UNIVERSITY OF BIRMINGHAM

DEVELOPMENT OF A MODEL TO ASSESS CLEANING AND DISINFECTION OF COMPLEX ROOT CANAL SYSTEMS

by

Firas Saddam Oglah Albaaj

A thesis submitted to the University of Birmingham for the degree of

DOCTOR OF PHILOSOPHY

School of Dentistry

College of Medical and Dental Sciences

The University of Birmingham

April 2018

ABSTRACT

The remaining debris and biofilm in the anatomical complexities of root canal systems can affect treatment outcomes. Files with asymmetric cross-section design may improve debris and biofilm removal from these difficult spaces during canal preparation. Tooth opacity and different densities of the remaining materials prevent the direct systematic assessment of the preparation process. The present study assessed remaining debris and biofilm using a novel transparent root canal model with novel approaches. Natural and simulated root canal samples with isthmus space were evaluated. Canal preparation by ProTaper Next and Revo-S asymmetric systems was evaluated in comparison to the standard ProTaper Universal symmetric system. The root canals were investigated by micro-computed tomography (micro-CT), confocal laser scanning microscopy (CLSM), and optical coherence tomography (OCT) imaging tools. Data analysis was undertaken with SPSS (V. 24). Files with asymmetric cross-section and constant taper removed more debris and biofilm from the complex root canal system. The model allowed direct assessment of remaining materials and confirmed the novel imaging approach with the OCT. In conclusion, the asymmetric design improves debris and biofilm removal especially when used with a constant taper. The model was verified as an ideal system for assessing root canal treatment *in vitro*.

I dedicate this thesis to my parents:

Mr Saddam Oglah and Mrs Ameera Lafta

ACKNOWLEDGEMENTS

First of all, I thank Allah (God), the Almighty, for granting me the capability to proceed successfully with this thesis.

I must acknowledge the Ministry of Higher Education and Scientific Research of Iraq for providing me with this PhD sponsorship. I extend my acknowledgement to the University of Birmingham and the School of Dentistry for this opportunity to undertake this research study.

I would like to express my deepest sense of gratitude to my supervisors, Professor Damien Walmsley and Dr Phillip Tomson, for their warm encouragement, thoughtful guidance throughout my study, also for their critical comments and correction of the thesis. I extend my gratitude to my supervisor Dr Rachel Sammons for her valuable guidance and instructions during the laboratory work.

Thank you for all laboratory technicians, especially, Gay Smith, Michelle Holder, Khawla Doudin, Sue Finny, and Jianguo Liu, for their technical guidance and endless cooperation. Thank you for post-graduate students, whom I met during my PhD journey, for sharing their research experiences and for their friendly companionship. I extend thanks to Rajvansh Juneja for the time and help provided in the microCT experimentation. Thank you for Dr Zhenyu Jason Zhang and Konstantina Simou for the cooperation provided to undertake the AFM analysis. Thank you for Dr. Luc van der Sluis and Rene' Dijkstra for their kind cooperation and support provided during the OCT experimentation.

Finally, I must thank my parents, sisters, brothers, wife, and children. Your patience and support inspired me the strength to continue my study.

List of Contents

List of Illustrations

List of Tables

List of abbreviations

Abbreviation	Meaning
µA	Microampere
AFM	Atomic force microscopy
ANOVA	Analysis of variance
BSA	Bovine serum albumin
CDFF	Constant depth film fermenter
CFU(s)	Colony forming unit(s)
CLSM	Confocal laser scanning microscopy
Cm	Centimetre
EPS	Extracellular polymeric substance
hr(s)	Hour(s)
IIF	Indirect immunofluorescence
kV	Kilovolt
LSD	Least significance difference
M	Molarity
MB	Mesiobuccal
microCT	Micro-computed tomography
min(s)	Minute(s)
ML	Mesiolingual
mL(s)	Millilitre(s)
mm(s)	Millimetre(s)

Abbreviation	Meaning
nm(s)	Nanometre(s)

nN	Nano-newton
NRRD	Nearly raw raster data
OCT	Optical coherence tomography
PBS	phosphate buffered saline
PTN	ProTaper Next
PTU	ProTaper Universal
RCS	Root canal system
RI	Refractive index
RP	Rapid prototyping
rRNA	Ribosomal ribonucleic acid
RS	Revo-S
rs	Spearman's correlation coefficient
SD	Standard deviation
SE	Standard error
sec(s)	Second(s)
SLA	Stereolithography
STL	Standard triangle language
TIFF	Tagged image file format
TRITC	Tetramethylrhodamine isothiocyanante
UV	Ultraviolet
VHN	Vickers hardness number

OVERVIEW

This thesis discusses the cleaning and disinfection of root canal system with complete isthmus using rotary file systems that have asymmetric cross-section design. The overview discusses the reasons for undertaking such research subject, materials, and analytic procedures.

The pulp is a loose connective tissue occupying the central space of the tooth (root canal system); in most situations, once it is traumatised or invaded by bacteria, it undergoes an inflammatory process termed as pulpitis. In severe and advanced cases, pulpitis can cause complete necrosis of the pulp tissue leaving a devascularized space, which is a favourable environment for bacterial growth and colonisation. The colonised bacteria and their toxins can invade the periodontal tissue surrounding the root apex initiating an inflammatory response termed as apical periodontitis. Apical periodontitis may lead to pain and swelling, which require root canal treatment or tooth extraction (Fava, 1998, Ricucci and Siqueira, 2010).

Root canal infection is mainly a bacterial disease of multiple phenotypes. Several species of bacteria have been isolated from such infections. Recent molecular studies have confirmed the existence of several genotypes of *E. faecalis* in both primary and secondary infections (Rôças et al., 2004, Hasson and Kadhem, 2017). This bacterium is an important species in endodontic failure linked to persistent apical periodontitis. Therefore, it is seen as a target for evaluating the efficacy of therapeutic measures in root canal infections (Dunavant et al., 2006, Wu et al., 2014, Wright and Walsh, 2017).

Endodontic procedures aim to '*prevent or treat apical periodontitis'* by *'either maintaining asepsis of the root canal system or disinfecting it adequately*' (European Society of Endodontology, 1994). In order to clean and disinfect the root canal system, it needs to be prepared and shaped with file instruments and an irrigant solution. Debris is produced mainly as a by-product of the mechanical process of instrumentation. Most debris will be removed coronally; however, some may be carried outside the canal through the apical foramen. There is evidence that the debris can be retained inside the canal and forced into fins, isthmi and accessory canals within the root system (Peters and Paqué, 2014, Versiani et al., 2016).

Debris can negatively affect root canal disinfection by either entombing bacteria or biofilm away from the disinfection procedure, or blocking dentinal tubules with infected material (Yusuf, 1982, Siqueira, 2001). The idea of entombing bacterial is possible in complex canals as debris was found to fill most of these spaces even after flushing the root canal system (RCS) with different irrigation protocols (Paqué et al., 2009, Versiani et al., 2016).

The RCS for most of teeth is not a simple rounded and tapered geometry to be ideally cleaned with the rounded tapered root canal files. Conversely, it is a highly complex system with a convoluted anatomy consisting of ramifications, protrusions and transverse anastomoses (isthmi). This is especially true in the posterior teeth (Vertucci, 1984). This complex anatomy is present throughout the root and often away from the main root canal. Hence, this part of the canal is not reached by the working field of the file instrument during preparation and subsequently not reached by the effective action of irrigant solutions. In summary, a large part of the canal system is remains untouched after preparation. This allows contaminated debris and biofilm to remain which will result in future problems (Siqueira Jr et al., 2018).

The isthmus is a partial or complete narrow communication between two root canals within the same root (Norman Weller et al., 1995). It has a higher prevalence in posterior to anterior teeth (Vertucci, 1984). In particular, the isthmus forms 21.4 % of the total root canal surface and 9.4 % of the total root canal volume (Endal et al., 2011). Consequently, it presents a considerable challenge to root canal treatment as it may harbour a significant amount of debris and bacteria both before and after root canal treatment. The thin wall of the isthmus and the difficult to reach areas of the tooth pose difficulties for research evaluation of these structures. Research used to evaluate the effectiveness of root canal treatment is mostly undertaken with scanning electron microscopy (SEM) and will require the root to be split in to two halves. It is difficult to split the tooth without damaging the thin walls of the tooth anatomy and in the past many samples were discarded because of the undesired root fracture (Heard and Walton, 1997). In the optical microscopy, horizontal sectioning is required to examine the root slice. With such sectioning, the biofilm and debris may be disrupted during the cutting procedure leading to false negative results. In both previous methods, evaluation is based on various qualitative scoring techniques where specific numbers are given to the collected specimens based on certain judgement criteria (Koçak et al., 2017, Yadav et al., 2017). The variations in these criteria may affect the interpretation of outcomes among experiments. Another technique uses a paper point or an appropriate instrument to culture samples from the root canal on an agar plate (Sathorn et al., 2007). This technique may not fully represent the situation inside isthmi because the sampling tool is always introduced to the main lumen. The results of all previous techniques were qualitative in nature and limited to a few samples rather than quantifying the debris and biofilm in the whole root canal system.

The use of extracted teeth does provide root canal samples with natural morphology. The variations in natural isthmus geometry could be considered as an uncontrolled variable, which might affect the outcome of the results. Controlling this variable by applying strict sample inclusion criteria with matched teeth of similar morphology is time consuming. Ethical approval for the use of human tissues in most laboratories can also lead to delays (Ahmed and Nicholson, 1996, Maskell et al., 2003).

To overcome such limitations, translucent models of root canals have been created by curing a clear resin around a straight or pre-curved silver point (Weine et al., 1975). Such simulated canals have been used extensively in endodontic research (Lim and Webber, 1985a, Dummer et al., 1991, Thompson and Dummer, 1997). Several forms of straight and curved simulated root canals, termed endo-blocks, are available for both research and education (Tchorz et al., 2015). Attempts to simulate a lateral canal or isthmus include using a thin wire and a thin metal strip respectively as templates at the apical level of the canal (Lee et al., 2004b). The invention of three dimensional printer machines offers an opportunity to develop a simulated root canal based on a previously set computer model (Martelli et al., 2016a). However, the technology for developing the root canal morphology remains limited to a simple conical shape, lacking the anatomical challenges that normally exist in natural teeth.

Research on the simulated root canal has focused on changes in root canal morphology following instrumentation with various instrument designs and techniques. Debris was also evaluated via pre-inclusion of natural dentine chips into a created groove in the apical portion of root canal blocks (Lee et al., 2004b). Endo-blocks containing *E. faecalis* have been used to research different irrigation protocols on biofilm removal using a spectrophotometer

(Townsend and Maki, 2009). These seem to be the early attempts for evaluation of debris and biofilm in resin root canals. Recently, single replicated root canals were used to measure biofilm that remained in the apical part using fluorescent and confocal microscopy (alarab Mohmmed et al., 2016, De Meyer et al., 2017, Mohmmed et al., 2017b). The samples were made by a stereolithography (SLA) printing technology using transparent resin materials. This material demonstrated a good surface for biofilm generation and evaluation with fluorescent and confocal microscopes.

Generally, the evaluation of debris and biofilm removal in simulated root canals has been limited to research on the impact of irrigation protocols. The impact of mechanical instrumentation was neglected, which makes the evaluation not as clinically relevant. Also, the evaluation is limited to the apical portion leaving the evaluation of biofilm and debris in the middle and cervical portions uncertain. This area should be included in the evaluation as high percentages (15.65 %) of root canal failure are seen following the coronal progression of root canal infection from cervical to the apical third of the root (Swartz et al., 1983, Tabassum and Khan, 2016).

Recent advances in file cross-sectional design have led to the development of asymmetric (off-centred) designs with one or two angles rather than whole angles contacts. These designs are primarily aimed to decrease stresses on the file surface and canal wall during canal instrumentation. Such design improvement is found to reduce cracks in the dentine (Yoldas et al., 2012). Instrument fatigue is decreased by reducing torsional and flexional stresses. Manufacturers claim that these instruments will provide more space within the canal wall. This

may allow debris to move outside the root canal facilitating its removal. However, the effect of asymmetric file design on debris accumulation in root canal is currently unknown.

The presence of debris in conjunction with biofilm in the RCS is recognized by many studies using 2D imaging tools (Peters et al., 2001, Metzger et al., 2010b). It is not possible with present technology to determine the relationship between remaining debris and biofilm within the same root canal sample at 3D level. Three dimensional imaging tools, such as cone beam computed tomography (CBCT) and microcomputed tomography (microCT), which uses x-ray beams, are sensitive to inorganic debris but are not able to detect organic tissues such as biofilm. Huang et al., (1991) developed a non-invasive optical scanning tool, termed optical coherence tomography (OCT), which is considered as an optical analogue to ultrasonic imaging in medical and biological fields. It utilizes a variety of optical properties, such as light absorption and scattering, to identify different tissue structures. Such ability is a recognized criterion, which can hold a promise for detection of debris and biofilm in the same root canal in a non-invasive 3D procedure.

In summary, the isthmus is a well-known space that harbours debris and bacteria during root canal treatment especially in posterior teeth where it constitutes a large volume of the root canal space. Such presence of debris and bacteria can interfere with the proper cleaning and disinfection goals toward successful root canal treatment.

Whilst remaining debris and remaining biofilm following treatment were independently evaluated, the extent to which debris contributed to biofilm was not fully clarified. Therefore, a comprehensive assessment to the treatment procedures within such difficult space seems

imperative for the systematic clarification of factors that impose challenges to the cleaning and disinfection procedures.

Unfortunately, due to the complexities of root canal anatomy and limitations of the current testing methods, a comprehensive *in vitro* evaluation of cleaning and disinfection of the root canal system is not possible.

Therefore, the overall aim of this thesis is to develop non-contact methods to undertake a systematic evaluation of cleaning and disinfection of root canal system with an isthmus using modern file designs.

To achieve this aim, the following objectives were considered.

1. To develop a simulated root canal model with realistic morphology.
2. To study cleaning and disinfection of the root canal system (RCS) with an isthmus using files with symmetric (centred) and asymmetric (off-centred) cross-sections
3. To establish a new non-invasive 3D technique for exploring debris and biofilm in the same root canal sample.

A general overview of the thesis structure is demonstrated in Figure 1. The experimental work and measurements were undertaken mainly by the thesis author. However, a collaborative work was required in certain experimentations.

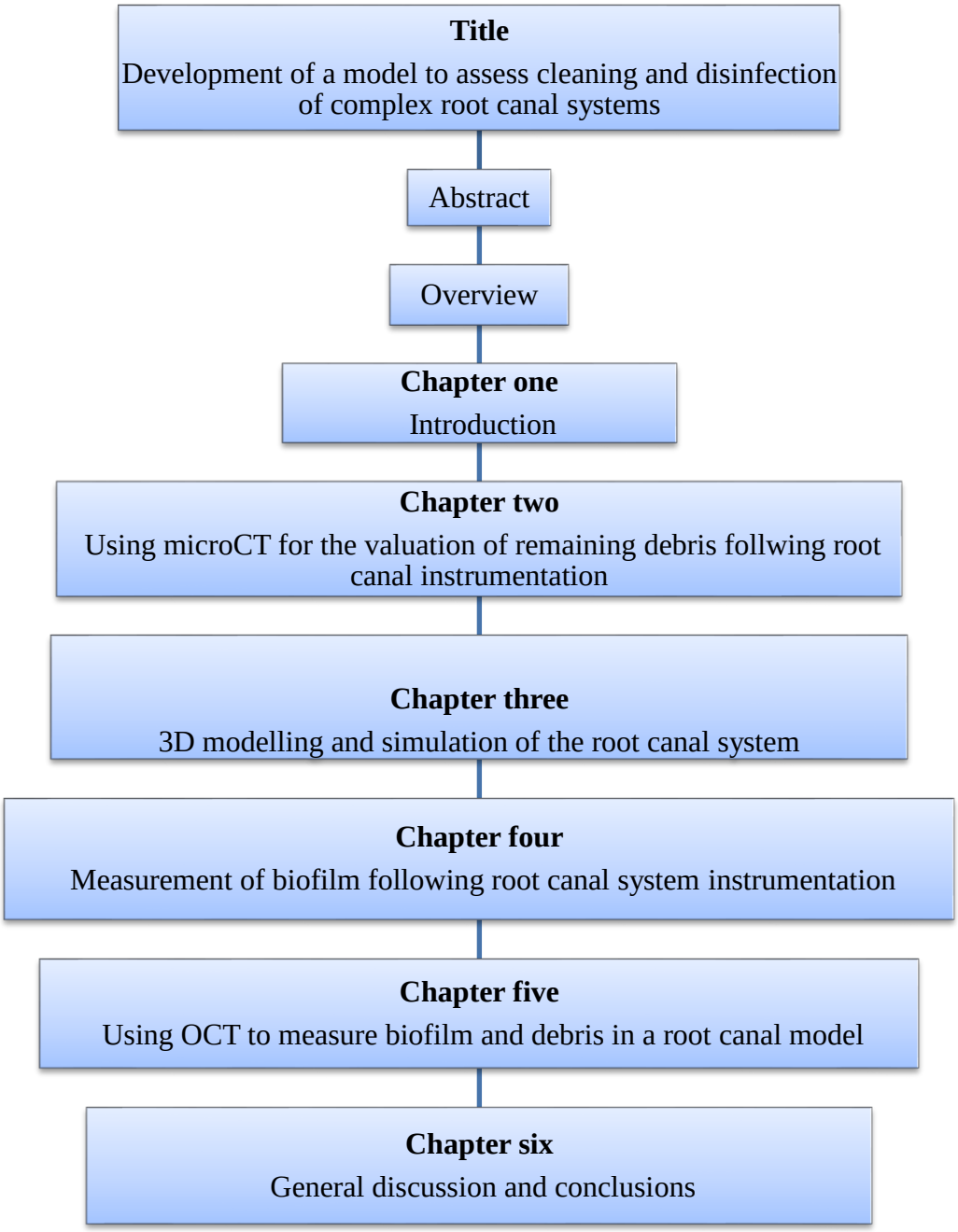

Figure 1: The Overview of the thesis structure.

CHAPTER ONE:

INTRODUCTION

This chapter discusses sequentially the biological, pathological, therapeutic, and evaluation aspects of pulp and periradicular diseases. The anatomy and composition of tooth structures are reviewed in order to understand how these structures can be involved in the mechanisms of disease progression and treatment modification. Dental caries and pulpitis are outlined as the dental diseases that lead ultimately to root canal infection and apical periodontitis. Root canal treatment is discussed with a detailed description of the mechanisms of root canal preparation. This review focuses on the isthmus space, which is an area of the root canal where preparation procedures are challenging especially in cleaning and disinfection protocols. The discussion is extended to include research methods used for the assessment of root canal cleaning and disinfection. The methods and applications of 3D printing technologies are evaluated for their potential of creating 3D root canal models for *in vitro* experimentation.

1.1. Tooth structure

The human tooth can be considered morphologically in two parts as shown in Figure 2; the crown and the root (Fitzgerald, 1992). These two parts are demarcated by the cementoenamel junction (CEJ) or the cervical line (Fouad et al., 2009). The structure of the tooth is composed of four unique tissues; enamel, dentine, pulp, and cementum, which relate to its form and function (Marsh et al., 2009).

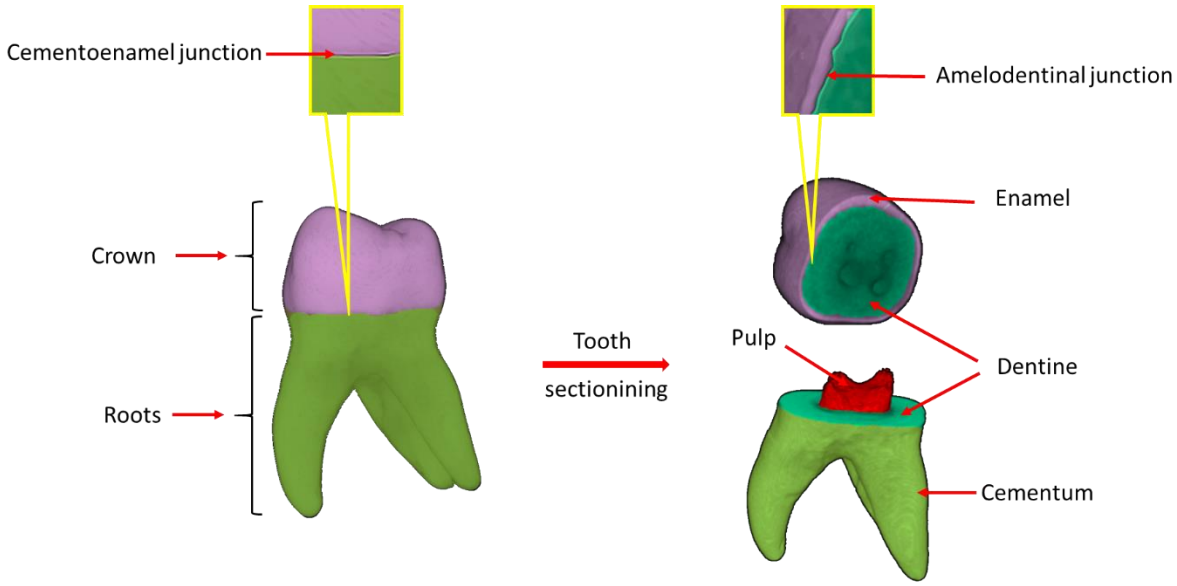

Figure 2: Tooth structure. Three-dimensional microCT images showing tooth parts and structures of a multi-rooted tooth.

1.1.1. Enamel

Enamel is a hard protective layer covering the whole crown with a variable thickness reaching its maximum at the cusp tips of premolars and molars (2–2.5 mm) to a very thin layer (knife edge) at the neck of the tooth (Avery and Steele, 2006). This hard layer enables the crown to withstand the high loads during mastication (Bhaskar, 1991). Enamel is a highly mineralized tissue composed of 96% inorganic matter and 4% organic matter, which includes water and protein (Permar and Melfi, 1994).

Amelodentinal junction (ADJ) refers to the microscopic scalloped line between enamel and dentine which has characteristic features of branched dentinal tubules and a spindled appearance (Avery and Steele, 1992).

1.1.2. Dentine

Dentine comprises the main bulk of the tooth providing the outline shape as it develops before enamel and cementum (Chandra et al., 2004). Embryologically, dentine is derived from the dental papilla via specialized ectomesenchymal cells called odontoblasts (Avery and Steele, 2006). Most of dentine structure consists of 65% inorganic substance and 35 % organic matter and water. The physical and chemical structure of the dentine are similar to those of the bone, it is a hard and porous tissue characterized by microtubules (dentinal tubules) running throughout its structure (Bhaskar, 1991). These tubules have a tapered structure with diameter of 2.5 to 3 µm near the pulp and 1 µm at the ADJ. The tubules orientation is different

throughout the tooth where they follow an S-shape pattern in the coronal portion, while they run in a straighter line in the root dentine. In addition, these tubules are responsible for the permeability of dentine by forming a network for the diffusion of nutrients (Nanci, 2014). Unlike enamel, dentine is a vital structure and can develop pain in response to cold and hot stimuli (Ten Cate, 1998).

Dentine is softer than enamel with a mean Vickers hardness number (VHN) range between 61.93 and 63.01 (Fuentes et al., 2003). Dentine hardness differs according to the age, tooth type and, whether it is located in the crown or in the root. The central part of dentine is harder than the peripheral part, which lies adjacent to the enamel or to pulp tissue (Bhaskar, 1991). This structure gives dentine a mild elasticity that acts as a cushion to support the brittle enamel layer against masticatory forces (Ten Cate, 1998). Dentine and pulp are considered as one functioning unit (dentine-pulp complex) because of their unique embryonic, structural and functional relationship to one another (Bath-Balogh et al., 1997).

1.1.3. The pulp

The pulp is a loose connective tissue of mesenchymal origin occupying the whole pulp chamber and root canal system. The mature pulp contains different cells with specialized functions for sensation, defence and providing a nutrient supply to the tooth. (Permar and Melfi, 1994). Histologically, the pulp tissue has two main zones, the odontogenic (peripheral zone) and the pulp proper (central zone). The odontogenic zone consists of four layers named sequentially toward inside of pulp as, the odontoblast layer, the cell free zone, the cell rich zone, and the

parietal plexus of nerves (Ten Cate, 1998) . The neurovascular supply of the pulp enters the tooth through the apical foramen at the apex of the root (Atkinson and White, 1992).

1.1.4. Cementum

It is a very thin calcified tissue that covers the whole root and is made of two different types: acellular cementum on the cervical and middle thirds, and cellular cementum on the apical third (Chandra et al., 2008, Nanci, 2014). It contains approximately 45 to 50 % inorganic substance and 50 to 55 % organic matter and water by weight (Chandra et al., 2008).

1.2. The root canal system (RCS)

This term refers to the space within the tooth, which is normally occupied by the pulp tissue, and follows the external contour of the tooth (Holliday, 2011). This system consists of two main parts: the pulp chamber, located in the crown of the tooth, and the root canal, which is located in the root portion of the tooth. At the end of the root, there are one or more orifices that communicate to the surrounding tissues outside the tooth called the apical foramen (Nelson and Ash, 2010).

There are other features within the root canal system such as isthmi, accessory canals, lateral canals, and apical deltas. The majority of these spaces were found in posterior teeth rather than anterior teeth with percentages of 20 to 59.5 % respectively (Vertucci, 1984). The higher incidence, based on the previous study, was found in the second premolar and in the first and

second molars of maxillary and mandibular teeth. Such features are regarded as difficult spaces or difficult anatomy as they lie in a lateral position to the main canal away from the field of preparing instruments (Holliday, 2011). By histological evaluation, bacterial biofilm was detected covering the wall of canal isthmi and ramifications in endodontically treated (80 %) teeth with persistent apical lesions such as abscesses, cysts, and granulomas (Ricucci and Siqueira, 2010). This might be the reason behind the higher percentage (7.58 %) of endodontic treatment failure in posterior teeth compared to the lower percentage (4.1 %) in anterior teeth (Salehrabi and Rotstein, 2004).

1.2.1. Isthmus

An isthmus is a ribbon-shaped anastomosis located between two canals within the same root (Norman Weller et al., 1995). It forms 21.4 % of the total root canal surface and 9.4 % of the total root canal volume (Endal et al., 2011). An isthmus could be classified as complete where it connects two canals through their cervicoapical length; or as partial where it connects two canals at certain levels (Villegas et al., 2004, Al-Qudah and Awawdeh, 2009).

Based on evaluation of histological stained sections, the term incomplete isthmus referred when two canals protrude toward each other without actual communication (Norman Weller et al., 1995, Teixeira et al., 2003). Once communication is observed, the terminology is changed to a complete isthmus. The prevalence of isthmus was recorded as 37.2 % in the apical 6 mm of mandibular teeth via evaluation of histological sections (Teixeira et al., 2003).

The high possibility (60 %) of having two main canals in the mesial roots of these teeth (Norman Weller et al., 1995) could increase the likelihood for the canals to develop an inter-connection compared to other teeth with a single canal. Vertucci (1984) found that the mesial root of the lower first molar followed by the mesial root of the upper first molar revealed the high percentage of partial isthmi 63 % and 52 % respectively in all root canal levels. However, in the Vertucci's study, root canals with complete isthmus were not described because such canal morphology was classified as a single canal volume.

The use of microCT in endodontic research, as 3D scanning device, has offered the advantage of evaluation of the whole RCS anatomy in a single image. The prevalence of isthmi in 36 lower 1st molars was recorded as 24 % - 50 % using microCT in a Chinese population where the younger age group (24-39 years) showed the higher percentage compared to the old age group (≥ 60 years) (Gu et al., 2008).

Through examining histological sections, biofilm has been detected covering the walls of canal isthmi and ramification in endodontically treated (80 %) and untreated (74 %) teeth, which were diagnosed with apical lesions such as abscesses, cysts, and granulomas (Ricucci and Siqueira, 2010). This research could reflect the difficulty in the disinfection measures used in the isthmus area because the endodontic treatment showed no improvement in the root canal sterility compared to untreated teeth.

1.3. Pathological conditions related to teeth

Dental caries and periodontal disease are two common diseases that affect the teeth. For the purposes of this thesis, dental caries and its consequences on the pulp and surrounding tissues will be considered.

1.3.1. Dental caries

Dental caries is a multifactorial disease affecting the calcified tissues of the tooth causing demineralization of the inorganic substance and subsequent destruction of the organic components (Summitt and dos Santos, 2006). Miller (1889) proposed the acidogenic theory, which assumed that the demineralization of the tooth structure occurs due to the effect of the acid which results from the fermentation of carbohydrates by oral bacteria. It is suggested by epidemiological studies that dental caries is caused by specific species of bacteria rather than a polymicrobial mass as two types of *streptococci* species (*mutants* and *sobrinus*) have been shown to be highly prevalent in carious lesions (Kidd and Joyston-Bechal, 1997). Other factors like dietary sugars and time are also important in disease development (Soames and Southam, 2005).

1.3.2. Pulp inflammation and necrosis

Pulpitis is a general term referred to the inflammation of the pulpal tissue (Cawso, 2002), which is usually caused by invasion of bacteria or an irritating substance to the RCS (Samaranayake, 2006). Depending on the severity of the inflammation, increasing blood flow and vascular permeability will raise intrapulpal pressure as there is no room for pulpal tissue expansion because it is confined by a rigid dentine case (Orstavik and Pitt Ford, 1998), and under unfavourable conditions may end with partial or complete tissue necrosis (Samaranayake, 2006).

1.3.3. Apical periodontitis

It is an acute or chronic microbial infection of dental origin affecting periradicular tissues as consequences to the pulpal tissue necrosis (Voruganti, 2008, Hargreaves et al., 2012). Long standing or severe apical inflammation can result in a high possibility of bone and soft tissue lysis (Wood and Goaz, 1997) and abscess formation (Scully et al., 2004). Periapical infection and flare up may be a result of either the extrusion of debris contaminated with bacteria to the periapical area, or through changing the environment in the root canal after incomplete eradication of microorganisms. The later causes disruption of the equilibrium status of endodontic microbiota (Siqueira, 2003).

After root canal treatment, apical periodontitis might appear as a complication because of inadequate cleaning and shaping (Estrela et al., 2009) especially in complex root canal anatomy

where parts of the RCS may prove difficult to be reached by instruments, irrigants and intra-appointment dressings aimed at disinfection (Nair et al., 2005a).

1.4. Root canal infections

These are classified according to their location into two main types; (1) Intraradicular, whereby microorganisms colonize the RCS (Fouad et al., 2009), and (2) extraradicular, which is characterized by bacterial invasion and proliferation into the periradicular tissues surrounding the apex of the root (Siqueira Jr, 2002, Marsh et al., 2009). The main routes by which bacteria can invade the pulp tissue are dentinal tubules, direct pulp exposure, periodontitis, and anachoresis, a process whereby microorganisms reach the damaged tissue through blood or lymphatic vessels (Fouad et al., 2009).

1.4.1. Endodontic microbiota

Although all microbial flora normally present in the oral cavity can invade exposed root canals, only restricted species (90 % anaerobic bacteria) have been isolated from infected canals (Figure 3). This was attributed to the special environment, such as nutritional demands and commensalism, inside these canals that allow for special species to survive and multiply (Sundqvist, 1992). In primary infection of root canal, by using checkboard DNA-DNA hybridization and polymerase chain reaction test on 53 infected teeth, *streptococci* were detected in 22.6 % of examined root canals, *Actinomyces* species in 9.4%, and *E. faecalis* in 7.5 % (Siqueira Jr et al., 2002b).

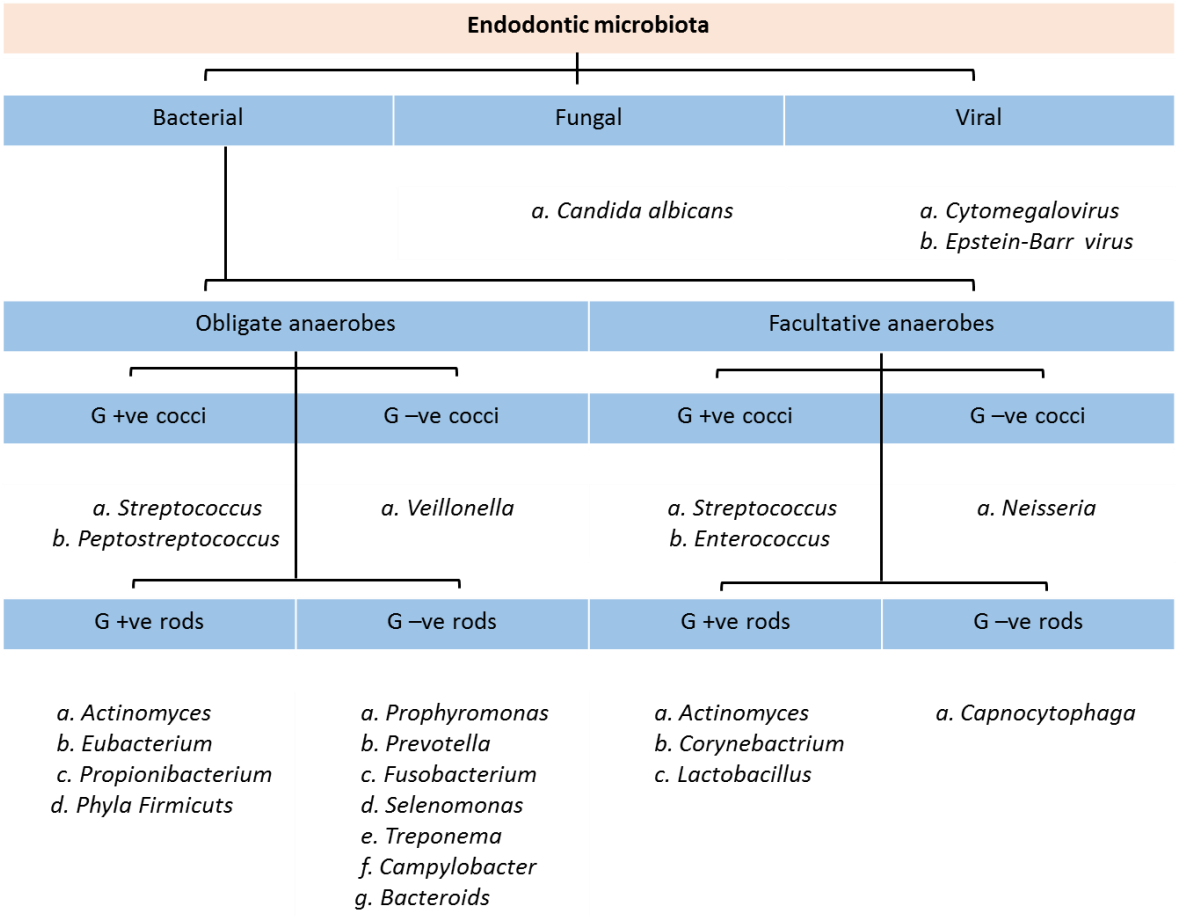

Figure 3: Endodontic microbiota. A flow chart shows the common bacterial phenotypes isolated *in vivo* from infected root canal (Nair, 1997, Siqueira, 2001, Siqueira Jr et al., 2002b, Ozbek et al., 2013, Jakovljevic et al., 2015, Nóbrega et al., 2016, Shah et al., 2016)

Under SEM, at the apical 2 mm of the infected roots, Molven et al., (1991) found that the gram negative rod- shaped bacteria are predominant among other types like filaments, spirochetes, and cocci, which collectively formed plaque similar structure covering the canal wall.

A molecular polymerase chain reaction (PCR) test, on nucleic acids extracted from pulverized teeth, has detected nucleic acids of *streptococcus milleri* and *streptococcus constellatus* in root canals with periapical lesions, while *Bacteroid forsythus* was detected in root canals with deep periodontal pockets (Smallwood et al., 1998).

Bacteroid genus was also predominant in teeth that had infected root canals with an acute periapical abscess. Seventy eight *Bacteroid* strains were isolated using anaerobic bacterial culture, however, *B. gingivalis*, *B. oris*, B. oralis, *B. intermedius*, and *B. denticola* were the most common strains (Haapasalo, 1989). Another study using quantitative PCR (qPCR) found that *S. anginosus* in 16.7 %, *F. nucleatum* 14.3 %, and *B. forsythus* in 7.1 % of cases with a periapical abscess (Siqueira et al., 2002a). Nóbrega et al., (2016) have recognized 59 cultivable bacteria in root canals with apical periodontitis using a qPCR analysis. The anaerobic gram-negative bacteria were the dominant species where *phyla Firmicutes* and *Bacteroidetes* form the majority of those species. Shah et al., (2016) have confirmed the presence of *Candida albicans* in 8 % of root canals with primary infection. Jakovljevic et al., (2015) and Ozbek et al., (2013) have isolated cytomegalovirus and Epstein-Barr Virus from apical periodontitis lesions of endodontic origin. Bacteria such as *Actinomyces israelii, Actinomyces naeslundii, and Arachnia propionicca,* have been found in root canal treatment failures (secondary infection) after a long-term evaluation of 2-5 years after root canal treatment for 79 teeth with single root and periapical lesion such cyst and abscess (Siqueira, 2001).

1.4.2. *Enterococcus faecalis*

E. faecalis are gram positive and facultative anaerobic cocci, which belong to the *Streptococcus* phenotype. They colonize normally the human intestine in abundance of 10^5-10^8 colony forming unit (CFU) in each gram of stool material (Koch et al., 2004). The genus *Enterococcus* have two main species; *E. faecium* and *E. faecalis*, which are opportunistic pathogens and the main species involved in nosocomial infections (Edmond et al., 1999). Twenty four strains of *E. faecalis* have been identified by Monstein et al., (1998) using broad-range PCR. The prevalence of *E. faecalis* in persistent root canal infections ranges from 24 % to 77 % (Stuart et al., 2006). It also has been found in a female genital tract (Younes et al., 2017) and with lesser extent in the oral cavity (de Paula et al., 2017). It is associated with different serious diseases such as endocarditis, bacteraemia, meningitis, also in wound and urinary tract infections. These bacteria are able to live in harsh conditions with low oxygen and depleted nutritional environment. *E. faecalis* showed ability to colonize tissue surfaces and resist detachment conditions like bowel motion (Barnes et al., 2017) and blood flow in case of bacterial endocarditis (Nallapareddy et al., 2006, Madsen et al., 2017). Several factors have been speculated to enhance *E. faecalis* adherence to the affected tissue:

1. Ace (adhesins of collagen from *E. faecalis*), which is also called collagen adhesion protein, is another surface protein found to mediate adhesion to specific collagens such as type I and type IV (Nallapareddy et al., 2000). The Ace has been detected as an important factor in the adhesion of *E. faecalis* to the dentine surface. (Hubble et al., 2003).

2. Enterococcus surface protein (Esp). This surface protein expected to mediate bacterial attachment to the urinary tract during infection (Shankar et al., 2001). On abiotic surfaces, A gene expression analysis has revealed that Esp was involved in the bacterial adhesion and biofilm development on polystyrene (Toledo-Arana et al., 2001b).
3. Aggregation substance, which is a hair-like surface glycoprotein that have a role in *E. faecalis* attachment to the human epithelium (Nallapareddy et al., 2000), however, the main role of this substance is the cell to cell adhesion to facilitate plasmid transfer between *E. faecalis* bacteria (Kreft et al., 1992).

1.4.2.1. Detection of *E. faecalis* in root canal infections.

E. faecalis is recognized as a distinct microbial participant in the pathogenesis of root canal infection stages especially after the invention of the molecular PCR test. This test is significantly more sensitive than the cultural method and enables detection of many non-cultivable genotypes (Gomes et al., 2006). In primary infection, a checkboard DNA-DNA hybridization and PCR test was recognized that *E. faecalis* constitute 7.5 % among bacterial species found in 53 infected root canals (Siqueira Jr et al., 2002b).

E. faecalis can colonize root canal surfaces and penetrate dentinal tubules (Louwakul et al., 2017). In a clinical study by Peciuliene et al., (2000) on 25 patients with persistent apical periodontitis, the authors found that *E. faecalis* appeared in 56 % of the 20 cases that showed positive culture. Seven genotypes of *E. faecalis* were detected in 23.8 % of cases with persistent apical periodontitis using bacterial culture and repetitive sequence-based qPCR (Delboni et al.,

2017). Rôças et al., (2004) used qPCR to investigate presence of *E. faecalis* in primary and secondary root canal infections. In both situations, the results showed that *E. faecalis* are mainly found in teeth with asymptomatic or chronic periapical lesion and rarely found in teeth with acute abscesses. Deo et al., (2016) isolated *E. faecalis* from primary root canal infection in both symptomatic and asymptomatic apical periodontitis using gene specific primer (16S rDNA) PCR method. The percentages were approximately similar in both situations as 33.3 % for symptomatic and 34.8 % for asymptomatic cases. Variation between both previous studies is likely related to the type of primer used for identification of bacterial species as generalized primer may recognize less bacterial genotypes than specialized one.

E. faecalis is able to develop a high or a moderate resistance to certain antibiotics such as cephalosporin, aminoglycosides, penicillin (Sood et al., 2008, Hall et al., 2017), gentamicin, vancomycin (Holliman and Smyth, 1989, Simonsen et al., 2003) doxycycline and azithromycin (Anderson et al., 2017), so they were found predominant in root canals with persistent infection following the antibiotic therapy.

1.5. Biofilm

Biofilm is a sessile aggregation of microbial cells in a hydrated polymeric structure (extracellular polymeric substance, EPS) on a biotic or abiotic surface (Costerton et al., 1999). The EPS composes 90 % of the biofilm structure and helps in providing; scaffold for the biofilm, water retention environment, and nutrient source for the colonizing bacteria (Flemming and

Wingender, 2010). Enzymes in the biofilm help in spreading of microorganisms by digestion and degradation of EPS matrix (Sauer et al., 2004).

The structure of biofilm is composed mainly of water (50-97%) circulating in microchannels (de Beer et al., 1994, Evans, 2003), and the extracellular products of microbial cells, such as polysaccharide, lipid and protein, with a wide range of enzymes, which control the structure integrity and stability (Sutherland, 2001). These products act as a dynamic matrix, which holds bacteria, fungi, or protozoa in a favourable survival environment during normal and harsh conditions (Sauer et al., 2004). The microbial cells in the biofilm are more resistant to the antimicrobial substances or host defence responses than planktonic bacteria (Sauer et al., 2004). It has been found that the EPS matrix retards the penetration of antibiotic through the biofilm mass to allow enough period for development of resistance phenotypes (Costerton et al., 1987). In addition, the local oxygen depletion in the biofilm causes bacteria to enter the stationary phase (slow growth) where bacteria are less susceptible to the antibiotics (Costerton et al., 1987, Fletcher, 1991, Walters et al., 2003, Hall-Stoodley and Stoodley, 2009). In polymicrobial biofilm, bacteria can modulate their pathogenic effect to be more virulent by a molecular interaction mechanism (Short et al., 2014). Therefore, biofilm, rather than planktonic bacteria, is considered as the causative factor in several persistent infections like chronic otitis media (Schachern et al., 2017), cystic fibrosis of the lung (Das and Manos, 2017) and apical periodontitis as will be discussed later. These findings pushed scientists to develop several *in vitro* culturing methods to simulate *in vivo* environments during biofilm generation as a measure for testing treatment modalities or studying biofilm behaviours.

1.5.1. Biofilm formation steps

There are general sequences for each biofilm to develop on any suitable surface substrate as described by (Svensäter and Bergenholtz, 2004) and (Stoodley et al., 2002):

1. Reversible adhesion phase: refers to the initial contact between bacteria and surface substrate.
2. Irreversible adhesion phase: refers to the aggregation of bacteria as microcolonies on substrate surface.
3. Biofilm maturation phase: refers when microcolonies are surrounded by EPS matrix
4. Dispersal phase: refers to the detachment of the bacteria to the surrounding medium.

During the initial step of biofilm development, the floating planktonic bacteria release protons and signalling molecules to explore proximal surfaces. They start to roll before adhesion and roll away if the surface is already colonised by bacteria of the same species forming a monolayer of bacteria of isolated colonies (Costerton, 1999). After the first step of attachment, bacteria upregulate specific adhesion genes to produce more EPS to enhance adherence to the surface and to other bacteria (Haapasalo, 1989). Such gene regulation will produce a phenotype different from the planktonic bacteria of the same species (Bhomkar et al., 2010). This higher production of EPS will change biofilm status from reversible to irreversible attachment (Costerton, 1999). In dispersal phase, the biofilm mass starts to degrade via the detachment of several bacteria to the medium as planktonic cells or as small fragments of biofilm that might adhere to a distant site (Stoodley et al., 2001). The biofilm degradation could happen either by

liquefaction of the central mass when certain bacteria upregulate to a bacteriophage to destroy bacterial colonies releasing survived bacteria (Webb et al., 2003) , or by an endogenous enzymatic degradation to the EPS matrix (Lee et al., 1996, Kostakioti et al., 2013). It is obvious that biofilm dispersal phenomenon affects both biomass structure and volume. Therefore, when evaluating biofilm removal, it is important to determine the onset of biofilm dispersal to avoid misinterpretation between physiologic and therapeutic degradation.

1.5.2. Methods of biofilm model generation

Biofilm models are generated by either static or dynamic biofilm systems. The static (constant) methods, such as the microtiter plate assay, the air-liquid interface assay, and the colony biofilms assay using agar plates, have the advantages of simplicity and being undertaken with the common laboratory tools. Also they can be used to study the biofilm at different developmental stage periods (Merritt et al., 2005). They are suitable for generation of biofilm for microscopic evaluation. In contrast, the dynamic (continuous flow) systems or fermenters, such as the constant depth film fermenter (CDFF) (Lei et al., 2016) and the centre for disease control (CDC) bioreactor (Yoon and Lee, 2017), provide continuous nutrient supplement with fresh growth medium. In addition, the biofilm maturation stage can be easily achieved in comparison to the static method (Merritt et al., 2005, Lei et al., 2016).

1.5.2.1. Microtiter plate assay

The method was developed by Fletcher in (1977) to test the ability for adhesion and biofilm generation of various bacterial species. This method provides quantification of the adhered biofilm, which is stained with crystal violet (Mawang et al., 2017) or methylene blue dye (Sai Saraswathi et al., 2017). The assay is usually performed in a 96-wells polystyrene tissue culture plate at different time intervals. The planktonic and floating parts of the biofilm are washed and removed from the culture plate's wells before the staining procedure (Azeredo et al., 2017). The amount of the biomass is determined by the amount of dye retained in the biofilm sample after washing. The retained dye is normally estimated by the estimating the absorbance amount for a passing light at a specified wavelength using a plate reader device (Sai Saraswathi et al., 2017).

1.5.2.2. Constant depth film fermenter (CDFF)

This culture procedure was intended to simulate the oral environment in order to study the biofilm on dental tissue and restorative materials (Coombe et al., 1984, Peters, 1988). The machine composed of a glass vessel of 18 mm diameter and 15 mm depth with an internal stainless steel rotating table contained 15 polytetrafluoroethylene sample pans. The table is rotating at a constant speed of 3 rpm (Wilson, 1999, Kocan et al., 2017). The machine is being work with a flow of air at 0.83 to 250 mL/min (Kinniment et al., 1996). The CDFF is designed to initiate gradual growth of a biofilm in recesses created on the pan surfaces. The culturing medium is dripped on the rotating table in front of a scraper blade. The scraper blade is placed at specific height from the pan to maintain a constant thick biofilm layer by scraping the excess

biofilm and keeping only thin film of nutrient over the developing biofilm (Kinniment et al., 1996). The shedding of the superficial biofilm layer was aimed to simulate the continuous shed of dental biofilm due to masticatory function (Wilson, 1999). In addition to its wide application for generation of oral biofilms (Al Groosh et al., 2016, Pratten et al., 2016), the CDFF was used to infect, *in vitro*, root canals with bacterial biofilm to mimic an induced *in vivo* infection (Patel et al., 2007). The results showed similar infections and therefore the CDFF is likely a suitable tool for generating clinically relevant root canal biofilm models.

1.5.3. Biofilm association with apical periodontitis

Several studies have revealed a typical biofilm structure in infected root canals with apical periodontitis. The biofilm was aggregated in all anatomical areas of the RCS as a single or Poly-microbial communities dominated by gram-negative anaerobes.

A SEM study on fifteen extracted teeth with attached periapical lesions showed extensive colonization of the root canal surface at all thirds inform of biofilm of mixed species. The species were mainly formed of cocci and rods while yeastlike cells appeared in one specimen (Siqueira Jr et al., 2002a). Nair et al., (2005b) examined a surgically resected apical portion of 16 mesial roots with apical periodontitis using the transmission electron microscopes. The results showed that 14 teeth have infection in the main canal and 10 roots have biofilm in isthmi and accessory canals despite canal irrigation with 5.25 % NaOCl and rinsing with 17 % EDTA. The effect was not limited to the intracanal biofilm, a clinical study investigated the presence of biofilm on the external surface of root canals of 16 tooth (Leonardo et al., 2002). The results showed a closed

association between the presence of periapical lesion and biofilm on the root surface after evaluation with SEM. Cocci, Bacilli, and filaments were dominating the biofilm SEM picture. Fluorescence in situ hybridization (FISH) was also used in conjugation with the confocal laser scanning microscopy (CLSM) to detect different types of bacterial species in asymptomatic treated teeth with periapical lesions. Lesions were surgically removed then labelled with different bacterial probes to be examined under the microscope. The results showed that an aggregation of microcolonies mainly formed gram negative anaerobic rods normally found in periodontal diseases such as *Tannerella forsythensis*, *Porphyromonas gingivalis*, and *Prevotella intermedia* (Sunde et al., 2003).

1.6. Treatment of pulpal and periradicular diseases

Whilst there are biological causes of pulpal and periradicular diseases, the treatment relies mainly on the mechanical and chemical removal of the affected tissues.

There are four main treatment procedures; pulp capping, pulpotomy, pulpectomy, and root canal treatment (Voruganti, 2008). The choice of each treatment depends on certain clinical and radiographical parameters. The pulp capping treatment relies on stimulating regenerative dentine formation by using an alkaline dressing paste (Stanley, 1989). Pulp capping can be categorized into; indirect pulp capping, where the dressing material is placed at the deepest part of a cavity if deemed to be close to the pulp. The intention is to induce the pulp to lay down tertiary dentine in order to protect itself (Ingle et al., 2008). In contrast, direct pulp capping is indicated when there is a pulp exposure during cavity preparation or traumatic injury with no

or minimal bleeding (Stanley, 1989). Recent advances in biomaterial technology have introduced new capping pastes such as mineral trioxide aggregate (MTA) and Biodentine which have improved both pulpal and dentinal tissue repair (Tomás-Catalá et al., 2018).

1.6.1. Root canal treatment

'*The purpose of root canal treatment is either to maintain asepsis of the root canal system or to disinfect it adequately*' (European Society of Endodontology, 2006). This involves the removal of vital and necrotic soft and hard tissues alongside canal disinfection using different types of instruments and various chemicals that are used as irrigants. This procedure is referred as biomechanical rather than mechanical instrumentation (Grossman, 1974). This term has been changed later to mechanochemical preparation (Hülsmann et al., 2005). Root canal preparation cannot always be performed to perfect technical standards. Due to certain limitations like inadequacies of instruments and techniques and complex canal anatomy, it is almost certain that the RCS will not be sterilised. Some debris and uncleansed surfaces will be left inside the canal which may allow bacteria to recolonize and result in failure of the treatment (Torabinejad and Walton, 2002). The mechanochemical preparation usually followed by filling the RCS with an adequate material to block the apical foramen and dentinal tubules to inhibit microorganisms and leaking fluids from invading the RCS and periapical tissues (European Society of Endodontology, 2006).

1.6.1.1. Root canal instrumentation

This process can be performed with manual (hand) file instruments or with engine driven (rotary) instruments using a rotational or reciprocating movement. There are different approaches to the use of such instruments and the success of each technique is shown mainly by *in vitro* experimentation.

1.7.1. Hand instrumentation - Step-back technique

Hand instrumentation is the traditional approach that uses hand files to debride the walls of the root canal. The aim of the step back technique is to produce an apically tapered canal, which allows easy obturation and irrigation of the RCS. This gradual taper technique was designed to overcome problems of apical transportation and perforation which can occur during instrumentation of a curved canal by stainless steel files (Ingle et al., 2008). It consists of two phases; phase I, the apical preparation (Ford et al., 2004), which aims to keep the apical constriction small and in its original position (Garg and Garg, 2008). Phase II includes preparation of the rest of the canal through gradual stepping back apico-coronally using a series of larger files (Ingle et al., 2008). In contemporary approaches, coronal flaring is established prior to the step-back procedure (Khademi et al., 2015).

1.7.2. Hand instrumentation - Crown-down technique

This technique differs from the step back approach as it commences with a flaring of the coronal third of the canal using hedstrom files followed by Gates-Glidden instruments (Kohli, 2010). The remaining part of the canal is prepared by sequentially decreasing size of the file as it progresses deeper into the canal until the instruments reach the apical constriction (Garg and Garg, 2010). The advantages of this technique are summarized as follows: minimizing coronal interferences with severe canal curvature helps reduce debris packing in the apical third (Baumann and Beer, 2011) and facilitate earlier penetration of the irrigant solution to the deeper parts of the canal (Patel and Duncan, 2011).

1.7.3. Hand instrumentation - Balanced – force technique

This technique employs a more complex finger movement by the operator where by the instrumentation process progresses in a corono-apical fashion using a 180^{o} clockwise rotation followed by 120^{o}-360^{o} counter clockwise rotation with apical pressure (Fouad et al., 2009). It appears that this technique is not as popular as the first two techniques (Roane et al., 1985), requiring more dexterity and time.

1.7.4. Nickel titanium (NiTi) rotary instrumentation

The first attempt to use NiTi files in root canal instrumentation was in 1988 when they were compared to stainless steel files of identical size, cross sectional design, and taper. Interestingly, NiTi was shown to be two to three times more flexible and have higher resistance to the torsional fracture (Walia et al., 1988). In the early 1990s, NiTi instruments were advocated for rotary file systems due to their more predictable root canal shaping (Del Fabbro et al., 2017), less fatigue to the practitioner and minimum postoperative sensitivity (Koch and Brave, 2002a). In addition, the use of rotary files is safer with little incidence of instrument failure. Despite rotary NiTi files having a simplified instrumentation process, they do not significantly improve treatment outcome or enhanced the removal of debris and biofilm from the RCS (Del Fabbro et al., 2017). A combined technique using hand and the rotary files in root canal preparation is currently a common procedure in root canal instrumentation. In this technique, hand instruments are used to negotiate the root canal and to create a smooth glide path for the rotary files (Alovisi et al., 2017, Zanesco et al., 2017).

1.8. Design characteristics of the rotary file

There are many design features that contribute directly to the file performance during root canal instrumentation.

The principle functions of the tip are to guide the file along the canal during the instrumentation. There are two main types of tip design: cutting and non-cutting (Hargreaves

and Cohen, 2011). Files with a cutting tip can better negotiate small calcified canals, nevertheless, there is great possibility of canal transportation if these files are held in the same position for more than one second (Koch and Brave, 2002a). Therefore, most of current rotary files use a non-cutting tip (Figure 4).

Files can be classified into two main categories; passive and active (Hülsmann et al., 2005). Passive files have a radial land (Figure 4) that removes a minimal amount of dentine by scraping or burnishing the canal wall (Peters, 2008). The larger surface area in contact with the canal wall keeps the file centred with little canal straightening (Kurtzman, 2007). Active instruments have better cutting efficiency but more tendency for canal transportation as they do not always follow the natural pathway of the canal (Walsch, 2004).

The pitch is described as the number of spirals per unit area on the file cutting surface (Figure 4) (Sanghvi and Mistry, 2011). Files designed with a constant helical angle and pitch have greater tendency to screw-into the canal compared to files with a variable helical angle (Koch and Brave, 2002b). The radial land is the surface axial projection between the file core and the cutting edge, which plays an adding peripheral strength to the file against torsional stresses.

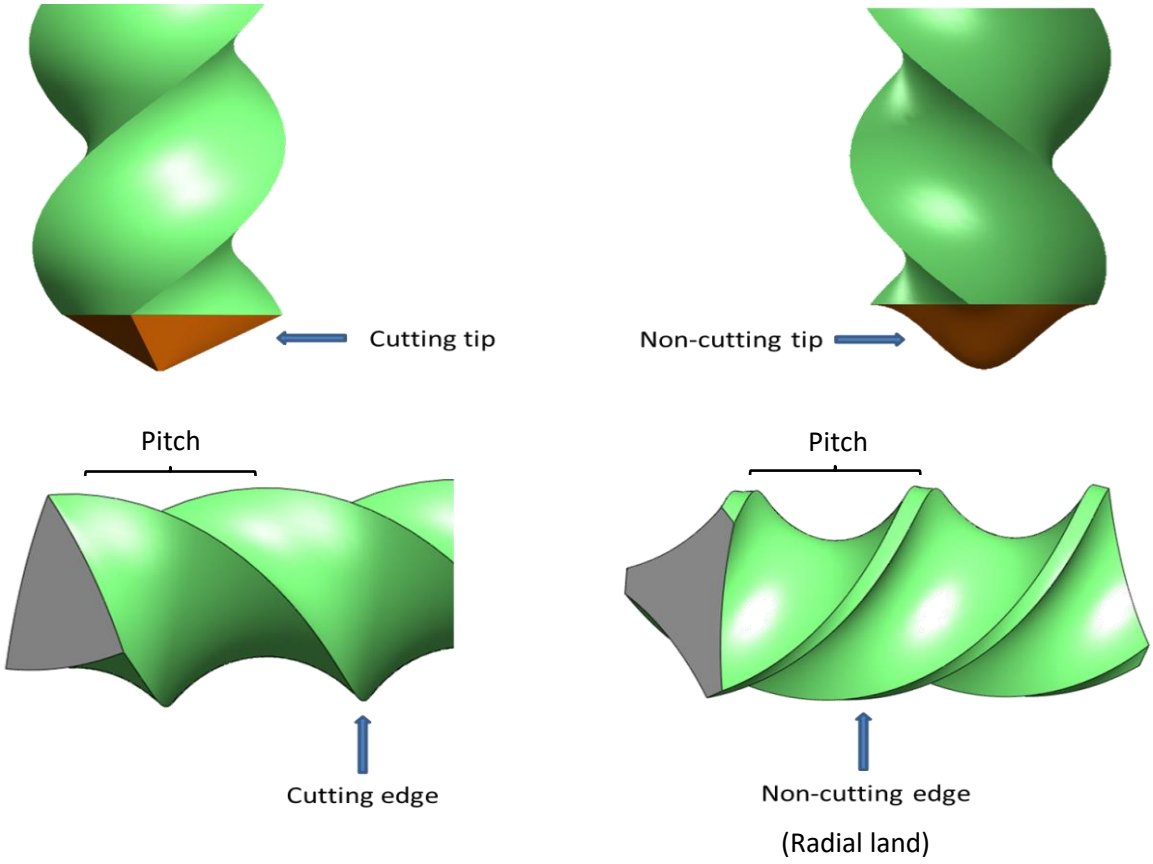

Figure 4: Design features of the endodontic file. A 3D diagram illustrates the tip and cross-sectional designs used for different file instruments. The upper panel show the cutting and the non-cutting tip (arrows), while the lower panel show the cross section and the lateral view for files with a cutting edge or with a non-cutting (landed) edge.

Also, it helps to keep the file centred inside the canal during instrumentation (Koch and Brave, 2002a). Some file systems, such as; ProTaper universal (Dentsply Maillefer, Ballaigues, Switzerland), Hero 642 (Micro-Mega, Besancon, France), EndoSequence (Brassler, Georgia, USA) and RaCe (FKG Dentaire SA, La Chaux-de-Fonds, Switzerland) do not have radial lands in their design (Sanghvi and Mistry, 2011) and have cutting edges.

Flexibility and lateral resistance during instrumentation is greatly affected by the cross-section design of the file's blank. Files with large cross-section and multiple contact points with the canal surface will generate high lateral forces, and thereby more torque to cut dentine (Kurtzman, 2007). However, small design, such as S-shape cross-section, leaves more spaces between the file and the canal wall that could facilitate debris removal (Newman et al., 1983).

The flute is a continuous groove extending along the working surface of the file in a helical pattern used to carry out soft and hard tissue debris (Hargreaves and Cohen, 2011). The depth and width of flutes are determined by cross section design and degree of helical angle (Elmsallati et al., 2006).

The helical angle represents the relationship between the cutting edge and the long axis of the file (Koch and Brave, 2002a). Files with variable helical angles along their working surface have a lower risk of screwing into the canal and it is possible to remove debris more efficiently when compared to those with constant angle (Sanghvi and Mistry, 2011). An example of such a file system is RaCe which utilizes a unique design called alternating helical design as a mean of reducing rotational torque (Koch and Brave, 2002a).

Recently, thermo-mechanical treatments to the NiTi alloy have been tried which have been shown to be more flexible than untreated nitinol and more resistant to file fracture (Gambarini et al., 2008). A number of manufacturers have produced file systems with treated NiTi alloys. For example, in 2007, M-Wire technology, developed by Dentsply, was introduced to the market. This product is produced by drawing raw NiTi file under specific tension and then heat treated at various temperatures. Such files like ProFile Vortex (Dentsply, Tulsa, USA), and Revo-s (Micro-Mega, Besançon, France), utilise this modified NiTi alloy (Basrani et al., 2011, Plotino et al., 2014b).

1.9. Classification of NiTi files.

Since their introduction there have been successive changes in the file design and these have been classified in term of different generations. Table 1 gives an overview of the changes of the file designs for each generation. The characteristic features of files belonging to the first generation are; landed cutting edges, neutral or negative rake angle, U-shape cross section, and fixed taper (Garg and Garg, 2010, Holliday, 2011). ProFile Vortex and Quantec (Tycom Corp., Irvine, CA) systems are examples of this generation, which require many file sequence to achieve the final design (Ruddle et al., 2013). To address some of the problems encountered by the first generation instruments, which include: high stress loads on files due to the landed cutting edges and screw-in effect, which resulted from a fixed taper design, second generation files were developed.

Table 1: Features of file generations. The main characteristic features of five file generations classified according to the modifications in the file design, material, and instrumentation motion.

	Characteristic features	**Examples of file systems**
First generation	Landed cutting edges, neutral or negative rake angle, U-shape cross section, and fixed taper	ProFile and Quantec
Second generation	None landed cutting edge, positive rake angle, variable taper, and alternating contact points.	ProTaper Universal and Endosequence
Third generation	New NiTi alloy technology based on special heating and cooling protocols.	ProFile GTX and the Twisted file
Fourth generation	Reciprocal movement and single file technology	Reciproc, Self-adjustable (SAF) and Waveone
Fifth generation	Asymmetric cross section design, active cutting edges, variable taper	Revo-S and ProTaper Next

There was also an attempt to reduce the number of files in each system (Ruddle et al., 2013). Examples include: (1) EndoSequence files with active cutting edges and alternating contact points to reduce rotational torque (Hargreaves and Cohen, 2011), (2) Protaper universal with variable taper which reduces the active cutting surface area at any one time whilst in operation (Ruddle et al., 2013).

The atomic structure of conventional NiTi alloy is composed of austenitic (hard / brittle) and martensitic (soft) crystalline lattices, the transformation from the hard to the soft structure is technically possible through different heating and cooling protocols under external tension (Peters and Paque, 2010). Taking the advantage of this technology led to the development of new file systems (third generation), such as ProFile GTX (Denstply, Tulsa Dental Specialties, Tulsa), and the Twisted file (TF) (Sybron Dental Specialties, Orange, CA) (Larsen et al., 2009).

It has been shown that a reciprocating motion can significantly reduce torsional stresses and hence file fracture by preventing file binding to dentine during clockwise rotation (You et al., 2010). Both the reciprocal movement and the single file technology are the main characteristic features of the fourth generation. The reciprocation could be; (1) up and down, like in the self-adjustable file (SAF) (ReDent Nova, Raanana, Israel) (Metzger et al., 2010a), or (2) clockwise and counter clockwise motion used in Waveone file (Dentsply, Ballaigues, Switzerland) (Webber et al., 2011).

Recently, the fifth generation files are produced with asymmetric cross section to reduce stresses on the file by minimizing engagement with the dentine. There is also a claim that this design could facilitate better file penetration and debris removal (Hashem et al., 2012). Diemer et al., (2013) found that the axial stresses along files with an asymmetric design are significantly lower than files with a symmetric design during preparation of resin-simulated root canals. Both Revo-S (Micro-Mega, Besanc¸on, France) and ProTaper Next (Dentsply Maillefer, Ballaigues, Switzerland) are an example of a file using asymmetric design. The Revo-S file has files with asymmetric triangular shaped cross-section design and three cutting edges located at different radii (Figure 5). The ProTaper next file has a rectangular cross section (Figure 5) which is offset and thus asymmetric which means when in motion it will only contact two surfaces of the canal wall at any one time (Capar et al., 2014).

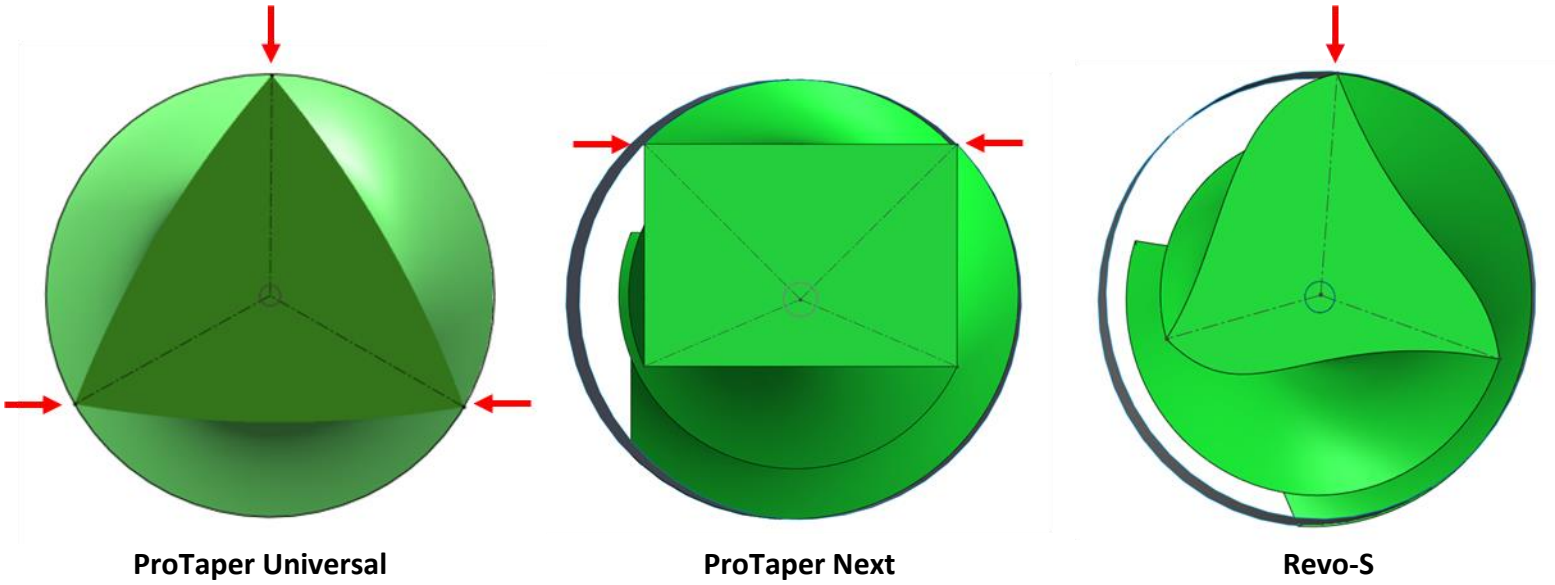

Figure 5: The cross-section design of three file systems. A diagrammatic illustration compares the asymmetric cross-section designs of ProTaper Next and Revo-S files to the symmetric design of the ProTaper Universal file. Arrows indicate the contact points of cutting edges with the root canal wall.

1.10. Root canal irrigation

Whilst mechanical preparation is important, the use of an irrigant is seen as a crucial step in root canal therapy. The irrigant solution is introduced into the RCS with a suitable tool and aims to '*eliminate microorganisms, flush out debris, lubricate root canal instruments and dissolve organic debris*' (European Society of Endodontology, 2006).

Many factors can influence achievement of these goals. Some of these factors belong to the delivery systems, while others belong to the confinement and anatomical complexities of the RCS. The available delivery systems failed to introduce the irrigant directly to the difficult spaces such as isthmus space; alternatively, they relied on the indirect flooding action through flushing of the main canal. The root confinement has been demonstrated to affect the dynamic flow of the irrigant solution and hence it's effective velocity (Verhaagen et al., 2012).

Gu et al., (2009) found that among 66 articles published between 1980 and 2008 about the impact of irrigation technique on root canal cleaning and disinfection, only 10 articles have used samples containing an isthmus space, and of these 10 studies, only one article has evaluated the biofilm using a histological method. This irrigation review might reflect the difficulty of direct exploration of such narrow space.

The simulation of the RCS could overcome challenges of sampling and visualization. The computational (Boutsioukis et al., 2010b, Chen et al., 2014, Adiguzel et al., 2016) and the physical (Lee et al., 2004b, Mohmmed et al., 2017b) simulation of RCS have been widely implemented in the evaluation of irrigation techniques. Rather these models lack the anatomical challenges as they were produced in a simple anatomy, the evaluation was not

as clinically relevant because these models did not address certain possible inferences to the irrigant flow associated with mechanical instrumentation. For example, changes in canal dimensions or the debris created during the canal shaping procedure. These limitations prioritize the need for developing a model that simulates the entire treatment procedure.

1.10.1. The standard syringe-needle irrigation

It is the earliest and the widely accepted technique among dentists. This method requires a syringe and needle or more recently cannula to introduce irrigant solution in to the root canal. The irrigation needles are designed to deliver the solution vertically towards the apical foramen or laterally to the root canal wall (Holliday and Alani, 2014). however, some designs have focused on placing few lateral vents and maintained a closed end to minimize the apical extrusion (Haapasalo et al., 2010). It produces a significant root canal cleaning and disinfection when compared to the treatment without irrigation (Lee et al., 2004a). However, syringe irrigation cannot effectively remove canal debris especially at the apical third when the canal diameter is narrow (Dalai et al., 2014), which is a possible effect of flow stagnation phenomenon (Verhaagen et al., 2012). Several disadvantages have been reported with the use of such technique. For instance, there is a higher rate of apical extrusion of irrigant solution (Charara et al., 2016) and lower effectiveness scores in cleaning of the isthmus area (Malentacca et al., 2017) compared to sonic and ultrasonic agitation methods. The wedging of the needle inside the root canal, the lack of the control on the flow rate, and the limited effect to an area closest to the needle vent are further drawbacks were reported with a such technique (Holliday and Alani, 2014).

1.10.2. Ultrasonic agitation

The use of ultrasonic agitation to an irrigant was started by Martin (1976) through using a titanium tip with 5.5 % sodium hypochlorite. He concluded that cavitation produced due to acoustic energy has direct bactericidal effect via destroying the bacterial cell wall or via increasing the antimicrobial activity of the irrigant solutions. The microstreaming could also bring these chemicals to the complex anatomies of the RCS (Van der Sluis et al., 2007).

The use of passive ultrasonic irrigation (PUI) was first demonstrated by Weller et al., (1980) who found a significant improvement in the cleaning efficiency of simultaneous root canals and extracted teeth when combining hand instrumentation with smooth wire agitated with ultrasonic machine. The PUI showed superior results to the syringe irrigation in single rooted canals. A study by Siqueira et al., (1997a) on extracted canines showed a non-significant difference between manual and ultrasonic irrigation with 4 % NaOCl. The use of NaOCl, as a potent antimicrobial agent, can mask the potential variations between irrigation methods.

Gutarts et al., (2005) and Leoni et al., (2017) found that PUI produces significant debridement scores in the isthmus area of the lower molars following hand and rotary instrumentation. A histological examination on cross sectional slices by Burleson et al., 2007 (2007) found significant reduction in the biofilm and necrotic debris in the isthmus upon using PUI for 1 min in lower molars. PUI shows less apically extruded debris through the apical foramen and minimum debris accumulation at the apical third compared to hand syringe irrigation (Alkahtani et al., 2014). A study showed that sodium hypochlorite at concentrations; 0.5 %, 1 %, 2.5 %, and 5.25 % can effectively remove pulp tissue remnants at the middle third of the canal when agitated by PUI (Baumgartner and Cuenin, 1992).

1.10.3. Irrigant solutions

They are low viscosity chemical solutions with certain requirements for the ideal irrigation process. It should have a broad spectrum of antibacterial activity, dissolve inorganic remnant in the root canal, non-toxic and non-irritant to the periapical tissue, and be able to clean the smear layer formed during canal instrumentation or prevent further smear formation (Zehnder, 2006).

1.10.3.1. Sodium hypochlorite (NaOCl)

Sodium hypochlorite is a clear and slightly yellowish solution that has a strong oxidative and antibacterial activity. When sodium hypochlorite dissolves in water, it will be degraded in to hypochlorous acid (HOCl) and hypochlorite ion (OCl^-) (Estrela et al., 2002). The disinfection property of NaOCl depends on the oxidative effect of the HOCl acid, which can easily diffuse through bacterial cell membrane causing damage to the cellular components (Karimi et al., 2016). The magnitude of the antibacterial activity is dose dependant and increases with higher concentrations. Much research has examined the effect of NaOCl on the root canal biofilm by using different concentrations (1 - 5.25 %). For instance, Frough-Reyhani., (2016) found that 2.5 % and 5 % NaOCl disinfected completely root canals infected with *E. faecalis* biofilm of ten weeks culture, while 1 % NaOCl caused incomplete biofilm reduction (78.62 %). Christo et al., (2016) found that 4 % NaOCl is more effective in root canal disinfection than 1 % concentration even when this low concentration was agitated with Er,Cr:YSGG laser. NaOCl is a powerful root canal disinfection solution compared to other irrigant solutions such as chlorhexidine digluconate and hydrogen peroxide (Arias-Moliz et al., 2015,

Ruiz-Linares et al., 2017). However, this material is highly toxic upon direct contact to the periapical tissue and it has been reported to cause a severe air emphysema related to its periapical extrusion following root canal treatment (de Sermeno et al., 2009). Recent studies showed a great possibility of apical extrusion of NaOCl when using the manual hypodermic or the Monoject syringe (Iriboz et al., 2015, Ariffin et al., 2016), however using this chemical with the Endovac system significantly reduced the extruded amount. Prolonged (1 hr) exposure of dentine to high concentration (5-9 %) of NaOCl can significantly reduce certain dental mechanical properties such as flexural strength and modulus of elasticity (Arias-Moliz et al., 2015). Gross surface roughness and spontaneous crack lines were developed on the dentine specimen surfaces rendering these samples brittle and less resistant to fracture during force application (Arias-Moliz et al., 2015).

1.10.3.2. Chlorhexidine digluconate (CHX)

At low concentration, CHX produces a bacteriostatic effect via leaking of phosphorus and potassium outside the cell (Athanassiadis et al., 2007). The CHX cation reacts with the negative charge on the bacterial surface to increase cell wall permeability through affecting the osmotic stability of the bacterial cells (Jones, 1997). At high concentrations of ≥ 2 %, it has a bactericidal effect, which enables CHX penetration to the cytoplasmic components causing precipitation of the intracellular components (Athanassiadis et al., 2007).

At concentrations of 0.2 %, 1 %, and 2 % and exposure time of 30 seconds, CHX showed a powerful antibacterial activity equivalent to 0.52 % of NaOCl against *E. faecalis biofilm* created by a tissue culture plate (TCP) method (Gomes et al., 2001). The CHX revealed

antibacterial activity against other bacterial species biofilms. For instance, single-species biofilms of Prevotella intermedia, Peptostreptococcus micros, Streptococcus intermedius, Fusobacterium nucleatum (Spratt et al., 2001). However, this antibacterial activity showed lower values when compared to NaOCl regardless of the concentration or the exposure time. CHX of 2.5 % has demonstrated a good ability to kill several bacterial phenotypes collected from root canals with persistent infection such as *Lactobacillus paracasei*, *Streptococcus gordonii,* and Streptococcus anginosus (de Paz et al., 2010). Accordingly, CHX has a broad spectrum of antibacterial activity and is effective in destroying biofilm in root canal infection. The CHX irrigant has revealed a minimal toxic effect on the living tissue when compared to the NaOCl (Önçağ et al., 2003). Although severe allergic reactions were reported when using CHX as an external antiseptic for surgeons (Egner et al., 2017), minimal or no allergic effects were found following the oral applications of such antibacterial agent (Amora-Silva et al., 2018). Unfortunately, CHX lacks the ability of NaOCl to disintegrate the organic tissue. Such ability is preferable in root canal irrigation to remove the organic debris remnants such as fragments of pulp tissue and collagen fibrils of shaved dentine.

1.11. The remaining debris following root canal preparation

Debris accumulation in the root canal following preparation is an inevitable complication especially at canal complexities (Peters and Paqué, 2014). Debris is generally categorised into organic (soft tissue) debris, which is the remnants of pulpal tissue and dentinal collagen fibrils, and inorganic (hard tissue) debris, which is the hydroxyapatite crystal particles of shaved dentine (Yamada et al., 1983). For the purpose of this thesis, the inorganic debris will be considered.

The amount of retained debris is greatly influenced by the type of the file system used. The self-adjustable file (SAF) left 1.7 % of that debris (Paqué et al., 2012) in comparison to ProTaper Universal and Waveone files, which left 10.6 % and 19.5 % respectively (Robinson et al., 2013). This debris produced during preparation has been demonstrated to contain bacterial presence within sizeable dentine shavings (Peters and Paqué, 2014), which can act as an obstacle for disinfection procedures (De-Deus et al., 2014). It may also prevent filling materials from flowing inside these spaces and entomb bacteria (Endal et al., 2011). Therefore, debris removal during root canal preparation seems as an important process that would improve root canal treatment outcome. Recently, a non-invasive method for estimating the amount of debris accumulation was used through measuring the canal volume changes after instrumentation by overlying reconstructed x-ray images of microCT machine (Paqué et al., 2012a, Robinson et al., 2013). The analysis of the remaining debris with the microCT received a considerable interest in endodontic research (Versiani et al., 2016, Verstraeten et al., 2017a). Debris can be counted by a specific analysis method applied for 3D image samples, which do not require pre-testing laboratory preparations. In addition, the images can be demonstrated in different colours given for root canal and debris to observe the real site of debris within the RCS.

1.12. 3D Imaging of the root canal system

This includes several imaging techniques that can non-invasively scan the tooth structure into hundreds of sections to analyse the complete root canal. The section can be reconstructed to produce 3D image with different axial and lateral spatial resolutions (*i.e.* ≥ 2 µm - < 5 mm) (Wagner et al., 2010).

1.12.1. Computed tomography (CT).

Computed tomography is a 3D X-ray imaging technique, which produces a series of sliced images via multiple radiation exposure sites called projections. These slices are collated into one 3D image using specifically designed computer software (Brenner and Hall, 2007). The concept of using computed tomography for imaging the root canal system commenced in 1990 when Tachibana and Matsumoto used the conventional CT used in hospitals for visualizing teeth of human volunteers (Tachibana and Matsumoto, 1990). Based on their findings, the anatomical configuration of the teeth, such as the number of roots and canals was clearly observed through a 3D image reconstructed by special software. However, the detailed anatomy of the root canal system was difficult to see because of the low resolution used in this technique (3-2 mm), and the scattering of the radiation via overlapping tissues.

1.12.2. Cone beam computed tomography (CBCT).

To increase the resolution and decrease the dose of radiation, Arai et al., (1999) developed CBCT to be specifically used for viewing the orofacial region. CBCT is a technique with higher resolution and minimum dose of radiation in comparison to the CT. This technique offered the advantage of producing isotropic voxels, whereby the reconstructed 3D-images have accurate dimensions compared to the anisotropic voxels of the conventional CT. In addition, there is possibility of focusing on a specific field of view. It has valuable applications in the diagnosis of patients for surgical and nonsurgical endodontic treatment (Cotton et al., 2007). CBCT has the ability to view precisely thin sagittal, coronal, and axial slices without common errors and difficulties, such as the superimposition of maxillary molars roots occur during imaging with the conventional 2D radiographic technique

(Johnson et al., 2011). In endodontic research, this tool showed promising results in evaluation of root canal anatomy (Matherne et al., 2008, Tahmasbi et al., 2017), and in detection of vertical root fracture (Hassan et al., 2009, Gaêta-Araujo et al., 2017) and preapical lesion (Estrela et al., 2008, Parker et al., 2017). Due to the resolution applied (0.4-0.125 mm), the use of this technology in endodontics is still limited to the diagnosis and assessment of treatment outcome (Scarfe et al., 2006, Durack and Patel, 2012).

1.12.3. Micro-Computed tomography (microCT).

For research purposes, Feldkamp et al., (1989) developed a method termed microCT to study the bone architecture using high isotropic (3D) resolution of 2.0 µm. MicroCT, such as Skyscan 1172 (BRUKER, Kontich, Belgium), is a device, which can take hundreds of images using an X-ray source from different angles through the object to a special X-ray detector. Furthermore, the distance of the sample can be adjusted to obtain the required magnification (Bruker, 2018).

Nielsen et al., (1995) found that microCT can show precisely the internal and the external features of a tooth without the need for sectioning. Further developments included a method to numerically calculate the change in the root canal volume after file instrumentation using special pack of software for analysis (Rhodes et al., 1999, Bergmans et al., 2001). These results proved that the microCT is an advanced system that could be used in endodontics research. This included measuring the amount of canal transportation and estimating the percent of the un-instrumented canal volume (Hübscher et al., 2003, Peters et al., 2003a, Paqué et al., 2005). Recently, microCT imaging enabled high-resolution

images to be developed which allowed debris to be easily differentiated from dentine walls. A co-registration method was developed to count and visualize the remaining debris in the original canal volume by using a mathematical operation, termed as a logical AND (Paqué et al., 2009). This operation combines the corresponding white pixels of two binary images into one image. However, the method was unable to identify the debris accumulated in the newly created canal spaces following preparation. In order to manage this problem, Robinson et al., (2012) extended the previous method to involve further imaging operations termed "morphological opening filtration" that recognised debris in the instrumented canal spaces.

1.13. Laboratory assessment of the root canal system

Generally, these assessments provide analysis down to microscale and nanoscale levels for accurate determination of cleaning and disinfection of the RCS.

1.13.1. Histological sectioning.

The RCS, especially the Isthmus space, is bounded by a thin and coalesced tooth structure, which is difficult to put in direct visualization under optical microscopes. Therefore, sectioning to several thin slices (200 µm to100 nm) was a routine laboratory work for performing a histological examination (Walton, 1976, Burleson et al., 2007, Adcock et al., 2011). In this technique, few sections are involved for the evaluation process. In these sections, the microscopic images taken for the debris or biofilm are analysed either by certain scoring procedures or by image analytic software. There are many complications

associated with the sample sectioning: the damaging of the section during preparation, the required area might not be included in the section, the actual size of the lesion cannot be guaranteed (Jablonski-Momeni and Stachniss, 2010).

1.13.2. Evaluation with scanning electron microscopy

With this method, the root canal can be examined in longitudinal sections. A groove with bur usually made along the mesial and distal root surface then split with chisel (Baker et al., 1975, B.S et al., 2014) or sectioning disc (Heard and Walton, 1997). The usual evaluation method is scoring or rating the efficacy of the preparation protocol from good to worse level. Three or five images from each root third were usually evaluated. Three or five scores were given to describe the amount of remaining debris, biofilm or the smear layer. However, this method is limited to a small area with a high possibility of disturbing or removing the root canal contents of debris and biofilm during sectioning procedure. Furthermore, it is difficult to section through the narrow isthmus and many tooth samples were damaged during sample preparation (Heard and Walton, 1997).

1.13.3. Bacterial culture method

Researchers preferred this method to assess the status of the intracanal microbiota *in vivo* (Gomes et al., 2006, Neves et al., 2016). This method offers direct sampling of the root canal using a paper point or a suitable file instrument (Bitter et al., 2017). Bacterial sample then detected by a culturing method or by a molecular method such as the PCR assay. The direct sampling of the isthmus area seems to be not possible in research due to the narrow

opening in such area. Alternatively, bacterial samples are collected from the main canal lumen. Therefore, this method appears not directly reflective to the microbial status of the isthmus area. In addition, cross-contamination of the root canal by oral bacteria is possible when a proper isolation of investigated teeth cannot be achieved.

1.14. Fluorescent labelling of bacterial biofilm

This method aims to study biofilms after staining with fluorescent dyes. The data is usually collected as light signals emitted from an excited dye by a suitable light source. In microbiology, this technique added advantage over the culture-based methods in that it can differentiate between live and dead bacteria within biofilm, also it can estimate different bacterial phenotype concentration in multiple species biofilm. The fluorescent dye can be applied directly to the biofilm or indirectly as conjugated to a molecular probe. Three examples of biofilm fluorescent labelling techniques are discussed in the following sections.

1.14.1. Live/Dead test

The test was primarily described for detection and quantification of live and dead cells of non-cultivable bacteria using the flow cytometry (Sachidanandham et al., 2005). Recently, the test has wide applications for oral and endodontic biofilm research for assessment of antibacterial protocols (Wang et al., 2012, Arias et al., 2016). This testing procedure uses two nucleic acid stains including SYTO9 and Propidium iodide. The SYTO9 is green fluorescing stain that can label all bacterial species in a biofilm as it can penetrate all bacterial cell membranes. In contrast, the Propidium iodide is a red fluorescing stain that

can only label the nucleic acid of damaged cell membranes (Shen et al., 2010b). The nucleic acid fluorescent dyes can also label the EPS substrate of the biofilm (Wu et al. 2014) due to the presence of DNA molecules in such substrate (Hall-Stoodley et al. 2008). Such ability is an added advantage over the other fluorescent stains that are conjugated to molecular probes, which are targeting bacterial cells only. However, the accuracy of live/dead test was criticized as it was demonstrated that an equal mixture of live and dead cells did not reflect an equal amount of emitted green and red lights (Netuschil et al., 2014). Additionally, this method showed unexplained increase in the bacterial viability of dental biofilm despite the application of a mouth-rinse antibacterial treatment (Hannig et al., 2013).

1.14.2. Fluorescence in situ hybridization test

Fluorescent *in situ* hybridization (FISH) is a cytochemical method to localize specific sequence of DNA or RNA molecules such as 16S and 23S rRNA (Giovannoni et al., 1988, Daims and Wagner, 2007). In this test, an oligonucleotide probe, which is a single-strand nucleic acid sequence of DNA or RNA, targeted their complementary part in the DNA or RNA of the examined tissue (Wallner et al., 1993, Moter and Göbel, 2000a). This technique used for bacterial identification in two ways. First, through hybridization of DNA that is extracted after the degeneration of the bacterial cell wall (Molander et al., 2002). The other way is by increasing the permeability of the bacterial surface with the lysosomal enzyme to allow the oligonucleotide to anneal their complementary nucleic part of ribosomal RNA (Al-Ahmad et al., 2009b, de Paz, 2012). However, the first way contributes to only low proportion of bacterial cells comparing to the actual bacterial concentration in an infected root canal

(Sedgley et al., 2006). In the last way, the fluorescent signal will be very low in the stationary stage of the bacterial growth due to the low ribosomal activity (Moter and Göbel, 2000a).

1.14.3. *In situ* immunofluorescence assay

This test uses an immunoglobulin (IgG) probe (*i.e*. antibody). Such probe is secreted by B-lymphocytes of different animals such Rabbit or Donkey (Aranda et al., 2015). These IgGs targeted specific proteins (epitopes) on the bacterial cells and allow for identification of the entire bacterial surface and hence the bacterial morphology (Wallner et al., 1993). These antibody probes are produced either as monoclonal where it can detect single genotype, or they produced as polyclonal where they can detect multiple genotypes. This type of probes does not require bacterial disintegration or lysis, which might disrupt the biofilm structure. The technique was described as highly specific in detection of bacterial species in different disease biofilm models (Jahns et al., 2014, Miklossy, 2016) including oral and root canal biofilms that were generated by *streptococcus mutans* (Ansari et al., 2017) and *enterococcus faecalis (*Martinho et *al.,* 2018*)* respectively.

1.15. 3D printing technology

3D printing technology was released to the market in 1988 by Charles W. Hull, who sold the first 3D printer that worked with stereolithography (SLA) technology (Martelli et al., 2016b). The 3D printers can generate a physical object from a model developed by computer aided design (CAD) software such as Solidworks and AutoCAD (Gross et al., 2014). Also, printers can generate prototypes from medical images developed by three dimensional scanning devices, such as CT and CBCT, for treatment (Cohen et al., 2009) or teaching purposes

(McMenamin et al., 2014). The images will be converted to a special format called STL (Standard Triangle Language), which provides an accurate communication with the printer software (Bibb et al., 2014, Gross et al., 2014). The STL formatting is basically based on covering the object surface with a mesh of triangular sections (Deering, 1995). By increasing the number of these sections, the resolution of the printed surface will be increased. However, the printing for a required resolution can be affected by the type of the printer and the used material.

There are four basic techniques used by 3D printers for developing objects: Stereolithography (SLA), inkjet-based systems, selective laser sintering (SLS), and fused deposition modelling (FDM). All of these techniques are based on building the sample layer by layer on a supporting stage. These techniques were effectively involved in the rapid prototyping (RP) concept where large number of objects can be produced with a significant reduction in the production time (Nguyen and Vai, 2010)

The SLA technology produces samples or prototypes from photo-curable resin materials using an UV laser beam. The prototype build-up is accomplished in a layering process where a 50 µm layer added each time. The layers of a resin liquid are cured gradually with the UV laser light followed by final curing to the whole specimen in a UV chamber. The light will cure the resin liquid on the surface of the moving stage in a resin reservoir. The moving stage will sink each time for a desired level to allow for another layer of liquid to accumulate on the surface for the next curing episode. This technology has wide application in the medical field (Ventola, 2014), for example, It benefits from 3D clinical imaging tools to prepare a fitted surgical splint for fractured mandible before the operation (Cohen et al., 2009). Recently, this technology was successfully applied to generate simulated root canal

samples with simple canal morphology (Mohmmed et al., 2017a). The Inkjet-based technique uses the same principles of SLA technology with difference in the supporting stage. The stage herein is a gel-like material, which can be washed easily after creation of the prototype that can be use immediately with no need for final curing. This method is cost effective when compared to the previous method and produced sample with higher resolution as the photopolymer resin dispensed in a thinner layer of 15 to 50 µm (Cima et al., 1995, Cohen et al., 2009). In SLS technique, the build-up layers are powder of different materials rather than the liquid resin. The powder beads are melted with a CO_2 laser beam to bond to each other forming a single layer (Ibrahim et al., 2009). The object produced by this technology is characterized by its opaque appearance and surface abrasiveness (Silva et al., 2008). The technology is widely applied to create prostheses for repairing craniofacial defects (Nyberg et al., 2017). A thermoplastic polymer is the material of choice for the FDM technique. The material is ejected on the stage in a semi-liquid stage through a thermal controlled nozzle. The movement of the nozzle is controlled according to the object model design. The ejected thermoplastic material will solidify in 0.1 sec to the join a previously developed layer (Salentijn et al., 2017). This technique has wide application in industrial field to fabricate small devices or printing of drug delivery tablets (Long et al., 2017).

In summary, root canal preparation is based on chemomechanical debridement and canal disinfection, which are still challenging the success rate due to the RCS anatomical complexities and the inherent limitation in the cleaning instruments. Although the basic instrumentation techniques have not been changed, the shaping and cleaning of the RCS have recently relied on the improvement of file design.

Due to their high flexibility and good physical properties compared to stainless steel files, nickel titanium instruments have achieved popularity as root canal files. These changes push the root canal instrumentation toward rotary file style due to their more predictable root canal shaping, less fatigue to the practitioner, and minimum postoperative sensitivity. Newer file systems, such as PTN and RS, have been introduced including differing cross-sectional design and taper with claims that they have improved canal debridement, although rigorous independent testing is always required to verify the results.

In addition to the inorganic debris, which appears as a by-product to the instrumentation, bacteria were found to colonize the RCS wall in form of a biofilm. The biofilm exists in both primary and secondary root canal infections. For better understanding the cleaning and disinfection procedures, visualization of debris and biofilm structure and distribution in the RCS is required at different scales such as CLSM and microCT imaging.

The use of microCT has offered a non-contact 3D evaluation to the remaining debris in the entire RCS with high isotropic resolution. However, such opportunity has not been implemented to the biofilm due to its lower structure density. Therefore, biofilm assessment has largely limited to the microscopic documentation of few sample sections. To agree with the notion that debris could prevent proper canal disinfection, a 3D method is required to evaluate the biofilm in the entire RCS.

The previous root canal models have not been realistic to the clinical situation. The 3D printing technology has the potential to significantly improve modelling of the natural root canal for *in vitro* investigations.

The specific aims of this thesis were:

1. To evaluate the remaining debris in root canals with a complete isthmus following instrumentation by rotary files with asymmetric cross-section design using microCT.
2. To evaluate the potential of using transparent rapid prototyping resin materials generated by high resolution printing technologies to produce accurate simulated root canal models.
3. To evaluate single-species biofilm removal, in the simulating root canals, following the instrumentation with asymmetric files and irrigation with different protocols using the *in situ* immunofluorescence technique.
4. To establish a new non-invasive 3D technique for quantifying debris and biofilm in the root canal models using OCT analysis.

CHAPTER TWO:

USING MICROCT FOR THE EVALUATION OF REMAINING DEBRIS

FOLLOWING ROOT CANAL INSTRUMENTATION

2.1. Introduction

This chapter investigates the remaining debris in the root canal of the mesial root of a lower molar following preparation with centred and off-centred cross-section rotary files using microCT.

Paqué et al., (2009) and Robinson et al., (2012) have developed a useful analytical method using microCT to quantify the amount of inorganic debris that remains in the root canal system following root canal preparation. This technique has advantages over traditional methods, such as SEM and optical microscopy, because it allows analysis of the whole volume of the root canal (*i.e.* not limited to few representative samples) without physical contact.

During mechanical preparation, debris accumulates in the root canal system (RCS) as a waste product of the breakdown of dentinal wall (Coffae and Brilliant, 1975, Littman, 1977). Packing of such debris in root canal recesses and isthmi has been recognized by several studies. Paqué et al., (2009) found that 29.2 % of the original canal volume was filled with the hard tissue debris following instrumentation with the ProTaper Universal (PTU) system (Dentsply Maillefer, Ballaigues, Switzerland). Robinson et al., (2012) revealed that 10.6 % to 19.5 % of the total debris was left in the RCS by the PTU system and WaveOne system respectively (Dentsply, Maillefer, Switzerland) following preparation. Versiani et al., (2016) found that 11.48 % was left in the mesial root of the lower molars following canal preparation with the BioRaCe rotary system (FKG Dentaire, La Chuax-de-fonds).

In addition to remaining debris, there were certain parameters that have been investigated in the previous three studies. These parameters included the RCS volume, the total amount of created debris during preparation, and the percentage of the instrumented root canal

surface. Changes in these parameters following root canal instrumentation were not statistically correlated to the changes in the amount of remaining debris. The establishment of positive or negative correlations is suggestive of an improved mechanism of debris removal. Furthermore, the quantification of the remaining debris has only considered the total amount in the RCS without detailed description of the amount of debris in each third of the canal. The assessment of debris at root canal levels was limited to an observational rather than, the more precise, quantification analysis. Quantification of debris in each canal third can explain the impact of differences in file designs along the file cutting edge. For instance, PTU and Revo-S (RS) systems have file sequences that were designed with progressive and fixed taper respectively, whereas, the ProTaper Next (PTN) system has been produced with progressive and regressive taper percentages along its cutting shaft. These variations might affect the manner by which each file cuts or distributes the debris within each third of the RCS.

The rotary file instruments with asymmetric cross-section design, such as PTN and RS systems have been claimed to improve debris removal in a coronal direction as discussed in the introduction chapter. However, to date, there is no independent research that has directly studied the effect of debris removal using asymmetric files using three-dimensional analysis.

The RS and PTN systems have been found to produce significantly less extruded debris than the PTU from the apical foramen during root canal preparation (Koçak et al., 2013, Ozsu et al., 2014). It is conceivable to assume that RS and PTN have either created less debris than the PTU file system or they have better debrided the RCS coronally. It has been found that RS cut significantly less amount of dentine (2.06 ± 0.73 mm^3) compared to PTU (4.67 ± 1.96

mm^3) using microCT scanning (Hashem et al., 2012). In a different study, the PTN produced less canal transportation at all levels of simulated root canals, which was attributed to the reduced cutting at the canal wall compared to the PTU (Al-Gharrawi and Fadhil, 2016). These findings have added credits to the asymmetric files to evaluate their direct impact on the amount of remaining debris.

In conclusion, systematic evaluation of the remaining debris in each canal third has not been determined during root canal instrumentation. In addition, the impact of the asymmetric cross-section design of the file instrument on the remaining debris was not investigated.

Aim:

To evaluate the percentage of remaining debris in the root canal with a complete isthmus, following instrumentation with symmetric (centred) and asymmetric (off-centred) cross-section rotary file systems including PTU, PTN, and RS, in three-dimensions using microCT.

Hypothesis:

There is no difference in the percentages of remaining debris when the root canal system prepared with PTU, PTN, or RS file systems.

Objectives:

1. To estimate the percentages of the remaining debris following root canal preparation with PTU, PTN, and RS file systems.
2. To assess the correlation between the percentages of the remaining debris with the percentages of; the root canal volume, the created debris, and instrumented (cleaned) surfaces.

2.2. Materials and methods

2.2.1. Teeth Selection

Ethical approval (REC Ref: 14/EM/1128) was obtained to conduct this project on human extracted molars (Appendix). Human mandibular 1st and 2nd molars (n = 297) were selected from the Birmingham Dental School Tooth Bank, where they were stored at -20°C. The following exclusion criteria were used.

(1) Extensive caries or filling materials,

(2) Visible cracks or any other external developmental and iatrogenic defects,

(3) Roots that are underdeveloped or with severe curvature (> 20^0) (Schneider, 1971).

After selection, the teeth were cleaned thoroughly under tap water to remove any attached soft or hard tissues using a spoon excavator, and stored at 4°C in plastic boxes with assigned experimental number codes. A summary of the procedures used to select and distribute teeth for three groups according to the three rotary file systems used is outlined in Figure 6.

2.2.2. Preliminary scanning.

This scanning process was aimed to select molars with mesial roots that had a complete isthmus between the MB and ML canals. A low resolution scan was carried out by a microCT scanner (Skyscan 1172; e2v technologies plc, Chelmsford, UK). A batch scanning technique was used with two teeth placed vertically in a translucent plastic tube and stabilized by a red wax (Figure 6).

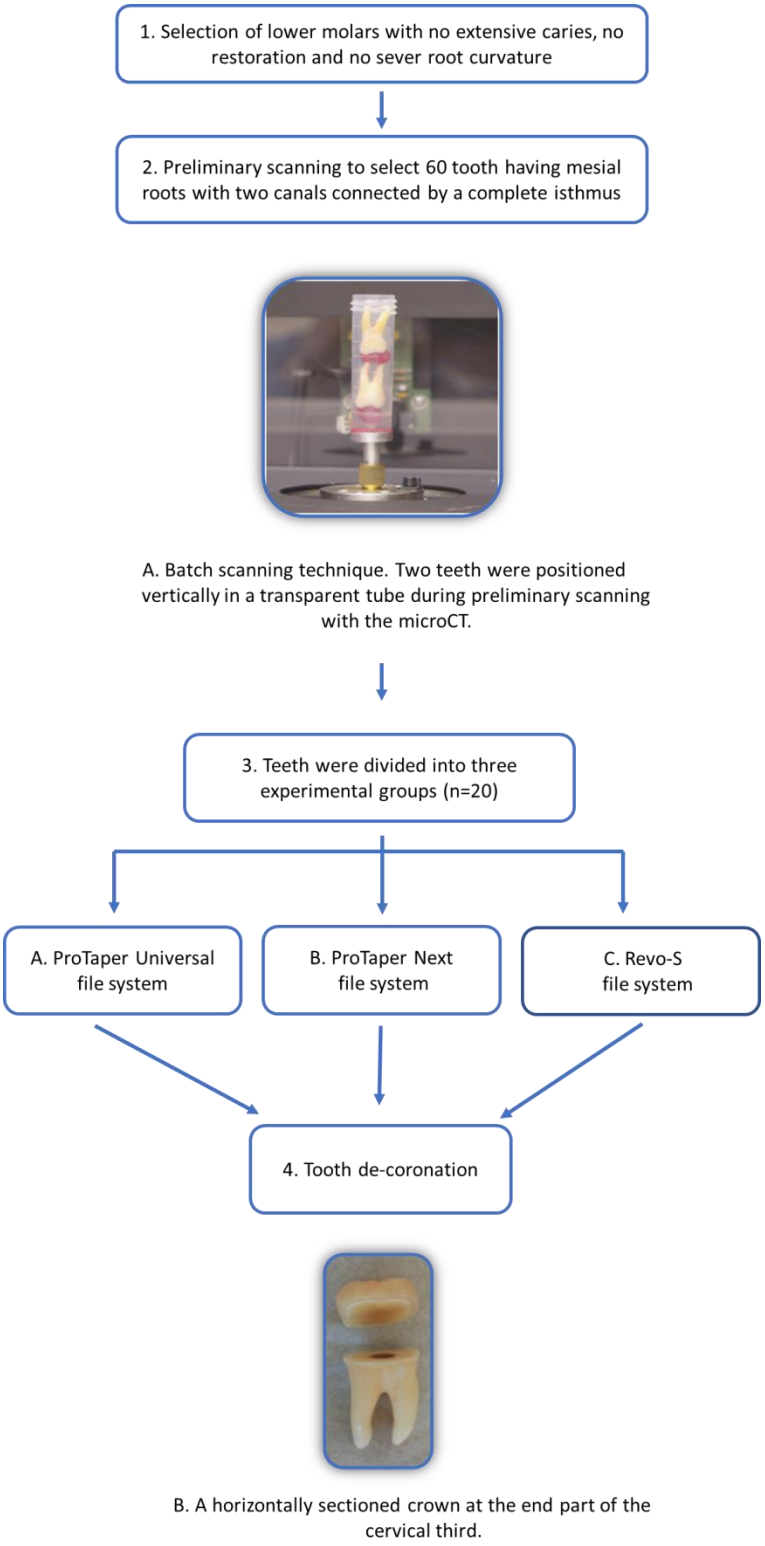

Figure 6: A diagram illustrates the process of teeth selection and distribution for group analyses.

The scanning procedure was created when the microCT was set on the parameters outlined in Table 2. After 4 mins scanning, the acquired longitudinal image slices, 38 per tooth, were reconstructed to 584 cross sectional slices using NRecon software, which was downloaded from the Bruker company website (http://www.skyscan.be/products /downloads.htm). The resulted 3D images were visualized by Data viewer software obtained from the same website.

Table 2: Settings applied for preliminary and experimental microCT scanning processes.

	Preliminary scanning	**Pre and post-preparation scanning**
Camera type	Large camera pixels	Medium camera pixels
Resolution	Low resolution of 27.7 µm	High resolution of 13.6 µm
Rotation degree	5	0.4
Frame (average)	9	9
Random movement	20	20
Stages rotation	180^0	180^0
Beam hardening filter	Aluminium-copper filter	Aluminium-cupper filter
Voltage	89 kV	89 kV
Current	110 µA	110 µA

The degree of the mesial root curvature was determined by estimating the angle formed by intersecting root canal long axes and canal curvature lines as described by (Schneider, 1971). This was accomplished using the angle measurement operation in ImageJ software (National institutes of Health, Maryland, USA), which is available from (http://fiji.sc /Downloads). Sixty teeth that met the strict inclusion criteria were chosen for the

experimental investigation. For unbiased assessment, the teeth were decoded and randomly divided into three equal groups (n = 20). The groups were then randomly assorted for each file systems. One group was assigned for the PTU file system as a control group. The other groups were assigned to either the PTN or RS file systems respectively (Figure 6). The selected teeth were decoronated with a water-cooled diamond disk fitted on a low speed saw at the CEJ (Figure 6). The sectioning process allowed a flat surface for reproducible positioning of the tooth on the microCT stage. The buccal surface of the tooth was then marked with a permanent ink to reproduce tooth direction during scanning cycles.

2.2.3. Pre-preparation scanning

This scanning process was aimed to estimate, at high scanning resolution, the RCS volume and hard tissue particles in the RCS before the root canal preparation (Table 2). In order to reduce ring artifacts (noise) produced during high resolution scanning, a flat-field correction was applied on a real-time image without tooth in the direction of the x-ray beam. Teeth were then scanned at high resolution (13.6 µm) to maximize contrast for accurate distinguishing between canal space and dentine. For each tooth, approximately 480 longitudinal images were obtained with image pixel definition of 2000 x 1200 pixels. The images were then reconstructed to approximately 1,169 cross sectional slices with pixel definition of 2000 x 2000 using NRecon software (Figure 7). The software was set at ring correction of 20 and beam hardening correction of 25 % to remove artefacts during the reconstruction process.

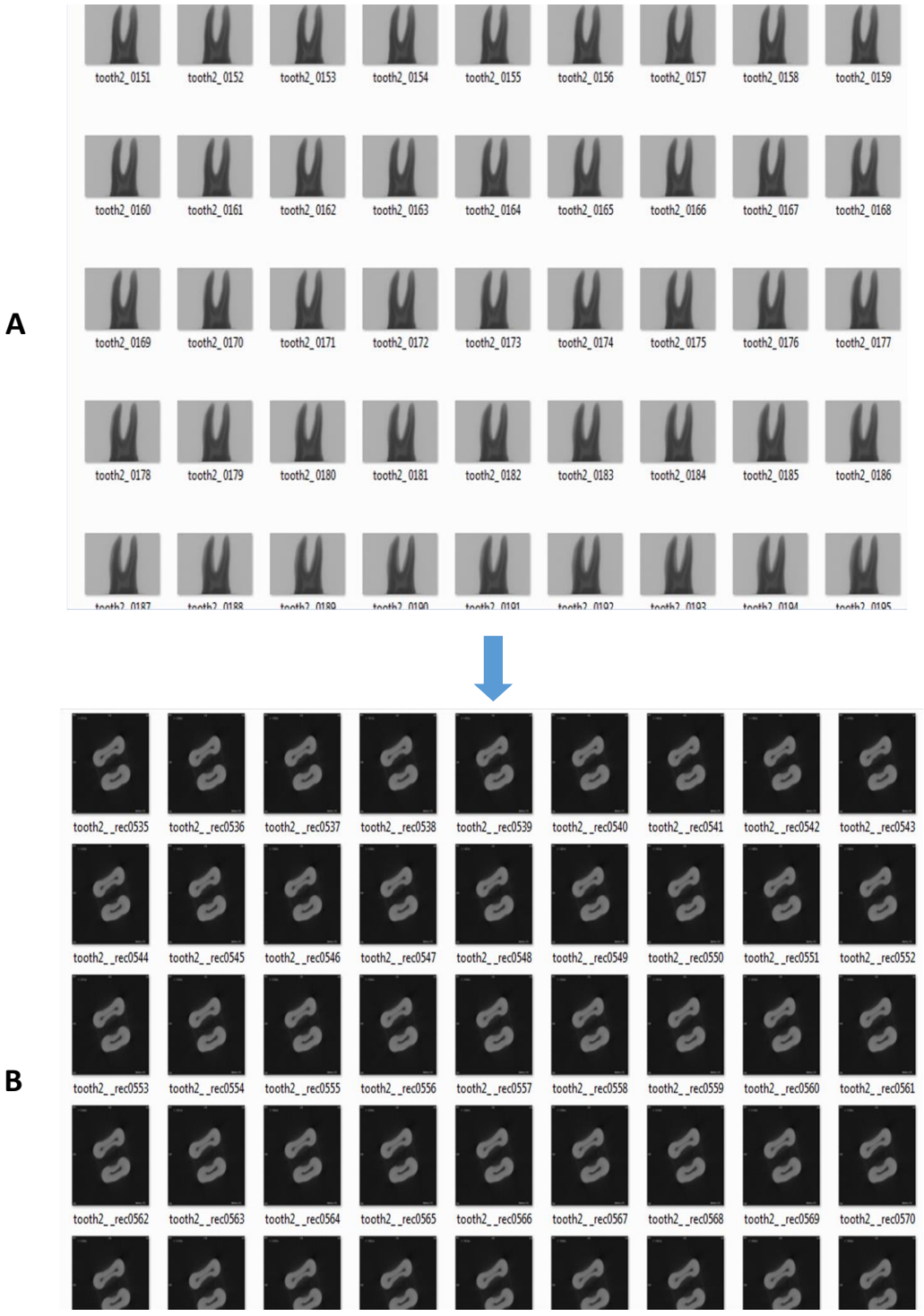

Figure 7: The acquired and reconstructed microCT image slices. (A) The primary vertical slices of the acquired microCT images in Tagged Image File (TIF) format. (B) The images following the reconstruction as horizontal slices in Bitmap (BMP) format.

2.2.4. Root canal preparation.

Both mesial root canals in each group were prepared with consistent instrumentation and irrigation techniques.

Each tooth was held firmly with operator fingers on a laboratory bench and kept approximately parallel to its long axis for the whole of the operative technique. The pulp chamber was accessed with a high-speed handpiece using a 501-tapered diamond bur (Micro Diamond Technologies, Afula, Israel) with water coolant. Remnants of the pulp tissue were then removed with a spoon excavator. The two mesial canals were negotiated with a size 08 K-file (Dentsply Maillefer, Balliegues, Swizterland) to ensure canal patency. Consequently, the working length was determined by visualisation of the apical foramen using an operating microscope (Global G3, DP Medical, UK) at 5.12x magnification (Figure 8). A size 10 K-file was placed in the canal and advanced until it was just visible at the foramen. The flat occlusal plane was used as the coronal reference point in order to accurately measure the length of the file to the apical foramen. From this length, 0.5 mm was subtracted to determine the working length so any subsequent preparation remained within the canal. A glide path to the working length was established up to the size 15 K-file. Four file sequences with variable tip sizes and taper (Table 3) were selected to enlarge and shape canals in each group using the crown-down technique. Files were driven in a continuous rotary movement at an endodontic handpiece connected to a micromotor (Waveone, Dentsply Maillefer, Ballaigues, Suisse) powered at 300 rpm and torque of 4 Ncm^2 (Figure 8). Files were manipulated in a vertical brushing motion against the root canal wall.

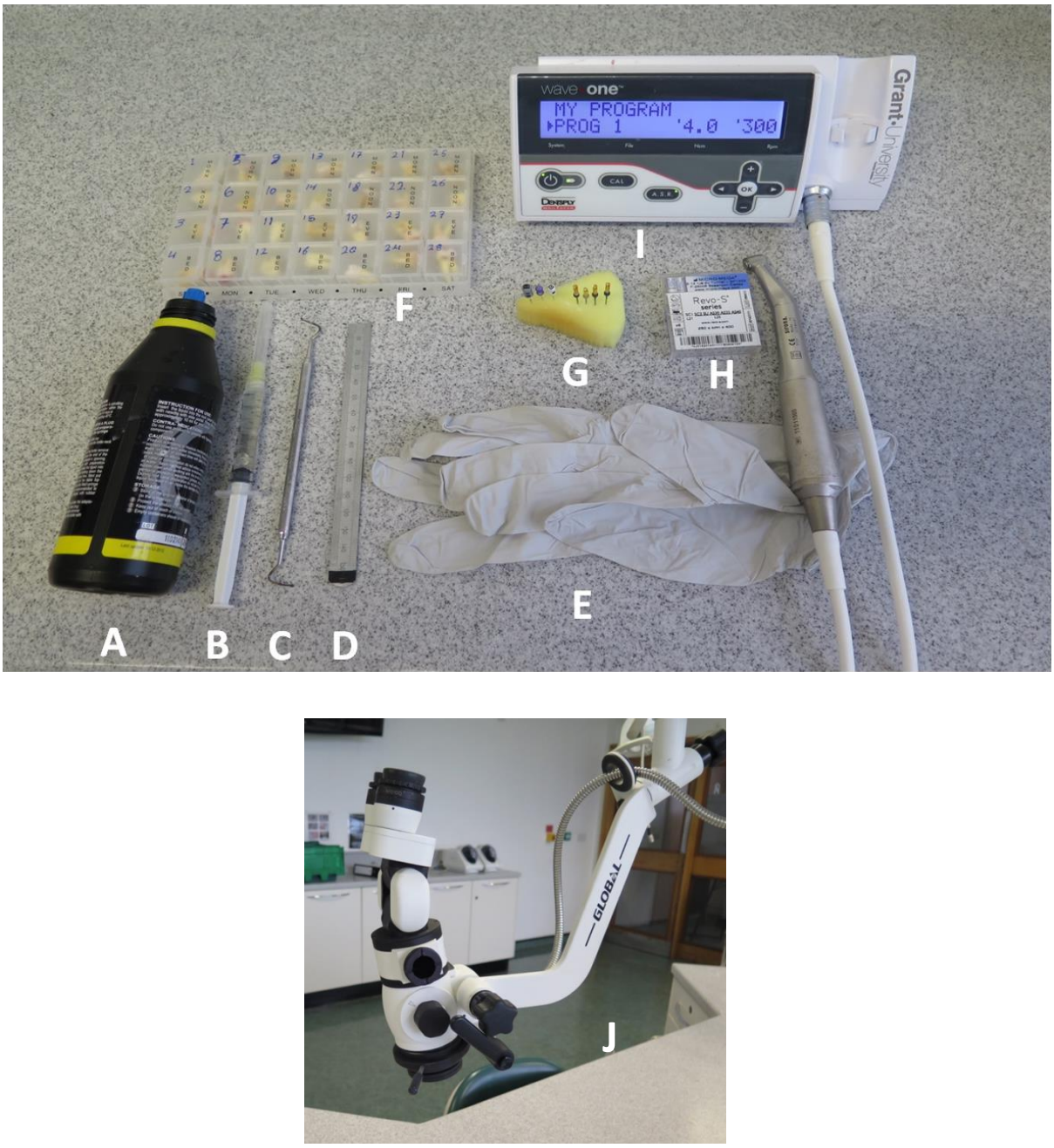

Figure 8: Photographs show the samples, materials and equipment used for the root canal preparation. (A) NaOCl irrigant solution, (B) side vented irrigating syringe, (C) spoon excavator. (D) Metal ruler, (E) plastic gloves, (F) teeth sample assorted in plastic boxes, (G) an endodontic sponge holding K-files and Revo-S files, (H) The Revo-S file kit, (I) endodontic micromotor and handpiece, and (J) a Global microscope used in working length determination at magnification of 5.12x.

Table 3: The file sequence name, tip size, and taper percent of PTU, PTN, and RS file systems.

File sequence name			file's tip size			file's taper percent		
PTU	**PTN**	**RS**	**PTU**	**PTN**	**RS**	**PTU**	**PTN**	**RS**
SX	SX	SC1	0.19 mm	19 mm	0.25 mm	3.5-9 %	3.5-9 %	6 %
S1	X1	SC2	0.17 mm	0.17 mm	0.25 mm	2-11 %	4-7.5 %, 7.5-6 %	4 %
S2	X2	SU	0.20 mm	0.25 mm	0.25 mm	4-11.5 %	6-7 %, 7-4 %	6 %
F1	X3	AS30	0.20 mm	0.30 mm	0.30 mm	5.5-7 %	6.5-4.5 %	6 %

File name meaning: SX, S1, S2, X1, X2, and X3 = Shaper files. SC1, and SC2 = shaper and cleaner files. SU = Shaper universal file,

F = Finishing file. AS = Apical shaper file.

The control group was instrumented with PTU system where the SX file was primarily used to pre-flare the coronal third. The canal was then shaped with S1 and S2 files, which were respectively advanced in an apical direction to the working length (canal terminus) whilst using a brushing motion against the root canal wall. The instrumentation process was then completed with the F1 file, which was gently advanced to the canal terminus (Table 4).

For the PTN group, coronal pre-flaring was achieved with the SX file. The canal was then enlarged with the X1 file which was advanced apically along the glide path to the canal terminus. The same process was repeated for the X2 file. The canal was finally shaped with the X3 file to the estimated working length (Table 4).

In the RS group, the canal 2/3 was primarily shaped with the SC1 file. Enlargment was then accomplished to the working length with the SC2 file. Thereafter, the SU files was used to smooth the canal. The apical portion was then finished by the AS30 file (Table 4).

For all groups, canal patency was maintined throughout instrumentation process using K-file size 10 following each file instrumentation. File flutes were regularly cleaned from dentine debris with a sponge. Each file was replaced with a new one following instrumentation of five roots (10 canals).

Root canal irrigation.

Root canal irrigation was performed in five cycles; following the establishment of a smooth glide path, and following the instrumentation with each of the four rotary files.

Table 4: The cutting motion applied with each file sequence including the depth of insertion during the RCS preparation

file system		**Instrumentation technique**									
	FS	WL	CM	FS	WL	CM	FS	WL	CM	FS	WL	CM
PTU	**SX**	2/3	Brushing	**S1**	full	Brushing	**S2**	full	Brushing	**F1**	full	Brushing
PTN	**SX**	2/3	Brushing	**X1**	full	Brushing	**X2**	full	Brushing	**X3**	Full	Brushing
RS	**SC1**	2/3	Brushing	**SC2**	full	Brushing	**SU**	full	Brushing	**AS1**	full	Brushing

FS = file sequence, WL = working length, CM = cutting motion, PT = Progressive taper.

A total of 5 ml of 5.25 % aqueous NaOCl (Cerkamed, Stalowa Wola, Poland) was introduced to each canal using a 27-G side-venting endodontic syringe (Monoject, Covidien, Mansfield, USA). 1 mL was introduced following each cycle at approximately 0.1 mL/sec flow rate. The flow rate was controlled following a period of training for the operator. The needle vent was always directed to the canal isthmus and moved constantly in an up/down movement with a short amplitude (2-3 mm) to prevent needle wedging in the canal.

2.2.5. Post-preparation scanning

The teeth were scanned immediately after preparation to avoid alteration of debris inside the canal that may result due to storage at low temperatures. The scanning and reconstruction processes were repeated as the pre-preparation setting.

2.2.6. Image analysis

The image analytic procedures were aimed primarily to filter (denoise) the acquired images. This was followed by image segmentation to isolate the root canal volume, the created debris volume, the remaining debris volume, and the surface area of the root canal. The segmented parts were then quantified in pixels for comparative evaluation. The reconstructed pre- and post-preparation images were opened in ImageJ software. A virtual stack denoiser operation was applied using the window of 3 and the standard deviation of 15 to reduce noise created during the reconstruction process (Figure 9).

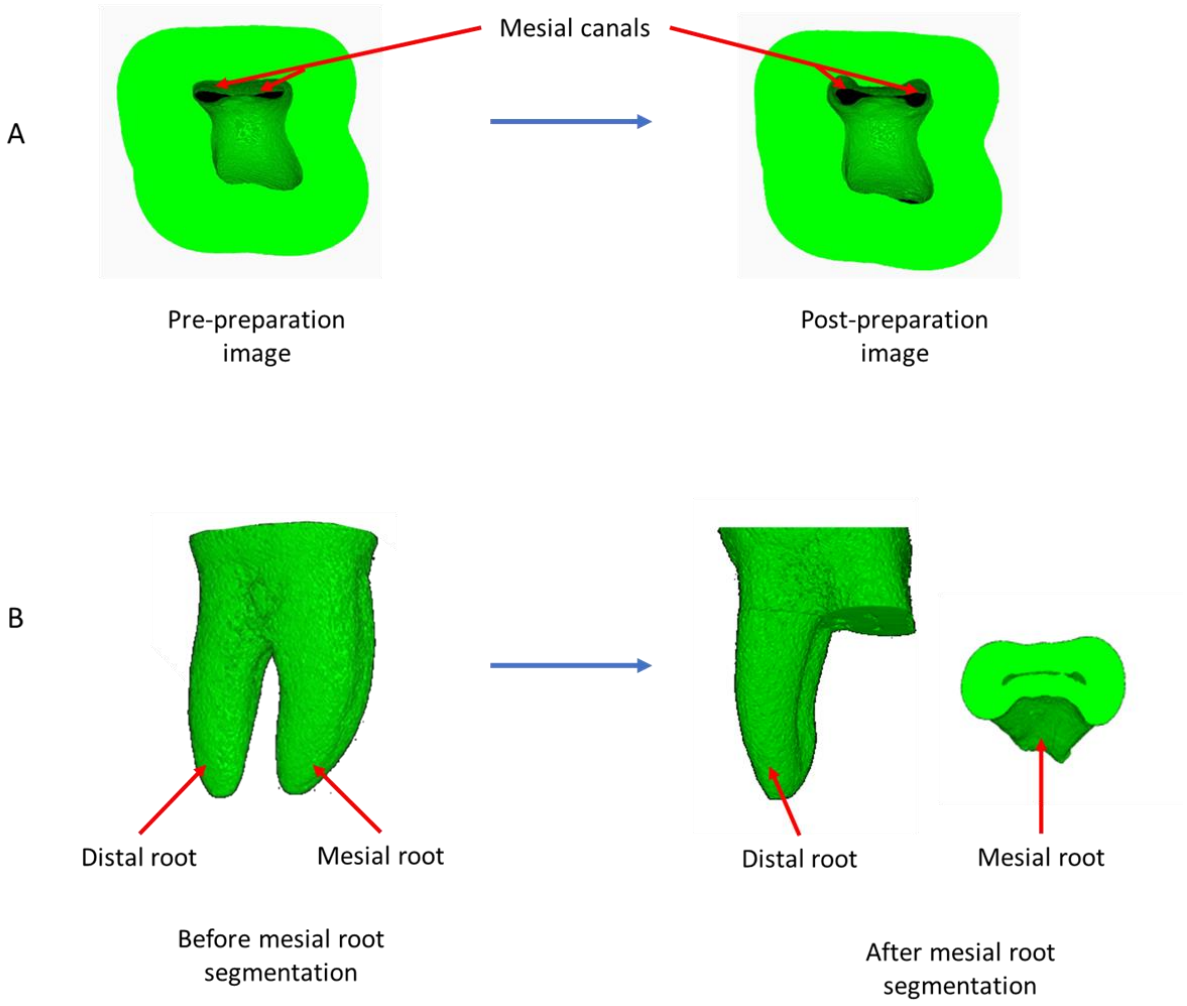

Figure 9: Image filtration and segmentation of the mesial root. (A) 3D images show Cross-sectional views of a lower molar tooth after the noise filtration process. The process has clearly distinguished the mesial root canals from the dentine (green) on pre- and post-preparation stages. (B) 3D images show longitudinal views of a lower molar tooth during the segmentation (isolation) of the mesial root.

New computer files were created to save the denoised images, which were reopened in the ImageJ software where the entire canal length for each tooth is isolated by the slice remover operation (Figure 9). The first slice is set immediately below the pulp chamber and the last slide was chosen at the end of the apical foramen in order to analyse the complete canal length. The resulting images were saved as *nrrd* (nearly raw raster data) format, which supports the scientific image processing.

A rigid co-registration (superimposition) of pre- and post-preparation images was then manipulated by 3D Slicer 4.4.0 (64-bit) software (https://www.slicer.org/) in order to identify changes following canal preparation (Figure 10). In this process, the pre-preparation image was used as template, while the post-preparation image moves through a translation and rotation to perform a full alignment. The two aligned images were saved as HDR (high dynamic range) image format for accurate marginal differentiation between canal space and canal wall.

2.2.6.1. Calculation of the remaining debris volume percentage

The following processes were then applied through ImageJ for isolation and estimation of remaining debris (Figure 10):

1. A threshold range of 90-150 pixels was used to create a binary image that defined dentine as a white colour with a pixel value of 255 and a black background colour with a pixel value of 0.

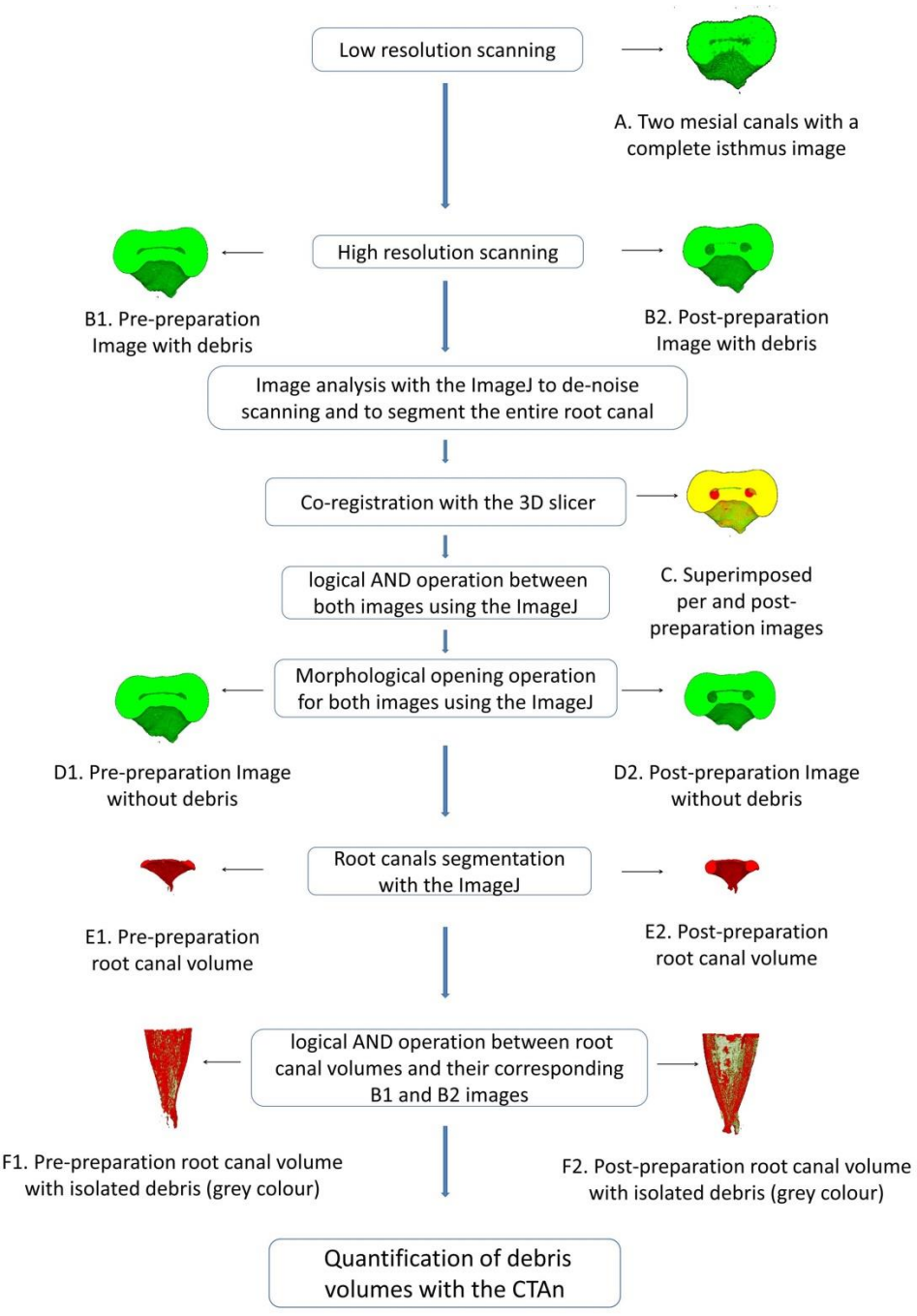

Figure 10: Quantification of remaining debris. A flow diagram shows methods used to identify, isolate, and quantify the remaining debris volume following root canal preparation.

2. To create a post-preparation image without debris in the non-instrumented spaces, a logical AND operation was applied between pre and post-preparation images (Paqué et al., 2009). The resulted image was used as the post-preparation image for the next steps, while the pre-preparation image was still unchanged.
3. A morphological opening operation was applied on both images to remove other debris (Robinson et al. 2013) as objects of octagon shape and 6-pixel radius. This will ensure removing the whole debris in the post-instrumented canal, together with the debris in the pre-instrumented canal. At this step, the canal spaces were enlarged in relation to the amount of debris removed by the two previous filtering processes.
4. Both canal spaces were then segmented to have a white colour of value 255 (solid volumes), while dentine marked as 0 value and a black colour (the inverse to the first segmentation process). Background pixels were removed using the ''subtract background operation'' in order to determine the white colour for the segmented canals only. The volume of each canal space (voxel / mm^3) was then calculated using CTAn software that is available in the previously mentioned Bruker company website. The difference between canal volumes was considered as the amount of debris created during the instrumentation procedure.
5. A second logical AND operation was used between the pre- and post-preparation segmented canals and corresponding images created in the step 1. The resulting images contained remaining debris only as it has the same pixel value (255) in both combined images. The total number of voxels in each image was estimated using CTAn software.

The total volume percentage of remaining debris was calculated using the following equation:

$$t = \frac{\mathrm{d3}}{\mathrm{d2} + \mathrm{d1}} \times 100$$

Where; t = the total percent of debris remained in the post-preparation canal, d1 = the volume of debris created during instrumentation procedure, d2 = the volume of debris in the pre-preparation canal, d3 = the volume of debris in the post-preparation canal.

2.2.6.2. Calculation of the created debris volume percentage:

The created debris refers to the amount of dentine that was shaved off the walls during the root canal shaping procedure. The shaping procedure is expected to increase canal volume by removing more dentine from the root canal wall. Hence, the difference between the pre and post-preparation volumes is equal to the amount of shaved dentine. The percentage of the created debris volume was calculated in relation to the post-preparation canal volume at each canal third (Figure 11).

2.2.6.3. Calculation of the instrumented (cleaned) surface area percentage

The purpose of this calculation was to define the percentage of the instrumented root canal surfaces in relation to the un-instrumented (un-touched) root canal surfaces. A convolve filtration process was applied using ImageJ software on the segmented pre and post-

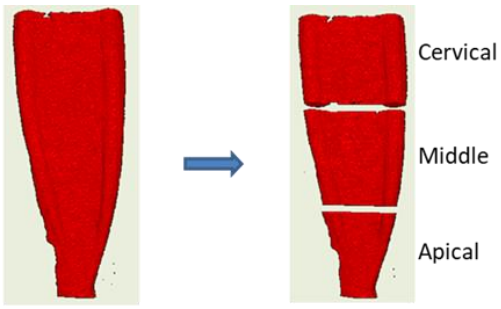

A. Splitting and calculation of the post-preparation root canal volume into cervical, middle, and apical thirds.

B. Calculation of the created debris (red voxels) by subtracting the pre-preparation canal volume (yellow voxels).

C. Calculation of the cleaned surface (red voxels) by subtracting the untouched surfaces (yellow voxels). The green voxels demonstrate the pre-preparation root canal surface.

Figure 11: Calculation of the canal third volumes, created debris, and cleaned surface. A pictorial flow diagram shows the methods used for isolation of canal third volume, created debris, and cleaned surfaces voxels for calculation.

preparation canal volumes (Figure 11). The operation returns the solid canal volume into a space lined with a canal surface. The difference between the two convolved canals represents the newly created root canal surfaces. Conversely, surfaces that were matching in both convolved images represent the un-touched surfaces.

2.2.6.4. Calculation of correlation percentages

The percentage of the remaining debris was mathematically correlated to the percentage root canal volumes, percentages of the created debris, and percentages of instrumented surfaces to expand knowledge about the dependency of the remaining debris on these parameters.

2.2.7. Statistical Analysis.

Statistical tests were applied for data analysis using the SPSS statistical software version 24. A descriptive analysis was applied primarily to explore data distribution using the Shapiro-Wilk normality test. As data showed abnormal distribution around the mean, non-parametric tests, including Kruskal-Wallis H and Mann-Whitney U, were performed between test groups to determine the significant differences. The level of significance was set at $p \leq 0.05$. The Mann-Whitney U test was applied between each two groups only when the Kruskal-Wallis H reveals a significant difference. The non-parametric Spearman's correlation test was applied to correlate the percentages of the remaining debris to the percentages of the root canal volumes, percentages of the created debris, and percentages of the cleaned surfaces. For visual

assessment, the Loess (local regression) curves were fitted to scatter plots for depicting the Spearman's correlations, which was set at a significance level of $p \leq 0.01$.

2.3. Results

2.3.1. The percentages of remaining debris

The initial analysis of the data by descriptive statistics (Figure 12) revealed that the RS file system produced the least mean percentage (4.9 % ± 3.1 %) of the remaining debris followed by the PTN file system (6.8 % ± 4.8 %). In contrast, the PTU showed the highest mean value (10 % ± 3.8 %). The Mann-Whitney U test revealed that the difference was significant ($p \leq 0.001$) between PTU and RS systems, also it was significant ($p \leq 0.05$) between PTU and PTN systems.

When canals are divided into thirds for analysis, the higher debris percentage was left in the cervical third followed by the middle and apical thirds respectively. This was true for all file systems as shown in Figure 12 except for the PTN system where debris percentages appear similar at all canal thirds. This similarity in the PTN system was seen attributed to the high debris values in the middle and apical thirds that minimize differences with the cervical third. For PTU and RS systems, the difference between the cervical and the apical thirds were significant (PTU - $p \leq 0.001$) and (RS - $p \leq 0.05$). Only the PTU showed a significant difference ($p \leq 0.05$) between middle and apical third.

In all groups, visual analysis of the post-preparation images showed that debris accumulates mainly in the canal isthmus and protrusion spaces (Figure 13). Complete and partial obliteration of the isthmus in the mesio-distal direction has been recognized at all canal levels. The main canals demonstrated less debris accumulation especially at the cervical and middle thirds.

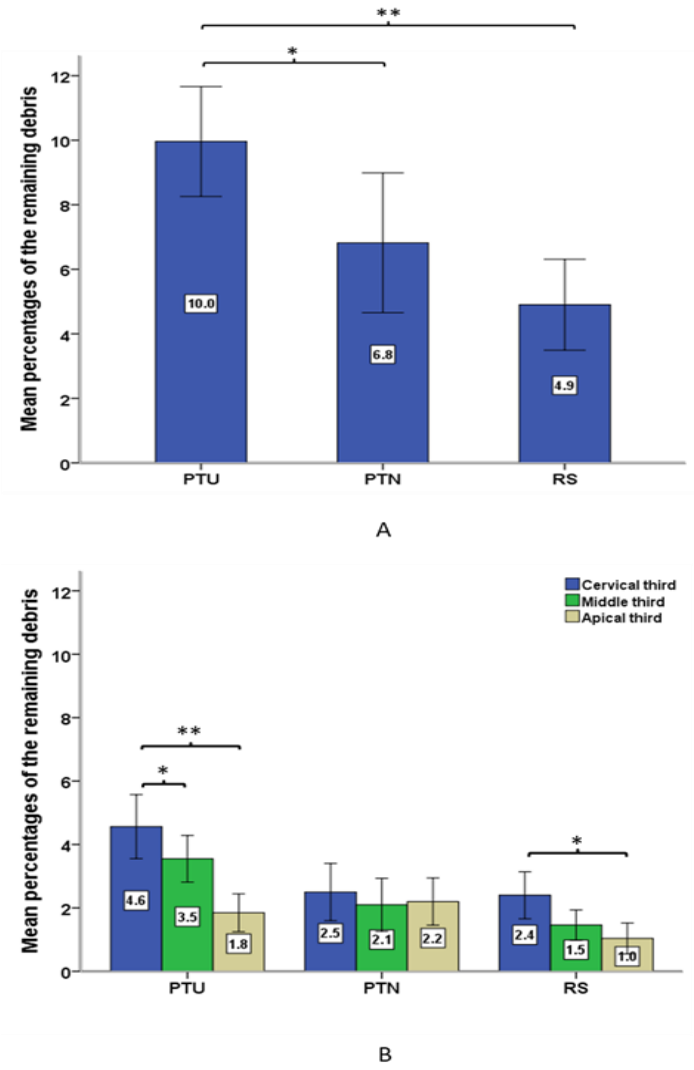

* = ($p \leq 0.05$).
** = ($p \leq 0.001$).

Figure 12: The percentages of the remaining debris using microCT. Bar charts with standard error bars show the mean percentages of the remaining debris volume in each group (A) and in each canal third (B) following the instrumentation with three file systems. Kruskal-Wallis H and Mann-Whitney U tests were applied to reveal the significance difference ($p \leq 0.05$).

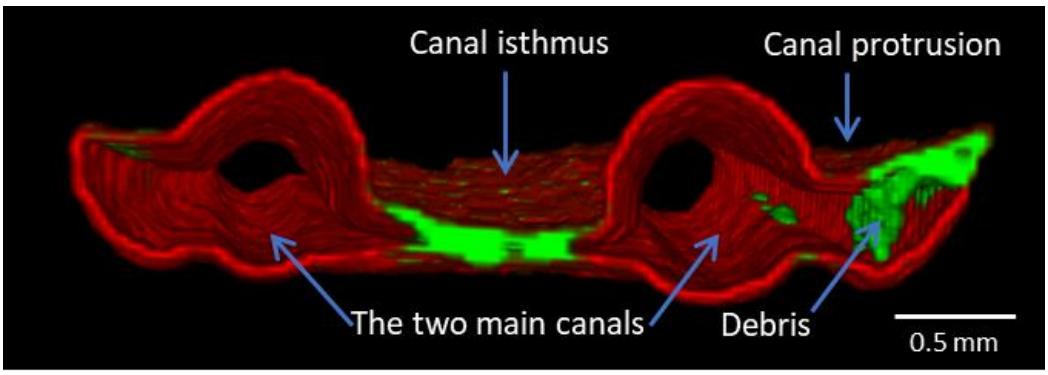

Figure 13: The distribution of hard tissue debris in the root canal system following preparation. A 3D section in the root canal system (red colour) of a mesial root image shows the accumulation of hard tissue debris (green colour) in the root canal isthmus and protrosion. The two main canals appear nearly empty of debris.

2.3.2. The percentage of created debris

According to the Figure 14 , the asymmetric file systems have cut more dentine than the symmetric file system during root canal instrumentation. The PTN creats the higher percentage of debris (53.9 % ± 19 %) followed by the RS (46.6 % ± 20.2 %) and the PTU (41.9 % ± 16.2 %). However, these differences were only significant between PTN and PTU systems.

The evaluation of the created debris at each canal third showed that all file systems created more debris in the cervical third compared to the middle and apical thirds respectively. The differences between these root canal thirds were significant within each group (Figure 14). The asymmetric file systems created more debris percentages in the middle and apical thirds and less debris percentages in the cervical third in comparison to the control symmetric system. In addition, the variations between the asymmetric systems at different canal levels also exist. The RS created more debris percentages at the cervical third and less debris percentages at the middle third (Figure 14). These differences were significant ($p \leq 0.05$) except between the middle thirds of root canal systems prepared by PTU and RS file systems. Observation of the 3D images revealed that the vast majority of debris was cut from the wall of the main root canal.

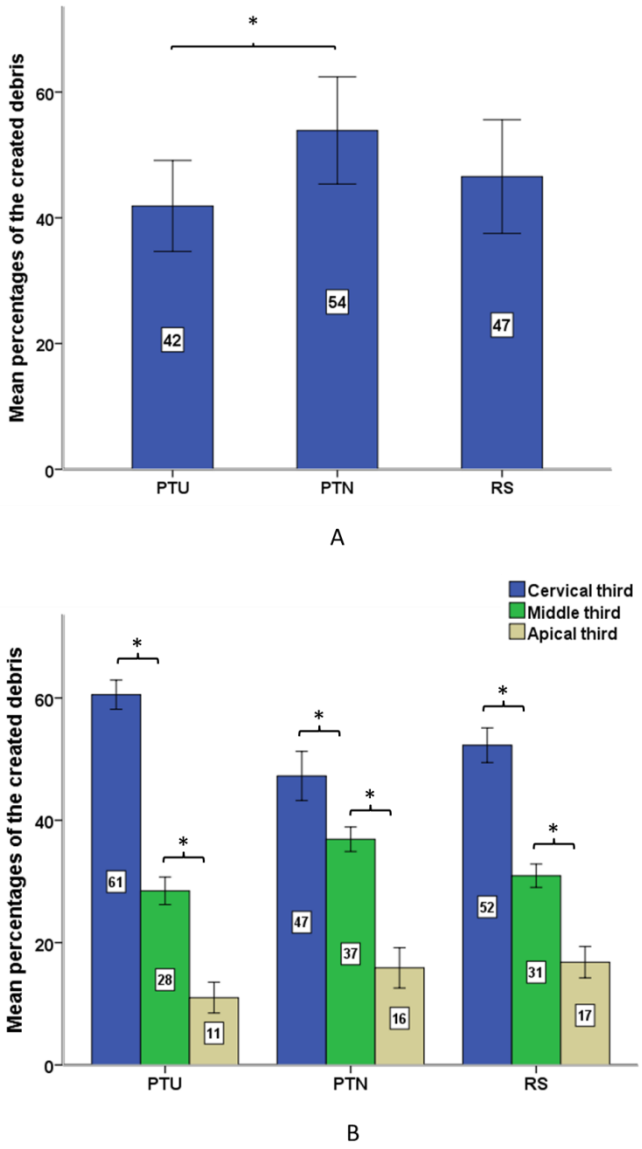

* = $p \leq 0.05$

Figure 14: The percentages of the created debris. Bar charts illustrating the mean and standard error bars of the created debris volume following the instrumentation with the three file systems. The created debris was reprented in the whole root canal (A), and within each canal third. Kruskal-Wallis H and Mann-Whitney U tests were applied to reveal the significance difference ($p \leq 0.05$).

2.3.3. The percentage of the instrumented surface

The mean percentages of the instrumented (cleaned) surfaces as demonstrated by Figure 15 revealed that none of the three file systems has completely cleaned the root canal surface. However, with a significant difference, the PTN showed the highest mean percetage (79.5 % ± 12.7 %) of cleaned surface when compared to the means of the RS (67.5 % ± 13.7 %) and the PTU (65.6 % ± 12.3 %) respectively. The difference between the PTU and the RS was statistically non-significant ($p > 0.05$).

Figure 15 also showed that the asymmetric files created the highest cleaning mean values in the apical third followed by the middle and cervical thirds respectively. Conversly, for the PTU, the highest mean value was shown in the cervical third while the lowest mean value was shown in the apical third. Significant differences were detected between cervical and the apical thirds of the PTU and PTN system.

The visual analysis of the images confirmed that canal surface that lined the isthmus and protrusion spaces remained untouched by file instruments. In contrast, most of the cleaned surfaces lie within the main canal path (Figure 16).

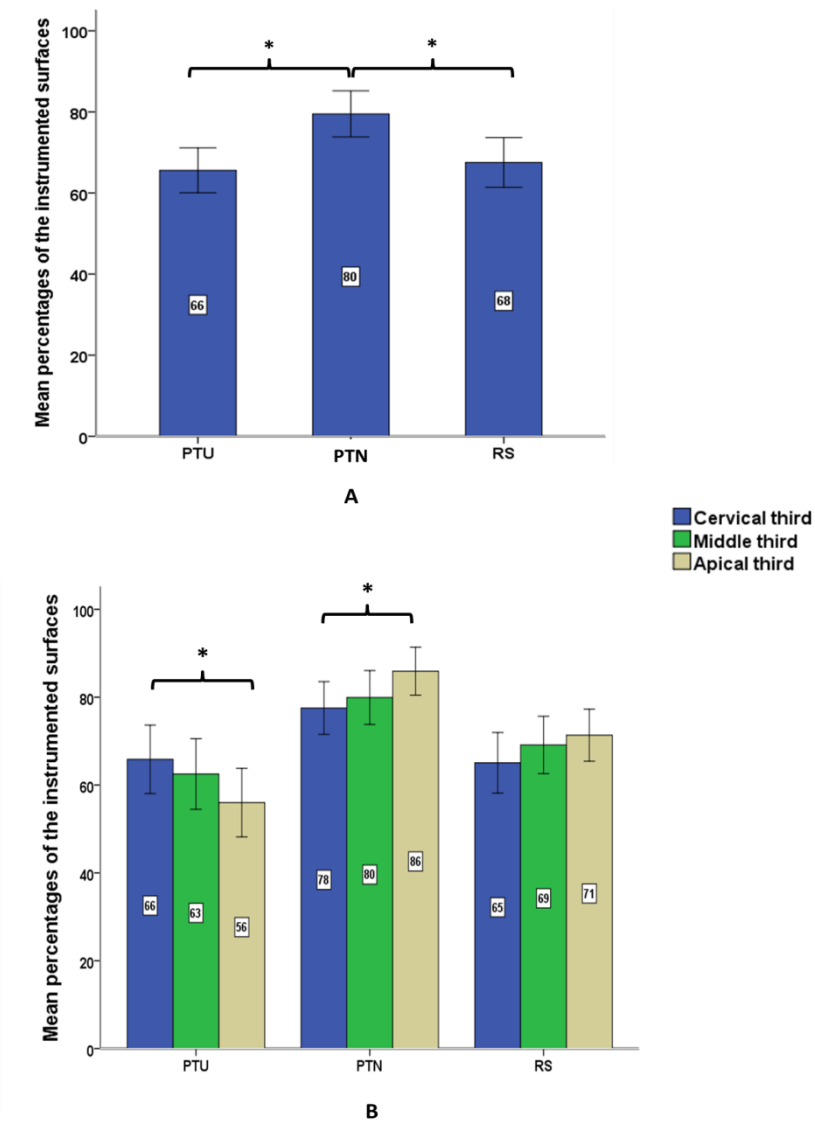

** = $p \leq 0.05$*

Figure 15: The percentages of the instrumented canal surfaces. Bar charts illustrating the means and standard error bars of the instrumented surfaces following the instrumentation with the three file systems. The instrumented surfaces were reprented in the whole root canal (A), and within each canal third (B). Kruskal-Wallis H and Mann-Whitney U tests were applied to reveal the significance difference ($p \leq 0.05$).

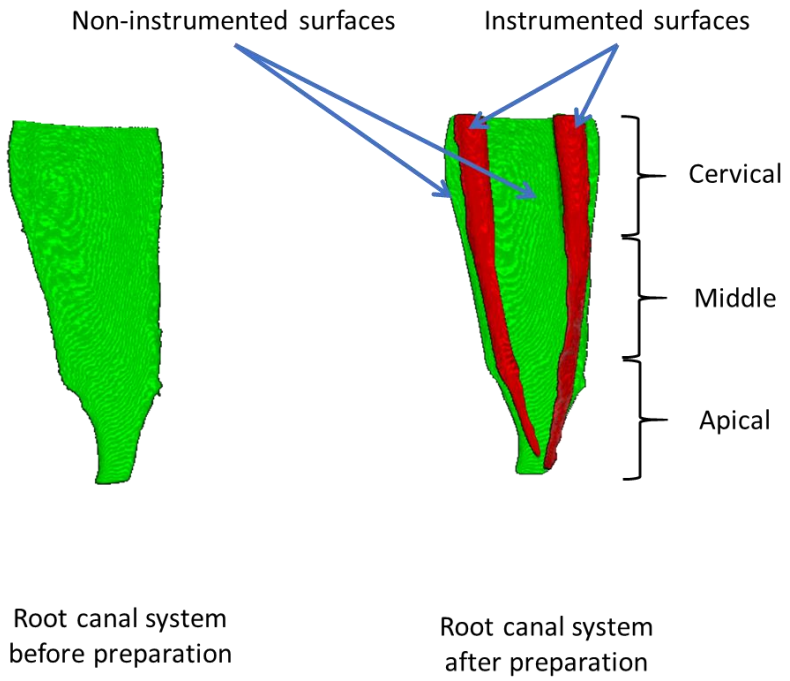

Figure 16: The locations of the instrumented and non-instrumented surface after root canal preparation. 3D images of the root canal system demonstrate the locations of the instrumented and non-instrumented (un-touched) surfaces after root canal preparation. The root canal isthmus and protrusion remained untouched by the file instrument. The touched surfaces can only be seen in the main two canals.

2.3.4. Correlation of percentages.

2.3.4.1. Remaining debris versus the canal volume.

The results revealed a positive corelation between the percentags of the remaining debris and the volume percentages of root canal thirds for all tested files (Figure 17).

Teeth that were prepared with the PTU system showed a strong correlation coefficient (r_s = 0.611) where percentage of remaining debris increases with the increasing of the percentage of root canal volume. In contrast, the PTN system produced very weak correlation coefficient (r_s = 0.035) while the correlation coefficient was moderate (r_s = 0.439) for teeth prepared with the RS system. The Loess curve demonstraes that there is a rapid increase in the percentages of remaining debris with increasing canal volume following preparation with the PTU system (Figure 17). However, the increment level was moderate with the RS system and very low with the PTN system. In summary, results showed that the remaining debris percentage increases in larger canal volumes except for the PTN system where the debris was approximately not dependent on the canal volume size.

2.3.4.2. Remaining debris versus created debris.

The results showed a positive correlation between the percentages of remaining debris and the percentages of the created debris (Figure 18). The correlation coefficient was strong (r_s = 0.582) when teeth are prepared by the PTU system, while it was moderate (r_s = 0.451) to very weak (r_s = 0.055) when teeth are prepared by the RS and PTN systems respectively.

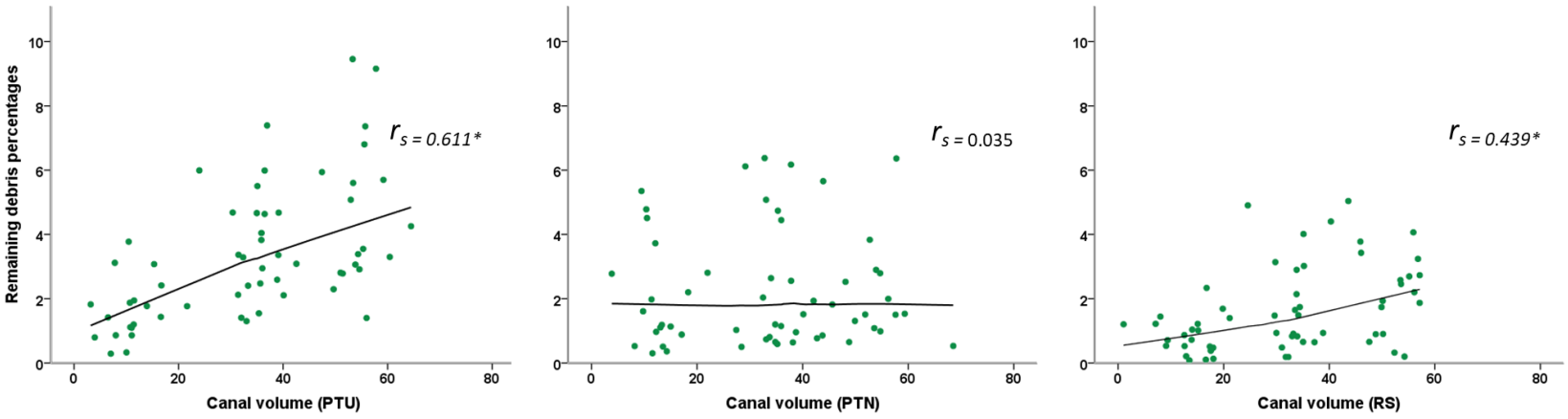

$^* = p \leq 0.01$

Figure 17: The correlation between remaining debris and the root canal volume. Scatter plot with Loess fitting curve demonstrate the Spearman's correlation between the percentages of remaining debris and the percentages of root canal volume thirds following instrumentation with three file systems. r_s = Spearman's correlation coefficient.

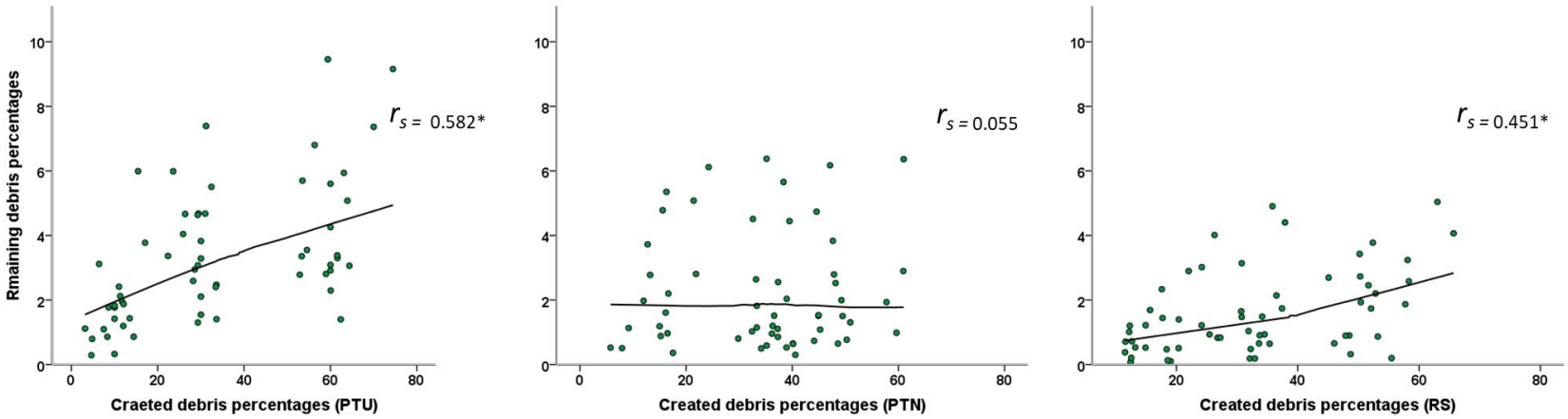

* = $p \leq 0.01$

Figure 18: The correlation between remaining debris and created debris. Scatter plot with Loess fitting curve demonstrate the Spearman's correlation between the percentages of remaining debris and the percentages of create debris in root canal thirds following instrumentation with three file systems. r_S = Spearman's correlation coefficient.

The Loess curves shows a pproximately a steady and smooth increasing in the percentaged of remaining debris during instrumentation with the PTU sytem. In contrast, the curve exhibits approximately no change throughout the scatter plot during the instrumentation with PTN system. For the RS system, the curve demonstrates a slower increasing trend in the lower percentages of the created debris followed by a faster increasing trend in the higher percentages of the created debris (Figure 18).

2.3.4.3. Remaining debris versus cleaned surfaces.

The percentages of remaining debris showed a negative correlation with the percentages of the cleaned surfaces in root canal thirds for all file systems (Figure 19) except for the PTN systm which showed approximately a no correlation (r_s = 0.076). A strong negative correlation coefficient was produced following instrumentation with the RS system (r_s = - 0.792). Whearas, the PTU systems showed a weak negative correlation coefficient (r_s = - 0.224). The Loess curve has shown a rapid declination in the RS system when compared to the slow declination in the PTU system or to the approximately zero declination in the PTN system.

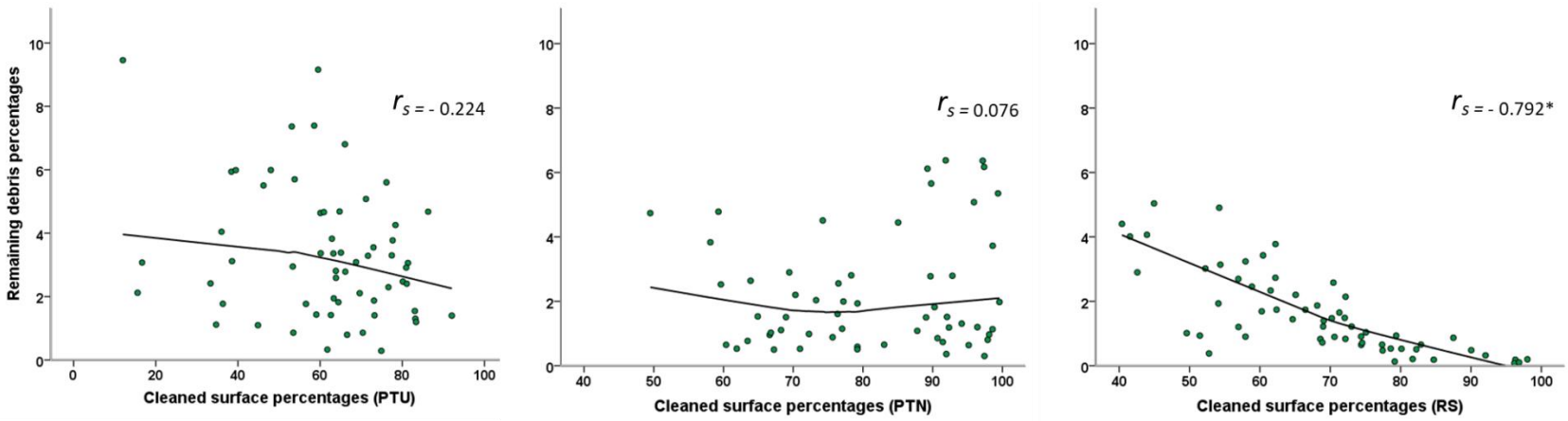

* = $p \leq 0.01$

Figure 19: The correlation between remaining debris and surface cleaning. Scatter plot with Loess fitting curve demonstrate the Spearman's correlation between the percentages of the remaining debris and the percentages of the cleaned surfaces in root canal thirds following instrumentation with three file systems. r_s = Spearman's correlation coefficient.

2.4. Discussion

The failure rates of root canal treatment have been shown to vary significantly (15 % - 41 %) in different cross sectional and longitudinal studies from 1921 to 2017 (Ng et al. 2007; Timmerman et al. 2017). Molar teeth have revealed the higher incidence of treatment failure (23.2 %) compared to premolars (13.3 %) and anterior teeth (14.4 %) (Azim et al. 2016). The high incidence (87.9 %) of the isthmus space in RCS of molars (Estrela et al. 2015) may attribute to such high percentage of treatment failure.

Among molar teeth, such challenging isthmi showed a high incidence (54.8 %) in the mesial root of the lower molar (De Pablo et al. 2010) and therefore, this tooth type is ideal for *in vitro* study models to create a challenge to study cleaning and disinfection of the RCS.

2.4.1. The percentages of remaining debris

The PTU has left the highest percentages of the total debris following preparation compared to the PTN and RS files. The results showed high standard deviation values, which are largely related to the variation in the root canal volumes of the tooth samples. These findings support the suggestion that asymmetric files enhance debris removal as there is more space between the flutes of the file and the canal wall allowing to be driven coronally. The RS system has left less debris percentage compared to the PTN system. This agrees with the previous suggestion because the triangular cross-section design of the RS has more space with the canal wall compared to the rectangular cross-section design of the PTN system. Until now, such data has not been reported on asymmetric files.

In respect to the debris percentages (10 %) left by the PTU system, the findings of the present study agree strongly with the finding of Robinson et al (2013), who showed that 10.6 % of the total debris was left in the mesial root canal of the lower molar using the same experimental design. A similar finding was also found by Paqué et al (2011) where 10.2 % of the root canal volume was filled with accumulated hard tissue debris by the PTU system.

Most of debris, with all file systems tested, accumulated in canal isthmi and some isthmi were completely obliterated with debris. Debris also accumulated in canal protrusions. These observations agree with previous studies, which utilized the microCT (Paqué et al. 2009; Paqué et al. 2012; De-Deus et al. 2015) or histological sections (Burleson et al. 2007; Susin et al. 2010; Adcock et al. 2011) for debris analysis in root canal with isthmus. Paqué et al. (2009) stated that debris in root canals is encouraged to be removed coronally from where it is contained and packed into the file flutes by resistance applied from the canal wall. However, on the side of isthmus opening, least resistance will encounter this process and debris is packed to the isthmus space rather than the file flutes.

In the canal thirds, both the PTU and RS systems left significantly more debris percentages in the cervical third followed by the middle and apical thirds respectively. Such variations may be attributed to the dimensional variations in the root canal volume percentages at each canal third. The results showed that the RCS volume is increasing progressively towards the cervical third and therefore, the cervical third may offer a larger volume for the debris to accumulate comparing to the other thirds. This suggestion disagrees with the finding of the PTN system where debris percentages were similar in all canal thirds. This could be used as evidence that the amount of the remaining debris is affected by file-related and tooth-

related factors. The results of the correlation of percentages were consistent with the previous discussion that the percentage of the remaining debris was dependent on canal volume for PTU and RS groups and non-dependent on canal volume for the PTN group.

2.4.2. The Percentages of created debris.

The amount of created debris is positively affected by the increasing diameter of the file. The results showed that the asymmetric files created more debris than the symmetric file. The tip diameters of the PTN and RS are larger than the tip diameter of the PTU. Increasing the instrument tip size causes a simultaneous increase in the instrument cross section diameter and consequently more dentine will be cut from the root canal wall. Peters et al., (2001) found that canal enlargement is related to the diameter of file instrument. In the present study, the file systems have cut more dentine in the cervical third than both the middle and apical thirds. Although, the PTN and RS systems have the same tip size at the last two file sequences, the taper percentages of the PTN are higher than the taper percentages of the RS as shown in Table 3. This could explain why the PTN system cut more dentine than the RS. The findings of our study agree with the findings of Deepak et al., 2015 where PTN produced significant dentine shaving and hence canal enlargement (transportation) compared to RS system. Therefore, files with small diameters can be used clinically to reduce created debris during instrumentation.

The results showed that there was a non-statistical difference between created debris percentages of PTU and RS. A study by Aydin et al., (2012) revealed that both files produced similar degrees of canal straightening and transportation from the original canal shape.

The results show that the percentages of the remaining debris are strongly dependent on the percentage of the created debris for PTU and RS groups. In contrast, the PTN group do not reflect any dependency between remaining debris percentages and created debris percentages.

2.4.3. The percentages of instrumented surfaces

Similar to previous studies (Peters et al., 2003b, Versiani et al., 2011, Siqueira et al., 2017), the findings showed that the root canal surface was partially instrumented. Certain percentages, 34.4 %, 20.5 %, and 32.5 % of the root canal surface remained untouched following instrumentation with PTU, PTN, and RS respectively. The visual analysis of images revealed that most of these untouched surfaces located in the isthmi and protrusions of the post-instrumentation canal. The root canal surfaces in the apical third showed higher percentages of cleaning compared with the middle and the cervical thirds respectively. Peters et al., (2001) found that rounded and small canals in apical thirds have more cleaned surface than the wide and oval canals in the middle and cervical thirds.

The PTN file system has cleaned more surface percentages of RCS comparing to the other two systems. This would be related to that the PTN shaved more dentine from the canal wall as demonstrated by the higher amount of created debris by this system.

For root canals prepared with PTU and RS systems, the correlation between the cleaned surfaces and the remaining debris was negative (inverse). More debris was found in association with less cleaned surfaces. Such a situation is most likely represented by the isthmus area. Conversely, approximately a zero correlation for root canals prepared with the PTN system.

2.5. Conclusions

The cross-section design and taper percentage (diameter) of the file instruments are shown to have a great influence on the percentage of remaining debris. In comparison to the symmetric design, files with asymmetric triangular or rectangular cross section provide an effective space with the canal wall that supports canal debridement coronally. However, The RS system has left the least percentages of debris compared to PTN and PTU systems respectively.

With respect to the canal levels, the file systems left significantly more debris percentages in the cervical third followed by middle and apical thirds. However, changing file tapering from progressive to a regressive along the PTN file length causes similar debris percentages in all canal thirds. Regarding tooth anatomy, most of debris was accumulated in the canal isthmi and protrusions. In contrast, the two main canals were occupied by minimal amount of debris.

For PTU and RS systems, the percentage of remaining debris was positively correlated to the either percentages of the root canal volume and created debris, while negatively correlated to the percentage of the instrumented surfaces. For the PTN system, no correlation has been reported between the percentages of remaining debris with the other parameters. According to the previous conclusion, the null hypothesis is rejected.

CHAPTER THREE:

3D MODELLING AND SIMULATION OF THE ROOT CANAL SYSTEM

3.1 Introduction

The chapter will consider the development of a novel root canal model system based on the mesial root of lower molar with a complete isthmus. The model system is created using rapid prototyping (RP) technology. It simulates a natural root canal system and can be used to evaluate various clinical cleaning and disinfection procedures. The model system allows direct visualization by optical scanning tools which will allow improved measurement of the success of root canal instruments without physical contact.

3.1.1. Rapid prototyping technology

Manufacturing technology now allows the production of a detailed 3D object from an image resource data (Frame and Huntley, 2012). The RP technology has been used in endodontics to produce root canal model blocks for teaching and research purposes. However, these models are less representative to the natural canal because they are drawn (sketched) as a simple cone-shape space with straight or curved path.

The advances in medical imaging, seen by the introduction of magnetic resonance imaging (MRI), CBCT and microCT scanners with high resolution, have led to the development of image-based modelling technology (Hieu et al., 2005). Three-dimensional models with detailed geometry were developed from image slices acquired by these scanners (Gibson, 2006). With image segmentation, the RP can produce an exact replica of any human organ (Petzold et al., 1999). Several medical training models and surgical splints have been developed for teaching and treatment purposes respectively (Gibson, 2006). Recently, a microCT scanning at resolution of 13.65 µm has produced a valid and detailed

computational model of a mandibular molar that successfully estimated the cuspal deformation under load using finite element analysis (Magne, 2007). Physical models with a natural anatomy were created for mandibular molars to evaluate the shaping performance of endodontic instruments (Ordinola-Zapata et al., 2014, Bonessio et al., 2017). These advances in RP increased the opportunities of creating novel simulated root canal models with realistic morphology.

3.1.2. Model validation

Validation of RP models for research purposes is required to assist comparisons between the artificial and natural root canal systems. The selection of validation tests depends usually on the questions required to be answered by a specific model (Sargent, 2013). Ideally, for example, a model that is designed to investigate root canal disinfection should provide the same environment of an infected canal in a clinical situation. Two general methods used to assess the results of validation tests: first, via comparing the test results with standard findings established by several previous studies and second, using the natural environment as a control to validate the artificial model (Gao et al., 2009, Shen et al., 2010a).

Few studies have been made to validate the physical root canal models. For example, (Lim and Webber, 1985b) found that no difference in shaping ability of file instrument between resin-based root canal samples and natural roots. Mohammed et al (2017a) have validated their root canal model by testing the surface wettability of a transparent 3D printed material in comparison the root dentine. In order to ensure robust validation of a resin-

based model prepared for the direct assessment of cleaning and disinfection of root canal system, several investigations, which include surface hardness, refractive index, contact angle (surface wettability), biofilm growth, and biofilm adhesion seem to be required.

3.1.2.1. Surface hardness

Material surface hardness of RP models may influence how root canal instrumentation works. Previous studies on surface hardness have revealed a negative relation to the resistance of resin-based materials to scratching forces (Özel et al., 2005, Passos et al., 2013, Gupta et al., 2016). It has been reported that resin-based artificial teeth have hardness values inferior to that of dentine (Loyaga-Rendon et al., 2007, Wang et al., 2017). It is likely that natural and resin-based teeth will behave differently with file instrumentation in term of stresses applied on the file surface during the shaping procedure (Bonessio et al., 2017). Further investigations will guide the future improvement of root canal samples to match the hardness value of dentine.

3.1.2.2. Refractive index (RI)

Refractive index (RI) measures the speed of light in vacuum in relation to the light speed in a specific medium. It indicates the amount of refraction when a ray of light passes from one medium to another (Avison, 2014).

Transparent materials have lower RIs values when compared to the opaque materials as the former produce minimal scattering effect on the incident light (Nakayama and Hayashi,

2007). Therefore, transparent materials are preferable as sample substrates in optical imaging research to produce high quality images (Hou et al., 2018).

In optical imaging, the refractive index influences image resolution by changing the number of light rays refracted toward the objective lenses of optical microscopes. Therefore, the angular aperture of these lenses are designed at an upper limit of 72^{o} to the direction of the light reflected from the standard microscopic slide (Rottenfusser et al. 2012). Accordingly, a model, which is planned for direct visualization with optical microscope should be transparent and have a RI similar to that of the microscopic slide.

3.1.2.3. Contact angle (Surface wettability)

Contact angle is a thermodynamic property that describes the wettability of solid materials where a small angle means better surface wettability (Marmur et al., 2017). Wettability of dentine surface is an important factor during root canal cleaning and disinfection. It brings the irrigant solution into intimate contact with debris and biofilm for an efficient removal during preparation (Abou-Rass and Patonai, 1982, Giardino et al., 2006).

Surface wettability also has a key role in the amount of grown biofilm mass on a particular material. The maximum amount of biofilm was found on surfaces with contact angles of 64^{o} and 74^{o} (Gottenbos et al., 2000, Zheng et al., 2016) including dentine surface (Prado et al., 2016). Therefore, a root canal model should be produced with contact angle similar to that of dentine to ensure an effective irrigation process and a proper biofilm growth mechanism.

3.1.2.4. Biofilm growth

Biofilm develops when bacteria and other microorganisms colonize the root canal system (de Paz, 2018). *In vitro,* biofilm models are used to test antibacterial regimens for disinfection of the root canal system (Bitter et al., 2017). Therefore, root canal samples should support realistic biofilm growth to comply with such a testing requirement. Several dynamic and static methods can be used to generate biofilm models. The microtiter plate is a common static method that is used to create biofilm models of different cultivable bacteria due to the simplicity and reliability of the culturing procedure (Harding and Daniels, 2017).

The concentration of viable bacterial cells before and after root canal treatment is widely used to indicate the efficacy of antibacterial medications (Ruiz-Linares et al., 2017, Bukhari et al., 2018). The efficacy of interventions might be misinterpreted if they are applied on biofilms that already have high concentration of non-viable bacteria. Also, the difference in the concentration between the viable and non-viable bacteria can be influenced by the age of the biofilm (Amorena et al., 1999, Lutskiy et al., 2015). Therefore, it seems important to determine the biofilm growth age associated with the higher concentration of viable bacteria before testing interventions that assess biofilm removal.

3.1.2.5. Biofilm adhesion

The biofilm on simulated root canals should exhibit adhesion integrity similar to that on dentine to simulate the clinical situation. Adhesion to surface substrate was described as the first process in biofilm growth. However, biofilms use different mechanisms to adhere to

different materials, such as dentine and resin polymer. This might cause variation in the biofilm adhesion integrity between surfaces and therefore the results may be not representative clinically.

Estimating the adhesion forces of surface biofilm may provide an insight into the variation in biofilm interaction with different substrates. An atomic force microscopy (AFM) has been demonstrated as a useful measuring tool for biofilm adhesion at a nanoscale (Razatos et al., 1998, Fang et al., 2000, James et al., 2016). In endodontology, the adhesion of bacterial biofilm to the root dentine surface has been estimated by AFM using a silicon nitride (SiNi) cantilever. The bacteria are coated on the cantilever tip and immobilized with a glutaraldehyde droplet. The cantilever is then approximated repeatedly to a root canal surface using perpendicular oscillatory motion to induce repeated adhesion and adhesion failure between bacteria and the root canal surface (Razatos et al., 1998, Kishen et al., 2008). The adhesion force was recorded at the maximum amount of cantilever deflection that is reached prior to the bacterial detachment. This test seems useful for measuring cell to cell or cell to surface adhesion at early stages of microbial aggregation. In mature biofilm, the test would be not applicable because bacterial cells will be embedded in the EPS matrix. In addition, the test is not representative clinically because perpendicular forces are not as common as shearing forces in root canal disinfection measures seen in mechanical debridement and irrigation process (Van Der Sluis et al. 2007).

A method with increasing lateral (shearing) forces, at the contact mode, with SiNi probe was developed by (Boyd et al., 2002). The method was applied to remove an overnight cultured biofilm on different substrata with different nanoscale forces. This method seems to be suitable for evaluation the adhesion of mature biofilm to root canal surface.

Aim:

To evaluate the potential of RP technology and materials in the manufacture of a simulated RCS which is valid for testing biofilm removal following root canal preparation.

Hypothesis:

The RP technology does not simulate the RCS to allow testing of different interventions to disinfect the root canal system.

Objectives:

1. To develop a 3D image of a mesial root of a lower molar aquired by microCT scanning as a 3D computational model.
2. To develop physical RCS samples using a material that mimics dentine and to assess its suitability for research through different physical and mechanical tests, including surface hardness, surface wettability, and refractive index.
3. To investigate the adhesion integrity of a generated biofilm on different material surfaces and compare its suitability to root dentine using AFM.
4. The overal objective is to produce a physical root canal model using rapid prototyping 3D printing technology. It is envisaged that this model will permit accurate testing, and research findings will guide for future development of different strategies of cleaning and disinfection that could improve treatment outcome.

3.2. Materials and methods

This investigation involved the use of computational modelling of the natural RCS followed by several physical, mechanical, and microbiological tests to validate different materials selected to create physical simulated root canal samples. The samples were 3D printed using the RP technique.

3.2.1. Creation of a novel root canal system model

The purpose of this work is to generate a novel model that represents a natural RCS morphology with a complete isthmus. The model will be used to generate identical root canal samples to be used for evaluation of biofilm removal following root canal preparation.

3.2.1.1. Creation of a computational model

An electronic model was created as a replica to the mesial root of a lower molar as shown in Figure 20. The replica was selected from the pre-preparation reconstructed microCT images of the 60 mesial roots. The roots were previously selected for the evaluation of remaining debris in the previous chapter. Evaluation of the roots included criteria of root canal length, inter-canal distance, and the range of isthmus width at the cervical opening. A root with an average of these criteria, 9.4 mm, 3.6 mm, and 0.08 – 0.312 mm respectively, was selected as a model for model generation.

Image processing:

The image processing steps are demonstrated sequentially by Figure 20. The selected image stack was filtered with the morphological opening algorithm to remove inorganic particles of octagon shape and 6-pixel radius within the RCS space. A Reslice operation was then applied to view image stack in a longitudinal section. The mesio-distal root curvature was then straightened to produce a flat sample for investigation. The root curvature was determined with the segmented line of the ImageJ. This was followed by the application of the line straightening operation, on the root. The root was then divided longitudinally into two equal halves in the mesio-distal direction. The external root surface was then modified to a rectangular shape of 8.2 mm length, 3.5 mm width and 9.4 mm depth (xyz) to improve sample handling during preparation. Thereafter, the two halves were converted to models by meshing their surfaces with geometrical triangles. The modelling was performed while images were displayed individually in the ImageJ 3D viewer at resampling factor of 2. Both model halves were then saved in STL, which is the common acceptable format for 3D printers input. A correction of improper meshing, such as missing or overlapping triangles, was followed using the Netfabb software (https://www.autodesk.com). This software was also used to rescale the model size to the correct dimensions using a scaling factor of 0.001.

3.2.2. Generation of a 3D frame model

This was aimed to reassemble the root canal sample during root canal preparation. A box shape frame was designed and drawn using the Solidworks software (http://www. solidworks.co.uk/).

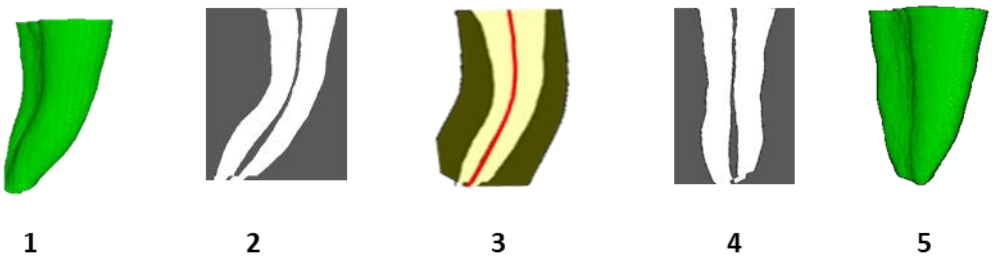

A. The selected mesial root (1) was resliced to a sagittal view (2), which allowed determination of root curvature using the wide segmented line (3). This was followed by curvature straightening to produce a straight canal and root (4 & 5).

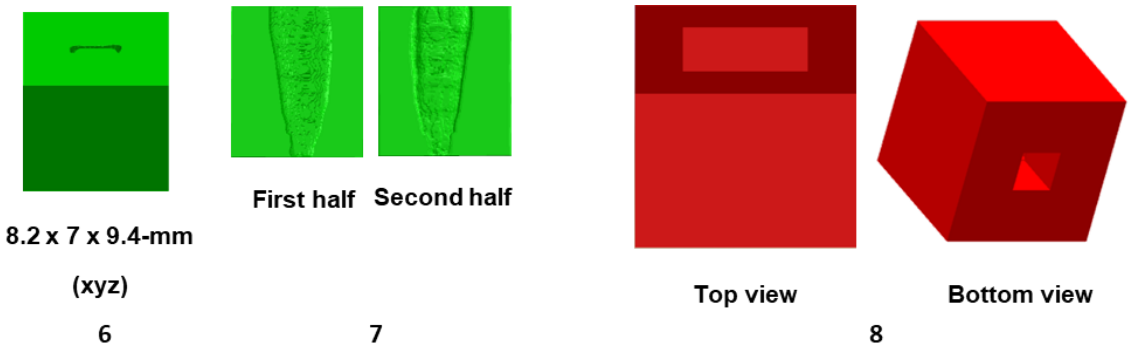

B. The external surface of the root was bounded with a rectangular geometry with a centrally located RCS (6). The canal system was then divided to equal halves (7). A cubic frame designed to hold the RCS halves during the instrumentation process (8).

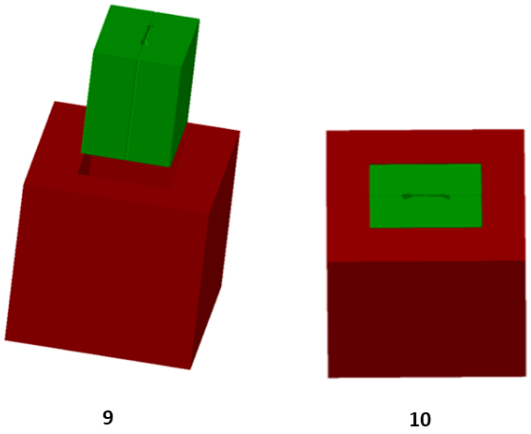

C. The alignment of the root canal model (9) before being fitted within the cubic frame 10).

Figure 20: Computational modeling of the RCS. A 3D diagram demonstrates the sequence of designing the novel RCS model.

The frame is 15 mm^3. An internal space was centrally located within the frame with same external dimensions of the joined root canal sample halves. A small window was placed in the base of the frame to assist in the apical sealing procedure and in sample extrusion following root canal preparation. A surface triangulated mesh was created with the same software followed by saving of the 3D image file in STL format.

A trial assembling of the model parts, including the RCS halves and the cubic frame, was assessed at the computational level using the Netfabb software. The assessment was aimed to detect any interference (overlapping) during seating of the RCS within the cubic frame. The assessment also included the measurements of the RCS and the cubic frame dimensions at xyz depths in comparison to the primary dimensions estimated by ImageJ and Solidworks software.

3.2.3. Material selection

Two transparent materials were used to evaluate the potential of creating simulated root canal samples using the 3D printing technology. These materials, Accura and EX200, are resin based liquids and polymerise in the presence of UV light using the SLA printing technology. Both materials were used to produce objects with ultra-high-resolution features.

To validate these resin-based materials for the physical simulation of RCS, different physical, mechanical, and biological parameters were evaluated to compare with root dentine as a control material.

3.2.3.1. Sample preparation of selected materials

Human lower third molars (n = 10) were collected from the Birmingham dental school tooth-bank (REC Ref: 14/EM/1128). The teeth were selected according to the following inclusion criteria; no caries, no restorations, and no visible crack. The buccal, lingual, mesial and distal surfaces of each tooth were flattened with a silicon carbide grinding paper grit 350 (Struers, Pederstrupvej, Denmark), which was fitted on a grinding and polishing machine (Struers, Pederstrupvej, Denmark) operating at speed of 250 rpm with water coolant. The flat surfaces enabled reproducible tooth alignment and stability during the sectioning procedure. The teeth were then decoronated by a low speed saw (Buehler, Illinois, USA) with water coolant. Mesial and distal sections of 1.8 ± 0.1 mm thick were taken from the root surfaces. The slices were adjusted to rectangular shapes of 5 mm ± 0.1 mm length, 4.5 mm ± 0.1 mm width, and 1.5 mm ± 0.1 mm thick using the low speed saw and a digital calibre (Duratool / Premier Farnell Company, Leeds, UK). The lower surface of each slice was marked with permanent ink (Steadtler, Mid Glamorgan, UK). The upper slice surfaces were finished with silicon carbide papers with decreasing abrasiveness of 1000, 2000, and 4000-grit for one min each paper. This was followed by polishing with a neutral aluminium oxide suspension of 0.02 µm for one min. The polishing suspensions were dispensed on a polishing cloth disc (Struers, Pederstrupvej, Denmark), which was magnetically fixed on the grinding and polishing machine. After polishing, samples were then washed under running tap water and cleaned for 5 mins with an ultrasonic bath to remove tooth debris and any remnants of polishing material. The samples were then kept in PBS in the ambient air incubator at 37^{o}C until use.

Large sample blocks of Accura and EX200 were printed using SLA and Projet technologies respectively. The blocks were cut to the same dimensions to match the dentine sample sizes (Figure 21). The cutting procedure was performed with the Buehler low speed saw followed by surface finishing and polishing process as mentioned above.

3.2.4. Sample testing

3.2.4.1. Evaluation of surface hardness

The purpose of this test was to compare the surface hardness of the Accura and EX200 materials to the surface hardness of root dentine.

Five samples of each material were used for this test. Five indentations, with a minimum of 100 µm separating distance, were made on each sample surface using the standard indenting machine (Struers, Rodovre, Denmark) at a dual time of 20 seconds and a load of 200 g (Figure 21). The length of the horizontal and vertical lines of the created diagonal indentation was measured at 40x magnification. The Vickers hardness number (VHN) was displayed automatically on the machine monitor.

3.2.4.2. Measurement of the contact angle (surface wettability)

The aim of this experiment was to measure the surface wettability of the test materials in comparison to the surface wettability of dentine.

Five block samples were used for each test material including dentine, Accura, and EX200.

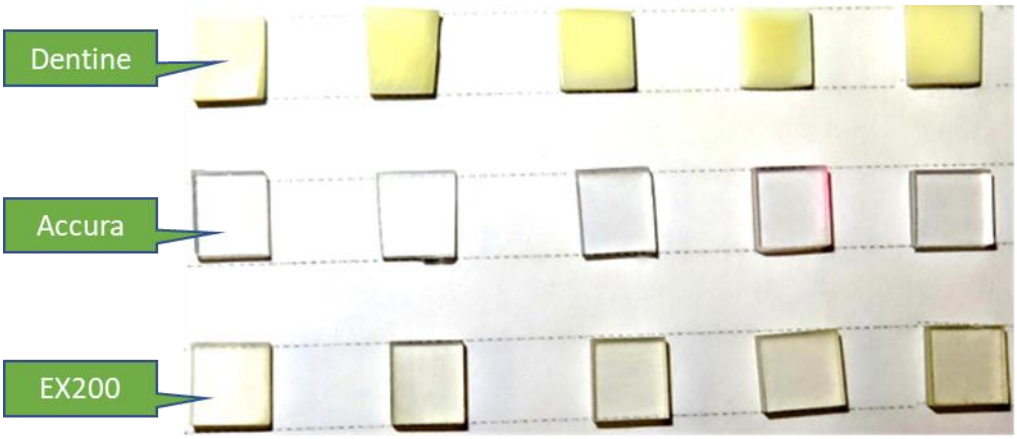

A

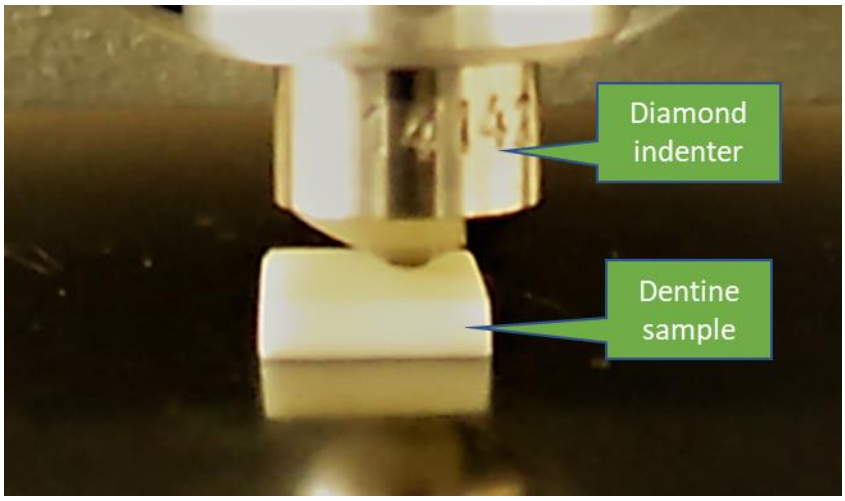

B

Figure 21: Material block samples and surface hardness testing. Photographs illustrating: (A) three material samples prepared with dimensions of 5 mm (± 0.1 mm) length, 4.5 mm (± 0.1 mm) width, and 1.5 mm (± 0.1 mm) thickness1; (B) load application with diagonal diamond indenter during hardness testing on the polished dentine surface.

Samples were mounted horizontally on an adjustable stage in front of a colour video camera (JVC, Wayne, USA). A distilled water droplet of 4 µl was then dispensed on the sample surface (Figure 22) using the 20 µl micropipette (Gilson, Villiers Le Be, France). An image was then captured using the Optimas 6.5 software and saved as PNG format. A semi-automatic analysis method was performed with the ImageJ software using the droplet analysis algorithm (Figure 22). The algorithm was originally written to estimate the contact angle for a droplet dispensed on reflective surfaces. Therefore, after being loaded, the droplet image was duplicated and then flipped vertically to simulate a reflected image for the original droplet. The droplet boundaries were then detected manually, whereas the contact angles, on both sides of the droplet, were detected and estimated automatically by the algorithm.

3.2.4.3. Measurement of the refractive index (RI)

The aim of this experiment was to determine the RI of the tested materials compared to the standard microscopic glass slide. The measurement was performed with the standard Abbe refractometer device (Carl Zeiss, Oberkochen, Germany) with an incandescent light of 40 voltages as advised by the device manual (Figure 23). The light source was put on distance of approximately 25 cm from the refractometer. The wavelength of the light source was determined because the refractive index varies with different wavelengths. The measurement was performed with a spectrometer (Ocean optics, Oxford, UK) connected to one end of a fibre optic cord of 400 µm diameter. The other end of the cord was put in direct contact with the lamp surface to measure in five different locations. An absolute irradiance (light intensity) curve was displayed on a laptop monitor at each measurement. The range of five wavelengths graph was then demonstrated using an excel worksheet.

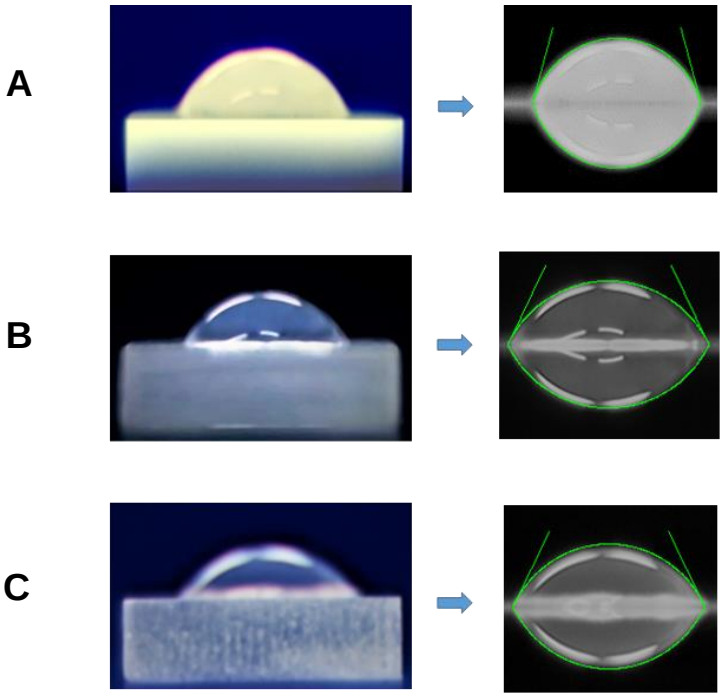

Figure 22: Contact angle measurement. An image panel demonstrates the water droplet dispensed on sample surfaces (left images), and contact angle determination on dentine (A), Accura (B), and Ex200 (C) materials using drop analysis algorithm (right images).

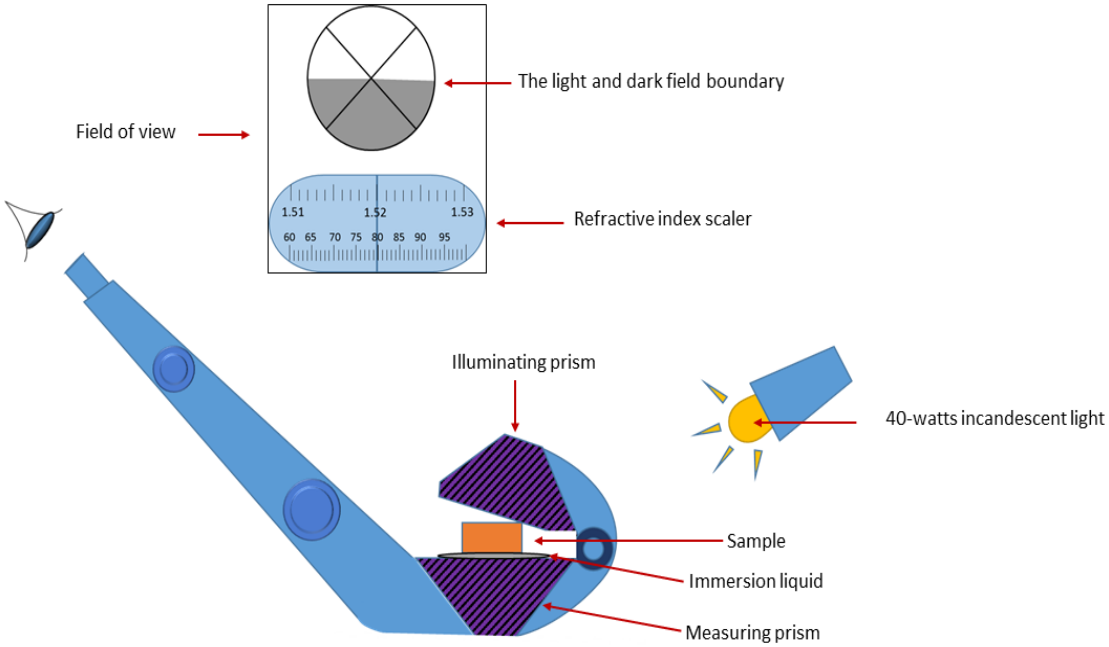

Abbe refractometer

Figure 23: Refractive index measurement. An illustration showing how the equipment, sample mounting and method used to measure the refractive indices for the evaluated samples.

Five sample blocks of Accura and EX200 materials with dimensions of 9 mm length, 7 mm width and 3.5 mm height were used for this test. Five glass slides were used as a control group in this experiment. The top and bottom surfaces of all samples were sequentially finished with silicon carbide papers using grits of 1000, 2000, and 4000. The top surface for each sample was then marked with a permanent ink at one corner while the bottom surface was further polished with neutral colloidal silica for 1 min. A droplet of an immersion liquid (1-bromonaphthalene) was dispensed on the surface of the measuring prism of the refractometer before sample placement to minimize air entrapment.

The sample bottom surface was then mounted on the measuring prism while the top sample surface was brought in direct contact with the movable illuminating prism. The apertures of the measuring and illuminating prisms were adjusted to produce a clear boundary between dark and light areas in the field of view. The clear boundary was brought into a close approximation with the cross section point as shown in Figure 23. The corresponding number on the Abbe scale was registered then included to a formula to estimate the refractive at 20^{o}C as following,

$$nD^{20} = [nD \text{ observed} + (20^{o}C)]\ 0.00045$$

Where, nD^{20} is the refractive index estimated at 20^{o}C, nD is the refractive index observed on Abbe scale, and 0.00045 is a constant number.

3.2.5. Generation of a single species biofilm on material surfaces

The aim of this experiment was to evaluate the potential of creation an *E. faecalis* biofilm on the surfaces of the test materials in comparison to the dentine surface.

Generation of a biofilm on simulated root canals required several steps:

- preparation of medium required for bacterial growth,
- performing tests necessary for confirming culture sterility,
- estimating bacterial inoculum required during culturing process,
- operating a biofilm growth assay to characterize biofilm growth behaviour over certain periods or with different treatment conditions,
- generation of the biofilm on block samples of the test materials.

3.2.5.1. Preparation of brain-heart infusion (BHI) broth and agar

The same growth medium constituents were used to cultivate *E. faecalis* during the experimental work in this project.

Powders of brain heart infusion (BHI) broth and BHI agar (Sigma-Aldrich, Gillingham, UK) of 37 g/L and 47 g/L respectively were separately dissolved in distilled water. The solutions were then shaken manually for one minute and left on the bench for five minutes at room temperature to ensure homogeneity (pH 7.4 ± 0.05).

The solutions were then sterilized at 121^{o}C for 22 mins in a 9 litre portable autoclave (Prestige Medical, Blackburn, UK) and then left to cool on the bench to an appropriate handling temperature. After cooling, the agar solution was poured onto 15 cm sterilized plastic petri-dishes (Fisher scientific, Loughborough, UK) inside a biological safety cabinet (Monmouth scientific, Somerset, UK) and allowed to solidify at room temperature. Both BHI broth and agar plates were left on the shelf until use.

3.2.5.2. Generation of *E. faecalis* colonies and growth culture

An *E. faecalis* standard strain (NCTC 12697, ATCC 29212) was collected as a freeze-dried pure culture in a flame-sealed glass ampoule (Culture Collection, Public health England, Wiltshire, UK). The seal was broken in a biological safety cabinet then bacteria were rehydrated for 5 mins with 0.5 mL of a sterile BHI broth. Then, 200 µL of the rehydrated culture were transferred with a micropipette to the surface of an agar plate (n = 3) and plated using sterile plastic loops. This was followed by an overnight incubation period (20-24 hr) in the CO_2 incubator at 37^{o}C.

3.2.5.3. Assessment of the purity of the bacterial culture

In order to ensure sample purity of the cultured *E. Faecalis the* following assessments were made: determination of colony morphology, gram staining and catalyse reaction.

The shape and texture of the produced colonies were observed visually and evaluated according to the criteria specified in the datasheet of the supplier (http://www.phe-culturecollections.org.uk/).

For the gram stain test, a single colony of an overnight culture was dispersed in a droplet of sterile distilled water (Millipore, Hertfordshire, UK) over a clean glass slide. The mixture was then allowed to dry for 5 mins at room temperature. The dried bacteria were then heat fixed with Bunsen burner for five seconds and stained by a gram staining kit (Pro-Lab Diagnostic, Wirral, UK) as demonstrated in Figure 24. Examination of the sample with the light microscope was followed using the 100x objective lens with oil immersion.

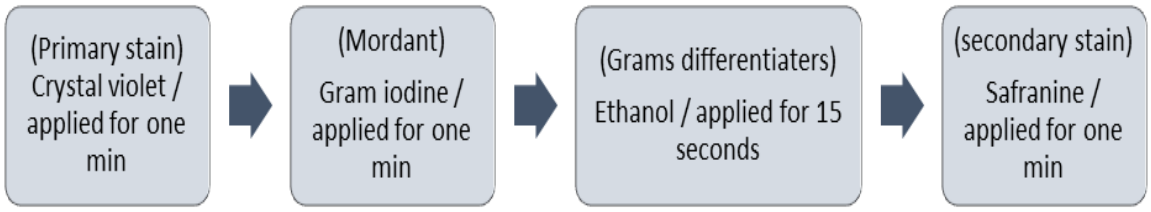

Figure 24: Gram-staining technique. Flow chart shows the steps of gram staining of *E. faecalis*. Each step was followed by washing with distilled water for approximately 10 seconds.

The catalyse reaction test was performed to distinguish between *E. faecalis* and other bacteria that may have similar morphology and positive reaction, such as *Staphylococcus epidermidis*. 1 mL of 3 % hydrogen peroxide (H_2O_2) solution was freshley prepared in a sterile small plastic tube (n=10). The solution was then inoculated with colonies of *E. faecalis* using a sterile wooden stick. The colonies were previously grown for 20 hr in the CO_2 incubator at 37^oC. An simple observation followed of the colony inoculation, for 60 seconds to detect elaborated O_2 bubbles in any of the test tubes.

3.2.6. Microtiter plate biofilm growth assay

This test was performed to evaluate the ability of the test *E.faecalis* strain to produce biofilm in an a static aerobic environment using a 48-wells tissue culture plate. Also to characterize biofilm growth and development in five time intervals. In this experiment, the volume of culture inoculum was primarly standarized.

3.2.6.1. Standarization of the culture inoculum

The aim of this calculation was to standarise bacterial concentration inoculated to each well throughout the biofilm growth assay.

A single colony of an overnight culture was inoculated to 10 mL of sterile BHI broth in a sterile plastic tube (n = 5) with a screw cap. A control group of the same sample size was left with a sterile broth. Thereafter, the ten samples were incubated overnight at 37^oC in the 5 % CO_2 incubator. Subsequently, samples were vibrated at medium speed for 10 secs to ensure homogenous dispersion of grown bacteria. 1 mL was then collected from each

sample in the test group using a plastic cuvette. The optical density (OD) of cuvette samples was then adjusted to 1 ± 0.005 at 550 nm wavelength using a spectrophotometer (Jenway, Staffordshire, UK). A fresh 1 ml of BHI broth was used as the zero standard to control the OD measurments. During the adjustment procedure, the higher OD number was reduced by replacing part of the culture with an equal amout of fresh broth in a rate of 100 µL for each 0.1 elavation in the OD.

3.2.6.2. Estimation of bacterial concentration

The bacterial concentration in a volume of 100 µL were counted using a flowcytometer. Five samples of 1 mL each were taken from the test and control group and dispensed separately in a 1.5 mm plastic tube with attached cap. At this stage, a further control group of sterile distilled water was included to the test. The 15 tubes were then centifugated for 3 mins at speed of 3000 rpm. This was followed by careful removal of the supernatent to avoid dislogement of the bacterial pellete at the base of the tube. The pellete was then resupended in 1 mL of filtered distilled water (0.22 µm pores filter) and shaken with a vibrator for 10 secs. This process was repeated for three times to wash bacteria from the remnants of the culture medium. Each tube was then mounted on the flowcytometer stage to count bacterial cells in 100 uL. Three runs set at medium speed were made for each sample.

3.2.6.3. Bacterial culturing process

An inoculum of 100 uL culture was diluted to 1/100 using a fresh BHI broth. The diluted culture was left inside the safety cabinate for 5 minutes to ensure homogenicity. Five tissue culture plates of 48-wells were inoculated with 0.5 mL of the diluted culture medium in each well (n = 20) using the 1000 µL micropipette. A tissue culture plate was added as a control group and inoculated with the same volume (0.5 mL) of a fresh BHI broth. All plates were incubated in the 5 % CO_2 incubator at 37^{o}C for different time intervals including 1, 7, 14, 21, and 28 days. The culture medium was refreshed every 48 hr where 0.45 mL of the cultute were replaced with 0.45 mL of fresh BHI broth. After the desired time interval, the culture medium was removed and replaced with an equal volume of 100 % (mg/mL) methylene blue dye. Biofilm staining was then allowed for 10 mins at room temperature. The methylene blue was then removed and washed with sterile PBS (pH 7.4 ± 0.05) two times for three minutes each. After that, 0.5 of the solubilizing solution (80 % ethanole with 20 % acetone) was added to each well to disolve the dye bound to the biofilm in 10 mins. The amount of light absorbance of dissolved methylene blue was estimated at 600 nm wavelength using a universal microplate reader (ELx 800, Bio-TEK instrument, Swindon, UK).

3.2.7. Evaluation of biofilm growth with serum albumins

The experiment was conducted to evaluate the possibility of maximizing the culture environment by adding protein compounds for improving bacterial adhesion and growth on root canal surface.

First group: Twenty wells of 48-wells tissue culture plate were coated with fibronectine as follows, 50 µL were added for each well then incubated for 1 hr at 37^{o}C in the CO_2 incubator. Following incubation period, 0.5 mL of the 1/100 diluted bacterial culture were added to each coated well and the incubated for 7 days.

Second group: Twenty wells of 48-wells tissue culture plate were inoculated with 0.5 mL of the diluted culture. 20 µL of bovine serum albumin (BSA) were then added to each well and incubated for 7 days using the first group culture environment. The biofilm was then labelled with the methylene blue dye then estimated with the microplate reader as described previously.

3.2.8. Evaluation of biofilm generation on RP materials

The aim of this experiment was to compare the amount and texture of a biofilm generated on Accura and EX200 surfaces to a biofilm generated on dentine surface.

Five sample blocks of each test material were autoclaved for 30 mins at 121^{o}C and placed in 24-well tissue culture plate and then incubated for 7 days with 2 mL of *E. faecalis* diluted culture at 37^{o}C in the CO_2 incubator. Regular culture refreshment with 1.8 mL of BHI broth was maintained every 48 hrs. Following the desired period, the culture medium was removed and samples were washed two times of three minutes each using a sterile PBS. Thereafter, samples were fixed for 10 mins in a buffer solution containing 2.5 % glutaraldehyde and 1 % M sodium-cacodylate. The fixed samples were washed two times as previous and allowed to dry out overnight in the fume hood at room temperature.

The samples were mounted onto aluminium pin stubs then sputter-coated (Emitech, K550x, Kent, UK) for 2 mins with a gold layer of approximately 15 nm thick. SEM imaging was achieved at a magnification of 1250x and 6000x with working distance of 14-15 mm.

Image analysis was performed using the ImageJ software (National Institute of Health, Maryland, USA). Five standardized images were taken for each sample, four in the corner and one in the middle. The trainable weka segmentation algorithm was applied using the ImageJ software to differentiate biofilm from material surface. The resulted coloured images were converted to 8-bit grey images and an automatic threshold was then applied to convert the biofilm to white pixels. The pixels were counted with the ImageJ for statistical analysis.

3.2.9. Evaluation of biofilm adhesion to the Accura surface

The purpose of this test was to evaluate the adhesion integrity of *E. faecalis* biofilm on the Accura material in comparison to the dentine using the AFM. Due to the material being unavailable, EX200 material was not included in this experiment.

Three block samples of each material including dentine and Accura were used. As in the previous experiment, the biofilm was generated on the samples surfaces for 7 days in the 5 % CO_2 incubator at 37^{o}C. Fixation and sample washing were achieved using the previous buffer and technique. After washing, samples were kept in a sterile plastic tube at 4^{o}C until testing.

Each sample was stabilised with a double adhesive tape on a glass slide, which was then mounted on an AFM apparatus (NanoWizard II, JPK Instruments, Germany). A droplet of

distilled water was then deposited on the sample surface to generate a liquid environment for imaging the biofilm. The measurements were carried out between the samples and a SiNi cantilever (Windsor Scientific Ltd, UK) with resonance frequency of 30 KHz, and spring constant of 0.27 Nm^{-1} on the contact mode at 18-20^{o}C room temperature. The data was displayed on the AFM monitor of the SPM control software (JPK Instruments, Germany). The cantilever was approaching automatically the surface of the sample and a preliminary first scan on an area of 10 µm x 10 µm or 15 µm x 15 µm was performed (Figure 25).

Low normal load (2 nN) was applied to capture the topography of the biofilm surface to ensure minimal destruction. Such preliminary scan was aimed to select a proper biofilm section for the subsequent load application tests.

Thereafter, five square areas of 2 μm^2 dimensions were assigned to five forces of 5, 10, 15, 20, and 25 nN using the contact mode scanning (Table 5). The purpose of applying an increasing load is to compare the effect of variable forces on removing the biofilm. The acquired topographic pictures, before and after load application, were saved in a JPK format and then opened in the JPK Data Processing software to perform image analysis.

Table 5: AFM scan setting. The setting parameters applied during the AFM scanning using the contact mode.

		Scan area size (µm)	Setpoint (nN)	Tip velocity (µm/sec)	Image pixel size
Preliminary scan area		15 x 15	2	23.51	512 x 512
	Before load	2 x 2	2	4.49	256 x 256
	After load	2 x 2	5, 10, 15, 20, and 25	4.49	256 x 256

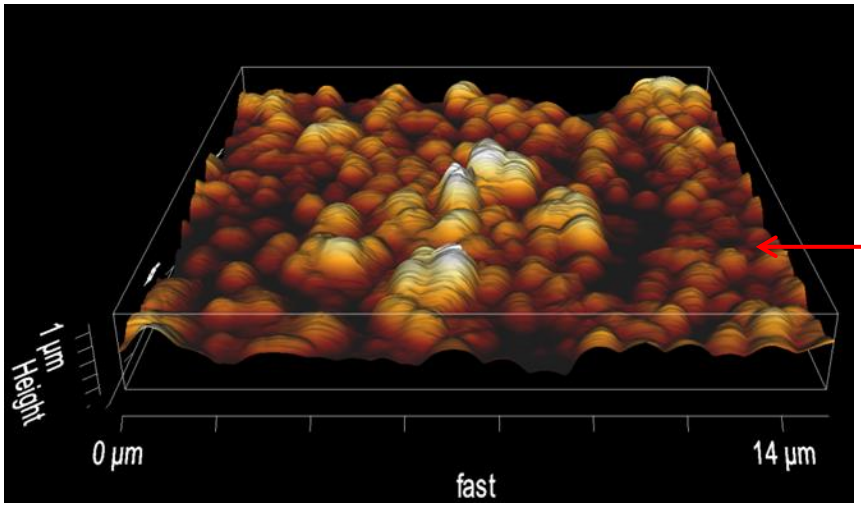

A ***E. faecalis*** **biofilm**

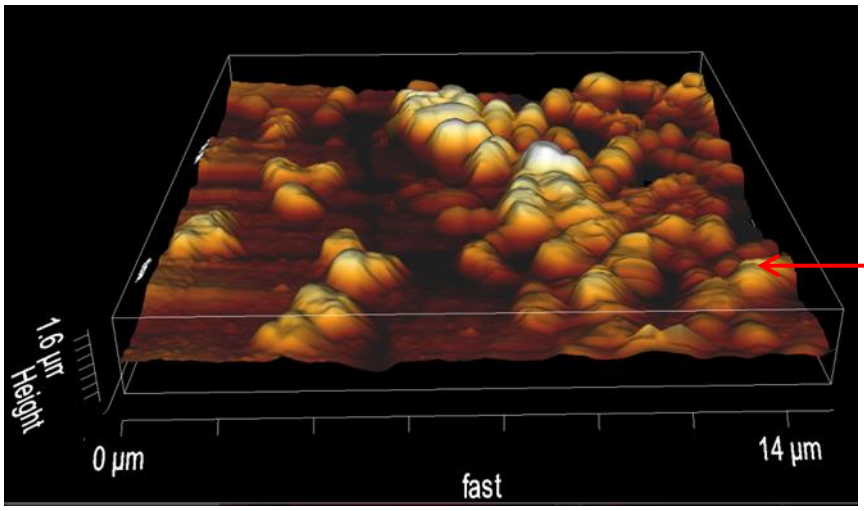

B

Figure 25: Preliminary AFM scanning. A fast scanning procedure was performed with the contact mode to select a proper area for variable load applications. Three-dimensional AFM views show biofilms generated on dentine surface (A) and Accura surface (B).

The images were filtered by the built-in JPK analytic software to remove the noise produced during scanning procedures. Visual analysis was adopted first to compare changes in biofilm following load application on both materials. Average height histograms were then plotted using the same software to evaluate the height of the biofilm before and after load application. The data of representative plots were saved as text files, which were processed later in an excel sheet to create superimposed plots for comparison.

3.2.10. Physical modelling of the novel root canal system model

The RCS model image files were submitted to a 3D printing company (3D Alchemy, Shropshire, UK), which is a University of Birmingham supplier. The Accura material (3D Alchemy, Shropshire, UK) was used to create RCS sample halves using the SLA technology. The printing resolution was made of successive layers of 50 µm thick and to a minimum surface feature of 0.3 mm.

The Rigur polypropylene like material (3D Alchemy, Shropshire, UK) was selected to create the cubic frame using the FDM printing technology. The printing resolution was made of successive layers of 250 µm thick and to a minimum surface feature of 1 mm.

3.2.11. Statistical analysis

The SPSS analytic pack, version 24, was used for the statistical evaluation of data. The variance and normality tests were initially applied for each data set to categorize data distributing around the data mean. The single factor Anova test and the post-hoc LSD test used to compare group difference at significance level set at $p \leq 0.05$.

3.3. Results

3.3.1. The computational root canal system model

The process revealed that microCT images of the RCS can be readily used to generate an accurate and realistic RCS model using the ImageJ and the Netfabb software (Table 6).

The computational assembling assessment with Netfabb software showed no interferences between the model halves and the cubic frame margins when visualized at higher zoom. Analysis of STL files with the Netfabb software revealed that both RCS and the cubic frame have retained the dimensions estimated with the ImageJ and Solidworks software respectively (Table 7).

Table 6: Spatial measurements of model parts. Surface areas, volumes, and surface mesh triangles as estimated by the Netfabb software.

	Surface area (mm^2)	Volume (mm^3)	Surface mesh (triangles)
Cubic frame	1707.1	2692.2	48
First half	280.8	269.9	344776
Second half	285.4	280.4	354584

Table 7: Computational and physical model pats dimensions. The xyz dimensions (mm) of the model parts as estimated by the ImageJ software, Netfabb software, and the Vernier calibre.

	X	Y	Z
ImageJ	8.2	3.5	9.4
Netfabb	8	3.5	9.5
Vernier calibre	8.22	3.65	9.54

3.3.2. Surface hardness

The surface of dentine was harder than the resin materials. This was represented by the higher VHNs of dentine (58.93 ± 3.5) compared to the Accura (14.8 ± 0.3) and EX200 (12.89 ± 0.2) materials as shown in Figure 26. The differences were significant ($p \leq 0.001$) following the parametric analysis with the LSD test. The Accura material showed a higher VHN mean value compared to the EX200 material but the difference was non-significant.

3.3.3. Refractive index

The wavelength of the light source was polychromatic located in the visible spectrum between 350.4 and 886.7 nm. The mean refractive indices of the glass slide, Accura, and EX200 are represented in Table 8 and showed approximately similar mean values.

Table 8: Refractive indices. A Statistical analysis table describes the refracted indices of the tested materials.

	Minimum	Maximum	Mean	SE	SD
Glass slide	1.52	1.53	1.5283	.00024	.00055
Accura	1.53	1.54	1.5362	.00262	.00585
EX200	1.53	1.54	1.5360	.00045	.00100

3.3.4. The contact angle (surface wettability)

The three tested materials; dentine, Accura, and EX200 showed hydrophilic surface criteria represented by contact angles of 71.36^{o} (± 5.3), 64.26^{o} (± 3.5), and 61.82^{o} (± 5.9) respectively. The LSD test revealed a significant difference ($p \leq 0.05$) between dentine and the other materials, whereas there was a non-significant difference between Accura and EX200 materials (Figure 26).

3.3.5. The purity of bacterial culture

The observation of the overnight culture growth on BHI agar plate showed small, white, smooth, shiny, convex and entire circular colonies. The colonies were semi-transparent; therefore, the petri-dishes were slightly tilted for proper observation of colony shapes. Figure 27 showed that bacteria are gram positive where purple stained cocci grouped in short and long chains under the oil immersion lens (100x). The result of the catalyse reaction test was negative as no oxygen bubbles were observed upon colony insertion in the H_2O_2 solution (Figure 27).

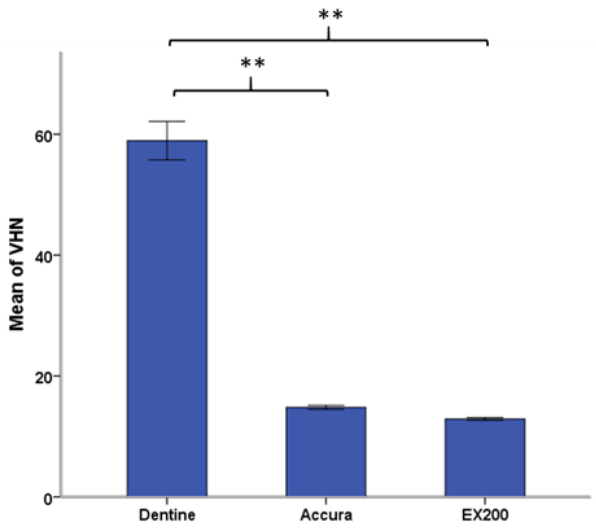

A

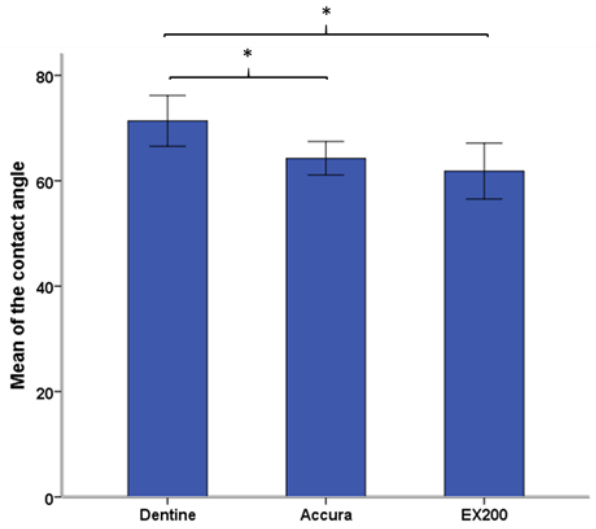

B

* = $p \leq 0.05$
** = $p \leq 0.001$

Figure 26: Surface hardness and contact angle measurement. Bar charts show the mean (± SE) surface hardness (A) and contact angle (B) measurements of Dentine, Accura, and EX200 materials. The VHNs estimated on material surfaces using 200 g load and dual time of 20 sec. Anova and LSD statistical tests were used to show the significance difference ($p \leq 0.05$).

3.3.6. Biofilm growth assay

The bacterial cell concentration in 100 uL of BHI broth at 1 OD revealed 1.66×10^6 ($\pm 8.4 \times 10^4$) bacteria, whereas, control groups of BHI and distilled water showed a proximately similar unit counts of 3.08×10^2 ($\pm 1.2 \times 10^2$) and 2.66×10^2 ($\pm 1.4 \times 10^2$) respectively (Figure 28).

E. faecalis showed successive biofilm formation after 24 hr static culture in the tissue culture plate (Figure 29). This growth was manifested visually as stained plaque at the centre and the periphery of the wells as shown in Figure 29. The absorbance value of the 24 hr biofilm (1.5) was significantly higher ($p < 0.05$) than the absorbance value of the negative control group (0.1). This group showed no visual evidence of biofilm plaque following 7 days of the incubation (Figure 29). Following 7 days, there was a marked increase in the biofilm volume ($p \leq 0.05$) represented by a higher absorbance value (2.5). However, the amount of the biofilm decreased gradually from week two to week four with absorbance values of 2.1, 1.7, and 0.6 for weeks one, two, and three respectively. The differences between absorbance values for the different growth periods were statistically significant ($p \leq 0.05$). However, none of the test groups showed an absorbance value lower than that of the negative control group.

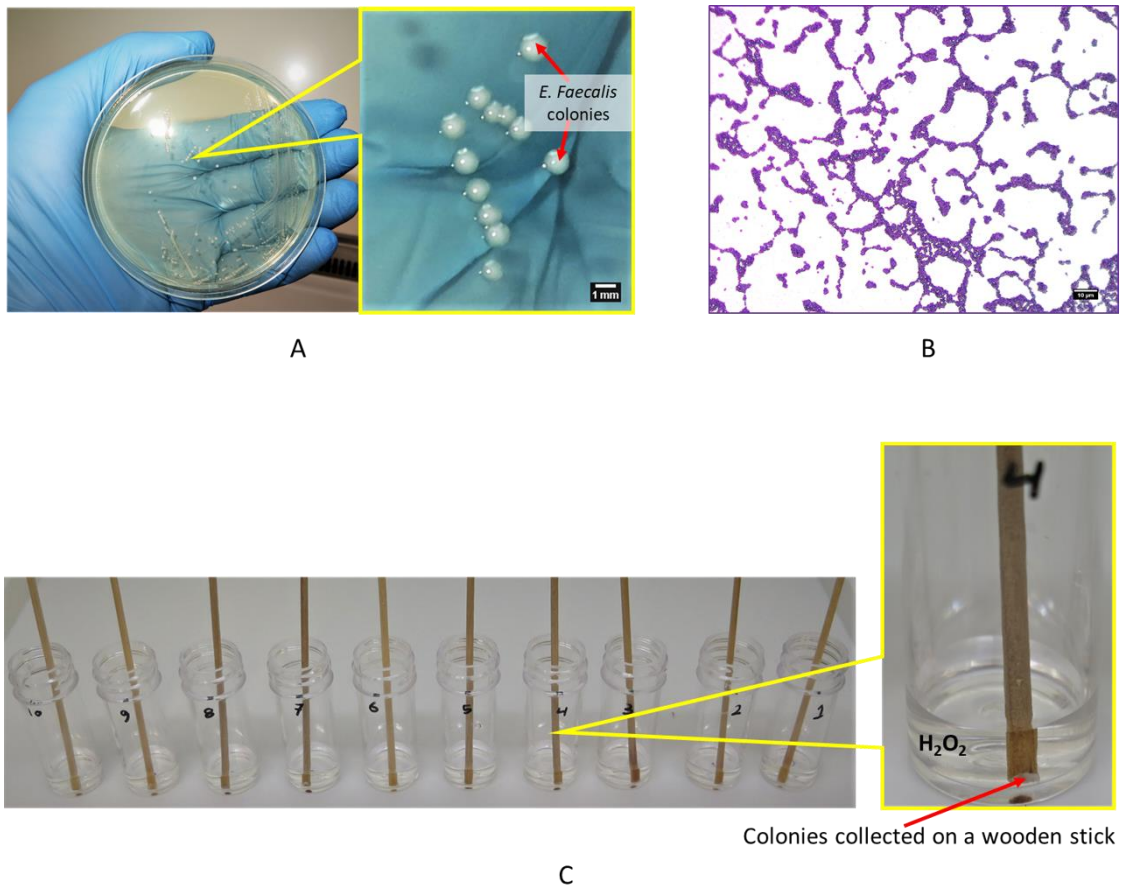

Figure 27: ***Enterococcus faecalis*** **culture purity tests.** An image panel shows a photograph of bacterial colony morphology after 24 hr growth on BHI agar (A); a stereomicroscope image (50x lens) showed the positive result of bacterial gram staining (B); a photograph shows ten plastic tubes with wooden sticks inoculating several colonies following 24 hr growth on an agar plate (C).

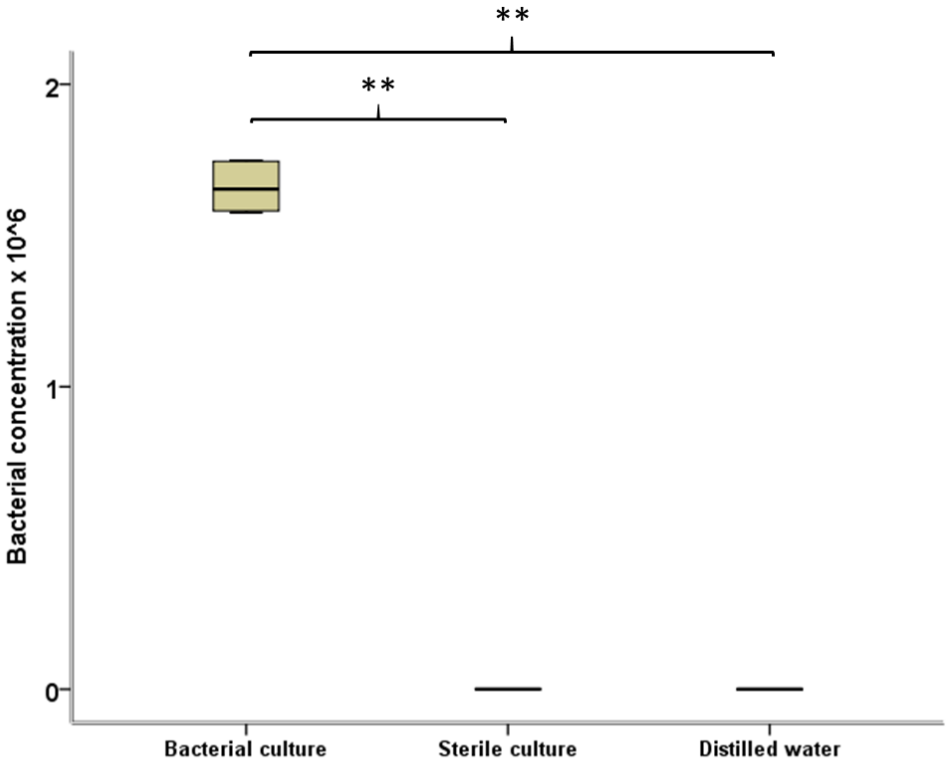

** = $p \leq 0.001$

Figure 28: Estimation of bacterial concentration. A boxplot chart shows the mean (± SD) concentration of *E. faecalis* at OD of 1 in comparison to the sterile culture of the BHI broth and to the distilled water as control groups. Each concentration was estimated in a volume of 100 µL. Anova and LSD test were used to reveal the significance difference ($p \leq 0.05$).

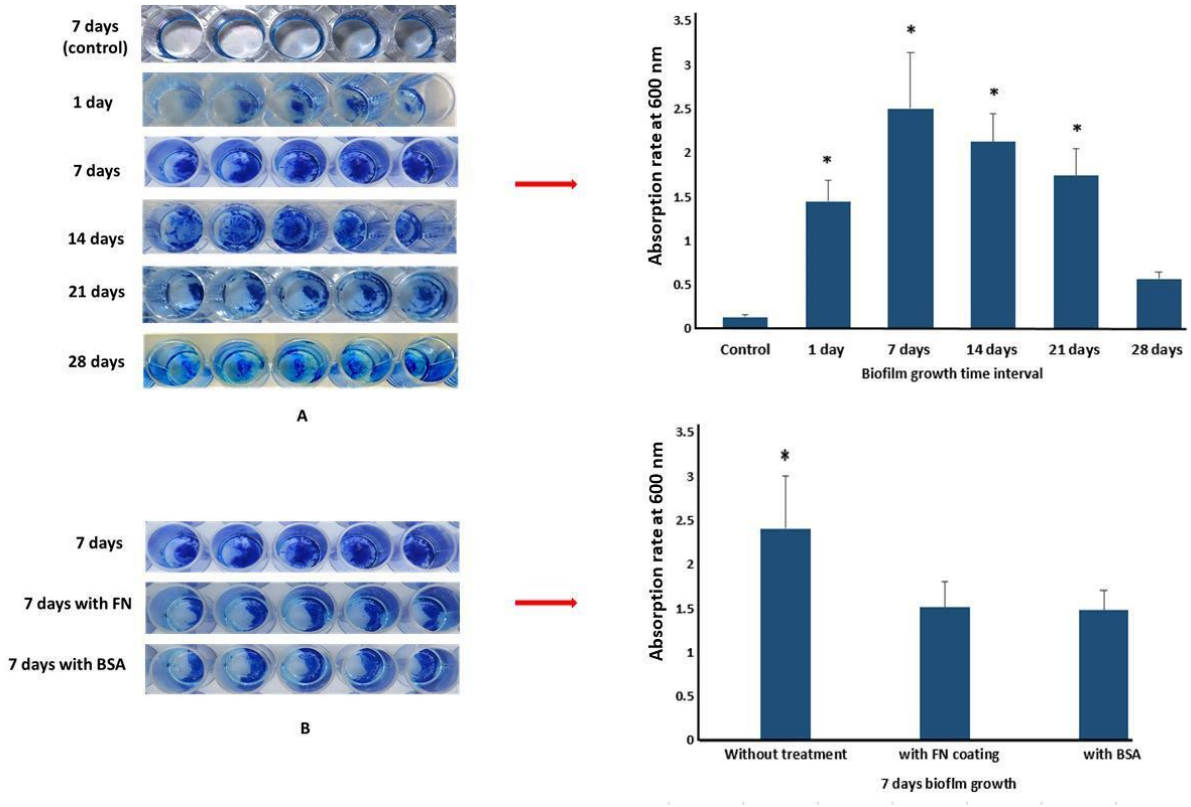

* = $p \leq 0.05$

Figure 29: Biofilm growth assay. 24-wells tissue culture plate (left) shows the biofilm stained with methylene blue following different growth time intervals (A) and treatment proteins (B). Bar charts (right) show the amount of biofilm following different time intervals (A) and different treatment proteins (B). ANOVA and LSD tests were applied for significance difference ($p \leq 0.05$).

3.3.7. Biofilm growth in relation to serum albumins

The amount of biofilm decreased following 7 days of incubation in tissue culture plates, which were coated with 20 µL of 5 µg/mL fibronectin or following the inoculation of 20 µL of 3 % (g/mL) BSA. The differences were significant when both protein effects were compared to the 7 days biofilm culture without treatment (Figure 29). The difference between biofilm absorbance values of 1.6 and 1.5 following fibronectin and BSA protein treatment respectively were statistically non-significant.

3.3.8. Biofilm growth on RP materials

SEM images showed a successive biofilm development on all material surfaces (Figure 30). The density of growth was approximately similar between resin materials (*i.e.* Accura and EX200). There were dispersed masses of mature biofilm composed of bacteria embedded in a large amount of biofilm matrix with scattered individual bacteria. The density of the biofilm was higher on dentine than that on the resin materials with no statistical difference ($p > 0.05$). The visual analysis showed that the dentine biofilm have minimum or no ESP matrix in comparison to obvious amount of biofilm matrix surrounding bacterial cells on resin materials. The statistical analysis revealed a higher mean value for biofilm on dentine surface followed by EX200 and Accura surface s respectively (Figure 30). The single factor ANOVA test revealed a non-significant difference ($p = 0.322$) between groups.

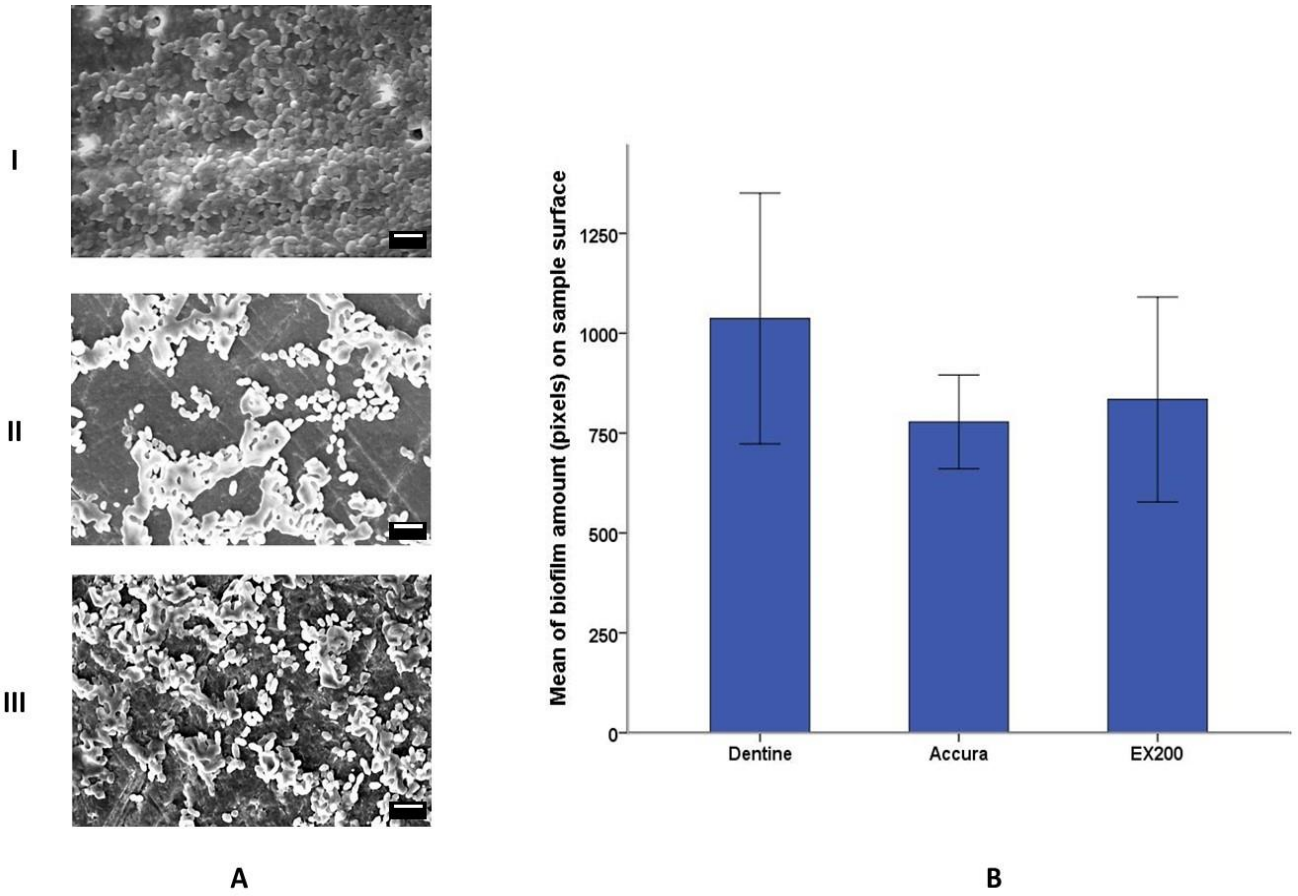

Figure 30: Biofilm growth on different materials. (A) Scanning electron microscope evaluation of biofilm generated by E. faecalis over 7 days incubation period on dentine (I), Accura (II), and EX200 (III) material surfaces. (B) A bar chart with SE bars demonstrates the mean differences of biofilm on material sample surfaces. ANOVA and LSD tests were applied for the statistical analysis. The scale bar represent 4 µm

3.3.9. Biofilm adhesion on the Accura and dentine surfaces

Topographic 3D AFM images with average height histograms, before and after load applications of 5 nN and 25 nN, were demonstrated herein as representative for the whole test results (Figure 31). Four bacterial species can be seen, in each image, embedded in the biofilm matrix. However, the biofilm appears higher on Accura surface compared to the dentine surface.

The five applied forces produced approximately comparable changes on the biofilm grown on dentine and Accura surfaces. Image observation showed that all forces failed to detach the biofilm from samples (Figure 31). The forces have removed the superficial layer leaving the four bacterial species in their original position. However, the scratching of the superficial layers was more intense with increasing load and that such result was more prominent after the application of 25 nN.

At many areas of the graphs, the after-load histogram showed a decreased height frequency compared to the before load one. However, histogram distribution remains approximately similar at both situations.

5 nN load

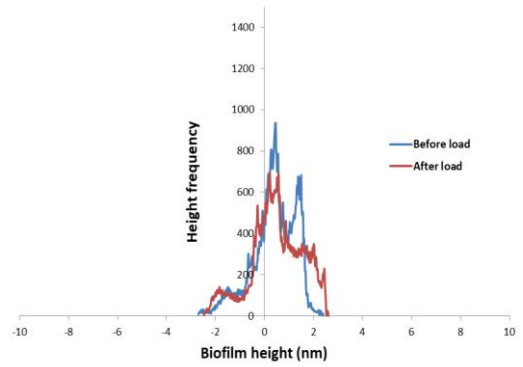

A. Biofilm height-histogram on the dentine surface

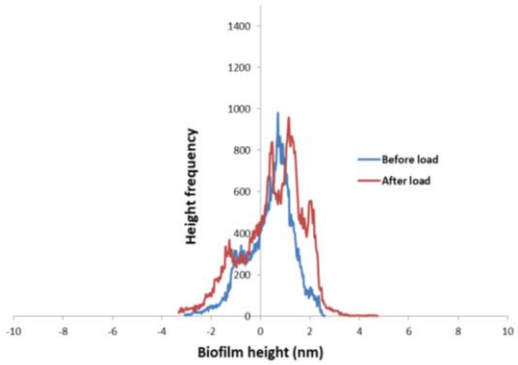

B. Biofilm height-histogram on the Accura surface

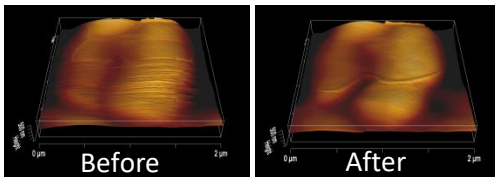

C. 3D images of biofilm on the dentine surface

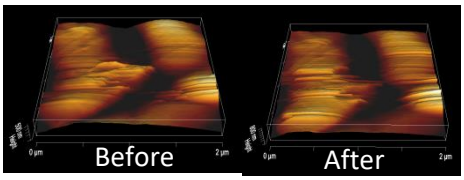

D. 3D images of biofilm on the Accura surface

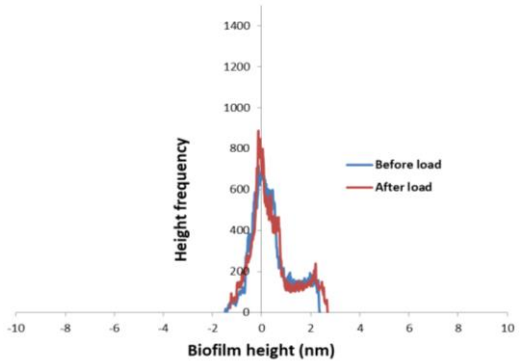

E. Biofilm height histogram on the dentine surface

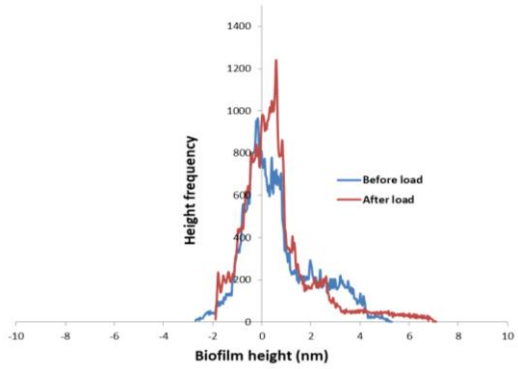

F. Biofilm height histogram on the Accura surface

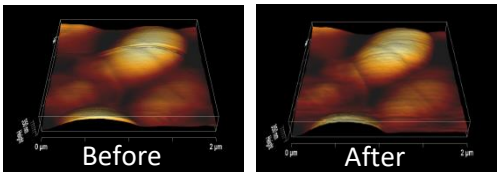

G. 3D images of biofilm on the dentine surface

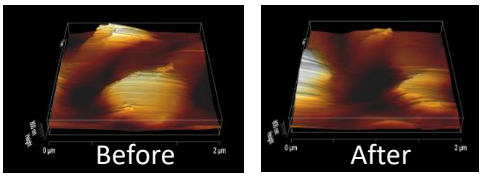

H. 3D images of biofilm on the Accura surface

Figure 31: Biofilm adhesion test. The results of the AFM adhesion test before and after load application on biofilm generated on dentine and Accura material surfaces. The effect of minimum (5 nN) and maximum (25 nN) loads were represented with histograms (A, B, E, and F), and with three dimensional images (C, D, G, andH).

3.3.10. The physical root canal system model

The model parts were included transparent simulated RCS halves and a white cubic frame (Figure 32). The physical measurements made with a vernier calibre showed that the model parts have the same xyz dimensions (± 0.2 mm) when compared to the computational model dimensions (Table 7). The RCS fitted precisely within the cubic frame using a moderate finger pressure. In addition, it can be readily removed from the frame using a moderate pushing force with a stainless-steel tweezer nozzle. Slight variations appear between spatial measurements of model halves regarding the surface area, volume and number of meshing triangles as shown in Table 6.

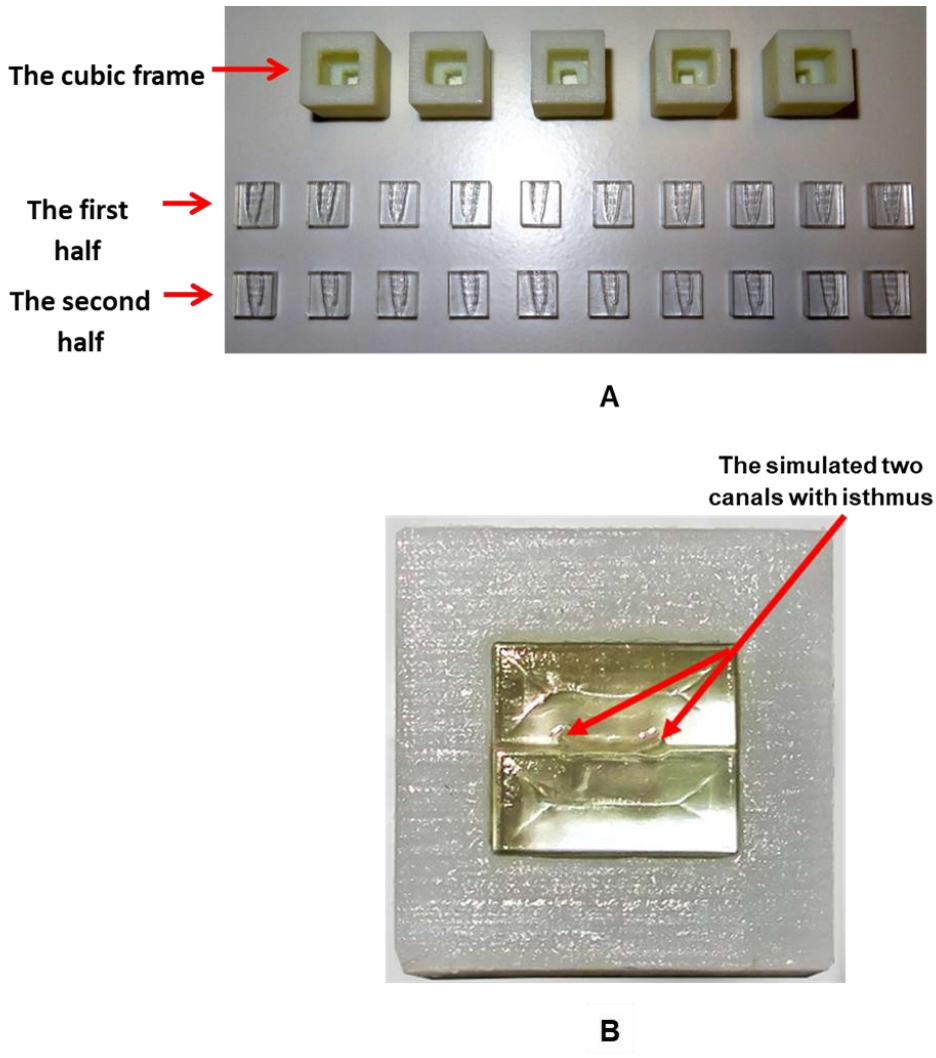

Figure 32: Parts of the root canal model. (A) Five cube-shape frames with external dimensions of 15 mm x15 mm x 15 mm, the first and the second root canal halves with dimensions of 9.5 mm length, 8.2 mm width x 3.5 mm thick. (B) Assembled model where the simulated root canal halves were assembled precisely within the cubic frame using finger pressure.

3.4. Discussion

3.4.1. Creation of the computational model

The results showed generation of an accurate 3D root canal system model using ImageJ and Netfabb software. For medical and dental model generation, variety of medical image processing programs were used in conjunction with different mesh correction programs, such as Mimics with Magics RP (Hieu et al., 2005), OsiriX with MeshLab (Frame and Huntley, 2012), and VGStudio with ABAQUS (Bonessio et al., 2017). In the current study, ImageJ with Netfabb were used to generate the root canal system model because both software programs have open sources that can be downloaded to the standard computers. In addition, the ImageJ is one of standard tools for the image processing and analysis in medical and dental fields for several years. This has provided valuable shared experiences between research students about the use of such software. This available knowledge supported the current procedure undertaken.

3.4.2. Surface hardness

The surface hardness of the tested resin material was significantly lower than root dentine. Although, the resin-based simulated root canals were scratched with 50 % of the forces required to scratch the dentine surface, no significant canal transformation was recognized after shaping in comparison to the natural canal (Lim and Webber, 1985a). This has validated the use of resin-based samples for the evaluations of instrumentation techniques (Schäfer and Florek, 2003, Dadresanfar et al., 2017).

However, the differences in the material structures between dentine and resin may result in differences with weight, size, and density of the debris particles. This could produce variation in the flushing performance of an irrigant when it is introduced into natural canals compared to the simulated root canals. Therefore, further future studies seem to be required to improve the hardness of the simulated root canal samples. For example, Many resin-based composite materials, such as VLink II (Nexus and Variolink, Schaan, Germany) and CV DuoCem (Colténe, Sussex, Germany) restorative materials have VHNs (45 – 60) similar to the VHNs of root dentine (Hofmann et al., 2001, Qing et al., 2006, Kazemipoor et al., 2017). Such materials can be modified to produce simulated root canals with comparable hardness values to the natural root canals. Unfortunately, these materials are currently not used by the RP technology to produce physical models.

3.4.3. Refractive index (RI)

The RIs of the resin based materials in the current study agree to the RI (mean = 1.548) of the clear unfilled cured resin of bisphenol A glycidyl methacrylate (Miletic et al., 2017) and to the RI (mean = 1.53) of the clear unfilled Bisphenol A epoxy resin (Tao et al., 2013).

With the polychromatic light source, the RIs of Accura and EX200 resin based materials have approximately matched the RI of the standard glass slide. Therefore, minimal or no image aberration could be seen if root canal samples are manufactured of these materials and evaluated directly or through a glass slide by an optical microscope. Mediums with close RIs should produce a similar angle of refraction on the penetrating light rays (Hell et al., 1993). This minimizes the effect of the spherical aberration phenomenon that attenuate light

intensity and hence resolution depth of the scanning procedure especially in confocal microscopy (Fouquet et al., 2015, Boothe et al., 2017). In addition, the default angular aperture of the objective lenses was set in accordance to light rays reflected from medium with RI of 1.5.

3.4.4. Contact angle measurement (surface wettability)

Both the resin based materials showed a contact angle less than 90^{o}. Thereby, they have a wettable surface criterion that reflects a suitable surface free energy for interaction with the aqueous culturing medium of bacterial species (Absolom et al., 1983, Minagi et al., 1985). The estimated degree of the contact angles lies within the estimated range for the resin based materials in other research (Namen et al., 2011, Syakur and Sutanto, 2017). The dentine surface showed significantly less wettability (larger contact angle) value compared to the two resin base materials. These finding disagree with Mohmmed et al., (2017a) who found the unpolished dentine shows more wettability (smaller contact angle) compared to the polished Accura material. This may be not surprising as the contact angle of dentine is positively related to the degree of surface polishing where it increases with the increased polishing degree (Wege et al., 2003). However, among studies, there is a wide variation (36.1^{o} to 75.4^{o}) in the estimates values of the contact angle on the dentine surface (Al-Omari et al., 2001, Mohmmed et al., 2017a). This is probably related to the variation in the exact time at which the contact angle is measured. After dispensing, the droplet has a subsequent relaxing time accompanied with a subsequent decrease in the contact angle value (Osti et al., 2009).

3.4.5. The biofilm growth assay

In addition to its common presence in root canal infections, *E. faecalis* is selected to generate mono-species biofilm due to their expected ability to adhere and generate biofilm on dentine and plastic surfaces by different adhesins on the bacterial cell wall. The mono-species biofilm can also simplify the immunofluorescence testing procedure because it requires a single antibody to label a single type of bacteria. To determine the optimal growth period, the *E. faecalis* biofilm was monitored over five time intervals. Bacterial incubation was performed at 37^{o}C in the CO_2 to ensure a humidity of 100% and to avoid dehydration of the culture medium. The bacteria showed a distinct ability to generate biofilm within 24 hours, which is consistent to several studies (Toledo-Arana et al., 2001a, Dale et al., 2017). The build-up of the biofilm mass continues in the first seven days then begins to decline gradually with a minimal mass observed at day 28 of growth. Floating parts of biofilm mass were obvious at 14, 21, and 28 days of time intervals during washing procedures. These parts could be sloughed during the dispersal phase of the biofilm (Chua et al., 2014) with failure of the dispersed bacteria to generate a new biofilm colonies in a limited sized well. These results seem consistent with results of Kishen et al., (2006) where same *E. faecalis* species biofilm showed a decreasing density in a 4-weeks period. The authors also found that the majority of bacterial cells were dead after four weeks of biofilm maturation as distinguished by the Live/Dead BacLight test.

3.4.6. Biofilm growth in relation to proteins

Many studies have advocated the coating with fibronectin or the inoculation of the BSA to improve bacterial attachment to material surfaces (Lyte et al., 2003, Christner et al., 2010).

In the current experiment, the biofilm values were decreased with fibronectin coating and BSA inoculation. The bacterial species used might lack the Enterococcal fibronectin-binding protein A (Efbp A), which is normally detected on certain *E. faecalis* genotypes, such as TX5707 (Singh et al., 2015). The deletion of such protein has significantly reduced the adhesion of the *E. faecalis* to fibronectin containing tissues. It has been confirmed that serum proteins, such as BSA, adsorb to the wall of polystyrene tissue culture plate (Parhi et al., 2010). This adsorption could prevent the direct adhesion of *E. Faecalis* to the tissue culture plate wall hence decreasing the opportunity for developing more biofilm amounts.

3.4.7. Biofilm generation on rapid prototyping materials

With the static culturing environment, the *E. faecalis* succeeded to generate a uniform biofilm layer on the material surfaces with similar biofilm density to that seen on the dentine. The results agree with Mohmmed et al., (2017a) who found that both dentine and Accura materials are favourable surfaces for the *E. faecalis* biofilm. However, there is no knowledge about using the EX200 as a substrate for biofilm generation. In endodontic research, *E. faecalis* strains show a recognizable ability to generate biofilm on natural and simulated root canals (Beltes et al., 2017, Bitter et al., 2017, De Meyer et al., 2017). This seems justifiable due to the presence of many adhesins, such as AS and Ace, on the bacterial surface that support their adhesion to biotic and abiotic surfaces (Madsen et al., 2017).

The biofilm structure was different on dentine compared to the resin-based materials. A deficient amount of EPS was recognized on dentine in comparison to the rich EPS on Accura

and EX200. It has been concluded that *E. faecalis* biofilm density and structure are affected by the chemistry of the substrate material (Sénéchal et al., 2004).

3.4.8. Evaluation of biofilm adhesion using the AFM.

At a nanoscale, the different load applications by the AFM cantilever revealed similar adhesion integrity between the dentine and Accura surfaces. The maximum load applied (25 nN) was not sufficient to remove the biofilm on both materials. The adhesion of *E. faecalis* biofilm to the dentine surface finished with 4000 carbide paper was found to be 0.4 nN after 14 hrs growth (Kishen et al., 2008). Adhesion increases with increasing age of biofilm due to further bacterial aggregation and accumulation of EPS (James et al., 2016). Surface chemistry of medical-grade polymer has a recognized effect on *E. faecalis* adhesion following increasing lateral forces applied with the SiNi cantilever. A lateral force of 19 nN was required to detach *E. faecalis* from polyurethane medical material after overnight culture of 18-20 hrs (Sénéchal et al., 2004).

3.4.9. Physical modelling of the novel RCS model.

The method of RP used has produced accurate physical RCS samples with the same spatial dimensions (± 0.2 mm) of the computational model. In addition to the Vernier calibration, the accuracy was manifested by the reproducible seating of the printed root canal halves within the printed cubic frame. The results are consistent to the results of (Khalil et al., 2016) who found that RP printers have produced teeth samples with very similar dimensions to their computational model.

3.5. Conclusions

The evaluated materials were validated to support generation of RCS sample for assessment of biofilm removal following root canal preparation. The surface wettability of the resin materials appeared better than root dentine. There was a uniform bacterial growth on both materials which was comparable to the bacterial growth on the dentine surface. However, the material toughness was inferior to dentine based on hardness values

At the nanoscale forces, the adhesion of the biofilm to the Accura surface was similar to the biofilm adhesion on the dentine surface and the material can be used to test the biofilm removal with mechanical means. Both materials can be used under optical imaging without producing aberration to the acquired images even when the classical glass slide used to support the material on a microscopic stage.

The use of microtiter method is a reliable and reproducible method that supported biofilm growth for a seven days period. However, coating the material surface with BSA and FN caused remarkable reduction in the biofilm mass.

The modelling of a RCS with complete isthmus was achievable when ImageJ and Netfabb images acquired with the microCT scanner were used. Accurate root canal samples are generated by the RP technology using the SLA printers and the Accura material within a short period and at a cost effective price. Based on the discussed findings, the null hypothesis was rejected.

CHAPTER FOUR:

MEASUREMENT OF BIOFILM FOLLOWING ROOT CANAL SYSTEM INSTRUMENTATION

4.1. Introduction

This chapter discusses the effectiveness of biofilm removal using asymmetric rotary file systems and different irrigation protocol with confocal laser scanning microscopy (CLSM).

The direct visualization and accurate quantification of the adherent bacteria following root canal preparation remain a significant challenge in endodontic research. The use of culture methods for quantification of colony forming units (CFUs) are selective to the site of sampling without giving information about morphology and the spatial distribution of the microorganism of the whole canal volume.

The application of a fluorescent marker to a biofilm renders the biomass to be visible by fluorescent microscopes such as epifluorescent and confocal microscopy. The use of CLSM to detect fluorescent dyes on labelled microorganisms has been shown to be an effective tool for quantification of single or multiple species biofilms, such as *E. faecalis* biofilm, or *S. oralis*, *E. sanguinis*, and *A. naeslundii* biofilms (Albuquerque et al., 2017, Bukhary and Balto, 2017, Hoedke et al., 2017, Nair et al., 2017).

In immunofluorescent technique, specific IgG probes anneal to their complementary proteins on the target bacterial cell without the need for bacterial lysis (Bergmans et al., 2005). The fluorescent dye is chemically conjugated to an antibody. The conjugation of the fluorescent dye is either direct to the primary antibody or indirect where the dye is conjugated to a secondary one (Moter and Göbel, 2000b). Although additional step used in the indirect method adds complexity to the staining procedure, it is cost effective and provides high intensity signal compared to the weak signal from the conjugated primary antibody (Immunolabeling. 2014).

The *in situ* indirect immunofluorescence (IIF) technique is used in microbiology for the identification of the bacterial species within their natural environment (Morimoto et al., 2008). The combination of the immunofluorescence method with confocal microscopy has successfully been used for direct identification of bacterial species in infected root canals (Morimoto et al., 2008, Peciuliene et al., 2008). The researchers found that the immunofluorescence method was useful to quantify the number of bacteria that were present in slices rather than the whole canal. Therefore, this chapter considers the developing of an approach to quantify biofilm along the whole canal with indirect immunofluorescence as this avenue of research has not been undertaken in detail.

Aim:

Quantification of biofilm in simulated root canal samples with a complete isthmus following instrumentation with different file systems, and following different irrigation protocols using the *in situ* IIF technique.

Hypothesis:

There is no difference in removing biofilm from root canals by different file systems and different irrigation protocols when measured by the *in situ* IIF technique.

Objectives:

1. To produce identical RCS samples using SLA printing technology.
2. To evaluate the labelling efficacy of polyclonal primary and secondary antibodies on *E. faecalis* biofilm.

3. To generate the *E. faecalis* biofilm on the root canal surface using the microtiter plate method.

4. To test the efficiency of canal instrumentation with PTU, PTN, and RS rotary file systems; and irrigant agitation with sonic and ultrasonic tips on removing biofilm from the RCS.

4.2. Materials and methods

4.2.1. Evaluation of the *in situ* IIF technique protocol

Thirty sterile and surface-treated rounded plastic coverslips (Thermo Fisher Scientific, Rochester, USA) of 13 mm diameter were placed in 24-wells tissue culture plate keeping their treated surfaces upwards. Small part of the coverslip margin was bended slightly with a sterile tweezer to facilitate handling. The coverslips were then cultured for 7 days with *E. faecalis* using the microtiter plate method. Each coverslip was placed in a well where the treated surface faced the tissue culture plate lid. Each well was then inoculated with 2 mL of the diluted culture of *E. faecalis* and incubated in an aerobic environment for 7 days at 37^{o}C in the 5 % CO_2 incubator. The culture was replenished every 48 hr with 1.8 mL of fresh BHI broth. After the desired period (7 days), samples were washed twice with 2 mL of a sterile PBS buffer for 3 mins each and fixed for 10 mins with 2.5 % glutaraldehyde. The fixed samples were then washed as previous.

A blocking buffer was prepared to block non-specific sites on the coverslip, such as surfaces that were not covered with the biofilm. This was aimed to prevent the non-specific deposition of the fluorescent dye, which could produce undesired background during image acquisition.

Three grams of BSA (Sigma Aldrich, St. Louis, USA) were dissolved for 1 hr in 100 mL of sterile distilled water at room temperature. The solution was filtered with a 0.22 µm pore size filter (Merck millipore, Cork, Ireland) for sterilization and removing undissolved BSA particles.

A polyclonal non-conjugated primary antibody (Rabbit anti *Enterococcus species*-MyBioSource, San Diego, USA) with a concentration of 4-5 mg/mL, and a polyclonal secondary antibody (Donkey Anti-Rabbit IgG H&L–Abcam, Cambridge, UK) with a concentration of 1 mg/mL were diluted each with the blocking buffer for five different concentrations (1/100, 1/200, 1/300, 1/400, 1/500). Aliquots of 1 mL each were kept in the fridge at 4^{o}C. The secondary antibody was conjugated to the tetramethylrhodamine isothiocyanante (TRITC) fluorescent dye (fluorochrome), which has excitation and emission spectrums of 547 nm and 572 nm.

Following biofilm fixation, samples were randomly divided into six groups (n = 5). Five groups were assigned for testing the IIF staining protocol while one group was left as a control without staining. For each corresponding dilution, 50 µL of the primary and secondary antibodies were applied sequentially on the biofilm using the 200 µL pipette in the biological safety cabinet. An overnight incubation (20 hr) in the fridge at 4^{o}C allowed the primary antibody to hybridize the *E. faecalis*. The samples were then washed for three times with 2 mL of the sterile PBS for 3 mins. This was followed by the application of 50 µL of the secondary antibody on the sample surface. The application of the secondary antibody was performed in a dark environment in the microbiological safety cabinet to avoid the depletion of the TRITC fluorescent dye. A period of sample incubation was allowed for the secondary antibody in the same incubation manner of the primary antibody. During incubation, the tissue culture plate was wrapped with an aluminium foil to maintain darkness. Samples were washed for three times as before, to remove unbounded secondary antibodies, and were left 1 hr to dry at room temperature in a new tissue culture plate. Thereafter, samples were kept in the fridge for 24 hrs until imaging by the CLSM.

During the imaging process, each coverslip was mounted on a glass slide without utilizing a mounting medium. The scanning parameters of the microscope were configured as shown in Table 9. Imaging was followed at magnifications of 5x, 10x, 20x, and 40x lenses at three places within each biofilm sample. A visual comparative analysis was performed for the quality of the acquired biofilm images among groups using Zen image processing software (Carl Zeiss, Oberkochen, Germany). The quality was assessed based on brightness, contrast, and resolution criteria. The fluorescent dye concentration, which produced the brightest biofilm image without affecting the contrast while maintaining a high resolution of bacterial species, was considered as appropriate for the current assay.

Table 9: The setting of CLSM. The setting criteria applied for CLSM parameters during the scanning procedure of the biofilm on the root canal surface. AF = auto-fluorescent.

	Scanning speed	Range (Frame)	Pin hole size	Gain master	Digital offset	Colour	Wave length (nm)
Track 1	3	2	54.2	732	0	Green (AF)	488
Track 2	3	2	54.2	732	0	Red (TRITC)	555

4.2.2. Validation of the potential reaction between irrigant solutions and the staining buffer

The following methodology was employed to examine the potential reaction between irrigant solutions (2 % CHX and 5 .25 % NaOCl) with the BSA blocking buffer or with the fluorescent dye.

To reveal the reaction with the blocking buffer, fifteen wells of a 96-well tissue culture plate were inoculated each with 100 mL of 3 % BSA using 200 mL micropipette. The wells were divided into three experimental groups (n = 5 wells for each group) according to the added liquid. A volume of 100 µL of distilled water was added to the control group whereas 100 µl of 2 % CHX and 100 µL of 5.25 % were added to the test groups. The wells were then observed over 5 mins period, at room temperature, for changes in the clarity of the BSA buffer. After that, 20 µL drops of the resulting reactions were deposited on glass slides. The drops were visualized by the CLSM at 5x lens.

To show the effect of CHX and NaOCl irrigants on the intensity of the fluorescent dye, 100 µL of each irrigant were added to 100 µL of the diluted (1/300) secondary probe, which is conjugated to the fluorescent dye, at room temperature in a dark environment. The test was performed using a 96-well tissue culture plate (n = 5 per group). A corresponding control group was prepared using the distilled water as a comparing liquid. The resulting liquids were then examined using the CLSM at 5x lens following 1 and 5 mins of the mixing time. Changes in the intensity of the fluorescent dye over the two periods were recorded as changes in the grey values using the surface plot algorithm operated by the ImageJ software. A square selection was applied on the entire image to plot the grey values for the tested groups. The plotting data were then saved to an excel sheet to estimate and compare the mean values between the two periods as shown in the result section (Figure 42).

4.2.3. Evaluation of the remaining biofilm

Biofilm development on root canal system samples:

Forty root canal samples were created by the Rapid Prototyping process and sterilized by an autoclave for 21 mins at 121^{o}C in plastic packaging. Root canal block halves were placed in the 24-well tissue culture plate based on one-half per one-well in a safety microbiological cabinet (Figure 33). Block surfaces that contained the root canal system were kept facing the tissue culture plate lid. Each well was then inoculated with 2 mL of a diluted (1/100) overnight culture of *E. faecalis* in BHI broth. The culture was then incubated for 7 days at 37^{o}C in the 5 % CO_2 incubator.

The culture medium was replenished regularly at a rate of 1.8 mL every 48 hrs (Figure 33). After the desired period (7 days), samples were randomly divided into four groups (n=10) including one control group, which was left without instrumentation, and three test groups. Samples were then washed with a sterile PBS (pH = 7.4 ± 0.05) for three times of 3 minutes each. Biofilm fixation was then followed for 10 mins at room temperature using 1 mL of 2.5 % glutaraldehyde. The fixative buffer was then washed for three times of 3 mins each.

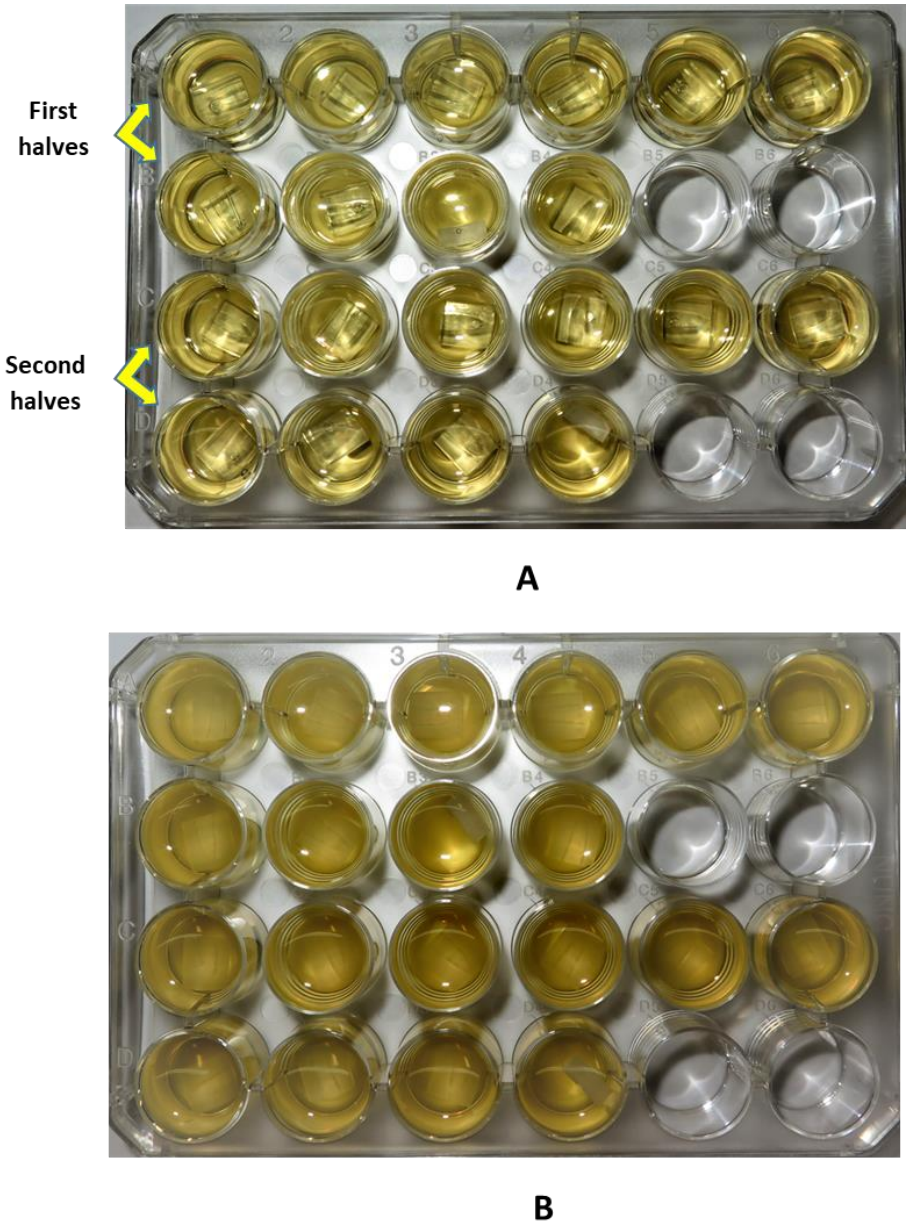

Figure 33: Photographs show the culturing process of the root canal system model in 24-well tissue culture plates. (A) The model halves seated in the culturing wells and inoculated with 2 mL of the culturing medium. (B) The same culture following 48 hrs of aerobic incubation with turbidity indicates bacterial growth.

Root canal preparation:

In the control group (Group 1), samples were left without preparation and labelled immediately after biofilm fixation and washing procedures. For the test groups, the simulated root canal halves were assembled in the polypropylene cubic frame. The root apices were sealed with a red wax to create a closed endodontic system (Figure 34). The model was then stabilized under firm finger pressure during root canal preparation.

Sample instrumentations were achieved using three rotary file systems as follow:

1. Group 2: The ProTaper Universal (PTU) system,
2. Group 3: The ProTaper Next (PTN) system,
3. Group 4: The Revo-S (RS) system.

Canal patency was primarily established by size 15 hand K-file that is placed at the working length (9.5 mm). The rotary file instruments were operated with an endodontic handpiece attached to the Waveone motor (Dentsply Maillefer, Ballaigues, Suisse) powered at 300 rpm speed and 4 Ncm^2 torque. Files were advanced gently within the canal using short amplitudes, approximately 3-4 mm, of vertical (crown-down) brushing motion. The motion was applied against the canal wall to enlarge and flare canal diameter until reaching the canal terminus. For PTU, the SX instrument was used to flare the coronal third of the canal. Consequently, S1 and S2 instruments used to flare the middle and apical thirds respectively. Canal then finished with F1 instrument to the working length. The instrumentation with the PTN was started with SX instrument to flare the canal coronally. Thereafter, X1, and X2 instruments were used to shape the middle and apical thirds respectively. The X3 instrument was applied as the master apical file to finish the canal shape.

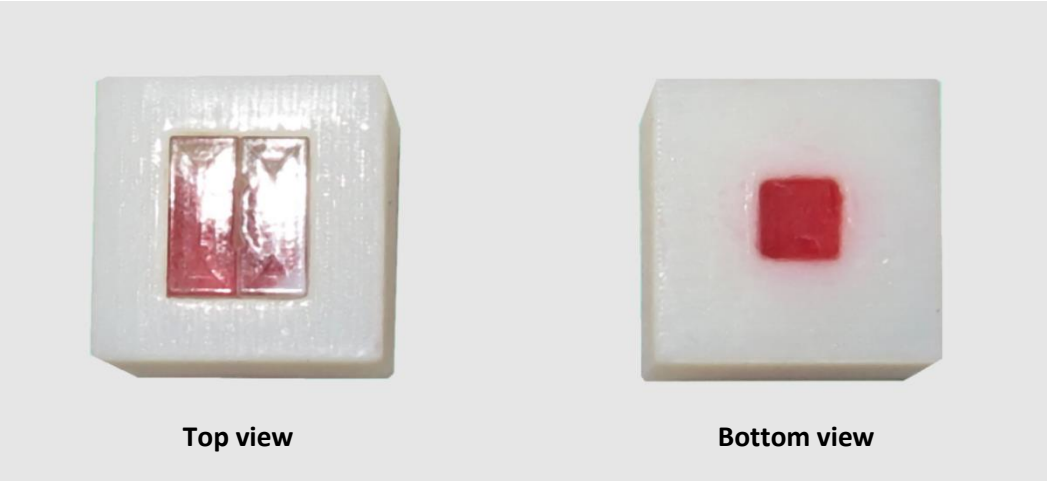

Figure 34: Sealing the apex with red wax. A photograph shows the top and bottom views of the RCS model with a red wax to close the root canal apices.

The coronal and middle thirds of the RS group were shaped with SC1 file. The SC2 was used to shape the canal at the apical third while the SU file has smoothen the resulting canal shape. The AS30 was applied as the last instrument to produce the final canal shaping at the apical third.

Five mL of 2 % chlorhexidine digluconate (CHX) solution was used to irrigate each canal (*i.e.* 10 mL for each root canal sample) throughout the instrumentation procedure. During each file-instrumentation, 1 mL was used to flush the canal using the Monoject hand syringe with needle. The irrigation solution was introduced at a flow rate of approximately 0.1 mL/sec while keeping the needle vent always toward the isthmus opening. The irrigating needle was prevented from binding to the canal wall by short amplitudes of up-and-down motion. A single trained operator (Author) undertook the procedures to control the flow rate. Training included discussion and undertaking 50 procedures in the same manner with supervision.

After root canal preparation, the sample halves were gently removed using stainless steel tweezer nozzles. Samples were then washed gently with PBS (pH 7.4 ± 0.05) for three times of 3 mins each to remove debris and remnants of irrigant solution. Thereafter, IIF staining was performed immediately for each half.

Biofilm labelling with the *in situ* IIF stain:

A volume of 50 µL of the diluted (1/300) unconjugated primary antibody buffer was initially applied on the root canal surface and incubated overnight (20 hrs) at 4^{o}C to label the *E. faecalis* biofilm. After that, samples were washed for three times of 3 mins each. Application of 50 µL of the diluted (1/300) secondary probe on the root canal surface was completed in a dark environment at room temperature. Samples were then incubated overnight in a dark environment at 4^{o}C. The excess secondary probes were then removed by

washing with PBS. Sample drying was performed for 1 hr in the dark in a new tissue culture plate at room temperature followed by 24 hrs incubation at 4°C until the imaging with the CLSM.

4.2.4. Evaluation of the remaining biofilm following irrigant agitation with sonic and ultrasonic tips

Twenty simulated root canal samples with biofilm were divided into two test groups (n=10) to evaluate two agitation systems following the instrumentation with the PTN system.

A total of 5 mL of 2 % CHX was introduced into each canal. However, there was an exception that after the last file instrumentation, each sample was mounted on a manual jack stage and bounded with a thick adhesive tape for stability (Figure 35). Irrigant, 0.5 mL, was then introduced into the canal at a rate of 0.016 mL/sec using a benchtop peristaltic pump (Watson-Marlow, Cornwall, UK). At this time, the irrigant was agitated for 30 sec with one agitation protocol. A passive ultrasonic irrigation (PUI) technique was performed using the Irrisafe file (IRR20/25, Acteon, St Neots, UK). The file was used in an ultrasonic handpiece (P5 Newtron XS, Acteon, St Neots, UK) set at a power of 7. The sonic agitation was performed using the EDDY irrigation tip (VDW, Munich, Germany) oscillating at 6000-Hz with a compressed air of 3 bars (Jun-Air, Bromsgrove, UK).

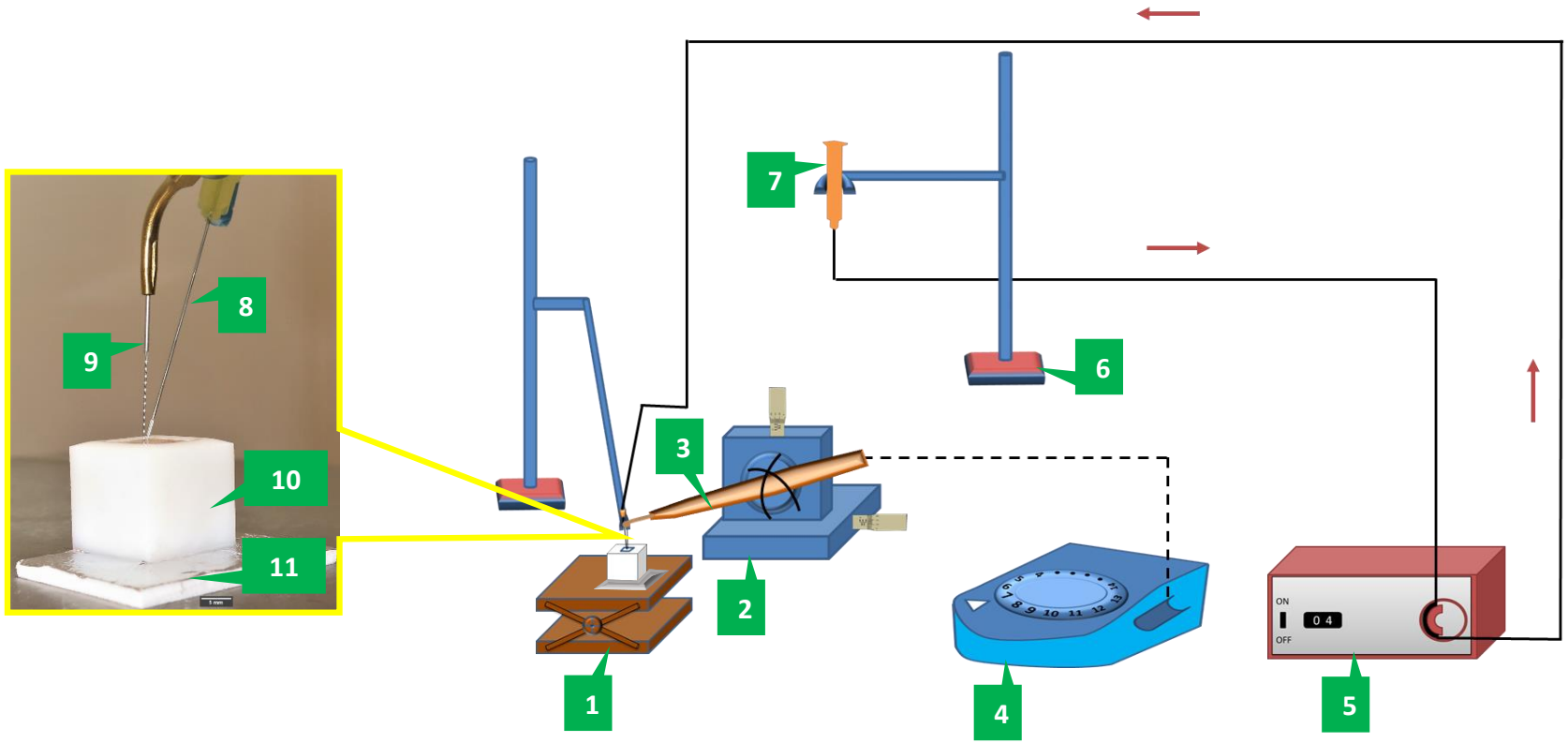

Figure 35: The assembly of the equipment during ultrasonic agitation. A diagram demonstrates the equipment used during introducing and agitation of 2% chlorhexidine digluconate using the piezo electric device. (1) A manual adjustable jack, (2) micrometre positioning stage, (3) Ultrasonic handpiece, (4) ultrasonic device, (5) peristaltic pump, (6) metal stand with clamp, (7) plastic syringe (20 ml) containing 2 % chlorhexidine digluconate, (8) Monoject needle, (9) the ultrasonic tip, (10) the RCS model, (11) adhesive tape. The arrows indicate the direction of the irrigant during pumping process between the syringe and the needle.

The tip was attached to a Sonicflex air scaler handpiece (Kavo, Biberach, Germany) connected to a portable dental unit (Kavo, Biberach, Germany). Both sonic and ultrasonic tips were inserted 1 mm away from the canal terminus.

A final flush was made with 0.5 mL of 2 % CHX with the Monoject hand syringe. To maintain a reproducible tip position between samples, the handpieces were mounted on a manual XYZ axis positioning stage (Thorlab, Ely, UK), which permits standard vertical and horizontal linear movements. The controlled vertical movement was used to insert the irrigation tips to the required working length, while the horizontal movement was used to move the tips between the two canals of each sample.

4.2.5. CLSM scanning and image processing

A special microscopic slide was customized to create standardized and reproducible method for the quantification of biofilm for the whole root canal system (Figure 36). A circular copper finder-grid (Agar scientific, Essex, UK) with 10 mm diameter was mounted onto approximately the centre of a standard glass slide (Menzel-Glaser, Braunschweig, Germany). The use of the grid was aimed to produce standardized biofilm images in term of size, and number. It had special guided patterns that were used to reproduce image positions during acquisition. The grid was fixed with clear glue (Mega-Fix, Iver, UK), applied carefully at the grid margin. A C-shape frame with right angles was cut from the previous polypropylene cubic frame. The cut frame was fixed on the glass slide to surround the copper grid as shown in (Figure 36).

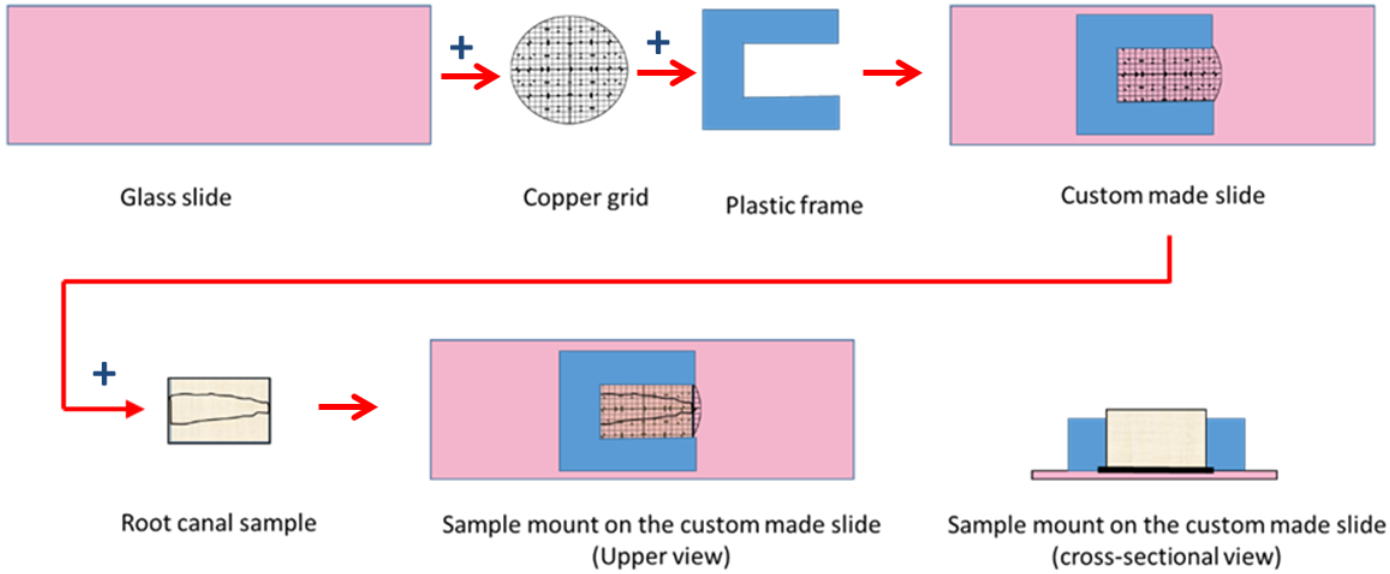

Figure 36: Fabrication of the glass slide for quantification of biofilm on the internal aspect of the root canal system. The illustration shows the sequence of assembling the special glass slide parts and the seating of root canal sample.

Such C-shape frame was aimed to create a precise and reproducible placement for the root canal samples during CLSM imaging. The midline of the grid was managed to be located approximately in the middle of the root canal. Due to geometric variations between the two halves of the root canal system, a customized slide was made for each half-set of samples. The slide was replaced once the copper grid looked contaminated with debris, as this interferes with laser light transmission and image resolution.

Sixteen images were acquired for each root canal including eight images per each root canal half (Figure 37). Each image included a square area containing four small squares in the grid. The number of images for each root canal third was distributed according to the canal third percentages in relation to the total canal volume as shown in (Figure 37). In addition, the inclusion of the isthmus and the main canal was considered during image allocations. Images were acquired with a 5x lens using the previous CLSM setting (Table 9) with pixel definition of 512 x 512 pixels. The cervical third was scanned initially followed by the middle and apical thirds.

The analysis was performed using the ImageJ software where a stack of eight images was manipulated. A square selection was applied to the region of interest to standardize image size (Figure 38). The stack was then split in to two colours. A red colour represented the biofilm whilst a green colour represented the root canal surface. The biofilm images were then filtered with the Unsharp-mask algorithm set at Mask weight of 0.8 and Radius of 3 to segment the biofilm pixels from the image background. The background was then removed using the subtract-math algorithm set at a value of 80.

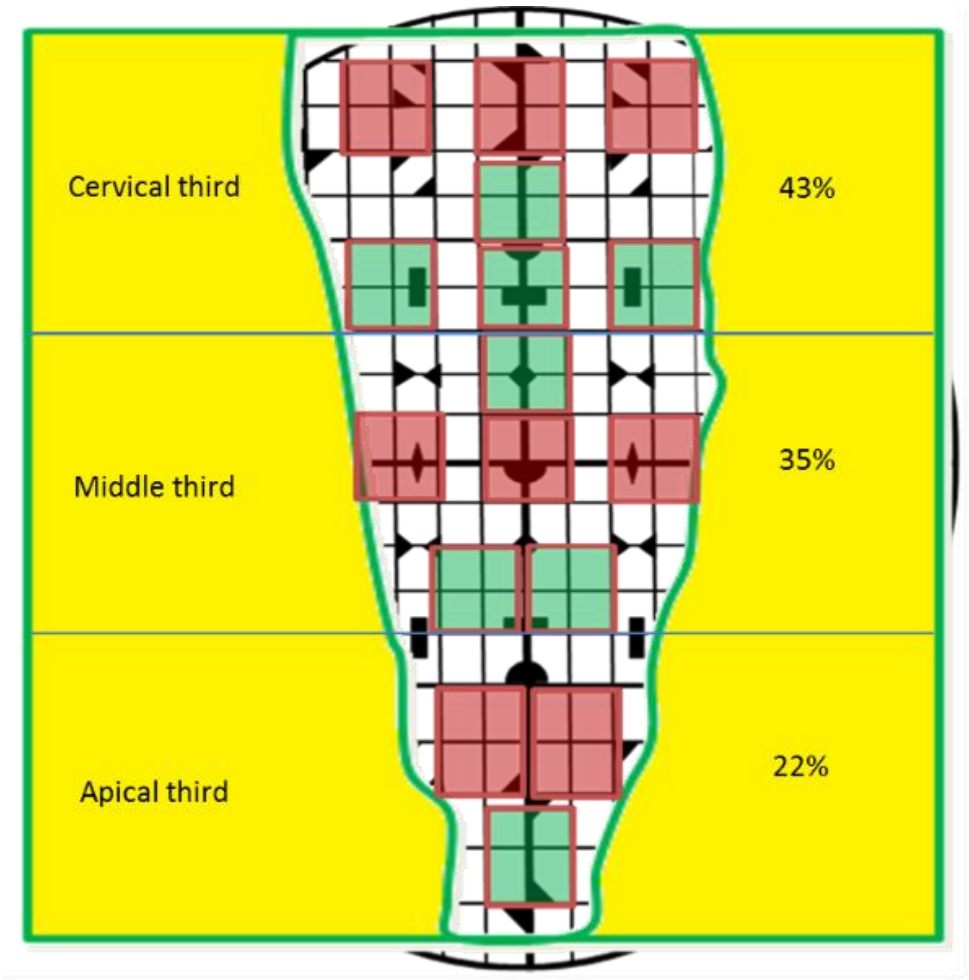

Figure 37: Biofilm quantification. An illustration shows the position and number of images acquired for the first half (red) and for the second half (green). Images were distributed in relation to the volume percentages of the root canal-thirds.

An automatic threshold application was followed on the biofilm pixels, which were then counted by the Voxel counter algorithm (Figure 38). For each group, the amount of the biofilm was quantified in the root canal. The amount of the biofilm was further classified according to each level of root canal thirds. The biofilm percentages in each canal third were estimated in relation to the corresponding group to show biofilm distribution and also to the untreated group to show the disinfection performance of each file system.

4.2.6. Statistical analysis

The distribution of data was explored by the Shapiro-Wilk normality test. Parametric tests including single factor ANOVA and the Post-Hoc LSD, were applied to compare data among groups. The statistical difference was set at $p \leq 0.05$. Bar charts (Figure 43, and Figure 46), plot chart (Figure 42), and statistical tables (Table 10, Table 11, and Table 12) were used to describe data means and percentages.

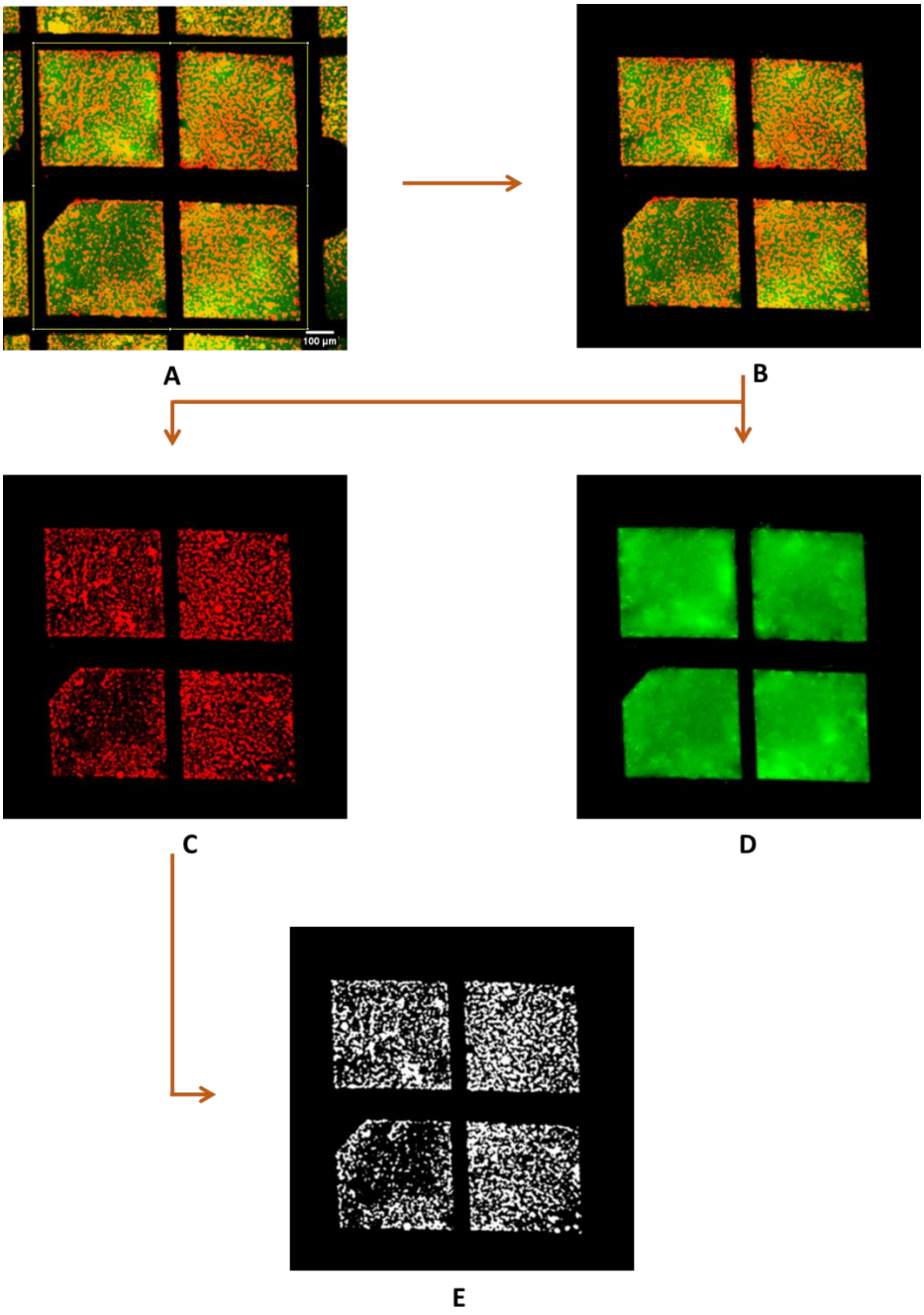

Figure 38: An image panel demonstrates the method sequence utilized for biofilm quantification by the ImageJ software. (A) The square selection is applied to the region of interest. (B) The outer-image was deleted. (C and D) Colours were split into red (biofilm) and green (root canal surface) images. (E) A threshold was applied to the biofilm image for quantification

4.3. Results

4.3.1. Biofilm labelling with *in sit*u IIF technique

The visual analysis revealed that the primary and secondary probes succeeded in hybridization *of E. faecalis*. The CLSM images revealed that a dilution factor of 1/300 produced the best image quality at different magnification according the evaluated criteria (Figure 39). The labelled E*. faecalis* were seen as single, double, or grouped in long chain with a distribution picture similar to the picture revealed by the bright-field image on the Stereomicroscope (Figure 40). It appears that the staining technique has involved the bacterial species alone because the EPS matrix was not visible in the acquired images. In the unlabelled control group, *E. faecalis* has not been detected by the CLSM despite the same scanning technique.

4.3.2. The potential reaction between irrigant solutions and the staining buffer

The observation of the tissue culture plate over 5 mins period revealed white precipitation developed after the inoculation of CHX to the BSA (Figure 41). The concentration of precipitation increased with time as indicated by the increased turbidity of the mixed liquid. The precipitates appear as an auto-fluorescent coagulation network when visualized by the CLSM at 488 nm wavelength using 5x lens (Figure 41). Conversely, no precipitates were seen following the inoculation of NaOCl. Instead, there was a yellowish discoloration, which becomes darker with increasing time. However, no changes were seen in the clarity of the BSA solution following the inoculation of distilled water.

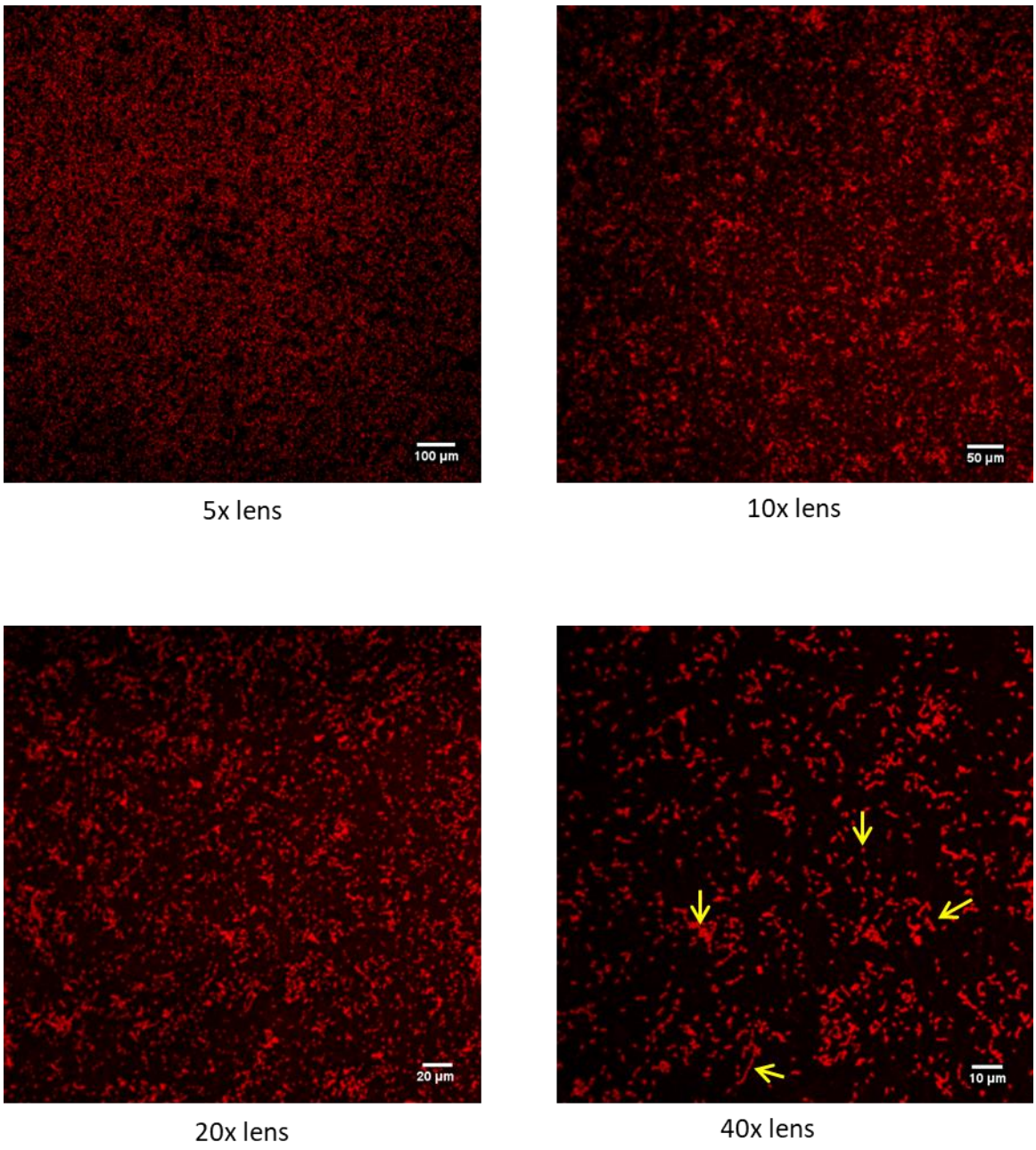

Figure 39: Visualization of biofilm labelling by CLSM. Confocal microscope images show the labelled *E. faecalis* biofilm (red) at four magnifications following 7 days growth period. Labelling was achieved using the IIF staining protocol at the dilution factor of 1/300. The bacterial species appear as single or aggregated in multiple forms (arrows) as shown by 40x lens image.

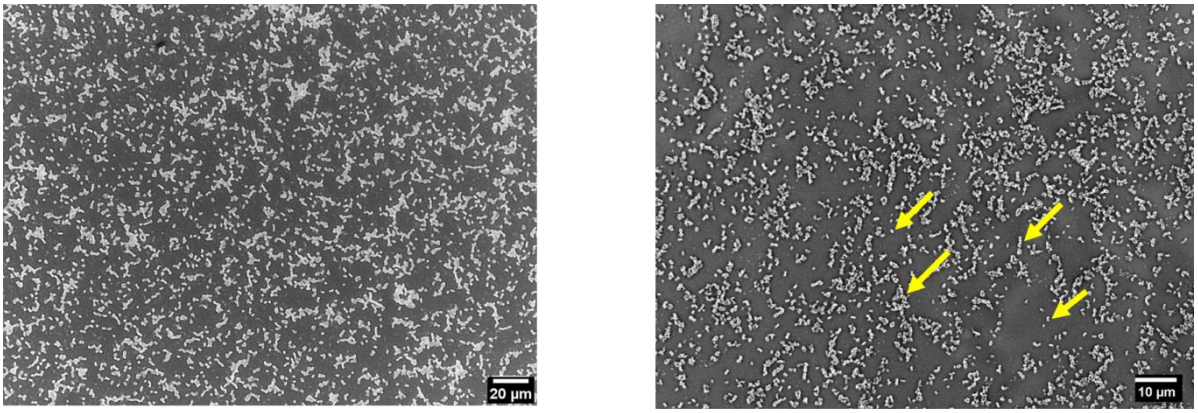

Figure 40: Visualization of the non-labelled biofilm by the Stereomicroscope. Bright-field images show the non-labelled *E. faecalis* biofilm following 7 days growth on cover slips at two magnifications. The arrows indicate the bacterial species that appear as a single cell or multiple form aggregations similar to their distribution in the labelled biofilm.

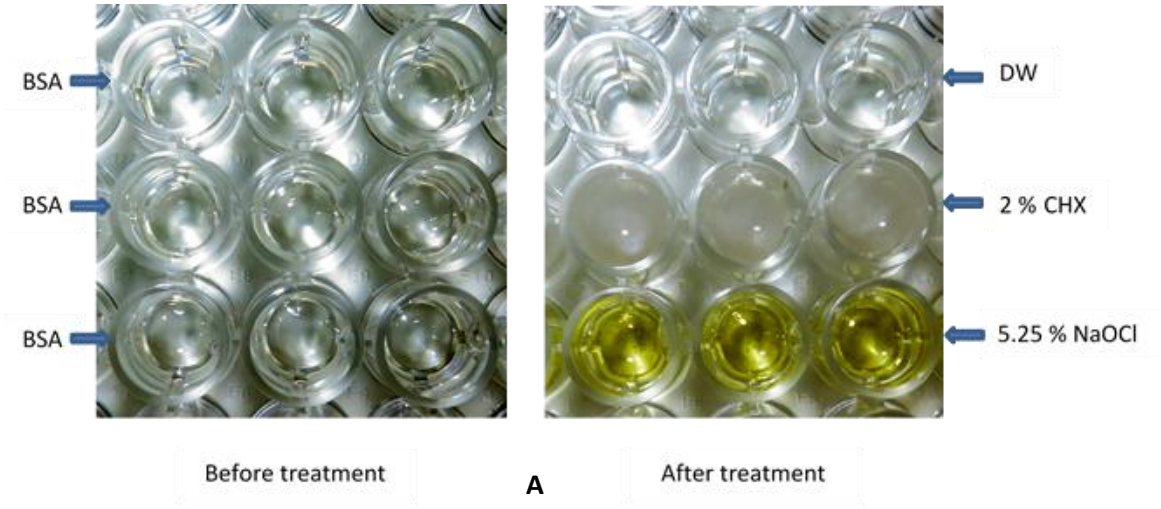

A

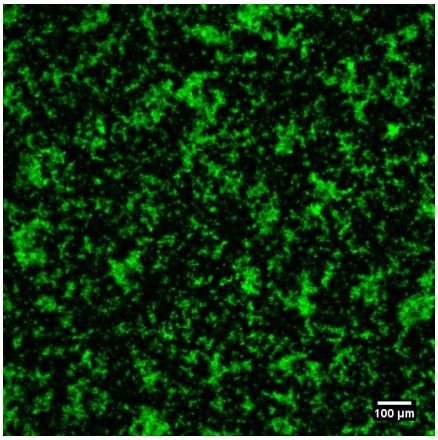

B

Figure 41: The reaction of the staining buffer with different irrigants. Photographs show the changes in the consistency and colour of the BSA buffer after the treatment with 2 % CHX and 5.25 % of NaOCl in 96-wells tissue culture plate. (A) White precipitates and yellowish discolouration can be seen following the inoculation of CHX and NaOCl respectively. (B) The auto-fluorescent white precipitates as seen by the CLSM at an excitation spectrum of 488 nm under 5x lens.

The effect of the irrigant solutions on the intensity of the fluorescent dye was demonstrated by the plot charts as shown in Figure 42. The inoculation of the irrigants to the fluorescent dye has significantly ($p \leq 0.05$) reduced the fluorescent intensity within 1 min in comparison to the control group. Minimal differences in the fluorescent intensity were seen in the CHX group within the 5 mins period. Conversely, the intensity value dropped to a zero value in the NaOCl group within 5 mins period. However, no difference or even minimal improvement in the fluorescent intensity was seen in the control group (Figure 42).

4.3.3. Remaining biofilm following instrumentation with asymmetric cross section files.

All root canal samples exhibited good control during the cutting procedures. Debris adhered to the flutes of the rotary files in a similar manner to the instrumentation of the natural root canal. The debris texture was in the form of grinded particles similar to that created during dentine shaving. The speed and torque applied was sufficient to achieve a smooth continuous taper without any concerns.

The three file systems produced a significant ($p < 0.001$) reduction in biofilm quantity when compared to the untreated (control) group as shown in Figure 43. The PTU, PTN, and RS file systems have removed 75 % (± 26 %), 73 % (± 11 %), and 85 % (± 8 %) of the biofilm quantity respectively in relation to the biofilm quantity of the untreated group. The difference was only significant ($p \leq 0.05$) between PTN and RS file systems.

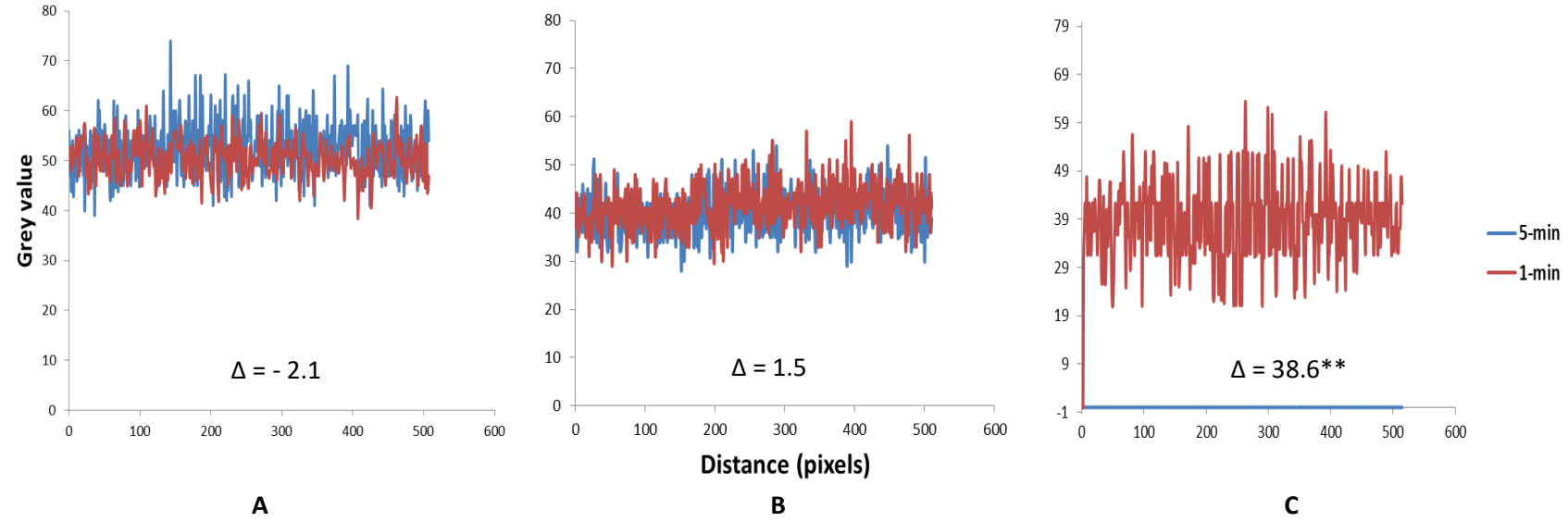

** = $p \leq 0.001$

Figure 42: Changes in the intensity of the fluorescent dye. Plot charts show the changes in the intensity of the fluorescetnt dye following 1 min and 5 mins of mixing with DW (A), 2 % CHX (B), and 5.25 % NaOCl (C). Δ = The difference between 1-min and 5 mins intensity mean values.

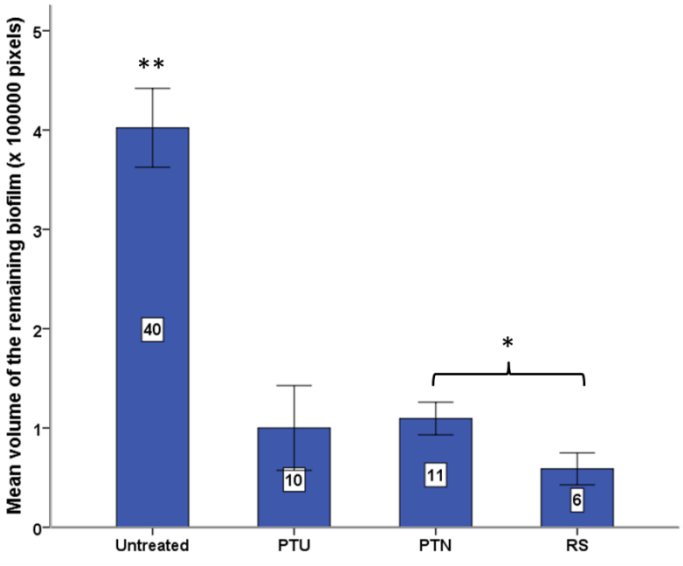

A

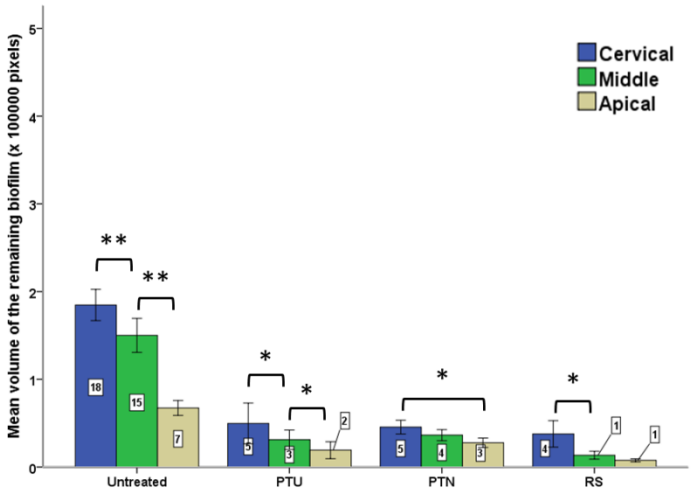

B

* = $p \leq 0.05$.
** = $p \leq 0.001$.

Figure 43: The remaining biofilm using the IIFA. Bar charts with SE bars that show the mean remaining biofilm in the simulated RCS for each group (A) and for each canal third (B) following the instrumentation with the three file systems. The biofilm percentages are relative to the untreated group. ANOVA and LSD tests were applied to compare means ($p \leq 0.05$).

The images showed that the biofilm in the main canal was almost removed (Figure 44). In the isthmus area, biofilm density was reduced rather than completely removed, except for the isthmus margins that lie close to the main canals where approximately total biofilm removal was achieved (Figure 45).

In the untreated (control) group, the larger amount of biofilm was found in the cervical third followed by the middle and apical third respectively. This pattern of biofilm distribution remains similar following the three treatment processes (Figure 43 and Table 10).

This difference was statistically significant ($p < 0.001$) among these thirds in the untreated group (Figure 43). However, the difference became non-significant between the middle and apical thirds for groups treated by PTN and RS systems.

Table 10: Distribution of biofilm percentages in root canal thirds. The mean percentage (± SD) of the remaining biofilm estimated in canal thirds following different instrumentation techniques. The percentages are relative to the total amount of the remaining biofilm in the corresponding group.

Groups	Untreated	PTU	PTN	RS
Cervical	46 % (± 3 %)	49 % (± 5 %)	41 % (± 6 %)	61% (± 16 %)
Middle	37 % (± 3 %)	32 % (± 5 %)	33 % (± 4 %)	24% (± 11 %)
Apical	17 % (± 2 %)	19 % (± 4 %)	25 % (± 5 %)	15% (± 7 %)

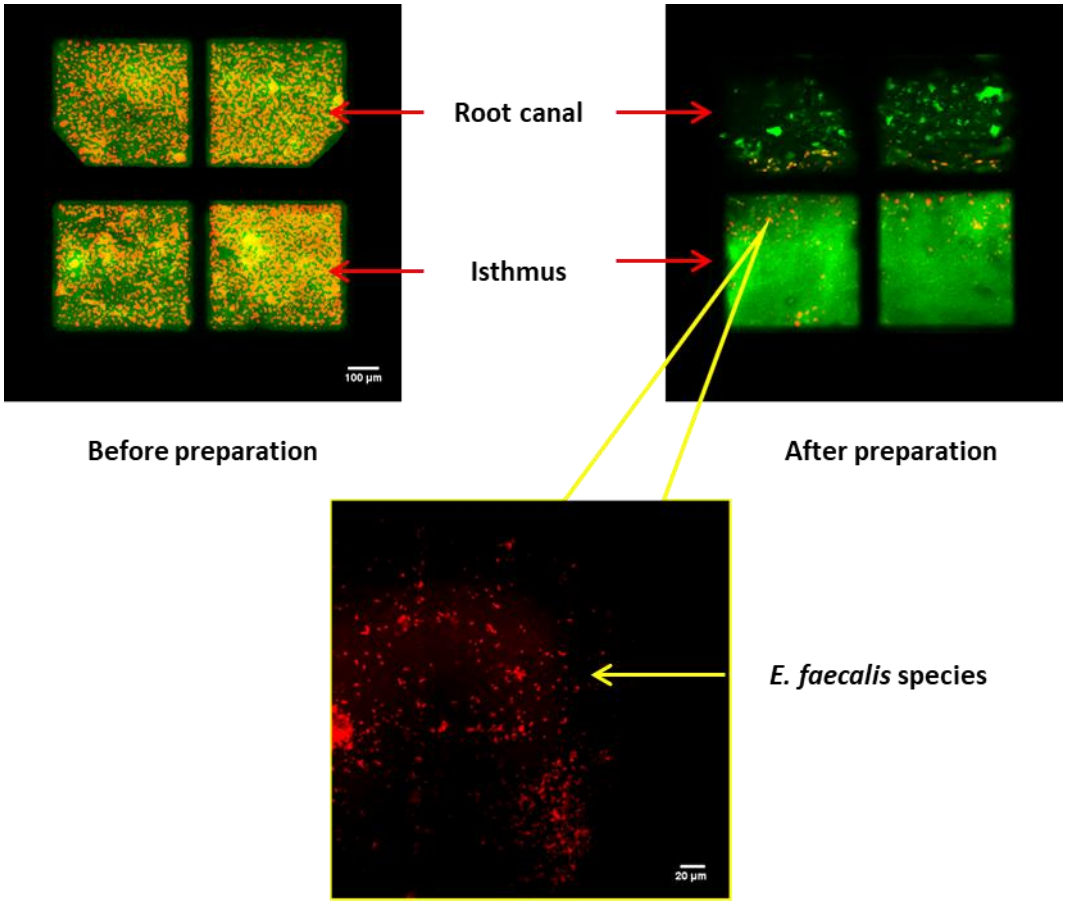

Figure 44: Biofilm removal in the main canal. Representative CLSM images demonstrate the labelled *E. faecalis* biofilm (red color) before and after the root canal preparation. There is a marked reduction in biofilm quantity at the main canal and at the isthmus area adjacent to the main canal after preparation.

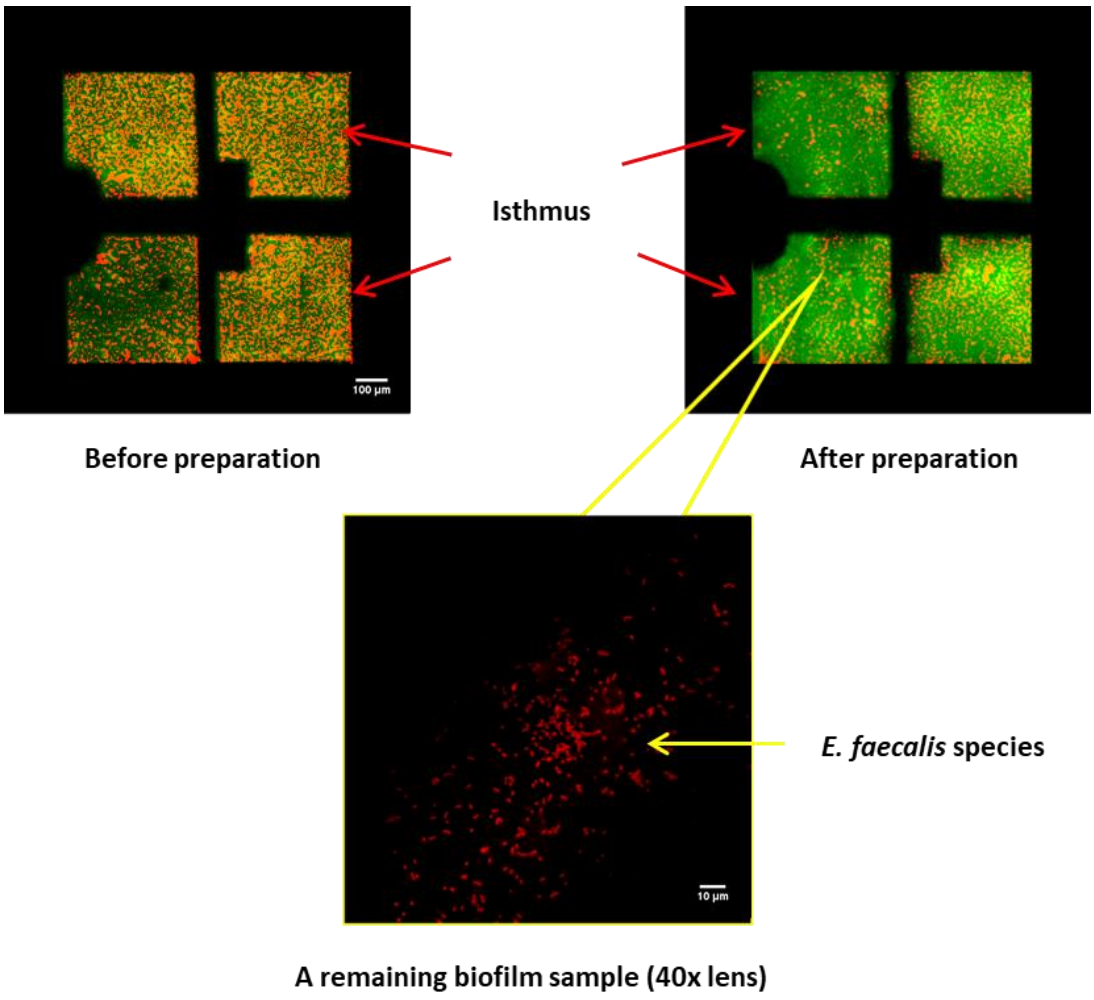

Figure 45: Biofilm removal in the isthmus area. Representative CLSM images demonstrate the labelled *E. faecalis* biofilm (red color) before and after the root canal preparation in the isthmus area. There is an obvious reduction in the biofilm after preparation

All file systems showed a better efficiency to remove biofilm from the middle third in comparison to the other third. There is an exception that, the PTN was equally effective in the coronal and apical thirds (Table 11). However, the PTN was the least effective in the apical third among the other systems. The best cleaning percentages can be seen in the middle, apical, and cervical thirds respectively of the RS system among all treatment groups (Table 11).

Table 11: The efficacy of file systems in removing biofilm at each canal third. The mean percentage (± SD) of the remaining biofilm at each canal third following different instrumentation techniques as relative to the control group thirds.

Groups	PTU	PTN	RS
Cervical	30 % (± 10 %)	25 % (± 3 %)	20 % (± 4 %)
Middle	24 % (± 6 %)	25 % (± 3 %)	9 % (± 1 %)
Apical	32 % (± 10 %)	42 % (± 5 %)	12 % (± 1 %)

4.3.4. Evaluation of biofilm removal with different irrigation techniques

Sonic and ultrasonic agitations for 30 secs have enhanced the biofilm removal when compared to the manual method alone. The enhancement was highly significant ($p \leq 0.001$) by the sonic tip and non-significant ($p > 0.05$) by the ultrasonic tip (Figure 46). For both groups, the distribution percentages of the remaining biofilm was higher in the cervical third than middle and apical thirds respectively in any of the tested groups (Table 12).

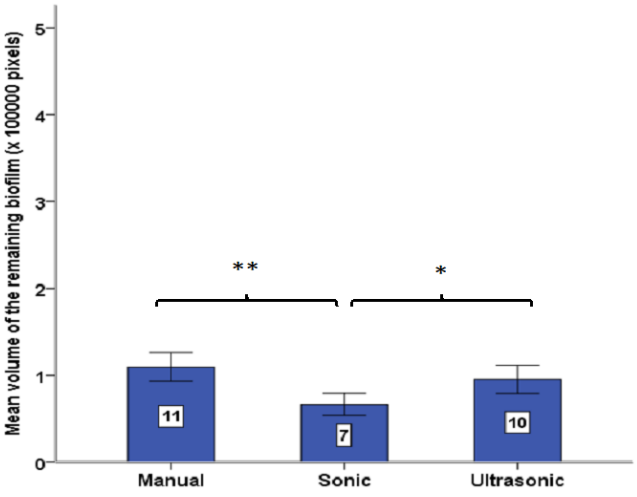

A

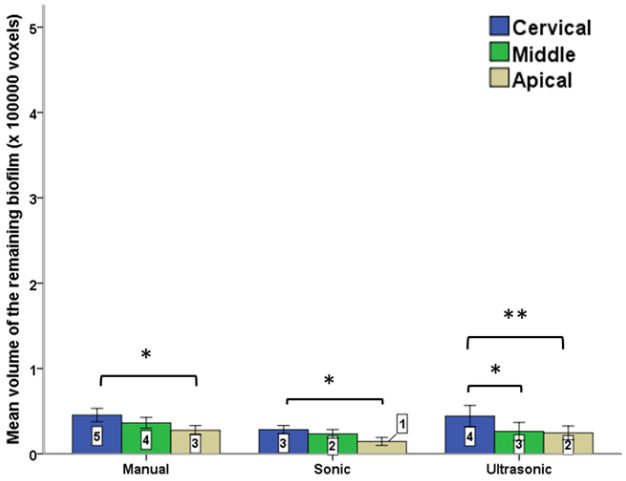

B

* = $p \leq 0.05$.
** = $p \leq 0.001$.

Figure 46: The remaining biofilm following irrigant agitation. Bar charts with SE bars representing the means of the remaining biofilm in each group (A) and each canal level (B) following the additional power agitation with sonic and ultrasonic tips in comparison to the manual irrigation alone. ANOVA and LSD test were applied to reveal the statistical difference ($p \leq 0.05$).

Table 12: The remaining biofilm percentages following different agitation protocols. The mean percentage (± SD) of the remaining biofilm on the surface of each canal third following different agitation protocols. The percentages are relative to the total amount of the remaining biofilm in the corresponding canal.

Groups	Manual	Sonic	Ultrasonic
Cervical	41 % (± 6 %)	44 % (± 9 %)	46 % (± 17 %)
Middle	33 % (± 4 %)	35 % (± 3 %)	28 % (± 17 %)
Apical	25 % (± 5 %)	21 % (± 7 %)	26 % (± 12 %)

The sonic tip was more effective than the ultrasonic tip at all canal levels (Figure 46). The results revealed that sonic tip has further removed 38 % (± 12 %), 35 % (± 13 %), and 48 % (± 21 %) of the remaining biofilm in the cervical, middle, and apical thirds respectively. However, the ultrasonic tip has further removed 3 % (± 2 %), 11 % (± 6 %), and 28 % (± 14 %) of the remaining biofilm in cervical, middle, and apical thirds respectively.

4.4. Discussion

In this experiment, the scanning parameters of the CLSM allowed for accurate images to be produced. The pin-hole size and the gain master represented the key parameters that controlled the amount of light required to illuminate the biofilm on the root canal surface. Narrowing the wavelength scale for each scanning track allowed for maximum separation between the fluorescent emission spectrums of the printed material and the fluorescent dye. Furthermore, controlling scanning speed and acquisition range functions yielded images with the same high resolution for reproducible analysis. The scanning depth criterion of the CLSM overcomes the image aberration that may arise when imaging a biofilm at different height levels on the irregular root canal surface. Such imaging flexibility made the segmentation and the quantification of the biofilm on the root canal surface possible compared to more conventional microscopes.

4.4.1. Biofilm labelling with *in situ* IIF technique

The signal produced with the *in situ* IIF technique allowed identification of the *E. faecalis* biofilm at 5x, 10x, 20x, and 40x magnifications and 1/300 dilution factor. At higher magnifications (*i.e.* 20x and 40x) It was clear that all the cell morphology is labelled by the combination of the primary and secondary antibody probes. This offers advantages over other fluorescent techniques that rely on the internal oligonucleotide hybridization of the nucleic acids. The fluorescent hybridization of *E. faecalis* biofilm appeared as a blurred collection of fluorescent mass rather than well-defined bacterial species (Al-Ahmad et al., 2009a).

Although at low magnifications (*i.e.* 5x and 10x) the individual bacteria cannot be seen, a larger area of the biofilm was viewed by the scanning process allowing a larger analytic procedure to take place. Therefore the 5x lens was selected to scan the root canal surface to capture biofilm data during the analytic procedure. Due to the high specificity of the primary antibody probe to the epitopes on the intact bacterial cell wall (Sims et al., 2006), the EPS was not seen during the scanning process.

Different studies have agreed that the *in situ* IIF is highly specific technique for detection of bacterial species target, such as *E. faecalis* (Waar et al., 2005, Brauner and Jäckel, 2016). The technique is reliable for estimation of bacterial concentration due to comparable results to the standard methods of evaluation (Caruso et al., 2000).

The use of the TRITC fluorescent dye to label the biofilm was used to minimize the overlapping between fluorescent spectrums emitted by the biofilm and the auto-fluorescent root canal surfaces of the 3D printed model. It has been reported that the resin-based plastic materials has an emission spectrum (525 nm) in the green region of the colour scale when excited with a laser light of 488 nm (Piruska et al., 2005).

4.4.2. The potential interaction between irrigant solutions and components of the staining buffer

Due to the denaturation and oxidation criteria of CHX and NaOCl respectively on protein compounds (Hjeljord et al., 1973, Becker et al., 1974, Portenier et al., 2002), the potential interaction between such chemicals and protein components of the staining buffer should be explored to avoid result misinterpretation.

The results showed the appearance of white precipitate and yellow discoloration following addition of CHX and NaOCl solutions respectively to the BSA buffer. The structure of the of the white precipitates was previously described by Hjeljord et al., (1973) as a salt of chlorhexidine-albumin, while the yellow discoloration is largely the cause of oxidative degradation of BAS structure (Estrela et al., 2002, Hawkins et al., 2003). These interactions might largely inhibit the function of the BSA as a blocking buffer and render an accurate *in situ* IIF method impossible.

The CLSM examination revealed that the white coagulates have an auto-fluorescent behaviour that could be falsely estimated as biofilm presence. The coagulation of the albumin into larger molecules may explain the green auto-fluorescence behaviour, which was previously manifested with other protein molecules (Matz et al., 1999, Zimmer, 2014).

The results showed that NaOCl has completely diminished the emitted light of the fluorescent dye after few minutes and that could be falsely estimated as biofilm absence. This may be explained by the oxidative degradation of the polypeptide structure of the IgG that could detach the conjugated dye (Chennamsetty et al., 2017) leading to the loss of the fluorescent signal. Beside chemical interactions, previous studies found that the BSA solution reduced the antibacterial activities of 2 % CHX and 5 % NaOCl against *E. faecalis* strains (Pappen et al., 2010, Quintana et al., 2017). These findings require the application of the staining buffer after the irrigation process to avoid false positive and false negative results also to avoid the attenuation of antibacterial activity of irrigant solution.

For this study, the CHX was selected instead of the NaOCl because the latter showed a robust antimicrobial activity (Bukhary and Balto, 2017, Farzaneh et al., 2017) that could

remove most of the biomass that is required to show treatment variations amongst the tested file systems.

4.4.3. The remaining biofilm following root canal instrumentation

Root canal preparation with all file systems produced significant disinfection of the treated RCS samples. The level of disinfection was higher with the RS compared to the PTU and PTN systems respectively. However, observational analysis showed that all file systems left minimum amount of biofilm in the main canals comparing to that left in the isthmus. Therefore, the variation among the three systems is dependent on the biofilm that remained in the isthmus space. These findings agree with previous findings that mechanical instrumentation reduces the vast majority of the biomass in infected canals (Bystrom and Sundqvist, 1981, Siqueira et al., 1999).

As isthmus space remained untouched during the instrumentation process; there is high possibility that biofilm removal in such space was dependent on the mechanical shearing and the chemical disintegration effects of the irrigation process (Van der Sluis et al., 2007, Mohammadi et al., 2017). One or both effects must have been responsible for the complete biofilm removal seen at several locations along the isthmus. The 2 % CHX has demonstrated ability to destroy *E. faecalis* within 2 min of direct contact (Bukhary and Balto, 2017). However, there is extremely limited knowledge about flow dynamics and shear forces of irrigants in the isthmus space.

It seems that these effects were attenuated toward the isthmus centre where the biofilm was reduced in density rather than removed completely. Obstacles such as the remaining

debris could either interfere with an effective flow or prevent direct contact with the biofilm material. Unfortunately, the changes in the irrigant flow-dynamic, in the presence of debris, remain unknown. The other possible factor is the impingement of irrigant flow in a narrow isthmus. It was found that the penetration depth of the irrigant solution was largely decreased in the narrow canals (Albrecht et al., 2004, Huang et al., 2008) and this consequently affects sufficient irrigant replacement (Boutsioukis et al., 2010a) that is required to maintain efficient biofilm removal.

Following instrumentation, biofilm was distributed along all canal thirds with higher amounts seen in the cervical, middle, and apical thirds respectively. It is clear that canal sections with larger volumes host more biofilm and therefore disinfection strategies should take this in consideration during the designing of the irrigation system. The delivery site and the flow rate of irrigant solutions require controlling at each canal level.

With all treatment groups, biofilm removal was more in the middle third than the apical third. During the current irrigation regimen, the needle vent was inserted in close position to the middle third with approximately 2.5 to 3.5 mm short of the canal working length. It was concluded that the irrigant solution must be delivered in close position to the material for an effective removal (Abou-Rass and Piccinino, 1982). A computational analysis study revealed that fluid shear stresses, on the root canal wall, reached the maximum around the needle vent and decrease at apical and coronal thirds respectively when the needle vent is placed at 3 mm from the apex at 0.1 mL/sec flow rate (Wang et al., 2015). Therefore, it appears it would be useful to modify the endodontic syringe tips to include several vents that open at all canal levels.

4.4.4. Biofilm removal with supplementary sonic and ultrasonic agitation techniques

In this project, the supplementary agitation of the root canal for 30 sec with either sonic or ultrasonic tips allowed for more disinfection than conventional syringe irrigation alone. The sonic tip performed better than the ultrasonic tip, which showed minimal difference to the manual method in this experimental set-up. A study by Alves et al., (2016), applied on mesial canals with isthmi, have agreed to the current findings that passive ultrasonic irrigation (PUI) produced a non-significant reduction to the amount of *E. faecalis* biofilm in comparison to the manual method.

Sonic and ultrasonic agitation techniques have been shown to maximize canal disinfection procedures when used in conjunction with the standard manual method (Bryce et al., 2017, Nakamura et al., 2017). However, the findings of these studies disagree to the current findings in that the ultrasonic tip showed better performance than the sonic tip. This would be affected by the experiment design where the previous studies were conducted on root canals with little or no anatomical challenges.

The ultrasonic file oscillates with high frequency and a lower magnitude standing wave of 3-4 antinodes (Lea et al., 2004). Conversely, the sonic file oscillates with lower frequency and higher magnitude wave with a single node at the free end (Walmsley et al., 1989). Both tips were shown to oscillate at higher magnitude at their apical part in comparison to the coronal part (Walmsley et al., 1989, Boutsioukis et al., 2013). The oscillation with higher magnitudes could improve irrigant streaming through the isthmus space that consequently enhances biofilm removal (Ahmad et al., 1987, Neelakantan et al., 2016a) as seen with the sonic file or with the apical ends of both files.

4.5. Conclusions

The *in situ* IIF technique is a reliable and reproducible method to label *E. faecalis* biofilm on simulated root canal surfaces. The CLSM is a powerful scanning tool to visualize the labelled *E. faecalis* before and after root canal preparation.

Root canal preparation with all file systems using 2 % CHX produced significant removal to the biofilm especially in the middle third. However, there was not total removal of the biofilm following treatment. The RS system was determined to be superior to the PTU and PTN systems respectively at all canal thirds. In contrast, the PTN system was inferior to the other systems especially at the apical third.

Biofilm in the isthmus space represents a challenge for disinfection procedures in comparison to the simply approached canals. Although, the material toughness of the simulated root canals was inferior to that of dentine, no technical problems arose during root canal instrumentation. All instrumentation parameters were kept similar to the instrumentation parameters applied during the instrumentation of the natural teeth.

The supplementary irrigant agitation improves canal disinfection especially with EDDY sonic tip. The use of the ultrasonic irrisafe file yields minimal benefit. The sonic tip was effective at all canal levels while the effect of the ultrasonic tip was limited to middle and apical thirds. The findings of this experiment have rejected the null hypothesis.

CHAPTER FIVE:

USING OCT TO MEASURE BIOFILM AND DEBRIS IN A ROOT CANAL MODEL

5.1. Introduction

A novel non-contact method is described to quantify debris and biofilm in simulated root canals with a complete isthmus following instrumentation with three rotary file systems using optical coherence tomography.

Optical coherence tomography (OCT) is a non-invasive imaging tool developed by (Huang et al., 1991). It works on interferometric principles where a light source is split into both a reference arm and a sample arm. The reference arm is used for interpretation of changes of the sample arm, such as the time delay of backscattered light by different layers within a semi-transparent material (Dunkers et al., 2001, Drexler and Fujimoto, 2015). It produces real time 3D images, as cross-sectional slices, at a microscale resolution and high acquisition rate. In modern OCT systems, imaging can be performed to a depth of 6 mm with an axial resolution of 2.6 to 10 µm and speeds of 50 to 80 image frames per second (Shemesh et al., 2007). However, the deep imaging ability of OCT is limited to semi-transparent materials and tissues (Stifter et al., 2003).

The OCT utilizes a variety of optical properties, such as light absorption and scattering, to identify different tissue structures with a safe non-ionizing light (Fercher et al., 2003). These properties make OCT a favourable tool for both clinical applications and basic research (Huang et al., 1991). It has received wide application in the biomedical field particularly in the evaluation of thin biological structures such as the retina and its underlying tissues (Coscas et al., 2016, Spaide and Curcio, 2017).

In dental research, the OCT is used to examine surface lesions such as dental caries, tooth fracture, and gaps produced between the tooth structure and restorations (Han et al., 2016, Mansour et al., 2016, Kim et al., 2017). When coupled with an imaging tube of 0.3-0.5 mm

diameter, the OCT is able to recognize debris left in root canal fins (Shemesh et al., 2007) and to observe vertical root fracture ((Shemesh et al., 2008, Wagner and Horn, 2017). However, such applications required the root canals to be enlarged to file size 50 to adapt the tube width. In addition, scanning depth was limited by tooth opacity which does prevent the differentiation of debris that adheres to the root canal wall. The effect of tooth opacity may be overcome by using a transparent simulated sample.

The cured transparent epoxy resin with a refractive index (RI) of 1.552 seems an ideal material for production of root canal samples especially that OCT is able to visualise microstructures included in this material (Dunkers et al., 2001). Accura is an example of this material that is currently used to generate high definition three-dimensional samples using the rapid prototyping technology (Green III et al., 2016).

Biofilm is a viscoelastic structure that may be easily disrupted on manipulation. Therefore any methods that lead to minimal sample disturbance are desirable for biofilm evaluation (Wagner and Horn, 2017). The OCT was established as a non-invasive imaging tool for *in situ* visualization of the biofilm structure and its dynamic behaviour in a transparent glass tube (Xi et al., 2006a, Haisch and Niessner, 2007). It has advantages over other imaging tools, such as the CLSM, as additional preparation steps, such as fixation or labelling of bacterial species, are not required. Furthermore, the biofilm structure including the EPS matrix can be observed at an increased penetration depth.

The axial resolution limit of OCT may interfere with the observation of a thin biofilm structure (less than 2.5 µm). An example would be the biofilm generated by *E. faecalis*. Thereby, species that generate a thick biofilm layer are easier to image accurately with OCT. Root canal biofilm can grow as single biomass, or as a multiple microorganism structure that

live in a symbiosis or competitive interaction (Wanner and Gujer, 1986). In symptomatic root canal infections, strong associations were determined between streptococci, such as *S. oralis,* and actinomyces, such as *A. naesulandii*. (Siqueira et al., 2002b, Xia and Baumgartner, 2003). Both species are initial colonizers that enhance biofilm adhesion to the tooth surface (Palmer Jr et al., 2003). Coaggregation-mediated interaction was seen between these two species. The interaction produced thick biofilm (14 μm) that was characterized by the rapid production of EPS matrix (Koo et al., 2010). For research purposes, biofilm fermenters, such as the CDFF, are preferable tools for generating thick poly-microbial biofilms on tooth structures (Kinniment et al., 1996, Kocan et al., 2017, Teranaka et al., 2017).

Apart from SEM evaluation, both debris and biofilm have been investigated individually due to the challenge in visualisation with a single tool. This is because both materials have different structure densities. Utilizing the OCT scanner with transparent resin simulated root canals may provide a novel methodology for visualisation and quantification of debris and biofilm in the same sample.

Aim:

Quantification of debris and biofilm in a novel simulated root canal following instrumentation with PTU, PTN, and RS file systems using the OCT scanner.

Hypothesis:

The OCT cannot quantify debris and biofilm in the simulated root canal and there is no difference among the three file system in cleaning and disinfection of the root canal system.

Objectives:

1. To investigate the use of an OCT scanner for detection of the root canal wall, debris, and biofilm in the same sample.
2. To generate a dual species biofilm in the root canal model using the constant depth film fermenter (CDFF).
3. To quantify debris and biofilm volumes that remained in the RCS following instrumentation with three rotary file systems.

5.2. Materials and methods

Dual species biofilm was generated in simulated root canal samples using the CDFF. The contaminated canals were then shaped with asymmetric rotary files and irrigated with 2 % chlorhexidine. A final rinse with a saliva buffer was performed after the initial canal preparation. Data was evaluated using the OCT (Ganymede, Thorlabs, New Jersy, USA) scanner to create 3D images, which were processed with ImageJ and 3D Slicer software.

5.2.1. Generation of simulated RCS samples

Forty RCS samples with a complete isthmus were generated using the stereolithography (SLA) rapid prototyping (RP) technology. The Accura material was selected to prepare the samples following modifications to the previous computational RCS model. These modifications include the external shape and dimensions of the model halves without affecting the internal surfaces of the RCS.

The cuboid shape of each half of the model was modified to a semi-cylinder (Figure 47) which allowed easy adaptation within the CDFF sample holders. The modification process was performed with the ImageJ software where a semi-circular selection was included for the image stack of each root canal half. Then, the white pixels that located outside of the selection were deleted to leave a semi-cylindrical object image stack.

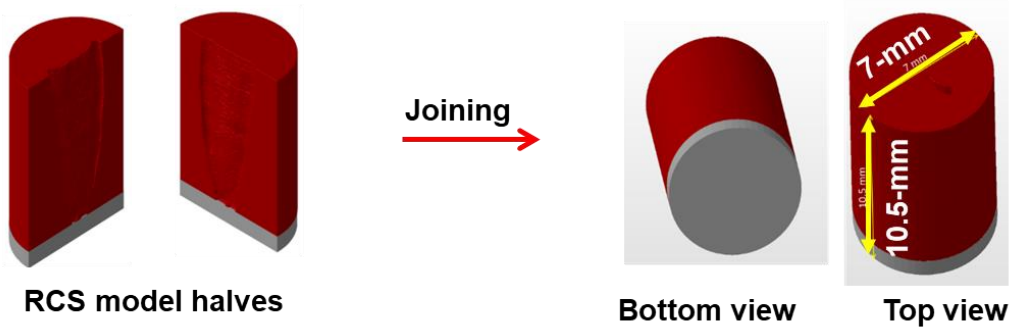

Figure 47: Modelling and simulation of RCS for the OCT analysis. (A) 3D images show the computational RCS model halves joined to a cylindrical shape of 7 mm diameter x 10.5 mm height. (B) Simulated root canal samples halves produced with RP technology and joined with a light cured resin adhesive liquid.

The resulted root canal half images were converted to a model where root canal surfaces were meshed with triangular facets. The information of the model halves were saved in STL file format. They were then opened in the Netfabb software to rescale dimensions from millimetre to micrometres using a scaling factor of 0.001; and to repair errors occurred during the meshing process, such as incorrectly oriented or overlapped triangles.

The apical end of the root model was closed with a 1 mm-thick solid disc image to create a closed endodontic system. The disc was designed as two equal halves using the Solidworks software and joined to the RCS model using the Netfabb software. The model was printed as two semi-cylindrical halves with a centrally located RCS. The two halves were then aligned in a transparent plastic tube and joined in the form of a cylinder with a light cure adhesive liquid applied around the contact line (Figure 47). Five consecutive curing times of 20 secs each were applied around the adhesive layer to ensure complete polymerization of the adhesive material.

Two samples were then used for trial placement in one sample ring of the CDFF bioreactor. The ring was filled with a silicon rubber-base material to create a stabilizing negative replica to hold samples during the incubation period. Autoclave sterilization (Varioklav, Oberschleißheim, Germany) was used to disinfect the CDFF components and the RCS samples.

5.2.2. Preparation of saliva buffer

The saliva buffer solution (pH 6.8) was prepared by mixing of 1 mM CaCl2, 2 mM of potassium phosphate buffer (K_2HPO_4 43.5 g/L and KH_2PO_4 34.0 g/L) with 50 mM KCl

solution. All salts were dissolved in distilled water using a magnetic stirrer (IKA, Wilmington, USA). The buffer was then autoclaved for 21 mins at 121^{o}C.

5.2.3. Preparation of the growth culture

A BHI broth enriched with yeast extract 1 g/mL (Oxoid, Hampshire, UK) was used as a culture medium. After sterilization, 5 mL of hemin was added with a micropipette. The hemin was prepared by mixing 50 mg of L-cysteine-HCl (Sigma Aldrich, St. Louis, USA) with 5 ml of 0.1 M NaOH (Merck, Kenilworth, USA) in 45 mL of distilled water. Thereafter, 1 mL of 1 % menadione sodium bisulphite (Sigma Aldrich, St. Louis, USA) was introduced to the medium with a micropipette. Both the hemin and menadione were sterilized by a 0.22 µm pore size filter (Millipore, Sigma Aldrich, St. Louis, USA) and then added to the autoclaved BHI broth. The broth was then stored at room temperature until use.

Two bacterial strains were used to create the dual species culture; *A. naeslundii* T14v-j1 and *S. oralis* j22. Bacteria were collected from frozen stocks at -80^{o}C.

S. oralis was cultured in aerobic conditions after being plated on a blood agar plate (Oxoid, Hampshire, UK) using a sterile loop. The agar plate was then incubated overnight in ambient air (Carbolite, Essex, UK) at 37^{o}C. The same procedure was repeated for the *A. naeslundii* but in an anaerobic cabinet (Laftech, Bayswater North, Australia) at 37^{o}C where the culture was allowed to grow overnight.

To standardize bacterial concentration, a single colony from each bacterial phenotype was inoculated into 10 mL of a fresh BHI broth in a 20 mL size glass test tube. The cultures were incubated for 24 hrs using the preferred conditions for each bacterial strain. Each 10 mL culture was then centrifuged (Beckman-Coulter, Indianapolis, USA) at 6341 g.

The supernatant was removed carefully to avoid dislodgement of the bacterial pellet, which was re-suspended in 10 mL of the sterilized saliva buffer. The process was repeated two times followed by sonication (Sonics & Materials Inc, Newtown, USA) of the suspension to break aggregates. Sonication was repeated three times 10 secs, with 1 min intervals to let the suspension cool in order to prevent overheating. During sonication, samples were placed in a glass jar with ground ice to avoid overheating. Following this a 10-fold dilution of the sonicated suspension was dispensed to the Bruker-Turk counting chamber. The number of bacterial cells in 32 squares was counted under the light microscope using a 40x lens magnification and the average was included to the following standard formula;

$$\text{bacterrial concentration } \left(\frac{\text{cell}}{\text{mL}}\right)$$

$$= \frac{\text{total number of bacteria}}{\text{number of squares}} x\ dilution\ factor\ x\ 4x10^7 (volume\ correction\ to\ mL)$$

The bacterial concentration was then diluted to 3 x 10^8 /mL and 1 x 10^8/mL for *S. oralis* and *A. naeslundii* respectively in one flask of saliva buffer totalling 100 mL of bacterial suspension.

5.2.4. Generation of dual species biofilm in the root canal samples

To initiate bacterial adhesion, samples were submerged in the bacterial culture of the saliva buffer and kept for 1 hr at 37°C in the ambient air. Samples were kept perpendicular during this incubation period of bacterial adhesion initiation. After this period, the bacterial culture medium was removed from the root canal samples with a micropipette. The sample canals were then washed with a saliva buffer solution (K_2HPO_4 0.174 g/L, KH_2PO_4 0.136 g/L, 1 mM $CaCl_2$, 50 mM KCl) for two periods of three minutes to remove non-adhered bacteria.

The CDFF parts were then reassembled in the microbiological safety cabinet. During this time, samples with the adhered bacteria were loaded to the bioreactor rings then the incubation chamber lid was secured with the built-in screws. The process of incubation included pumping the fresh BHI on a regular basis (0.5 mL/min) while keeping the main ring rotating at a slow speed. The incubation process was performed in aerobic conditions at 37 ^{o}C. After 4 days of incubation, the samples were removed from the bioreactor discs then dislodged from the silicon material. All samples were kept in the saliva buffer at room temperature before root canal instrumentation to avoid biofilm dehydration.

Thirty of the forty samples were randomly divided into three test groups. Each group was allocated for the preparation with one of the three file systems to be tested. There was a negative control group (n = 10) where samples were left sterile without biofilm generation. As these were not cultured in the CDFF, they were used to verify OCT detection on the RCS wall, also the detection of the remaining debris after RCS preparation.

5.2.5. Scanning procedure by OCT

Cyclic OCT scans at 930 nm were arranged to show the differences throughout the root canal space in 3D levels following different treatments (Figure 48).

A pre-instrumentation scanning was made to investigate the root canal volume with its content of the generated dual species biofilm. In addition, the pre-instrumentation image stack was used as a reference to the proposed remaining biofilm after root canal preparation. A post-instrumentation scanning was made two times for each sample; one after the canal preparation and other after rinsing the prepared canal with an extra volume of the saliva buffer.

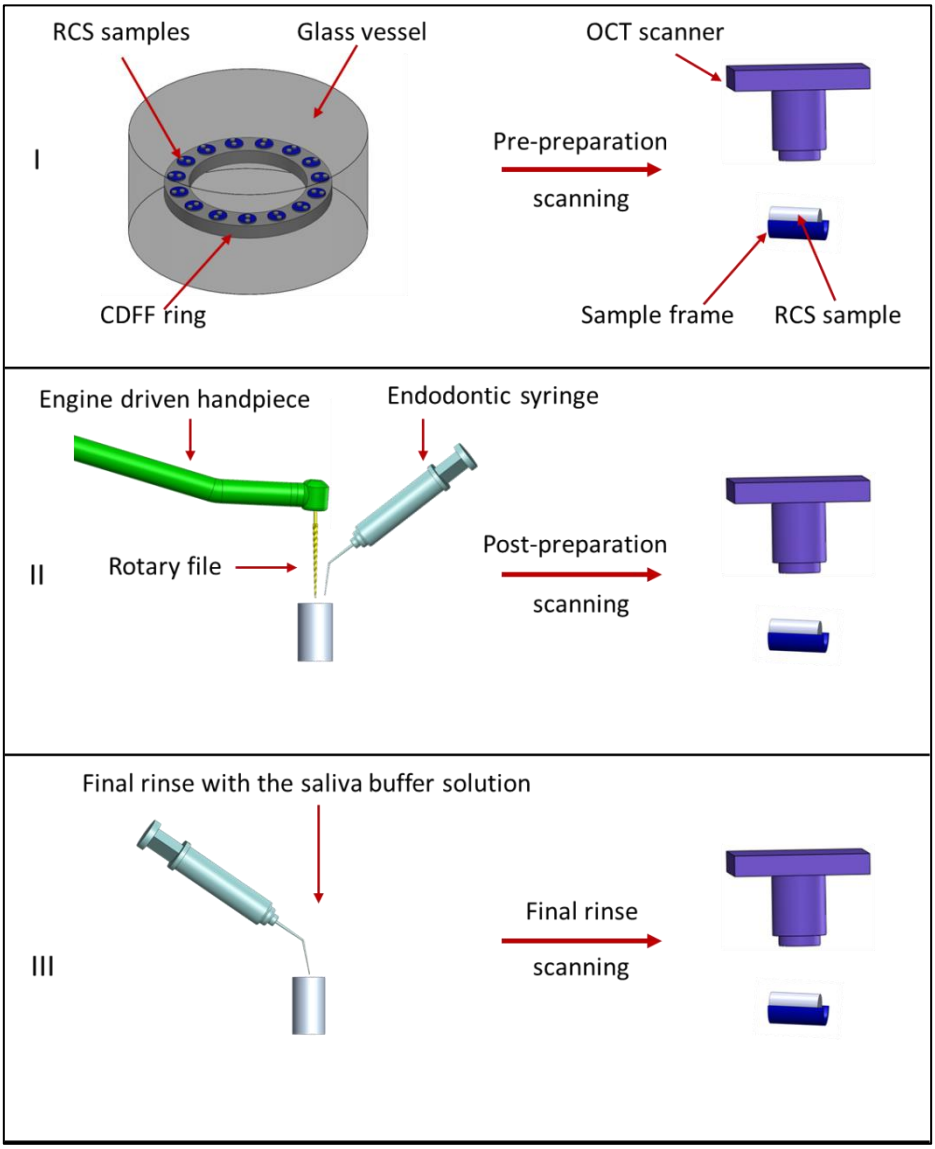

Figure 48: The OCT evaluation of remaining debris and biofilm. An illustration demonstrates the three sequences of sample preparation and sample scanning with the OCT. Three scanning steps were performed for each sample following; biofilm generation (I), root canal preparation (II), and final rise with 2.5 mL CHX (III).

A universal frame was made from a silicon rubber material to stabilize each sample in a reproducible position during the scanning procedure (Figure 48). Samples were lined individually in a longitudinal position under the scanning camera. The scanning procedure was set to visualize the entire canal volume involving the root canal surface. The wavelength of the device was 930 nm with an exposure time of 27 sec. The resulting image was made from a stack of 500 slices in a TIF format and a pixel size of 1000 width x 165 height. Three scanning procedures were performed on each sample including pre-instrumentation, post-instrumentation, and post-final rinse scanning.

5.2.6. Root canal preparation

The instrumentation technique was consistent for the four groups in regards to the number of included files and the volume of the irrigant solution. The negative control group was prepared with the PTU as a standard file system. The three test groups were instrumented with PTU, PTN, or RS. The instrumentation started with a hand stainless steel K-file size 15, of 0.02 taper, to create a smooth glide path. This was followed by canal shaping with the first four files in a sequential manner. The working length was universal for all groups as 9.5 mm ± 0.1 mm represented the cervico-apical sample length. This length was determined on each file instrument by a stainless-steel ruler and guided by the file rubber stopper. Each sample was griped firmly with the operator index, thumb fingers, and stabilized vertically on the laboratory bench in a clean plastic dish. With the different file systems, the root canal was prepared in a rotary movement driven by a contra-angle handpiece connected to a Waveone engine set at speed of 300 rpm and torque of 4 Ncm^2 (Dentsply Maillefer, Ballaigues, Switzerland).

Irrigation technique:

The Irrigation procedure followed the same principles in the previous experiments. Chlorhexidine digluconate (2 %) was used as an irrigant solution with a total volume of 5 mL for each canal and 10 mL for each root. A manual irrigation method was used to flush root canal samples using the endodontic syringe and needle. The needle shaft was bent in the middle to approximately 45^{o} to maintain a perpendicular irrigant injection to the canal space. The needle was moved in short up and down cycles (2-3 mm) to prevent its binding for an effective irrigant delivery. Manual pressure was maintained on the syringe piston to introduce the irrigant solution in a flow rate of approximately 0.1 mL/sec. One mL was used to flush the canal during each instrumentation process. A total of 5 mL were introduced to each canal using approximately 0.1 mL/sec flow rate. The canals were not dried and the samples were immediately transferred to the OCT scanner.

For SEM evaluation, three RCS samples were prepared by the same technique used for the negative control group. Following preparation, a 1.5 mm thick slice was sectioned from each canal thirds using the Buehler saw machine. The slices were left to dry for 24 hrs in a plastic box contained silica gel granules. Each dried slice was mounted on an aluminium stub then sputter coated with a thin gold film before SEM imaging. An image was captured for each slice at 49x magnification to include the mesio-distal width of the canal.

5.2.7. Final rinse with a buffer solution

The purpose of this experiment was to investigate the effectiveness of final flushing with a buffer solution on cleaning and disinfection of the root canals.

The saliva buffer solution (K_2HPO_4 0.174 g/L, KH_2PO_4 0.136 g/L, 1 mM $CaCl_2$, 50 mM KCl) was used to perform this irrigation step. Before the final flush, the root canal was scanned with OCT. The irrigant buffer solution was manually introduced to the root canal sample in a continuous manner as previously described. The samples were then immediately transferred to the OCT for the second post-instrumentation scanning.

5.2.8. Image analysis

Two analytic software programs (ImageJ and 3D Slicer) were applied on the image stacks to calculate the biofilm generated in the root and biofilm after root canal preparation and after the final rinse. In addition, the analysis was extended to calculate debris remaining. ImageJ was applied for image filtration, segmentation, thresholding and quantification; whereas, 3D Slicer was applied for image registration.

The original image stack, in TIFF format, was dragged and dropped into the ImageJ software. The 16-bit pixel depth colour was then converted to 8-bit to comply with the applied processing algorithms. The inherent low-energy scanning background noise was removed with a Virtual stack algorithm that was set at a window of 3 and a standard deviation of 15. At this stage, the profile of grey values of debris and biofilm in the RCS of the negative and the positive groups was estimated using the Plot profile algorithm. Three line selections of

0.6 mm each were placed on debris or biofilm found in cervical, middle, and apical thirds of first five samples of each group.

The denoised process was then repeated to ensure maximum eradication of scanning noise. Image background pixels were then homogenised using a Rolling ball algorithm at a radius value of 50 pixels. This algorithm removes pixels that have sizes less than the specified number. The contrast was adjusted to a minimum value of 10. These filtration processes yielded a grey-scaled root canal image on a black background. Gaussian blur filter was then applied to smooth the image objects and to close holes produced during denoised operation. Image stacks were than save as NRRD file format.

Figure 49 shows the sequence of the image analytic process used for extraction then quantification of debris and biofilm. The pre and post-instrumentation images were then registered with the 3D Slicer software using the Transform operation. Such operation brings the same features on the two images in close approximation. This was followed by the General registration operation using rigid and fine features function to produce an accurate alignment and superimposition.

The aligned images then opened in the ImageJ software where the root canal wall was removed with a morphological erosion operation, which included the vertical line structures of 6-pixels size. This produced a pre-instrumentation image with the generated biofilm, and a post-instrumentation image with both the remaining debris and the remaining biofilm. The two images were then operated with the mathematic AND algorithm to extract objects with the same grey pixels. This permits isolation of the remaining biofilm. The remaining biofilm image was then subtracted from the post-instrumentation image using the Subtract mathematic operation.

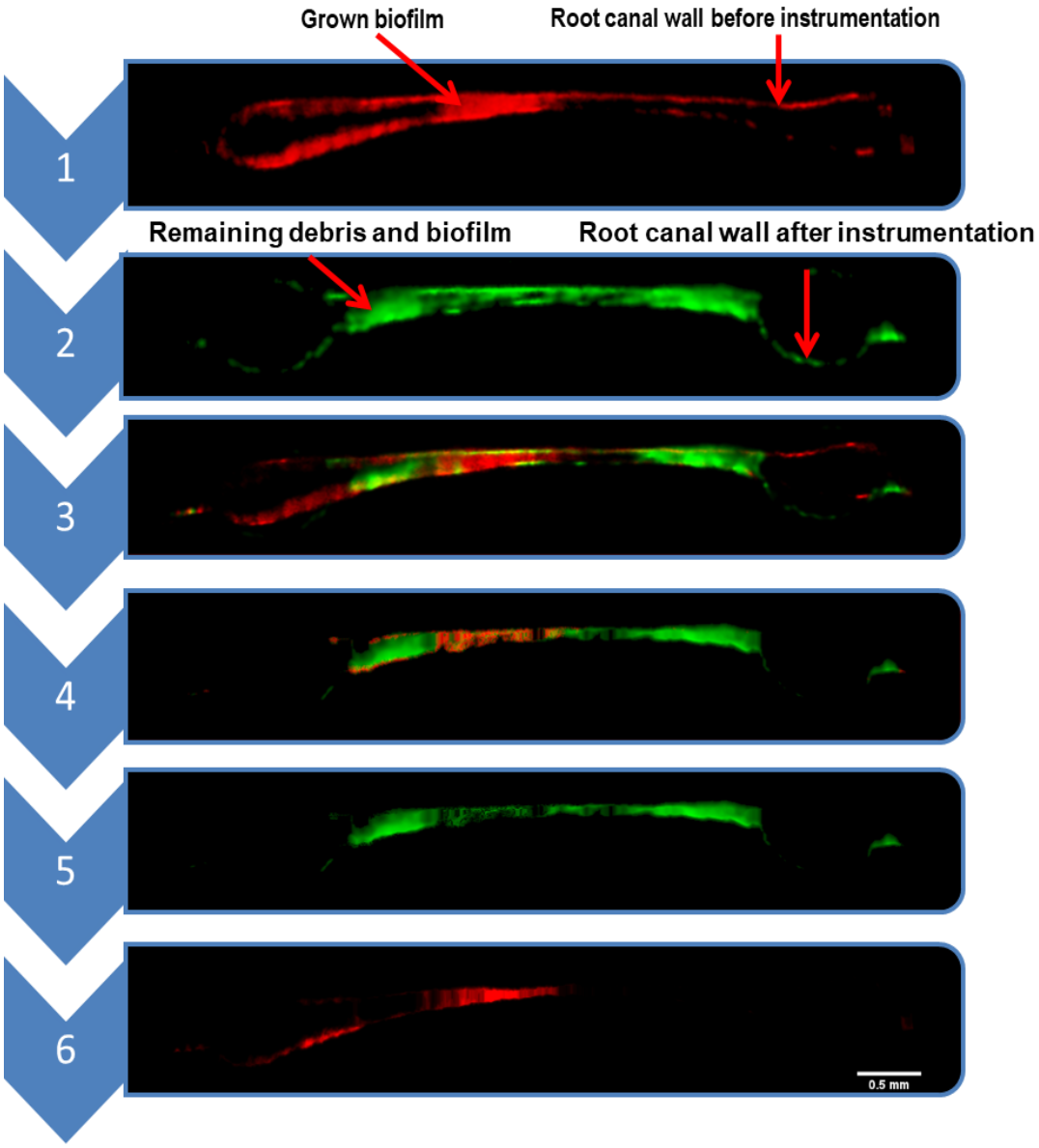

Figure 49: Segmentation of the OCT image stacks. Pictorial OCT images demonstrate the methodology sequence for segmentation and isolation of debris and biofilm. (1) Pre-instrumentation image with biofilm, (2) post-instrumentation image with the remaining debris and biofilm, (3) Registration of pre and post-instrumentation images, (4) segmentation of the remaining debris (green) and the remaining biofilm (red). (5 & 6) Isolation of debris and biofilm for quantification.

This produced a new image with the remaining debris. A threshold of 10-255 was then applied for the resulted images to count debris and biofilm using the Voxel counter plugin.

The remaining debris and biofilm volumes were counted in each sample and in each third where the number of image stack was divided into three equal parts as cervical, middle, and apical. The percentages of the remaining biofilm volume were estimated in relation to the untreated biofilm volume.

To determine a possible effect of debris on disinfection procedure, the volume of the remaining debris was correlated to the volume of the remaining biofilm.

5.2.9. Statistical analysis

The Shapiro-Wilk normality test revealed that data of remaining biofilm percentages and remaining debris volumes of treated groups have normal distribution around the means. Therefore, analysis were performed with the LSD Post-Hoc test as data has equal variance (*F statistic* = 2.5, *F critical* = 3.1). However, data evaluation in each canal third showed abnormal distribution ($p \leq 0.05$) due to the large dispersion of data sets form the mean values. Accordingly, non-parametric analyses were performed using the Kruskal-Wallis H and Mann-Whitney U tests. The level of significance was set at $p \leq 0.05$. The correlation between the remaining debris and the remaining biofilm was analysed using the non-parametric Spearman's correlation test. Correlations were represented with scatter plots and Loess fitting line while level of significance was set at $p \leq 0.01$.

5.3. Results

5.3.1. The negative control group

The OCT pre-preparation scanning to the RCS samples has detected the whole boundaries of the RCS as shown in Figure 50. An empty root canal space was readily identified through the observation of the image stack with the Image software (Figure 50).

After preparation, presence of debris was seen in the RCS as newly found white pixels in an already empty space (Figure 50). This remaining debris was also detected through the observation of the SEM images at all canal thirds (Figure 51). The distribution pattern of debris was similar to the distribution pattern of the natural debris as recognized with the microCT in a previous experiment. Changes in the root canal geometry, after the instrumentation process, were clearly manifested via image observations by ImageJ software.

5.3.2. The biofilm in the RCS sample

Before root canal preparation, the visual examination of the washed transparent root canal samples revealed biofilm generation in the RCS space manifested as a white plugging, which was dominant in the apical region. The pre-preparation scanning of the biofilm samples showed accumulation of biofilm as white pixels in an already empty canal space. The pattern of the scanned biofilm was generally similar to the biofilm pattern on the visual examination. The observation of the 3D images showed that the generated biofilm tends to cover the RCS space especially in the isthmus region or to line the canal wall especially in the main canals (Figure 49 and Figure 50).

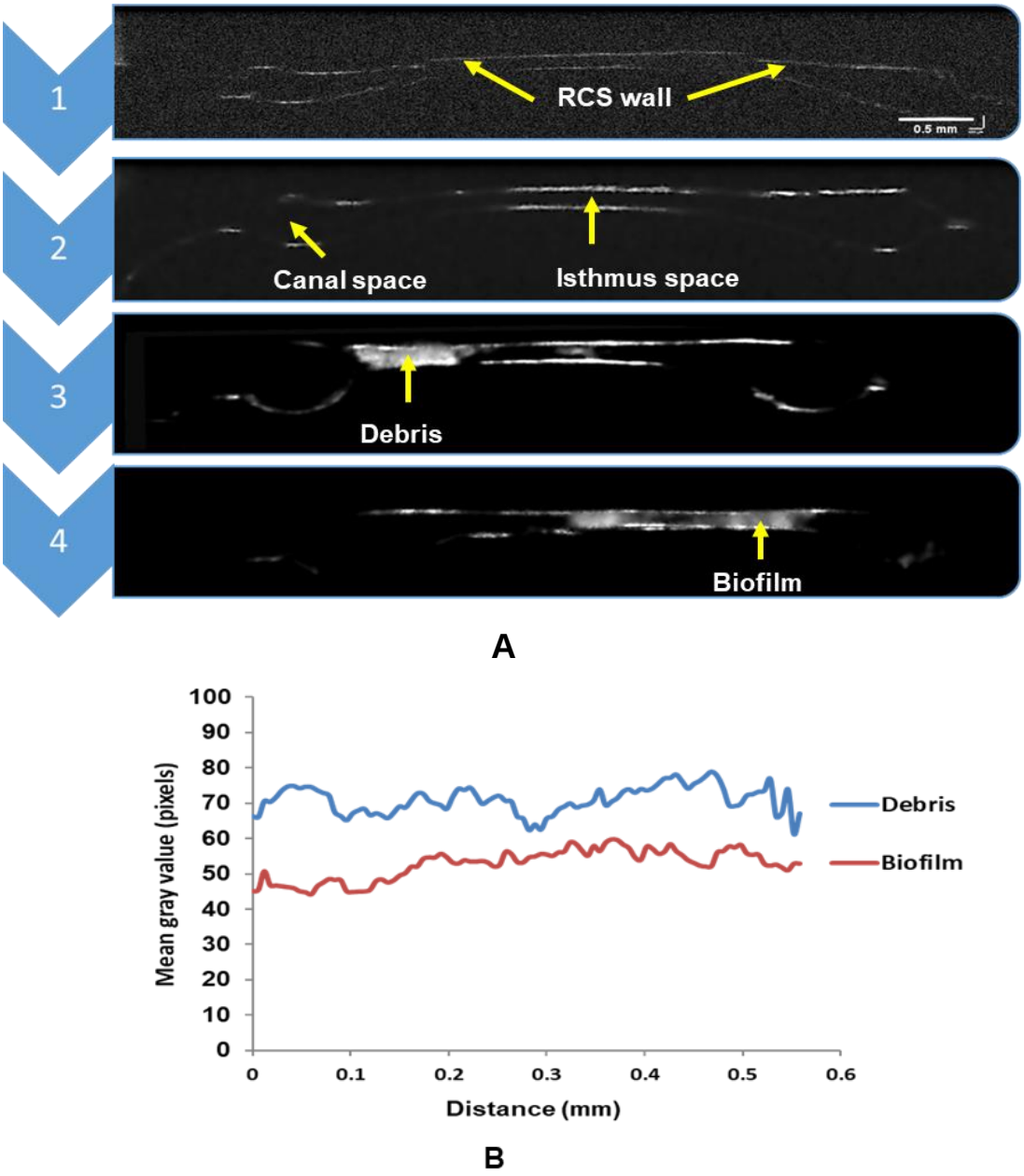

Figure 50: Differentiation of the RCS objects with the OCT scanner. (A) A pictorial chart shows the unfiltered initial image (1), and filtered pre and post-instrumentation images (2 and 3) of the negative control and the filtered pre-instrumentation image 4) of the positive control group. (B) A plot chart demonstrates the range of grey scale values for the debris and the biofilm.

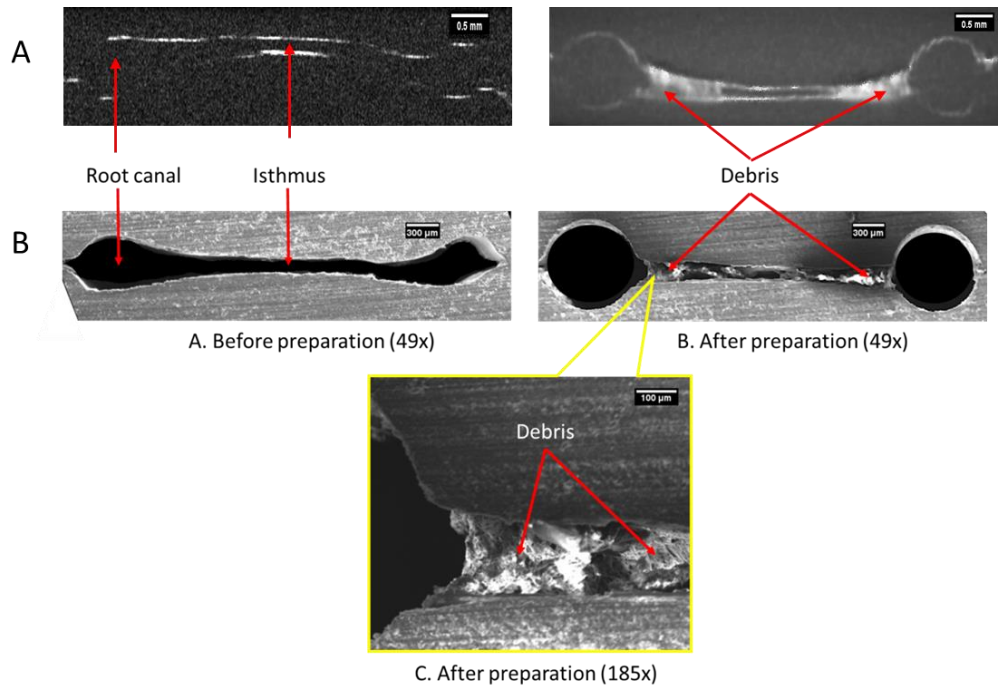

Figure 51: The detection of the remaining debris with SEM and OCT. An image panel shows how the OCT can distinguish the remaining debris in the root canal model after root canal preparation (A) in comparison to the standard SEM method (B). These images were acquired from the middle third of the RCS.

The results showed clearly that biofilm has a lower grey value range (40 pixels– 60 pixels) compared to the higher grey value range (60 pixels– 80 pixels) of debris (Figure 50). However, overlapping between debris and biofilm grey values were seen in different individual samples. The statistical analysis revealed that more biofilm was generated in the apical third compared to the middle and cervical thirds respectively. The difference was only significant ($p \leq 0.001$) between the apical and the cervical thirds in all control (untreated) groups (Figure 52).

Significant biofilm removal ($p \leq 0.001$) was seen after root canal preparation although complete removal of the biofilm was not achieved (Figure 52). A higher percentage (95 % ± 4 %) of biofilm removal was seen after instrumentation with the RS system, whereas the lowest percentage (92 % ± 6 %) was seen after the instrumentation by the PTN system (Figure 53). The observation of 3D images revealed that most of the remaining biofilm was left in the isthmus space. Conversely, the minimum amount of biofilm was noticed in the main canals of each sample.

The final flush removed more biofilm from the root canal system in all treatment groups with a significant removal ($p \leq 0.05$) seen only in the group treated with the PTN file system (Figure 53). The reduction percentages were higher in the PTN group (62 % ± 25 %) and lower for the RS group (40 % ± 25 %). For the PTU group, the reduction percentage was 52 % (± 36). The percentages were estimated in relation to the initial preparation biofilm values.

With respect to root canal thirds, smaller amounts of biofilm were noticed in the middle third compared to the cervical and apical thirds for all treatment groups. Further canal rinsing has reduced biofilm percentages in all thirds without achieving complete disinfection (Figure 52) or significance differences between corresponding root canal thirds.

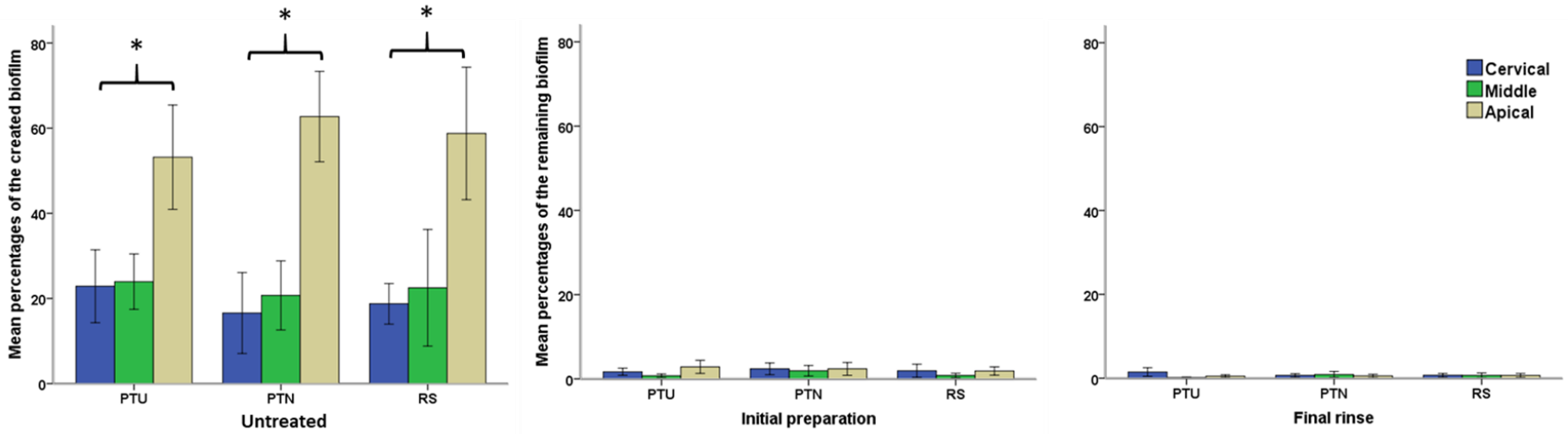

* = *P ≤ 0.001*

Figure 52: Analysis of the remaining biofilm using the OCT scanning. The mean percentages (± SE) of debris remained in each third of the simulated RCS following initial preparation with PTU, PTN, and RS file systems and following final rinse with 5 mL of saliva buffer in comparison to the untreated group. Kruskal-Wallis H and Mann-Whitney U tests were applied to show significant differences (*p ≤ 0.05*).

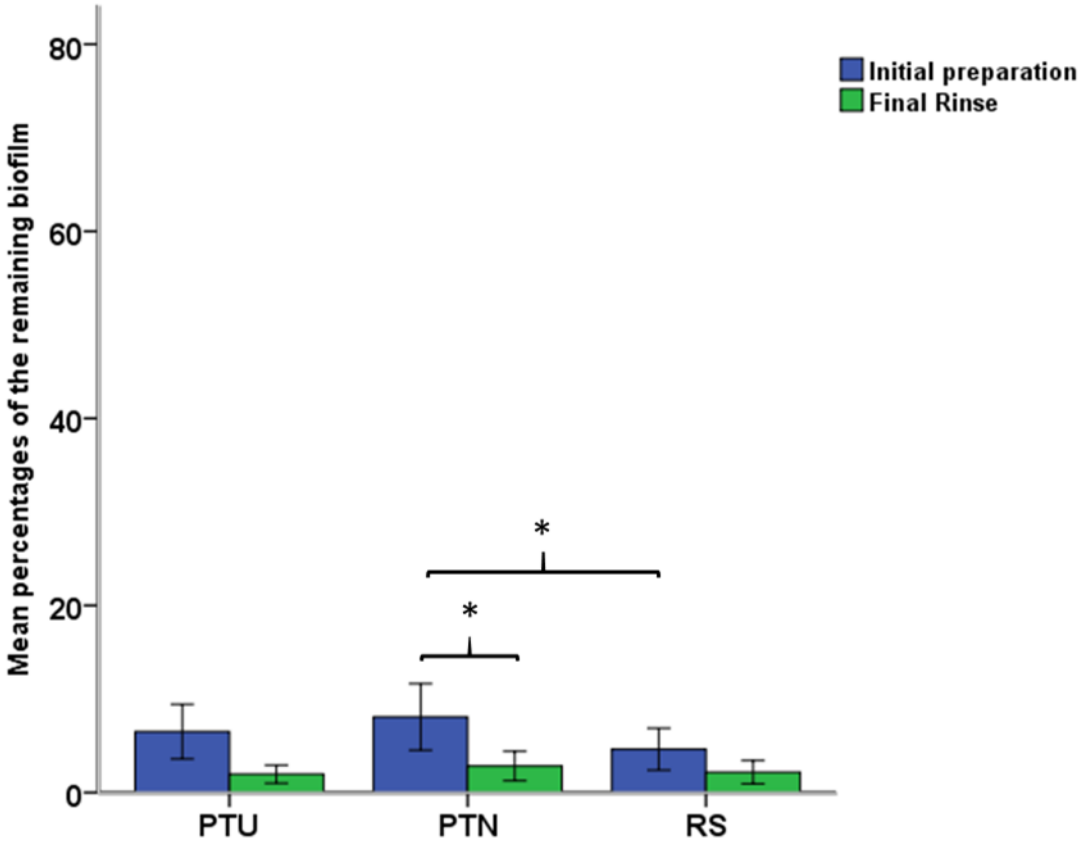

* = $p \leq 0.05$

Figure 53: The remaining biofilm following the initial preparation and final rinse of the RCS. A Bar chart shows the percentages of the remaining biofilm following the Initial RCS preparation with PTU, PTN, and RS file systems, and following final rinse with the saliva buffer. ANOVA and LSD tests were used for the statistical evaluation ($p \leq 0.05$).

All file instrument systems showed more efficiency in removing biofilm from the apical third compared to the middle and cervical thirds respectively. This can be clearly seen in the representative pie charts where the remaining biofilm is related to its corresponding amount of untreated biofilm (Figure 54). However, within each sample, the differences were not significant except for the PTN system where the biofilm removal efficiency in the apical third was significantly better ($p \leq 0.001$) than the cervical third.

5.3.3. The remaining debris in the RCS samples:

Following the initial preparation, the results revealed that debris was found in the RCS with all file system groups. Canal instrumentation with PTN system has accumulated higher debris values compared to the other instruments (Figure 55) with a significant difference only with the RS system. No significant difference was found between PTU and RS groups despite more debris accumulated by the PTU group (Figure 55). The final rinse of RCS samples with 5 mL of the saliva buffer has significantly reduced, but not completely removed, the debris volume in all tested group ($p \leq 0.05$). Although, variations between the groups remain similar, the differences in debris volumes became non-significant ($p > 0.05$). In addition, the PTN group showed the higher percentage of reduction (60 % ± 12 %) in the debris volume compared to the PTU (52 % ± 12 %) and RS (58 % ± 21 %) groups.

The visual analysis of the 3D images showed that debris was present mostly in the isthmus space. Minimal debris volumes were seen in the main two canals of each sample. The complete occlusion of the isthmus space, for 2 to 3 mm of the canal length, was the common feature found in all three tested groups.

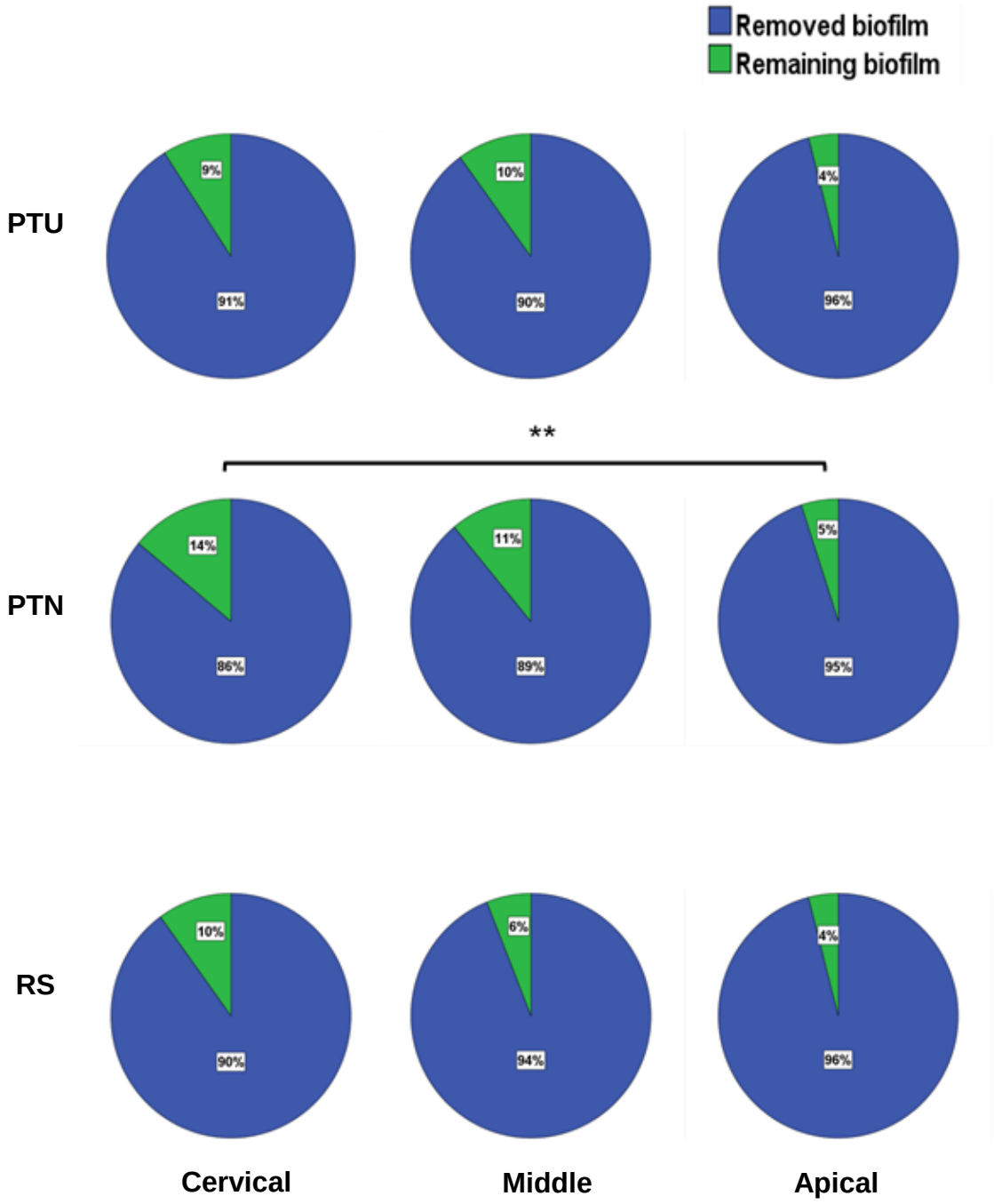

** = $p \leq 0.001$

Figure 54: The biofilm removal efficacy. Pie charts demonstrate the efficacy of biofilm removal by each file system in each canal third following the initial preparation. Kruskal-Wallis H and Mann-Whitney U test were applied to show the statistical difference ($p \leq 0.05$).

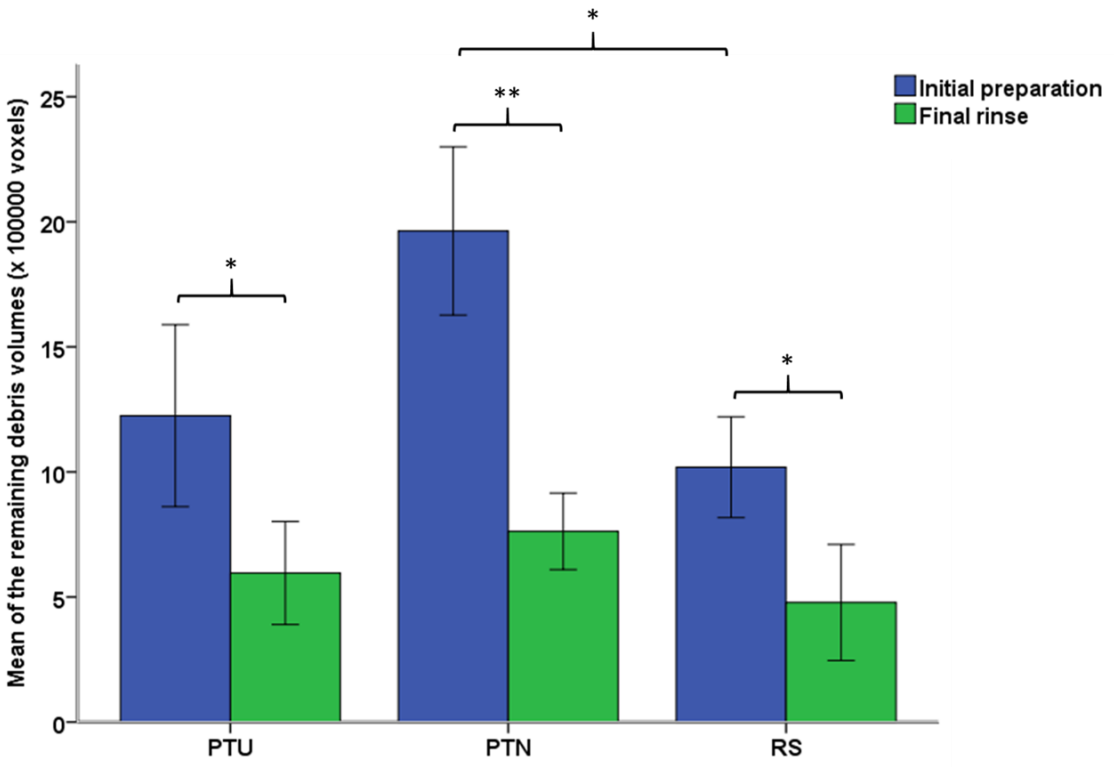

. * = *P ≤ 0.05.*
** = *P ≤ 0.001.*

Figure 55: The remaining debris volume in each group using OCT. A bar chart shows the mean values ± SE of debris volume in the root canal models following the initial preparation and the final rinse processes with the three file systems. ANOVA and LSD tests were applied for statistical analysis (*p ≤ 0.05*)

With respect to each canal third, the debris volumes following the initial preparation showed higher values in the cervical third compared to the middle and the apical third respectively (Figure 56). The difference was significant ($p \leq 0.05$) between the cervical and the apical thirds whereas non-significant ($p > 0.05$) in other pairwise groups. It is obvious that the final rinse was reduced the significant differences in debris values to a non-significant level except for the cervical third of the PTU group, which showed significance differences with the other two thirds (Figure 56).

5.3.4. The Correlation between debris and biofilm

For the three tested groups, the result showed a positive correlation between the volume of the remaining debris and the remaining biofilm in both initial preparation and final rinse procedures. With increasing debris volume, the biofilm volume has increased as demonstrated by the scatter plot and the Loess fitting line (Figure 57). The correlation was significant ($p \leq 0.01$) in the RS group for both treatment stages, whereas, a weak correlation was seen in the PTU and PTN groups (Figure 57).

Regardless of treatment type, the Spearman's test revealed a significant correlation ($p \leq 0.01$) when comparing the remaining biofilm to the accumulated debris of all groups (r_s = 0.502).

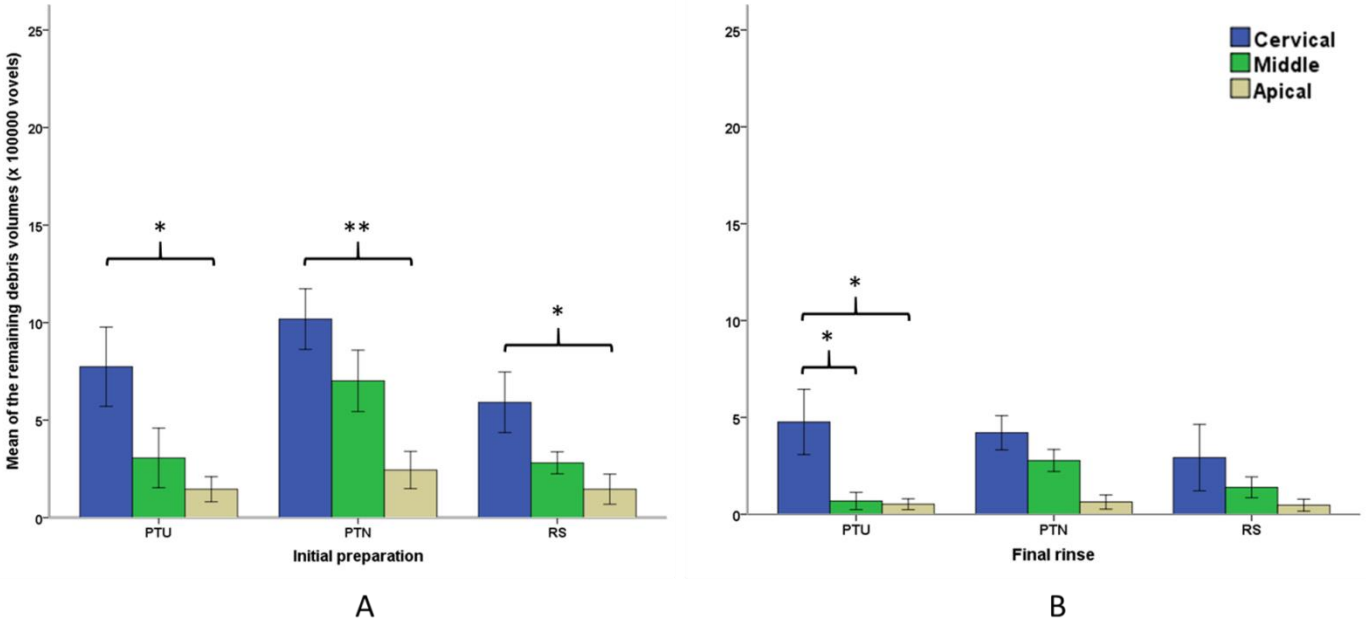

* = $p \leq 0.05$

* = $p \leq 0.001$

Figure 56: The remaining debris volumes in root canal thirds using OCT. The mean values ± SE of the remaining debris volumes of the three tested file systems in each root canal third following the initial preparation (A) and the final rinse (B) processes. Kruskal-Wallis H and Mann-Whitney U test were applied to show the statistical difference ($p \leq 0.05$).

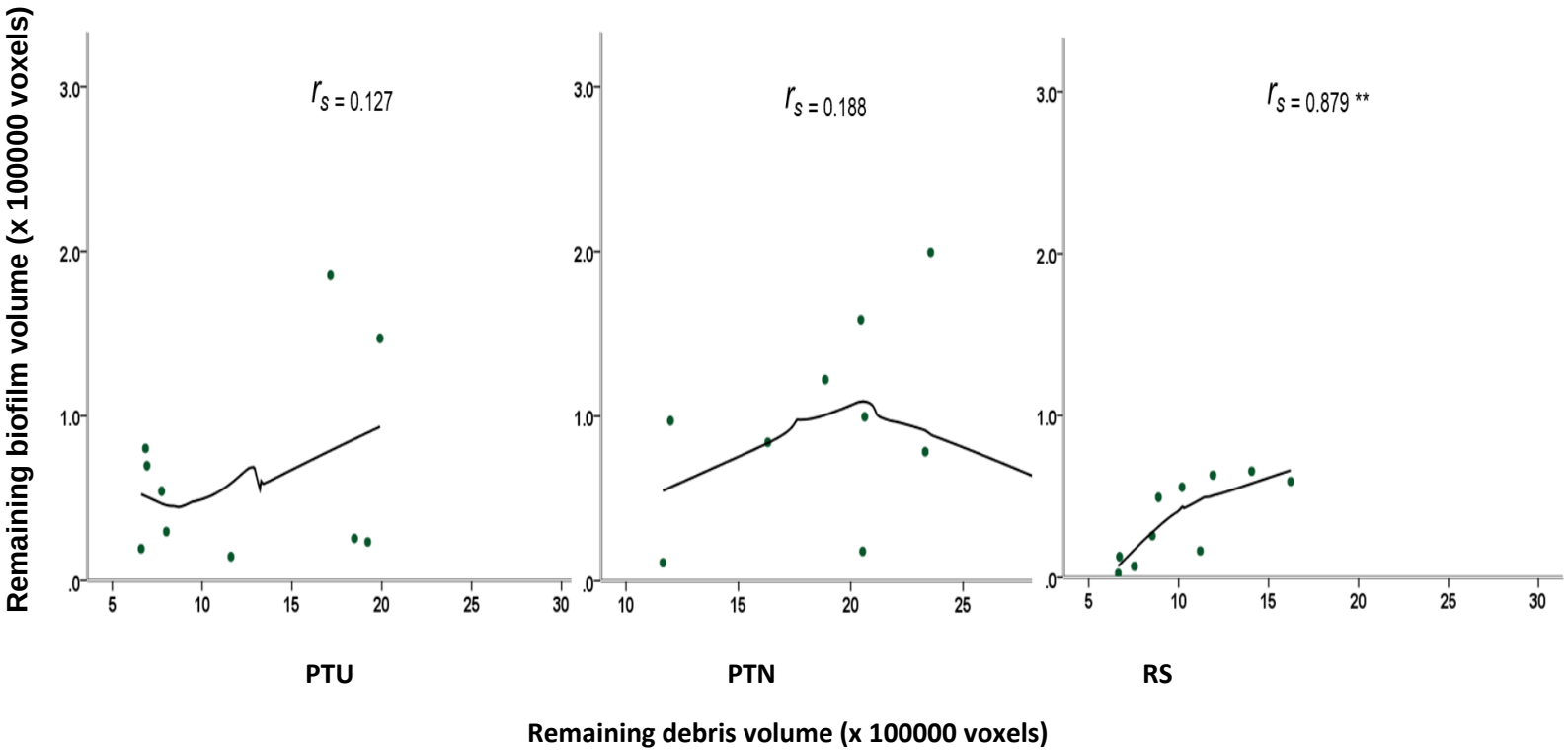

** = ***p ≤ 0.001***

Figure 57: Correlation between the remaining debris and the remaining biofilm. Spearman's correlation coefficient (r_s), scatter plot, and Loess fitting line show the positive correlation between the remaining debris and the remaining biofilm following the initial preparation of the tested groups ($p \leq 0.01$).

5.4. Discussion

This experiment effectively used the OCT as a non-contact tool for 3D quantitative evaluation of debris and biofilm in the entire RCS. The short scanning time of 27 sec seems convenient when compared to 3900 sec scanning time required by microCT for a single sample. However, scanning noise was the major disadvantage that was encountered during the imaging process. Such default noise was not avoidable as it usually affects scanning systems that use low light energy (Bozic et al., 2017, Martin et al., 2017).

Binarization has been described as a noise management measure by isolation of the foreground objects, such as biofilm and debris, from the noisy background by pixels' threshold range application (Wagner and Horn, 2017). For an effective binarization, reduction of noise through filtering algorithm is required for accurate threshold application. In order to preserve object edges, the nonlinear Median filter was widely applied during the processing of OCT images (Arias-Castro and Donoho, 2009). In the current work, the Median filter alone was not sufficient to eradicate the whole background noise pixels. Thus, another non-linear filter called Virtual Stack Denoiser was applied and showed dramatic improvement in image resolution. These two filters have advantages of being applicable on the image stack and maintain the intensity of the image signal by using the Boolean mathematical function (Delibasis et al., 1997).

5.4.1. The control group

The current findings showed that the RCS wall, debris, and biofilm were detected by the OCT as grey pixels with higher values (*i.e.* white) whereas RCS space was detected as grey pixels with lower values (*i.e*. black).

Although, the root canal samples were made from transparent material, the boundary of the RCS was visible during scanning. This would be caused by the immediate change of the RI between the RCS sample (RI = 1.5) and air (RI = 1) at the canal space. This change causes reflection of the passing light (Zhu et al., 2009) at the sample/air interface. This reflection possibly made the RCS surface detectable by the OCT scanner.

Interestingly, the remaining debris in the RCS was detected by the OCT despite that debris was cut from the same transparent material of the RCS sample. This would be explained by the change in the material transparency after the canal shaving process. In the amorphous structure, the polymeric resin materials are transparent with an RI similar to that of pure glass. This less stable non-refractive amorphous form will change to the stable refractive (*i.e.* visible) crystalline from when an insult is applied to the polymer structure (White and Spruiell, 1981, Yu, 2001).

The preliminary control study showed successful biofilm development after 4 days of incubation. The biofilm appeared as grey pixels with lower intensity in comparison to the high intensity of the grey pixels of the remaining debris. Such intensity differences are probably caused by the differences in the RIs (*i.e.* optical properties) of both materials (Podoleanu, 2012).

The recognition of biofilm in the simulated RCS was not surprising as OCT was routinely used for volumetric evaluation and quantification of biofilm in different research reports (Fortunato et al., 2017, Wagner and Horn, 2017) through transparent substrates (Xi et al., 2006a, Haisch and Niessner, 2007).

In the control group, the pre-instrumentation scanning provided important information about the empty status of the RCS cavity. The information was used as a guide for detection of changes, such as debris, that deposited in the RCS after instrumentation. The current results agree with other results that spaces appear as black pixels during the OCT scanning process. The OCT has wide application in detection of spaces resulted from diseases, such as macular hole and retinal detachment (van Velthoven et al., 2007, Wu et al., 2018).

5.4.2. The biofilm in the RCS sample.

With the CDFF method, the biofilm was generated with a larger volume in the apical third followed by middle and cervical thirds respectively. This is probably related to the basic mechanism used by the CDFF where biofilm is created in a gradual rhythm from the base toward the top of the sample (Wilson, 1999). This mechanism might give an early opportunity for the apical third to host more biomass before the middle and cervical thirds respectively.

The results revealed that root canal preparation produced a large reduction in the amount of the biofilm; however complete root canal sterilization was not possible with any of file systems. This is consistent with the previous findings from other studies (Bortoluzzi et al., 2015, Neves et

al., 2016). The effect of file design was similar to the current finding of the CLSM experiment that the RS system left the least amount of the biofilm while the PTN system left the highest amount of the biofilm.

The supplementary rinsing allowed more biofilm to be removed from the canal space. Canals with more biofilm mass, such as the PTN group, benefited more from this action when compared to other treatment groups with less remaining biofilm mass. This agrees with other findings that supplementary rinsing attempts decreased the level of biofilm in root canals (Alves et al., 2011, Paiva et al., 2012). These findings would clinically necessitate the final rinsing as a supplementary step to improve canal disinfection.

5.4.3. The remaining debris in the RCS samples

The results indicated that the RS files left the minimum amount of debris in contrast to the PTN files which left the maximum amount. These findings appear to be identical to the previous findings of the remaining biofilm with respect to the effectiveness of each file system. This might indicate that cleaning and disinfection are interrelated processes during root canal preparation.

The vast majority of the debris was seen in the canal isthmus in a similar picture to debris distribution found in natural teeth using the microCT technique. In addition, similarity was seen in debris distributed at canal thirds where the cervical third occupied by the largest value followed by the middle and apical third respectively. This debris picture may be explained as

the effect of variation in file cross-section diameter and variation in canal volume capacity to create and retain debris respectively. These findings, in turn, highlight the validity of the printed samples to simulate canal debridement, and, emphasise OCT as a reliable debris measuring imaging tool.

The final rinsing with the saliva buffer solution produced a remarkable reduction in the quantity of the remaining debris. This goes in agreement with other studies (Druttman and Stock, 1989, Sedgley et al., 2005, Al-Ali et al., 2012) where it was found that the final rinse was effective in removing debris from canal isthmus at all canal levels. Most of these studies concluded that increasing irrigant volume and extending time of irrigation were behind the improvement in the canal debridement.

5.4.4. The Correlation between debris and biofilm

In the current experiment, the presence of debris contributed to the presence of the biofilm. Image observations showed that biofilm remnants were entombed by debris remnants by closing isthmus entrance. Thus, debris might act as a barrier against the mechanism of the irrigation protocol which aims to disrupt the biofilm in the isthmus space. Accordingly, minimizing the amount of debris is important in the disinfection of the RCS.

5.5. Conclusions

The OCT scanner with 930 nm wavelength is a reliable device for quantification of the remaining debris and biofilm in transparent root canal models. The technique has provided rapid direct scanning of the entire RCS. The non-contact approach permitted cyclic scanning to be applied on the same sample following different treatment interventions. The real time imaging has eliminating the necessity for biofilm sample preparation, such as fixation or staining steps which are features of other imaging techniques.

The RS file system was the most effective system in the debriding and disinfecting the RCS, while the PTN was the least effective among the three file systems. The isthmus space harboured most of the debris and biofilm following root canal preparation.

The amount of the remaining debris is greatly affected by the cross-section design, cross-section diameter, and canal third volume. Supplementary final rinsing was an effective measure to enhance cleaning and disinfection goals. The presence of debris is directly related to the presence of the biofilm following root canal preparation. Based on these findings, the null hypothesis is rejected.

CHAPTER SIX:

GENERAL DISCUSSION AND CONCLUSIONS

Cleaning and disinfection of the root canal system (RCS) are mandatory goals for successful endodontic therapy. However, there are some technical and anatomical challenges in achieving these goals. This thesis investigated the effects of these challenges in terms of quantitative and qualitative evaluation of the remaining debris and biofilm following root canal preparation. Emphasis has been directed towards the anatomical complexity of the RCS and the cross-section design of the file system. Both of these have a major contribution in the effectiveness of cleaning and disinfection procedures (Siqueira et al., 1997b, Neelakantan et al., 2016b, Machado et al., 2017). In this research, the mesial root of a lower molar with a complete isthmus was used. The rotary file systems were chosen with symmetric (centred) and asymmetric (off-centred) deigns. These were tested in simulated canals *in vitro*.

In order to improve our understanding of the debridement and disinfection processes, the influence of the file design on the remaining debris and biofilm in the RCS was evaluated. Such research will also guide future development of new file designs. In addition, the establishment of reproducible methods for testing root canals with complex anatomy may be used for improving treatment modalities.

In the current study, three imaging techniques were used to test the RCS volumes both at micrometre and millimetre scales. The imaging tools used were microCT, CLSM in combination with IIF assay, and OCT. The latter two imaging tools were used with novel root canal samples (*in vitro* model systems), which were developed as part of this thesis.

6.1. The remaining debris using microCT imaging.

MicroCT is a reliable tool for scanning tooth structure at high spatial resolution. The microCT images were used to assess different estimations, such as canal volume, instrumented canal surfaces (Peters et al., 2003b) and remaining debris (Paqué et al., 2009, Robinson et al., 2012). However, the application of this imaging tool was highly restricted to samples with high structural density while resolution has a limit of approximately 6 µm. Thus, evaluation of low density biological and microbiological structure at cellular levels is required an optical imaging tool, such as SEM or CLSM, at nanometre or micrometre scale resolution.

The results showed the presence of high percentages of un-instrumented (un-touched) surfaces that lined canal isthmi and protrusion spaces following preparation. Large parts of these spaces were occluded by debris. The debris percentages distributed mainly at larger canal volumes, such as the cervical third, and to a lesser extent at the middle and apical thirds respectively. These findings support previous results (Verstraeten et al., 2017b) that un-touched spaces have a negative effect on canal debridement and work as pools for debris during instrumentation.

With respect to the file design, more debris remained at canal thirds that corresponded to wider cross sections on the file shaft. It was demonstrated that more dentine is cut as the file diameter is increased. These findings suggest that increasing cross-section file diameter will increase the remaining debris. This caused by increasing the created debris and vice versa. This concept might be noticed in the PTN file system where taper regression cervically has reduced the remaining debris percentage at the cervical level. However, in the design principles of the file instrument, the cross-section diameter increases at coronal direction. The idea is that canal

coronal flaring is recommended to enhance irrigant flow dynamics for efficient debridement apically (Coldero et al., 2002). Therefore, such taper regression would reduce coronal flaring and hence more debris percentage is seen at the apical region in the PTN group.

It was interesting to see that the asymmetric file systems create more debris. However, this was compensated by their efficiency in removing debris. In contrast, the symmetric file created less debris but was not efficient in removing it. These findings support the idea that spaces left between file cutting edges and the root canal wall may assist in removing debris out of the RCS. Based on the methodology used in the current experiment, the estimated remaining debris percentages were proportional to the amount of the created debris (Robinson et al., 2012) and this did not reflect the actual amount left in the RCS (Paqué et al., 2009). Thus, it would be possible to expect that files could leave more debris amount despite their relative efficiency in removing debris. This will be further explained in the finding of the OCT experiment.

6.2. Modelling of the root canal system

In the biomedical field, modelling is routinely used to simulate human tissue. This overcomes practical and ethical barriers for undertaking *in vivo* experiments (Dermol-Černe and Miklavčič, 2018). In endodontics, the available RCS models do not comply with the anatomical, physical, and biological challenges that naturally exist during root canal treatment. In addition, there are limited verification or validation tests conducted on such models.

Anatomical objects that are produced with precision by rapid prototyping technology are ideal for improving RCS modelling. The aim was to develop samples with realistic anatomical features. In this research, the RCS models that were produced had to fulfil certain requirement for the direct assessment of the biofilm under optical scanning means. These required the model had to be constructed from transparent materials that supported biofilm growth and enabled direct visualization with minimal aberration of the produced images in order to test their reliability for such experiments.

The tested resin materials showed good surface energy (wettability), which was promising for generation of a biofilm (Schnurr and Allen, 2015). It has been demonstrated that biofilm is generated when covalent attractive forces developed between bacteria and material substrate (Dufrêne, 2015). Such attraction would be replaced with repulsive inhibitory forces when surface energy is low. This surface property allowed good adhesion of the biofilm.

Additionally, the model produced supported growth of surface biofilm without surface treatment with fibronectin or bovine serum albumin. This reduced experimental steps and eliminated early interactions between proteins and irrigant solution during canal preparation stages. The transparent structure with refractive indices (RIs) similar to that of the glass slide highlighted the suitability of the resin materials for direct optical imaging. These criteria have eliminated the need for sectioning of the samples as undertaken by other researchers (Cruz et al., 2017). The materials do not required a specific method of sterilization and it could simply be autoclaved.

A disadvantage was that the surface hardness of the resin materials was inferior to that of dentine. Therefore the simulated root canal samples is not applicable for future testing of stresses generated during canal instrumentation (Kwak et al., 2017, Pedullà et al., 2017).

The use of a microtiter plate is a widely applied approach for characterizing biofilm growth and for testing biofilm treatment on the well surfaces (Fleer and Verhoef, 1989, Wakimoto et al., 2004, Gaudreau et al., 2018) or on surfaces of tested biomaterials (Han et al., 2017, Núñez-Beltrán et al., 2017, Oliveira et al., 2017). In addition, this method revealed advantages of being reproducible and generate an even layer of biofilm on the sample surfaces. In root canal infections, biofilm has been identified as the common living environment for the infectious bacteria which causes problem in root canal treatment. In biofilm, there are viable and non-viable bacteria with percentages varied according to the developmental stage. In order to ensure the maximum number of viable bacteria for the testing procedure, a biofilm assay was run in a 24-well microtiter plate for five time intervals using the standard *E. faecalis* species. The results of the assay indicated that 7 days growth produced the maximum absorption value and hence the maximum biofilm amount (Magalhães et al., 2017). These findings precluded other growth periods to generate the biofilm model as It was demonstrated that the biofilm amount is increased with increasing number of viable bacteria (Zhang et al., 2013).

6.3. The remaining biofilm using the *in situ* indirect immunofluorescence technique

Biofilm evaluation is best undertaken by different imaging scales. This allows understanding the structural and the physiological properties of this biomass. The nanometre or micrometre scales permit to explore the distribution of bacterial populations (the forming units for the biofilm). Imaging techniques, such as SEM (Sousa et al., 2017) and CLSM (Kishen et al., 2017), are useful in this request. Conversely, the millimetre scale has been used for investigating the biofilm EPS matrix using imaging techniques such as OCT and MRI (Fortunato et al., 2017, Renslow et al., 2017).

It has been demonstrated that *in situ* IIF technique can effectively label target microorganisms collected from infected root canals (Gohean et al., 1990). The repeatability, reliability, sensitivity and specificity of the immunofluorescence method for detection of bacterial IgG and IgM antibodies were similar to the enzyme-linked immunosorbent assay (Muleme et al., 2016). The staining protocol showed high affinity to label bacterial species as displayed in the CLSM images. Because the target of the labelling antibody is the IgG epitope on the bacterial surface, the test does not require increasing permeability of the bacterial cell wall to allow dye penetration to the intracellular nucleotide (Frickmann et al., 2017) hence cell morphology remained intact. In addition, surface labelling is promising as the test is not detecting bacteria with a damaged cell wall (the hostile of epitopes). This provided a great opportunity for testing the antibacterial activity of CHX that works by destroying the bacterial cell wall at 2 % concentration (Freitas et al., 2003).

The results showed that RS file system was more effective in removing biofilm while the PTN file system was the least effective among the three tested systems. Complete disinfection was not possible with all treatment groups.

Both file taper and the position of the needle vent have influenced the remaining amount of biofilm in each canal third and hence in the entire canal. For PTU and RS, which have continuous tapers, the positon of needle vent at the end level of the middle third was effective in removing more biofilm from the middle and apical thirds respectively. This also would be the reason that the disinfection process was less effective in the cervical third, which remains distance from the needle vent.

Regarding the PTN file system, the change in the tapering continuity from progressive to regressive at the middle and cervical third might have interfered with the irrigation flow dynamics at the apical region. This will have caused a reduction in its efficiency at this level. Such effects on the remaining biofilm were similarly seen previously on the remaining debris.

6.4. The remaining debris and biofilm using the OCT

The OCT uses a non-ionizing radiation with short scanning time that make it a promising tool for the real time imaging of biological and non-biological tissues. The OCT can image semi-transparent materials, such as biofilm, through a transparent substrate, such as the current root canal model (Xi et al., 2006b). The novel application of the OCT allowed the assessment of the debris and the biofilm. It also allowed the utilization of all the canal preparation

procedures. The non-contact approach permitted multiple scanning for the same sample for different treatment interventions. There were no need for preparatory steps, such as fixation and staining, which are required when imaging with confocal microscopy. The other advantage is that the scanning procedure is accomplished in real time.

The results of the remaining biofilm was similar to the immunofluorescence method where the RS file system was the most effective in the disinfection procedure while the PTN file system was the least effective among the three tested groups. In addition, none of the file systems has completely disinfected the RCS. The isthmus space harbours most of the remaining biofilm. The findings are consistent with a recent study by Siqueira et al., (2017) who showed that the isthmus space of the mesial root remained untouched followed preparation. It was filled with bacteria, inorganic debris and remnant of pulp tissue. These findings can inter-validate both techniques for assessment of disinfection protocols in simulated root canals.

The RS file system debrides the canals more than the other file systems while the PTN was the poorest in achieving debridement. The use of identical RCS samples has controlled the variability in root canal volume. It has allowed group comparison of the remaining debris amount rather than the remaining debris percentage. The OCT findings revealed that the file system that leaves more debris will leave more biofilm and vice versa. There were positive correlations between debris and biofilm following preparation of infected RCS.

6.5. Conclusions

6.5.1. Debris removal

- None of the tested file systems were capable of complete debridement and disinfection of the RCS.
- The asymmetric cross section file displayed higher efficiency to remove higher proportion of the created debris when compared to the file with symmetric cross-section.
- Between the asymmetric, the RS system was the most efficient. Higher debris percentages were found in association with larger RCS volume, more created debris, and wider un-instrumented surface areas.
- Files with wider cross-sections, such as PTN created more debris than files with narrower cross-section, such as RS and PTU respectively.
- The file system with one contact point with the canal wall such as the RS has left less debris percentages than files with two or three contact points such as PTN and PTU respectively.

6.5.2. Biofilm removal

- The RS file system has left the least amount of the biofilm while the PTN file system has left the largest amount of biofilm following root canal preparation.

- The taper variation of PTN files along their shafts interfered with the debridement and disinfection processes at the apical third of this group.
- The isthmus and protrusion spaces following root canal preparation remained un-instrumented and occupied by most of the remaining debris and biofilm especially at the larger RCS volumes.
- The supplementary agitation with sonic instrument and final rinsing with saliva buffer were effective in reducing debris and biofilm levels following preparation.

6.5.3. The root canal system model

- Modelling of RCS with image-based RP technology produces predictable samples with accurate dimension.
- The samples showed good surface energy that supported growth of single and dual species biofilm and showed a promising adhesion records with the *E. faecalis* biofilm.
- The direct imaging of biofilm and debris in RCS samples was highly possible with optical imaging tools due to the sample transparency with minimum refractivity.
- The model was verified as an ideal system for assessing root canal treatment *in vitro.*

6.5.4. Imaging techniques

- The microCT provides detailed anatomical 3D scan to the tooth structure that allowed multiple assessments to the root canal system before and after root canal preparation.

- The CLSM is powerful technique especially when coupled with the *in situ* immunofluorescence method to quantify biofilm on simulated RCS.
- The OCT is an effective and fast non-contact tool for evaluation of debris and biofilm in the simulated RCS.

6.6. Recommendations for future studies

1. Evaluation of the of root canal cleaning and disinfection using root canal model that mimic anatomical and structural components of the root dentine, such as the inclusion of collagen fibrils and dentinal tubules. In addition, using a material with similar toughness to the root dentine.
2. Evaluation of the irrigation flow dynamics in the root canal isthmus space using different kinds of irrigations systems. The evaluation should include all canal levels with and without root canal preparation to compare the effect of the remaining debris on the effectiveness of any irrigation regimen used.
3. Assessment of the effect of using irrigation needles with multiple openings at all canal thirds on the cleaning and disinfection of root canals with complete isthmus. The assessment should be made on both computational and physical model of the proposed needle.

Appendix:

The Ethical approval for using human extracted teeth

REFERENCES

ABOU-RASS, M. & PATONAI, F. J. 1982. The effects of decreasing surface tension on the flow of irrigating solutions in narrow root canals. *Oral Surgery, Oral Medicine, Oral Pathology,* 53**,** 524-526.

ABOU-RASS, M. & PICCININO, M. V. 1982. The effectiveness of four clinical irrigation methods on the removal of root canal debris. *Oral Surgery, Oral Medicine, Oral Pathology,* 54**,** 323-328.

ABSOLOM, D. R., LAMBERTI, F. V., POLICOVA, Z., ZINGG, W., VAN OSS, C. J. & NEUMANN, A. W. 1983. Surface thermodynamics of bacterial adhesion. *Applied and Environmental Microbiology,* 46**,** 90-97.

ADCOCK, J. M., SIDOW, S. J., LOONEY, S. W., LIU, Y., MCNALLY, K., LINDSEY, K. & TAY, F. R. 2011. Histologic Evaluation of Canal and Isthmus Debridement Efficacies of Two Different Irrigant Delivery Techniques in a Closed System. *Journal of Endodontics,* 37**,** 544-548.

ADIGUZEL, O., GOKCEN, M. G. & OLCAY, A. B. 2016. Evaluation of the Effect of Needle Tilting Angle on Irrigant Flow in the Root Canal Using Side-Vented Needle by an Unsteady Computational Fluid Dynamics Model. *International Dental Research,* 6**,** 1-8.

AHMAD, M., FORD, T. R. P. & CRUM, L. A. 1987. Ultrasonic debridement of root canals: an insight into the mechanisms involved. *Journal of Endodontics,* 13**,** 93-101.

AHMED, A. & NICHOLSON, K. G. 1996. Delays and diversity in the practice of local research ethics committees. *Journal of Medical Ethics,* 22**,** 263-266.

AL-AHMAD, A., MÜLLER, N., WIEDMANN-AL-AHMAD, M., SAVA, I., HÜBNER, J., FOLLO, M., SCHIRRMEISTER, J. & HELLWIG, E. 2009a. Endodontic and Salivary Isolates of Enterococcus faecalis Integrate into Biofilm from Human Salivary Bacteria Cultivated In Vitro. *Journal of Endodontics,* 35**,** 986-991.

AL-AHMAD, A., MÜLLER, N., WIEDMANN-AL-AHMAD, M., SAVA, I., HÜBNER, J., FOLLO, M., SCHIRRMEISTER, J. & HELLWIG, E. 2009b. Endodontic and Salivary Isolates of Enterococcus faecalis Integrate into Biofilm from Human Salivary Bacteria Cultivated In Vitro. *Journal of Endodontics,* 35**,** 986-991.

AL-GHARRAWI, H. & FADHIL, M. A. 2016. A Comparative Study to Evaluate Canal Transportation and Centering Ratio at Different Levels of Simulated Curved Canals Prepared by iRaCe, ProTaper NEXT and ProTaper Universal Files. *Journal of American Science,* 12.

AL-ALI, M., SATHORN, C. & PARASHOS, P. 2012. Root canal debridement efficacy of different final irrigation protocols. *International Endodontic Journal,* 45**,** 898-906.

AL-OMARI, W., MITCHELL, C. & CUNNINGHAM, J. 2001. Surface roughness and wettability of enamel and dentine surfaces prepared with different dental burs. *Journal of Oral Rehabilitation,* 28**,** 645-650.

AL-QUDAH, A. & AWAWDEH, L. 2009. Root and canal morphology of mandibular first and second molar teeth in a Jordanian population. *International Endodontic Journal,* 42**,** 775-784.

AL GROOSH, D., PRATTEN, J. & HUNT, N. 2016. The effects of polishing the fitting surface of acrylic base retainers on Methichillin resistance staphylococcus aureus; a laboratory study. *Iraqi Dental Journal,* 38**,** 137-141.

ALARAB MOHMMED, S., VIANNA, M. E., PENNY, M. R., HILTON, S. T., MORDAN, N. & KNOWLES, J. C. 2016. A novel experimental approach to investigate the effect of different agitation methods using sodium hypochlorite as an irrigant on the rate of bacterial biofilm removal from the wall of a simulated root canal model. *Dental Materials,* 32**,** 1289-1300.

ALBRECHT, L. J., BAUMGARTNER, J. C. & MARSHALL, J. G. 2004. Evaluation of apical debris removal using various sizes and tapers of ProFile GT files. *Journal of Endodontics,* 30**,** 425-428.

ALBUQUERQUE, M. T. P., NAGATA, J. & BOTTINO, M. C. 2017. Antimicrobial Efficacy of Triple Antibiotic–eluting Polymer Nanofibers against Multispecies Biofilm. *Journal of Endodontics,* 43**,** S51-S56.

ALKAHTANI, A., AL KHUDHAIRI, T. D. & ANIL, S. 2014. A comparative study of the debridement efficacy and apical extrusion of dynamic and passive root canal irrigation systems. *BMC Oral Health,* 14**,** 12.

ALOVISI, M., CEMENASCO, A., MANCINI, L., PAOLINO, D., SCOTTI, N., BIANCHI, C. & PASQUALINI, D. 2017. Micro-CT evaluation of several glide path techniques and ProTaper Next shaping outcomes in maxillary first molar curved canals. *International Endodontic Journal,* 50**,** 387-397.

ALVES, F. R., ANDRADE-JUNIOR, C. V., MARCELIANO-ALVES, M. F., PÉREZ, A. R., RÔÇAS, I. N., VERSIANI, M. A., SOUSA-NETO, M. D., PROVENZANO, J. C. & SIQUEIRA, J. F. 2016. Adjunctive steps for disinfection of the mandibular molar root canal system: a correlative bacteriologic, micro–computed tomography, and cryopulverization approach. *Journal of Endodontics,* 42**,** 1667-1672.

ALVES, F. R. F., ALMEIDA, B. M., NEVES, M. A. S., MORENO, J. O., RÔÇAS, I. N. & SIQUEIRA, J. F. 2011. Disinfecting Oval-shaped Root Canals: Effectiveness of Different Supplementary Approaches. *Journal of Endodontics,* 37**,** 496-501.

AMORA-SILVA, B. F., RIBEIRO, S., VIEIRA, C., MENDES, F., VIEIRA-NETO, A., ABDON, A., COSTA, F. & CAMPOS, A. 2018. Clinical efficacy of new α-bisabolol mouthwashes in postoperative complications of maxillofacial surgeries: a randomized, controlled, triple-blind clinical trial. *Clinical Oral Investigations***,** 1-8.

AMORENA, B., GRACIA, E., MONZÓN, M., LEIVA, J., OTEIZA, C., PÉREZ, M., ALABART, J.-L. & HERNÁNDEZ-YAGO, J. 1999. Antibiotic susceptibility assay for Staphylococcus aureus in biofilms developed in vitro. *Journal of Antimicrobial Chemotherapy,* 44**,** 43-55.

ANDERSON, A. C., ANDISHA, H., HELLWIG, E., JONAS, D., VACH, K. & AL-AHMAD, A. 2017. Antibiotic Resistance Genes and Antibiotic Susceptibility of Oral Enterococcus faecalis Isolates Compared to Isolates from Hospitalized Patients and Food. Boston, MA: Springer US.

ANSARI, J. M., ABRAHAM, N. M., MASSARO, J., MURPHY, K., SMITH-CARPENTER, J. & FIKRIG, E. 2017. Anti-biofilm activity of a self-aggregating peptide against Streptococcus mutans. *Frontiers in Microbiology,* 8**,** 488.

ARAI, Y., TAMMISALO, E., IWAI, K., HASHIMOTO, K. & SHINODA, K. 1999. Development of a compact computed tomographic apparatus for dental use. *practice,* 12**,** 15.

ARANDA, F., BLOY, N., PESQUET, J., PETIT, B., CHABA, K., SAUVAT, A., KEPP, O., KHADRA, N., ENOT, D. & PFIRSCHKE, C. 2015. Immune-dependent antineoplastic effects of cisplatin plus pyridoxine in non-small-cell lung cancer. *Oncogene,* 34**,** 3053.

ARIAS-CASTRO, E. & DONOHO, D. L. 2009. Does median filtering truly preserve edges better than linear filtering? *The Annals of Statistics***,** 1172-1206.

ARIAS-MOLIZ, M. T., ORDINOLA-ZAPATA, R., BACA, P., RUIZ-LINARES, M., GARCIA, E. G., DUARTE, M. A. H., BRAMANTE, C. M. & FERRER-LUQUE, C. M. 2015. Antimicrobial activity of Chlorhexidine, Peracetic acid and Sodium hypochlorite/etidronate irrigant solutions against Enterococcus faecalis biofilms. *International Endodontic Journal,* 48**,** 1188-1193.

ARIAS, M. P. C., MALIZA, A. G. A., MIDENA, R. Z., GRAEFF, M. S. Z., DUARTE, M. A. H. & ANDRADE, F. B. D. 2016. Effect of ultrasonic streaming on intra-dentinal disinfection and penetration of calcium hydroxide paste in endodontic treatment. *Journal of Applied Oral Science,* 24**,** 575-581.

ARIFFIN, A. F., HARUDIN, M. H., KANAGASINGAM, S., RAHMAN, M. M. & NOORINA, W. A. W. 2016. Apical extrusion of sodium hypochlorite irrigation during root canal treatment using monoject or hypodermic irrigation needle. *Bangladesh Journal of Medical Science,* 15**,** 575-578.

ATHANASSIADIS, B., ABBOTT, P. & WALSH, L. J. 2007. The use of calcium hydroxide, antibiotics and biocides as antimicrobial medicaments in endodontics. *Australian Dental Journal,* 52**,** S64-S82.

ATKINSON, M. E. & WHITE, F. H. 1992. *Principles of anatomy and oral anatomy for dental students*, Churchill Livingstone.

AVERY, J. K. & STEELE, P. F. 1992. *Essentials of oral histology and embryology: a clinical approach*, Mosby.

AVERY, J. K. & STEELE, P. F. 2006. *Essentials of oral histology and embryology: a clinical approach*, Mosby.

AVISON, J. 2014. *The world of physics*, Nelson Thornes.

AZEREDO, J., AZEVEDO, N. F., BRIANDET, R., CERCA, N., COENYE, T., COSTA, A. R., DESVAUX, M., DI BONAVENTURA, G., HÉBRAUD, M. & JAGLIC, Z. 2017. Critical review on biofilm methods. *Critical Reviews in Microbiology,* 43**,** 313-351.

B.S, H., CHANDU, G. S. & SHIRAGUPPI, V. L. 2014. Scanning Electron Microscopic Evaluation of Root Canal Surfaces Prepared with LightSpeed & Endowave Rotary System. *Journal of Clinical and Diagnostic Research : JCDR,* 8**,** ZC35-ZC38.

BAKER, N. A., ELEAZER, P. D., AVERBACH, R. E. & SELTZER, S. 1975. Scanning electron microscopic study of the efficacy of various irrigating solutions. *Journal of Endodontics,* 1**,** 127-135.

BARNES, A. M., DALE, J. L., CHEN, Y., MANIAS, D. A., GREENWOOD QUAINTANCE, K. E., KARAU, M. K., KASHYAP, P. C., PATEL, R., WELLS, C. L. & DUNNY, G. M. 2017. Enterococcus faecalis readily colonizes the entire gastrointestinal tract and forms biofilms in a germ-free mouse model. *Virulence,* 8**,** 282-296.

BASRANI, B., ROTH, K., SAS, G., KISHEN, A. & PETERS, O. A. 2011. Torsional Profiles of New and Used Revo-S Rotary Instruments: An< i> In Vitro</i> Study. *Journal of Endodontics,* 37**,** 989-992.

BATH-BALOGH, M., FEHRENBACH, M. J. & THOMAS, P. 1997. *Illustrated dental embryology, histology, and anatomy*, Saunders.

BAUMANN, M. A. & BEER, R. 2011. Endodontology.

BAUMGARTNER, J. C. & CUENIN, P. R. 1992. Efficacy of several concentrations of sodium hypochlorite for root canal irrigation. *Journal of Endodontics,* 18**,** 605-612.

BECKER, G. L., COHEN, S. & BORER, R. 1974. The sequelae of accidentally injecting sodium hypochlorite beyond the root apex: Report of a case. *Oral Surgery, Oral Medicine, Oral Pathology,* 38**,** 633-638.

BELTES, C., ECONOMIDES, N., SAKKAS, H., PAPADOPOULOU, C. & LAMBRIANIDIS, T. 2017. Evaluation of antimicrobial photodynamic therapy using indocyanine green and near-infrared diode laser against enterococcus faecalis in infected human root canals. *Photomedicine and Laser Surgery,* 35**,** 264-269.

BERGMANS, L., MOISIADIS, P., VAN MEERBEEK, B., QUIRYNEN, M. & LAMBRECHTS, P. 2005. Microscopic observation of bacteria: review highlighting the use of environmental SEM. *International Endodontic Journal,* 38**,** 775-788.

BERGMANS, L., VAN CLEYNENBREUGEL, J., WEVERS, M. & LAMBRECHTS, P. 2001. A methodology for quantitative evaluation of root canal instrumentation using microcomputed tomography. *International Endodontic Journal,* 34**,** 390-398.

BHASKAR, S. N. 1991. *Orban's oral histology and embryology*, Elsevier India.

BHOMKAR, P., MATERI, W., SEMENCHENKO, V. & WISHART, D. S. 2010. Transcriptional response of E. coli upon FimH-mediated fimbrial adhesion. *Gene Regulation and Systems Biology,* 4**,** 1.

BIBB, R., EGGBEER, D. & PATERSON, A. 2014. *Medical modelling: the application of advanced design and rapid prototyping techniques in medicine*, Woodhead Publishing.

BITTER, K., VLASSAKIDIS, A., NIEPEL, M., HOEDKE, D., SCHULZE, J., NEUMANN, K., MOTER, A. & NOETZEL, J. 2017. Effects of Diode Laser, Gaseous Ozone, and Medical Dressings on Enterococcus faecalis Biofilms in the Root Canal Ex Vivo. *BioMed Research International,* 2017.

BONESSIO, N., ARIAS, A., LOMIENTO, G. & PETERS, O. A. 2017. Effect of root canal treatment procedures with a novel rotary nickel titanium instrument (TRUShape) on stress in mandibular molars: a comparative finite element analysis. *Odontology,* 105**,** 54-61.

BOOTHE, T., HILBERT, L., HEIDE, M., BERNINGER, L., HUTTNER, W. B., ZABURDAEV, V., VASTENHOUW, N. L., MYERS, E. W., DRECHSEL, D. N. & RINK, J. C. 2017. A tunable refractive index matching medium for live imaging cells, tissues and model organisms. *eLife,* 6.

BORTOLUZZI, E. A., CARLON, D., MEGHIL, M. M., EL-AWADY, A. R., NIU, L., BERGERON, B. E., SUSIN, L., CUTLER, C. W., PASHLEY, D. H. & TAY, F. R. 2015. Efficacy of 3D conforming nickel titanium rotary instruments in eliminating canal wall bacteria from oval-shaped root canals. *Journal of Dentistry,* 43**,** 597-604.

BOUTSIOUKIS, C., GOGOS, C., VERHAAGEN, B., VERSLUIS, M., KASTRINAKIS, E. & VAN DER SLUIS, L. 2010a. The effect of apical preparation size on irrigant flow in root canals evaluated using an unsteady Computational Fluid Dynamics model. *International Endodontic Journal,* 43**,** 874-881.

BOUTSIOUKIS, C., VERHAAGEN, B., VERSLUIS, M., KASTRINAKIS, E. & VAN DER SLUIS, L. 2010b. Irrigant flow in the root canal: experimental validation of an unsteady Computational Fluid Dynamics model using high-speed imaging. *International Endodontic Journal,* 43**,** 393-403.

BOUTSIOUKIS, C., VERHAAGEN, B., WALMSLEY, A., VERSLUIS, M. & SLUIS, L. 2013. Measurement and visualization of file-to-wall contact during ultrasonically activated irrigation in simulated canals. *International Endodontic Journal,* 46**,** 1046-1055.

BOYD, R. D., VERRAN, J., JONES, M. & BHAKOO, M. 2002. Use of the atomic force microscope to determine the effect of substratum surface topography on bacterial adhesion. *Langmuir,* 18**,** 2343-2346.

BOZIC, I., EL-HADDAD, M. T., MALONE, J. D., JOOS, K. M., PATEL, S. N. & TAO, Y. K. Year. Multi-volumetric registration and mosaicking using swept-source spectrally encoded scanning laser ophthalmoscopy and optical coherence tomography. *In:* Optical Coherence Tomography and Coherence Domain Optical Methods in Biomedicine XXI, 2017. International Society for Optics and Photonics, 1005326.

BRAUNER, P. & JÄCKEL, U. 2016. Automated Image Analysis for Determination of Antibody Titers Against Occupational Bacterial Antigens Using Indirect Immunofluorescence. *The Annals of Occupational Hygiene,* 60**,** 643-648.

BRUKER. 2018. *SKYSCAN 1172: high resolution desk-top micro-CT* [Online]. Available: http://bruker-microct.com/products/1172.htm [Accessed 3/30/2018].

BRYCE, G., MACBETH, N., GULABIVALA, K. & NG, Y. L. 2017. The efficacy of supplementary sonic irrigation using the EndoActivator® system determined by removal of a collagen film from an ex vivo model. *International Endodontic Journal*.

BUKHARI, S., KIM, D., LIU, Y., KARABUCAK, B. & KOO, H. 2018. Novel Endodontic Disinfection Approach Using Catalytic Nanoparticles. *Journal of Endodontics*.

BUKHARY, S. & BALTO, H. 2017. Antibacterial Efficacy of Octenisept, Alexidine, Chlorhexidine, and Sodium Hypochlorite against Enterococcus faecalis Biofilms. *Journal of Endodontics,* 43**,** 643-647.

BURLESON, A., NUSSTEIN, J., READER, A. & BECK, M. 2007. The in vivo evaluation of hand/rotary/ultrasound instrumentation in necrotic, human mandibular molars. *Journal of Endodontics,* 33**,** 782-787.

BYSTROM, A. & SUNDQVIST, G. 1981. Bacteriologic evaluation of the efficacy of mechanical root canal instrumentation in endodontic therapy. *European Journal of Oral Sciences,* 89**,** 321-328.

CARUSO, G., ZACCONE, R. & CRISAFI, E. 2000. Use of the indirect immunofluorescence method for detection and enumeration of Escherichia coli in seawater samples. *Letters in Applied Microbiology,* 31**,** 274-278.

CAWSO, R. A. 2002. Cawson's essentials of oral pathology and oral medicine.

CHANDRA, S., CHANDRA, S. & CHANDRA, G. 2008. Textbook of Operative Dentistry (with MCQs).

CHANDRA, S., CHANDRA, S., CHANDRA, M. & CHANDRA, N. 2004. Textbook of Dental and Oral Histology and Embryology with MCQs. *Jaypee Brothers, Medical Publishers: India*.

CHARARA, K., FRIEDMAN, S., SHERMAN, A., KISHEN, A., MALKHASSIAN, G., KHAKPOUR, M. & BASRANI, B. 2016. Assessment of Apical Extrusion during Root Canal Irrigation with the Novel GentleWave System in a Simulated Apical Environment. *Journal of Endodontics,* 42**,** 135-139.

CHEN, J. E., NURBAKHSH, B., LAYTON, G., BUSSMANN, M. & KISHEN, A. 2014. Irrigation dynamics associated with positive pressure, apical negative pressure and passive ultrasonic irrigations: a computational fluid dynamics analysis. *Australian Endodontic Journal,* 40**,** 54-60.

CHENNAMSETTY, N., HELK, B., KAYSER, V., TROUT, B. & VOYNOV, V. 2017. Methods for identification of sites for IgG conjugation. Google Patents.

CHRISTNER, M., FRANKE, G. C., SCHOMMER, N. N., WENDT, U., WEGERT, K., PEHLE, P., KROLL, G., SCHULZE, C., BUCK, F., MACK, D., AEPFELBACHER, M. & ROHDE, H. 2010. The giant extracellular matrix-binding protein of Staphylococcus epidermidis mediates biofilm accumulation and attachment to fibronectin. *Molecular Microbiology,* 75**,** 187-207.

CHRISTO, J. E., ZILM, P. S., SULLIVAN, T. & CATHRO, P. R. 2016. Efficacy of low concentrations of sodium hypochlorite and low-powered Er,Cr:YSGG laser activated irrigation against an Enterococcus faecalis biofilm. *International Endodontic Journal,* 49**,** 279-286.

CHUA, S. L., LIU, Y., YAM, J. K. H., CHEN, Y., VEJBORG, R. M., TAN, B. G. C., KJELLEBERG, S., TOLKER-NIELSEN, T., GIVSKOV, M. & YANG, L. 2014. Dispersed cells represent a distinct stage in the transition from bacterial biofilm to planktonic lifestyles. *Nature Communications,* 5**,** 4462.

CIMA, M., SACHS, E., FAN, T., BREDT, J. F., MICHAELS, S. P., KHANUJA, S., LAUDER, A., LEE, S.-J. J., BRANCAZIO, D. & CURODEAU, A. 1995. Three-dimensional printing techniques. Google Patents.

COFFAE, K. P. & BRILLIANT, J. D. 1975. The effect of serial preparation versus nonserial preparation on tissue removal in the root canals of extracted mandibular human molars. *Journal of Endodontics,* 1**,** 211-214.

COHEN, A., LAVIV, A., BERMAN, P., NASHEF, R. & ABU-TAIR, J. 2009. Mandibular reconstruction using stereolithographic 3-dimensional printing modeling technology. *Oral Surgery, Oral Medicine, Oral Pathology, Oral Radiology, and Endodontology,* 108**,** 661-666.

COLDERO, L., MCHUGH, S., MACKENZIE, D. & SAUNDERS, W. 2002. Reduction in intracanal bacteria during root canal preparation with and without apical enlargement. *International Endodontic Journal,* 35**,** 437-446.

COOMBE, R. A., TATEVOSSIAN, A. & WLMPENNY, J. W. T. 1984. Factors affecting the growth of thin bacterial film in vitro. *Bacterial Adhesion and Preventive Dentistv.* Oxford: IRL, Press.

COSCAS, F., GLACET-BERNARD, A., MIERE, A., CAILLAUX, V., UZZAN, J., LUPIDI, M., COSCAS, G. & SOUIED, E. H. 2016. Optical coherence tomography angiography in retinal vein occlusion: evaluation of superficial and deep capillary plexa. *American Journal of Ophthalmology,* 161**,** 160-171. e2.

COSTERTON, J. W. 1999. Introduction to biofilm. *International Journal of Antimicrobial Agents,* 11**,** 217-221.

COSTERTON, J. W., CHENG, K., GEESEY, G. G., LADD, T. I., NICKEL, J. C., DASGUPTA, M. & MARRIE, T. J. 1987. Bacterial biofilms in nature and disease. *Annual Reviews in Microbiology,* 41**,** 435-464.

COSTERTON, J. W., STEWART, P. S. & GREENBERG, E. P. 1999. Bacterial biofilms: a common cause of persistent infections. *Science,* 284**,** 1318-1322.

CRUZ, A. T. G., GRECCA, F. S., PIASECKI, L., WICHNIESKI, C., WESTPHALEN, V. P. D., CARNEIRO, E., FARINIUK, L. F., NETO, S. & DA, U. X. 2017. Influence of the Calcium Hydroxide Intracanal Dressing on Dentinal Tubule Penetration of Two Root Canal Sealers. *European Endodontic Journal,* 2**,** 14.

DADRESANFAR, B., MOHAMMADZADEH-AKHLAGHI, N., SHAHAB, S., SHAHBAZIAN, S. & PARIROKH, M. 2017. Comparison of transportation and centering ability using RECIPROC and iRace: A cone-beam computed tomography study. *Journal of Oral Health and Oral Epidemiology,* 6**,** 159-164.

DAIMS, H. & WAGNER, M. 2007. Quantification of uncultured microorganisms by fluorescence microscopy and digital image analysis. *Applied Microbiology and Biotechnology,* 75**,** 237-248.

DALE, J. L., NILSON, J. L., BARNES, A. M. & DUNNY, G. M. 2017. Restructuring of Enterococcus faecalis biofilm architecture in response to antibiotic-induced stress. *npj Biofilms and Microbiomes,* 3**,** 15.

DAS, T. & MANOS, J. 2017. Pseudomonas aeruginosa Extracellular Secreted Molecules Have a Dominant Role in Biofilm Development and Bacterial Virulence in Cystic Fibrosis Lung Infections. *Progress in Understanding Cystic Fibrosis.* InTech.

DE-DEUS, G., MARINS, J., DE ALMEIDA NEVES, A., REIS, C., FIDEL, S., VERSIANI, M. A., ALVES, H., LOPES, R. T. & PACIORNIK, S. 2014. Assessing accumulated hard-tissue debris using micro–computed tomography and free software for image processing and analysis. *Journal of Endodontics,* 40**,** 271-276.

DE BEER, D., STOODLEY, P. & LEWANDOWSKI, Z. 1994. Liquid flow in heterogeneous biofilms. *Biotechnology and Bioengineering,* 44**,** 636-641.

DE MEYER, S., MEIRE, M., COENYE, T. & DE MOOR, R. 2017. Effect of laser-activated irrigation on biofilms in artificial root canals. *International Endodontic Journal,* 50**,** 472-479.

DE PAULA, V. A. C., OLIVEIRA, Q. B., DE OLIVEIRA BRITO, I. R., DE CARVALHO FERREIRA, D., CAVALCANTE, F. S., TEIXEIRA, L. M., DOS SANTOS, K. R. N. & PRIMO, L. G. S. 2017. Identification of Enterococcus faecalis by PCR in saliva of pediatric patients. *Archives of Oral Research,* 9**,** 171-176.

DE PAZ, L. E. C. 2012. Development of a multispecies biofilm community by four root canal bacteria. *Journal of Endodontics,* 38**,** 318-323.

DE PAZ, L. E. C. 2018. Aetiology of Persistent Endodontic Infections in Root-Filled Teeth. *Apical Periodontitis in Root-Filled Teeth.* Springer.

DE PAZ, L. E. C., BERGENHOLTZ, G. & SVENSATER, G. 2010. The Effects of Antimicrobials on Endodontic Biofilm Bacteria. *Journal of Endodontics,* 36**,** 70-77.

DE SERMENO, R. F., DA SILVA, L. A. B., HERRERA, H., HERRERA, H., SILVA, R. A. B. & LEONARDO, M. R. 2009. Tissue damage after sodium hypochlorite extrusion during root canal treatment. *Oral Surgery Oral Medicine Oral Pathology Oral Radiology and Endodontology,* 108**,** E46-E49.

DEERING, M. Year. Geometry compression. *In:* Proceedings of the 22nd Annual Conference on Computer Graphics and Interactive Techniques, 1995. Association for Computing Machinery, 13-20.

DEL FABBRO, M., AFRASHTEHFAR, K. I., CORBELLA, S., EL-KABBANEY, A., PERONDI, I. & TASCHIERI, S. 2017. In Vivo and In Vitro Effectiveness of Rotary Nickel-Titanium vs Manual Stainless Steel Instruments for Root Canal Therapy: Systematic Review and Meta-analysis. *Journal of Evidence Based Dental Practice,* 18**,** 59-69.

DELBONI, M. G., GOMES, B. P. F. A., FRANCISCO, P. A., TEIXEIRA, F. B. & DRAKE, D. 2017. Diversity of Enterococcus faecalis Genotypes from Multiple Oral Sites Associated with Endodontic Failure Using Repetitive Sequence-based Polymerase Chain Reaction and Arbitrarily Primed Polymerase Chain Reaction. *Journal of Endodontics,* 43**,** 377-382.

DELIBASIS, K., UNDRILL, P. & CAMERON, G. 1997. The design of stack filters for image restoration using genetic algorithm. *University of Aberdeen, Foresterhill, Aberdeen, AB25 2ZD, UK*.

DEO, B. D., SHASHIKALA, K. & BHAT, K. G. 2016. Detection of Enterococcus Faecalis In Symptomatic And Asymptomatic Endodontic Infections By Culture And Pcr Method. *World Journal of Pharmaceutical and Medical Research,* 2**,** 62-68.

DERMOL-ČERNE, J. & MIKLAVČIČ, D. 2018. From Cell to Tissue Properties—Modeling Skin Electroporation With Pore and Local Transport Region Formation. *IEEE Transactions on Biomedical Engineering,* 65**,** 458-468.

DREXLER, W. & FUJIMOTO, J. G. 2015. *Optical coherence tomography: technology and applications*, Springer.

DRUTTMAN, A. & STOCK, C. 1989. An in vitro comparison of ultrasonic and conventional methods of irrigant replacement. *International Endodontic Journal,* 22**,** 174-178.

DUFRÊNE, Y. F. 2015. Sticky microbes: forces in microbial cell adhesion. *Trends in Microbiology,* 23**,** 376-382.

DUMMER, P., ALODEH, M. & AL-OMARI, M. 1991. A method for the construction of simulated root canals in clear resin blocks. *International Endodontic Journal,* 24**,** 63-66.

DUNAVANT, T. R., REGAN, J. D., GLICKMAN, G. N., SOLOMON, E. S. & HONEYMAN, A. L. 2006. Comparative evaluation of endodontic irrigants against Enterococcus faecalis biofilms. *Journal of Endodontics,* 32**,** 527-531.

DUNKERS, J. P., PHELAN, F. R., SANDERS, D. P., EVERETT, M. J., GREEN, W. H., HUNSTON, D. L. & PARNAS, R. S. 2001. The application of optical coherence tomography to problems in polymer matrix composites. *Optics and Lasers in Engineering,* 35**,** 135-147.

DURACK, C. & PATEL, S. 2012. Cone beam computed tomography in endodontics. *Brazilian Dental Journal,* 23**,** 179-191.

EDMOND, M. B., WALLACE, S. E., MCCLISH, D. K., PFALLER, M. A., JONES, R. N. & WENZEL, R. P. 1999. Nosocomial bloodstream infections in United States hospitals: a three-year analysis. *Clinical Infectious Diseases,* 29**,** 239-244.

EGNER, W., HELBERT, M., SARGUR, R., SWALLOW, K., HARPER, N., GARCEZ, T., SAVIC, S., SAVIC, L. & EREN, E. 2017. Chlorhexidine allergy in four specialist allergy centres in the United Kingdom, 2009–13: clinical features and diagnostic tests. *Clinical & Experimental Immunology,* 188**,** 380-386.

ELMSALLATI, E. A., WADACHI, R., EBRAHIM, A. K. & SUDA, H. 2006. Debris retention and wear in three different nickel-titanium rotary instruments. *Australian Endodontic Journal,* 32**,** 107-111.

ENDAL, U., SHEN, Y., KNUT, Å., GAO, Y. & HAAPASALO, M. 2011. A High-resolution Computed Tomographic Study of Changes in Root Canal Isthmus Area by Instrumentation and Root Filling. *Journal of Endodontics,* 37**,** 223-227.

ENDODONTOLOGY, E. S. O. 1994. Consensus report of the European Society of Endodontology on quality guidelines for endodontic treatment. *International Endodontic Journal,* 27**,** 115-124.

ENDODONTOLOGY, E. S. O. 2006. Quality guidelines for endodontic treatment: consensus report of the European Society of Endodontology. *International Endodontic Journal,* 39**,** 921-930.

ESTRELA, C., BUENO, M. R., LELES, C. R., AZEVEDO, B. & AZEVEDO, J. R. 2008. Accuracy of cone beam computed tomography and panoramic and periapical radiography for detection of apical periodontitis. *Journal of Endodontics,* 34**,** 273-279.

ESTRELA, C., ESTRELA, C. R., BARBIN, E. L., SPANÓ, J. C. E., MARCHESAN, M. A. & PÉCORA, J. D. 2002. Mechanism of action of sodium hypochlorite. *Brazilian Dental Journal,* 13**,** 113-117.

ESTRELA, C., SYDNEY, G. B., FIGUEIREDO, J. A. P. & ESTRELA, C. R. D. A. 2009. Antibacterial efficacy of intracanal medicaments on bacterial biofilm: a critical review. *Journal of Applied Oral Science,* 17**,** 1-7.

EVANS, L. V. 2003. *Biofilms: recent advances in their study and control*, CRC press.

FANG, H. H., CHAN, K.-Y. & XU, L.-C. 2000. Quantification of bacterial adhesion forces using atomic force microscopy (AFM). *Journal of Microbiological Methods,* 40**,** 89-97.

FARZANEH, S., PARIROKH, M., NAKHAEE, N. & ABBOTT, P. 2017. Effect of two different concentrations of sodium hypochlorite on postoperative pain following single-visit root canal treatment: a triple-blind randomized clinical trial. *International Endodontic Journal,* 51**,** e2-e11.

FAVA, L. 1998. Acute apical periodontitis: incidence of post-operative pain using two different root canal dressings. *International Endodontic Journal,* 31**,** 343-347.

FELDKAMP, L. A., GOLDSTEIN, S. A., PARFITT, M. A., JESION, G. & KLEEREKOPER, M. 1989. The direct examination of three-dimensional bone architecture in vitro by computed tomography. *Journal of Bone and Mineral Research,* 4**,** 3-11.

FERCHER, A. F., DREXLER, W., HITZENBERGER, C. K. & LASSER, T. 2003. Optical coherence tomography-principles and applications. *Reports on Progress in Physics,* 66**,** 239.

FITZGERALD, M. 1992. A Colour Atlas and Textbook of Oral Anatomy, Histology and Embryology. *Journal of Anatomy,* 181**,** 386.

FLEER, A. & VERHOEF, J. 1989. An evaluation of the role of surface hydrophobicity and extracellular slime in the pathogenesis of foreign-body-related infections due to coagulase-negative staphylococci. *Journal of Investigative Surgery,* 2**,** 391-396.

FLEMMING, H.-C. & WINGENDER, J. 2010. The biofilm matrix. *Nature Reviews Microbiology,* 8**,** 623-633.

FLETCHER, M. 1977. The effects of culture concentration and age, time, and temperature on bacterial attachment to polystyrene. *Canadian Journal of Microbiology,* 23**,** 1-6.

FLETCHER, M. 1991. The physiological activity of bacteria attached to solid surfaces. *Advances in Microbial Physiology,* 32**,** 53-85.

FORD, H. P., FORD, T. P. & RHODES, J. 2004. *Endodontics: Problem-Solving in Clinical Practice*, CRC Press.

FORTUNATO, L., QAMAR, A., WANG, Y., JEONG, S. & LEIKNES, T. 2017. In-situ assessment of biofilm formation in submerged membrane system using optical coherence tomography and computational fluid dynamics. *Journal of Membrane Science,* 521**,** 84-94.

FOUAD, A., TORABINEJAD, M. & WALTON, R. E. 2009. *Endodontics: principles and practice*, Elsevier Health Sciences.

FOUQUET, C., GILLES, J.-F., HECK, N., DOS SANTOS, M., SCHWARTZMANN, R., CANNAYA, V., MOREL, M.-P., DAVIDSON, R. S., TREMBLEAU, A. & BOLTE, S. 2015. Improving axial resolution in confocal microscopy with new high refractive index mounting media. *PloS One,* 10**,** e0121096.

FRAME, M. & HUNTLEY, J. S. 2012. Rapid prototyping in orthopaedic surgery: a user's guide. *The Scientific World Journal,* 2012.

FREITAS, C. S. D., DINIZ, H. F. O., GOMES, J. B., SINISTERRA, R. D. & CORTÉS, M. E. 2003. Evaluation of the substantivity of chlorhexidine in association with sodium fluoride in vitro. *Pesquisa Odontológica Brasileira,* 17**,** 78-81.

FRICKMANN, H., ZAUTNER, A. E., MOTER, A., KIKHNEY, J., HAGEN, R. M., STENDER, H. & POPPERT, S. 2017. Fluorescence in situ hybridization (FISH) in the microbiological diagnostic routine laboratory: a review. *Critical Reviews in Microbiology,* 43**,** 263-293.

FROUGH-REYHANI, M., GHASEMI, N., SOROUSH-BARHAGHI, M., AMINI, M. & GHOLIZADEH, Y. 2016. Antimicrobial efficacy of different concentration of sodium hypochlorite on the biofilm of Enterococcus faecalis at different stages of development. *Journal of Clinical and Experimental Dentistry,* 8**,** e480-e484.

FUENTES, V., TOLEDANO, M., OSORIO, R. & CARVALHO, R. M. 2003. Microhardness of superficial and deep sound human dentin. *Journal of Biomedical Materials Research Part A,* 66**,** 850-853.

GAÊTA-ARAUJO, H., DE SOUZA, G. Q. S., FREITAS, D. Q. & DE OLIVEIRA-SANTOS, C. 2017. Optimization of Tube Current in Cone-beam Computed Tomography for the Detection of Vertical Root Fractures with Different Intracanal Materials. *Journal of Endodontics,* 43**,** 1668–1673.

GAMBARINI, G., GRANDE, N. M., PLOTINO, G., SOMMA, F., GARALA, M., DE LUCA, M. & TESTARELLI, L. 2008. Fatigue resistance of engine-driven rotary nickel-titanium instruments produced by new manufacturing methods. *Journal of Endodontics,* 34**,** 1003-1005.

GAO, Y., HAAPASALO, M., SHEN, Y., WU, H., LI, B., RUSE, N. D. & ZHOU, X. 2009. Development and Validation of a Three-dimensional Computational Fluid Dynamics Model of Root Canal Irrigation. *Journal of Endodontics,* 35**,** 1282-1287.

GARG, N. & GARG, A. 2008. *Review of Endodontics and Operative Dentistry*, JAYPEE BROTHERS PUBLISHERS.

GARG, N. & GARG, A. 2010. *Textbook of endodontics*, Boydell & Brewer Ltd.

GAUDREAU, A., LABRIE, J., GOETZ, C., DUFOUR, S. & JACQUES, M. 2018. Evaluation of MALDI-TOF mass spectrometry for the identification of bacteria growing as biofilms. *Journal of Microbiological Methods,* 145**,** 79-81.

GIARDINO, L., AMBU, E., BECCE, C., RIMONDINI, L. & MORRA, M. 2006. Surface tension comparison of four common root canal irrigants and two new irrigants containing antibiotic. *Journal of Endodontics,* 32**,** 1091-1093.

GIBSON, I. 2006. *Advanced manufacturing technology for medical applications: reverse engineering, software conversion and rapid prototyping*, John Wiley & Sons.

GIOVANNONI, S. J., DELONG, E. F., OLSEN, G. J. & PACE, N. R. 1988. Phylogenetic group-specific oligodeoxynucleotide probes for identification of single microbial cells. *Journal of Bacteriology,* 170**,** 720-726.

GOHEAN, R. J., PANTERA, E. A. & SCHUSTER, G. S. 1990. Indirect immunofluorescence microscopy for the identification of Actinomyces sp. in endodontic disease. *Journal of Endodontics,* 16**,** 318-322.

GOMES, B., FERRAZ, C., ME, V., BERBER, V., TEIXEIRA, F. & SOUZA-FILHO, F. 2001. In vitro antimicrobial activity of several concentrations of sodium hypochlorite and chlorhexidine gluconate in the elimination of Enterococcus faecalis. *International Endodontic Journal,* 34**,** 424-428.

GOMES, B. P. F. A., PINHEIRO, E. T., SOUSA, E. L. R., JACINTO, R. C., ZAIA, A. A., FERRAZ, C. C. R. & DE SOUZA-FILHO, F. J. 2006. Enterococcus faecalis in dental root canals detected by culture and by polymerase chain reaction analysis. *Oral Surgery, Oral Medicine, Oral Pathology, Oral Radiology, and Endodontology,* 102**,** 247-253.

GOTTENBOS, B., MEI, H. & BUSSCHER, H. J. 2000. Initial adhesion and surface growth of Staphylococcus epidermidis and Pseudomonas aeruginosa on biomedical polymers. *Journal of Biomedical Materials Research,* 50**,** 208-214.

GREEN III, J. M., LAWSON, S. T., LIACOURAS, P. C., WISE, E. M., GENTILE, M. A. & GRANT, G. T. 2016. Custom anatomical 3D spacer for temporomandibular joint resection and reconstruction. *Craniomaxillofacial Trauma & Reconstruction,* 9**,** 082-87.

GROSS, B. C., ERKAL, J. L., LOCKWOOD, S. Y., CHEN, C. & SPENCE, D. M. 2014. Evaluation of 3D printing and its potential impact on biotechnology and the chemical sciences. ACS Publications.

GROSSMAN, L. I. 1974. Endodontics: a peep into the past and the future. *Oral Surgery, Oral Medicine, Oral Pathology,* 37**,** 599-608.

GU, L.-S., KIM, J. R., LING, J., CHOI, K. K., PASHLEY, D. H. & TAY, F. R. 2009. Review of contemporary irrigant agitation techniques and devices. *Journal of Endodontics,* 35**,** 791-804.

GU, L., WEI, X., LING, J. & HUANG, X. 2008. A Microcomputed Tomographic Study of Canal Isthmuses in the Mesial Root of Mandibular First Molars in a Chinese Population. *Journal of Endodontics,* 35**,** 353-356.

GUPTA, N., RAI, R., SIKDER, A., NANDI, S., TANWAR, A., KHATOKAR, R., PASK, S. D. & MITRA, S. 2016. Design and development of a poly (acrylonitrile-co-methyl methacrylate) copolymer to improve the viscoelastic and surface properties critical to scratch resistance. *RSC Advances,* 6**,** 37933-37937.

GUTARTS, R., NUSSTEIN, J., READER, A. & BECK, M. 2005. In vivo debridement efficacy of ultrasonic irrigation following hand-rotary instrumentation in human mandibular molars. *Journal of Endodontics,* 31**,** 166-170.

HAAPASALO, M. 1989. Bacteroides spp. in dental root canal infections. *Dental Traumatology,* 5**,** 1-10.

HAAPASALO, M., SHEN, Y., QIAN, W. & GAO, Y. 2010. Irrigation in endodontics. *Dental Clinics of North America,* 54**,** 291-312.

HAISCH, C. & NIESSNER, R. 2007. Visualisation of transient processes in biofilms by optical coherence tomography. *Water Research,* 41**,** 2467-2472.

HALL-STOODLEY, L. & STOODLEY, P. 2009. Evolving concepts in biofilm infections. *Cellular Microbiology,* 11**,** 1034-1043.

HALL, C. L., LYTLE, B. L., JENSEN, D., HOFF, J. S., PETERSON, F. C., VOLKMAN, B. F. & KRISTICH, C. J. 2017. Structure and dimerization of IreB, a negative regulator of cephalosporin resistance in Enterococcus faecalis. *Journal of Molecular Biology*.

HAN, A., TSOI, J. K. H., MATINLINNA, J. P., ZHANG, Y. & CHEN, Z. 2017. Effects of different sterilization methods on surface characteristics and biofilm formation on zirconia in vitro. *Dental Materials*.

HAN, S.-H., SADR, A., TAGAMI, J. & PARK, S.-H. 2016. Non-destructive evaluation of an internal adaptation of resin composite restoration with swept-source optical coherence tomography and micro-CT. *Dental Materials,* 32**,** e1-e7.

HANNIG, C., BASCHE, S., BURGHARDT, T., AL-AHMAD, A. & HANNIG, M. 2013. Influence of a mouthwash containing hydroxyapatite microclusters on bacterial adherence in situ. *Clinical Oral Investigations,* 17**,** 805-814.

HARDING, M. W. & DANIELS, G. 2017. In Vitro Assessment of Biofilm Formation by Soil-and Plant-Associated Microorganisms. *Biofilms in Plant and Soil Health***,** 253.

HARGREAVES, K. M. & COHEN, S. 2011. Pathways of the Pulp. *St. Louis: Mosby Co*.

HARGREAVES, K. M., GOODIS, H. E. & TAY, F. R. 2012. *Seltzer and Bender's dental pulp*, Quintessence Publishing Company.

HASHEM, A. A. R., GHONEIM, A. G., LUTFY, R. A., FODA, M. Y. & OMAR, G. A. F. 2012. Geometric analysis of root canals prepared by four rotary NiTi shaping systems. *Journal of Endodontics,* 38**,** 996-1000.

HASSAN, B., METSKA, M. E., OZOK, A. R., VAN DER STELT, P. & WESSELINK, P. R. 2009. Detection of vertical root fractures in endodontically treated teeth by a cone beam computed tomography scan. *Journal of Endodontics,* 35**,** 719-722.

HASSON, A. H. & KADHEM, S. A. 2017. Identification of Enterococcus faecalis Isolated from Infected Human Tooth Root Canals Human by Using Polymerase Chain Reaction. *Ibn AL-Haitham Journal For Pure and Applied Science,* 28**,** 246-253.

HAWKINS, C., PATTISON, D. & DAVIES, M. J. 2003. Hypochlorite-induced oxidation of amino acids, peptides and proteins. *Amino Acids,* 25**,** 259-274.

HEARD, F. & WALTON, R. E. 1997. Scanning electron microscope study comparing four root canal preparation techniques in small curved canals. *International Endodontic Journal,* 30**,** 323-331.

HELL, S., REINER, G., CREMER, C. & STELZER, E. H. 1993. Aberrations in confocal fluorescence microscopy induced by mismatches in refractive index. *Journal of Microscopy,* 169**,** 391-405.

HIEU, L., ZLATOV, N., VANDER SLOTEN, J., BOHEZ, E., KHANH, L., BINH, P., ORIS, P. & TOSHEV, Y. 2005. Medical rapid prototyping applications and methods. *Assembly Automation,* 25**,** 284-292.

HJELJORD, L., RÖLLA, G. & BONESVOLL, P. 1973. Chlorhexidine–protein interactions. *Journal of Periodontal Research,* 8**,** 11-16.

HOEDKE, D., ENSELEIT, C., GRUNER, D., DOMMISCH, H., SCHLAFER, S., DIGE, I. & BITTER, K. 2017. Effect of photodynamic therapy in combination with various irrigation protocols on an endodontic multispecies biofilm ex vivo. *International Endodontic Journal***,** n/a-n/a.

HOFMANN, N., PAPSTHART, G., HUGO, B. & KLAIBER, B. 2001. Comparison of photo-activation versus chemical or dual-curing of resin-based luting cements regarding flexural strength, modulus and surface hardness. *Journal of Oral Rehabilitation,* 28**,** 1022-1028.

HOLLIDAY, R. 2011. Cohen's pathways of the pulp. *British Dental Journal,* 210**,** 242-242.

HOLLIDAY, R. & ALANI, A. 2014. Traditional and contemporary techniques for optimizing root canal irrigation. *Dental Update,* 41**,** 51-61.

HOLLIMAN, R. & SMYTH, E. 1989. Gentamicin-resistant enterococci and endocarditis. *Postgraduate Medical Journal,* 65**,** 390-393.

HOU, J., VEEREGOWDA, D. H., VAN DE BELT-GRITTER, B., BUSSCHER, H. J. & VAN DER MEI, H. C. 2018. Extracellular Polymeric Matrix Production and Relaxation under Fluid Shear and Mechanical Pressure in Staphylococcus aureus Biofilms. *Applied and Environmental Microbiology,* 84**,** e01516-17.

HUANG, D., SWANSON, E. A., LIN, C. P., SCHUMAN, J. S., STINSON, W. G., CHANG, W., HEE, M. R., FLOTTE, T., GREGORY, K. & PULIAFITO, C. A. 1991. Optical coherence tomography. *Science (New York, NY),* 254**,** 1178.

HUANG, T. Y., GULABIVALA, K. & NG, Y. L. 2008. A bio-molecular film ex-vivo model to evaluate the influence of canal dimensions and irrigation variables on the efficacy of irrigation. *International Endodontic Journal,* 41**,** 60-71.

HUBBLE, T., HATTON, J., NALLAPAREDDY, S., MURRAY, B. & GILLESPIE, M. 2003. Influence of Enterococcus faecalis proteases and the collagen-binding protein, Ace, on adhesion to dentin. *Molecular Oral Microbiology,* 18**,** 121-126.

HÜBSCHER, W., BARBAKOW, F. & PETERS, O. 2003. Root-canal preparation with FlexMaster: canal shapes analysed by micro-computed tomography. *International Endodontic Journal,* 36**,** 740-747.

HÜLSMANN, M., PETERS, O. A. & DUMMER, P. M. 2005. Mechanical preparation of root canals: shaping goals, techniques and means. *Endodontic Topics,* 10**,** 30-76.

IBRAHIM, D., BROILO, T. L., HEITZ, C., DE OLIVEIRA, M. G., DE OLIVEIRA, H. W., NOBRE, S. M. W., DOS SANTOS FILHO, J. H. G. & SILVA, D. N. 2009. Dimensional error of selective laser sintering, three-dimensional printing and PolyJet™ models in the reproduction of mandibular anatomy. *Journal of Cranio-Maxillofacial Surgery,* 37**,** 167-173.

INGLE, J. I., BAKLAND, L. K. & BAUMGARTNER, J. C. 2008. *Ingle's endodontics 6*, PMPH-USA.

IRIBOZ, E., BAYRAKTAR, K., TURKAYDIN, D. & TARCIN, B. 2015. Comparison of Apical Extrusion of Sodium Hypochlorite Using 4 Different Root Canal Irrigation Techniques. *Journal of Endodontics,* 41**,** 380-384.

JABLONSKI-MOMENI, A. & STACHNISS, V. 2010. Serial sectioning of teeth and microscopy in cariology research. *Microsc Sci Tech Appl Edu***,** 785-91.

JAHNS, A. C., KILLASLI, H., NOSEK, D., LUNDSKOG, B., LENNGREN, A., MURATOVA, Z., EMTESTAM, L. & ALEXEYEV, O. A. 2014. Microbiology of hidradenitis suppurativa (acne inversa): a histological study of 27 patients. *Apmis,* 122**,** 804-809.

JAKOVLJEVIC, A., ANDRIC, M., KNEZEVIC, A., SOLDATOVIC, I., NIKOLIC, N., KARALIC, D. & MILASIN, J. 2015. Human Cytomegalovirus and Epstein-Barr Virus Genotypes in Apical Periodontitis Lesions. *Journal of Endodontics,* 41**,** 1847-1851.

JAMES, S. A., POWELL, L. C. & WRIGHT, C. J. 2016. Atomic Force Microscopy of Biofilms—Imaging, Interactions, and Mechanics. *Microbial Biofilms-Importance and Applications.* InTech.

JONES, C. G. 1997. Chlorhexidine: is it still the gold standard? *Periodontology 2000,* 15**,** 55-62.

KARIMI, M., DAVIES, M. J. & PATTISON, D. I. 2016. 18 - Characterisation of the Novel Products of Protein Oxidation by the Inflammatory Oxidant Hypochlorous Acid (HOCl) Using Raman Spectroscopy. *Free Radical Biology and Medicine,* 100, Supplement**,** S24-S25.

KAZEMIPOOR, M., AZAD, S. & FARAHAT, F. 2017. Concurrent Effects of Bleaching Materials and the Size of Root Canal Preparation on Cervical Dentin Microhardness. *Iranian Endodontic Journal,* 12**,** 298-302.

KHADEMI, A., SAATCHI, M., SHOKOUHI, M. M. & BAGHAEI, B. 2015. Scanning Electron Microscopic Evaluation of Residual Smear Layer Following Preparation of Curved Root Canals Using Hand Instrumentation or Two Engine-Driven Systems. *Iranian Endodontic Journal,* 10**,** 236.

KHALIL, W., EZELDEEN, M., VAN DE CASTEELE, E., SHAHEEN, E., SUN, Y., SHAHBAZIAN, M., OLSZEWSKI, R., POLITIS, C. & JACOBS, R. 2016. Validation of cone beam computed tomography–based tooth printing using different three-dimensional printing technologies. *Oral Surgery, Oral Medicine, Oral Pathology and Oral Radiology,* 121**,** 307-315.

KIDD, E. A. & JOYSTON-BECHAL, S. 1997. Essentials of dental caries.

KIM, J.-M., KANG, S.-R. & YI, W.-J. 2017. Automatic detection of tooth cracks in optical coherence tomography images. *Journal of Periodontal & Implant Science,* 47**,** 41-50.

KINNIMENT, S. L., WIMPENNY, J. W., ADAMS, D. & MARSH, P. D. 1996. Development of a steady-state oral microbial biofilm community using the constant-depth film fermenter. *Microbiology,* 142**,** 631-638.

KISHEN, A., GEORGE, S. & KUMAR, R. 2006. Enterococcus faecalis-mediated biomineralized biofilm formation on root canal dentine in vitro. *Journal of Biomedical Materials Research Part A,* 77**,** 406-415.

KISHEN, A., SHRESTHA, A. & DEL CARPIO-PEROCHENA, A. 2017. Validation of Biofilm Assays to Assess Antibiofilm Efficacy in Instrumented Root Canals after Syringe Irrigation and Sonic Agitation. *Journal of Endodontics,* 44**,** 292-298.

KISHEN, A., SUM, C.-P., MATHEW, S. & LIM, C.-T. 2008. Influence of irrigation regimens on the adherence of Enterococcus faecalis to root canal dentin. *Journal of Endodontics,* 34**,** 850-854.

KOÇAK, S., BAĞCI, N., ÇIÇEK, E., TÜRKER, S. A., CAN SAĞLAM, B. & KOÇAK, M. M. 2017. Influence of passive ultrasonic irrigation on the efficiency of various irrigation solutions in removing smear layer: a scanning electron microscope study. *Microscopy Research and Technique,* 80**,** 537-542.

KOÇAK, S., KOÇAK, M. M., SAĞLAM, B. C., TÜRKER, S. A., SAĞSEN, B. & ER, Ö. 2013. Apical extrusion of debris using self-adjusting file, reciprocating single-file, and 2 rotary instrumentation systems. *Journal of Endodontics,* 39**,** 1278-1280.

KOCAN, J., WEIR, M. & MELO, M. 2017. Investigation of Bacterial Adhesion on Nanoparticle Filler-Reinforced Dental Composites after Different One-Step Finishing Timing Using a Constant-Depth Film Fermenter. *Nano Res Appl,* 3**,** 11.

KOCH, K. & BRAVE, D. 2002a. Real World Endo: Design features of rotary files and how they affect clinical performance. *Oral Health,* 92**,** 39-49.

KOCH, S., HUFNAGEL, M., THEILACKER, C. & HUEBNER, J. 2004. Enterococcal infections: host response, therapeutic, and prophylactic possibilities. *Vaccine,* 22**,** 822-830.

KOHLI, A. 2010. Textbook of endodontics. *Elsevier***,** 161.

KOO, H., XIAO, J., KLEIN, M. & JEON, J. 2010. Exopolysaccharides produced by Streptococcus mutans glucosyltransferases modulate the establishment of microcolonies within multispecies biofilms. *Journal of Bacteriology,* 192**,** 3024-3032.

KOSTAKIOTI, M., HADJIFRANGISKOU, M. & HULTGREN, S. J. 2013. Bacterial biofilms: development, dispersal, and therapeutic strategies in the dawn of the postantibiotic era. *Cold Spring Harbor Perspectives in Medicine,* 3**,** a010306.

KREFT, Á., MARRE, R., SCHRAMM, U. & WIRTH, R. 1992. Aggregation substance of Enterococcus faecalis mediates adhesion to cultured renal tubular cells. *Infection and Immunity,* 60**,** 25-30.

KWAK, S. W., HA, J.-H., CHEUNG, G. S.-P., KIM, H.-C. & KIM, S. K. 2017. Effect of the Glide Path Establishment on the Torque Generation to the Files during Instrumentation: An In Vitro Measurement. *Journal of Endodontics,* 44**,** 496-500.

LARSEN, C. M., WATANABE, I., GLICKMAN, G. N. & HE, J. 2009. Cyclic fatigue analysis of a new generation of nickel titanium rotary instruments. *Journal of Endodontics,* 35**,** 401-403.

LEA, S., WALMSLEY, A., LUMLEY, P. & LANDINI, G. 2004. A new insight into the oscillation characteristics of endosonic files used in dentistry. *Physics in Medicine and Biology,* 49**,** 2095.

LEE, S. F., LI, Y. H. & BOWDEN, G. H. 1996. Detachment of Streptococcus mutans biofilm cells by an endogenous enzymatic activity. *Infection and Immunity,* 64**,** 1035-1038.

LEE, S. J., WU, M. K. & WESSELINK, P. 2004a. The effectiveness of syringe irrigation and ultrasonics to remove debris from simulated irregularities within prepared root canal walls. *International Endodontic Journal,* 37**,** 672-678.

LEE, S. J., WU, M. K. & WESSELINK, P. 2004b. The efficacy of ultrasonic irrigation to remove artificially placed dentine debris from different-sized simulated plastic root canals. *International Endodontic Journal,* 37**,** 607-612.

LEI, C., JIYAO, L., HK, X. H. & XUEDONG, Z. 2016. Demineralization and Remineralization. *Dental Caries.* Springer.

LEONARDO, M. R., ROSSI, M. A., SILVA, L. A. B., ITO, I. Y. & BONIFÁCIO, K. C. 2002. EM Evaluation of Bacterial Biofilm and Microorganisms on the Apical External Root Surface of Human Teeth. *Journal of Endodontics,* 28**,** 815-818.

LEONI, G., VERSIANI, M., SILVA-SOUSA, Y., BRUNIERA, J., PÉCORA, J. & SOUSA-NETO, M. 2017. Ex vivo evaluation of four final irrigation protocols on the removal of hard-tissue debris from the mesial root canal system of mandibular first molars. *International Endodontic Journal,* 50**,** 398-406.

LIM, K. & WEBBER, J. 1985a. The validity of simulated root canals for the investigation of the prepared root canal shape. *International Endodontic Journal,* 18**,** 240-246.

LIM, K. C. & WEBBER, J. 1985b. The validity of simulated root canals for the investigation of the prepared root canal shape. *International Endodontic Journal,* 18**,** 240-246.

LITTMAN, S. H. 1977. Evaluation of root canal debridement by use of a radiopaque medium. *Journal of Endodontics,* 3**,** 135-138.

LONG, J., GHOLIZADEH, H., LU, J., BUNT, C. & SEYFODDIN, A. 2017. Application of fused deposition modelling (FDM) method of 3D printing in drug delivery. *Current Pharmaceutical Design,* 23**,** 433-439.

LOUWAKUL, P., SAELO, A. & KHEMALEELAKUL, S. 2017. Efficacy of calcium oxide and calcium hydroxide nanoparticles on the elimination of Enterococcus faecalis in human root dentin. *Clinical Oral Investigations,* 21**,** 865-871.

LOYAGA-RENDON, P. G., TAKAHASHI, H., HAYAKAWA, I. & IWASAKI, N. 2007. Compositional characteristics and hardness of acrylic and composite resin artificial teeth. *Journal of Prosthetic Dentistry,* 98**,** 141-149.

LUTSKIY, M.-Y., AVNERI-KATZ, S., ZHU, N., ITSKO, M., RONEN, Z., ARNUSCH, C. J. & KASHER, R. 2015. A microbiology-based assay for quantification of bacterial early stage biofilm formation on reverse-osmosis and nanofiltration membranes. *Separation and Purification Technology,* 141**,** 214-220.

LYTE, M., FREESTONE, P. P. E., NEAL, C. P., OLSON, B. A., HAIGH, R. D., BAYSTON, R. & WILLIAMS, P. H. 2003. Stimulation of Staphylococcus epidermidis growth and biofilm formation by catecholamine inotropes. *The Lancet,* 361**,** 130-135.

MACHADO, M. E. D. L., NABESHIMA, C. K., CABALLERO-FLORES, H., ELMADJIAN-FILHO, M., DUARTE, M. A. H., ODINOLA-ZAPATA, R. & CAI, S. 2017. Instrument Design May Influence Bacterial Reduction During Root Canal Preparation. *Brazilian Dental Journal,* 28**,** 587-591.

MADSEN, K. T., SKOV, M. N., GILL, S. & KEMP, M. 2017. Virulence Factors Associated with Enterococcus Faecalis Infective Endocarditis: A Mini Review. *The Open Microbiology Journal,* 11**,** 1.

MAGALHÃES, R., FERREIRA, V., BISCOTTINI, G., BRANDÃO, T. R., ALMEIDA, G. & TEIXEIRA, P. 2017. Biofilm formation by persistent and non-persistent Listeria monocytogenes strains on abiotic surfaces. *Acta Alimentaria,* 46**,** 43-50.

MAGNE, P. 2007. Efficient 3D finite element analysis of dental restorative procedures using micro-CT data. *Dental Materials,* 23**,** 539-548.

MALENTACCA, A., UCCIOLI, U., MANNOCCI, F., BHUVA, B., ZANGARI, D., PULELLA, C. & LAJOLO, C. 2017. The comparative effectiveness and safety of three activated irrigation techniques in the isthmus area using a transparent tooth model. *International Endodontic Journal,* 51**,** e35-e41.

MANSOUR, S., AJDAHARIAN, J., NABELSI, T., CHAN, G. & WILDER-SMITH, P. 2016. Comparison of caries diagnostic modalities: A clinical study in 40 subjects. *Lasers in Surgery and Medicine,* 48**,** 924-928.

MARMUR, A., DELLA VOLPE, C., SIBONI, S., AMIRFAZLI, A. & DRELICH, J. W. 2017. Contact angles and wettability: Towards common and accurate terminology. *Surface Innovations,* 5**,** 3-8.

MARSH, P. D., MARTIN, M. V., LEWIS, M. A. & WILLIAMS, D. 2009. *Oral microbiology*, Elsevier Health Sciences.

MARTELLI, N., SERRANO, C., VAN DEN BRINK, H., PINEAU, J., PROGNON, P., BORGET, I. & EL BATTI, S. 2016a. Advantages and disadvantages of 3-dimensional printing in surgery: A systematic review. *Surgery,* 159**,** 1485-1500.

MARTELLI, N., SERRANO, C., VAN DEN BRINK, H., PINEAU, J., PROGNON, P., BORGET, I. & EL BATTI, S. 2016b. Advantages and disadvantages of 3-dimensional printing in surgery: A systematic review. *Surgery,* 159**,** 1485-1500.

MARTIN, H. 1976. Ultrasonic disinfection of the root canal. *Oral Surgery, Oral Medicine, Oral Pathology,* 42**,** 92-99.

MARTIN, S. S., ALBRECHT, M. H., WICHMANN, J. L., HÜSERS, K., SCHOLTZ, J.-E., BOOZ, C., BODELLE, B., BAUER, R. W., METZGER, S. C. & VOGL, T. J. 2017. Value of a noise-optimized virtual monoenergetic reconstruction technique in dual-energy CT for planning of transcatheter aortic valve replacement. *European Radiology,* 27**,** 705-714.

MARTINHO, F. C., GOMES, C. C., NASCIMENTO, G. G., GOMES, A. P. & LEITE, F. R. 2018. Clinical comparison of the effectiveness of 7-and 14-day intracanal medications in root canal disinfection and inflammatory cytokines. *Clinical Oral Investigations,* 22**,** 523-530.

MASKELL, N., JONES, E. & DAVIES, R. 2003. Variations in experience in obtaining local ethical approval for participation in a multi-centre study. *Qjm,* 96**,** 305-307.

MATHERNE, R. P., ANGELOPOULOS, C., KULILD, J. C. & TIRA, D. 2008. Use of cone-beam computed tomography to identify root canal systems in vitro. *Journal of Endodontics,* 34**,** 87-89.

MATZ, M. V., FRADKOV, A. F., LABAS, Y. A., SAVITSKY, A. P., ZARAISKY, A. G., MARKELOV, M. L. & LUKYANOV, S. A. 1999. Fluorescent proteins from nonbioluminescent Anthozoa species. *Nature Biotechnology,* 17**,** 969-973.

MAWANG, C. I., LIM, Y. Y., ONG, K. S., MUHAMAD, A. & LEE, S. M. 2017. Identification of α-tocopherol as a bioactive component of Dicranopteris linearis with disrupting property against preformed biofilm of Staphylococcus aureus. *Journal of Applied Microbiology,* 123**,** 1148-1159.

MCMENAMIN, P. G., QUAYLE, M. R., MCHENRY, C. R. & ADAMS, J. W. 2014. The production of anatomical teaching resources using three-dimensional (3D) printing technology. *Anatomical Sciences Education,* 7**,** 479-486.

MERRITT, J. H., KADOURI, D. E. & O'TOOLE, G. A. 2005. Growing and Analyzing Static Biofilms. *Current Protocols in Microbiology,* 0 1**,** Unit-1B.1.

METZGER, Z., TEPEROVICH, E., ZARY, R., COHEN, R. & HOF, R. 2010a. The self-adjusting file (SAF). Part 1: respecting the root canal anatomy—a new concept of endodontic files and its implementation. *Journal of endodontics,* 36**,** 679-690.

METZGER, Z., ZARY, R., COHEN, R., TEPEROVICH, E. & PAQUÉ, F. 2010b. The Quality of Root Canal Preparation and Root Canal Obturation in Canals Treated with Rotary versus Self-adjusting Files: A Three-dimensional Micro-computed Tomographic Study. *Journal of Endodontics,* 36**,** 1569-1573.

MIKLOSSY, J. 2016. Bacterial amyloid and DNA are important constituents of senile plaques: further evidence of the spirochetal and biofilm nature of senile plaques. *Journal of Alzheimer's Disease,* 53**,** 1459-1473.

MILETIC, V., JAKOVLJEVIC, N., MANOJLOVIC, D., MARJANOVIC, J., ROSIC, A. A. & DRAMIĆANIN, M. D. 2017. Refractive indices of unfilled resin mixtures and cured composites related to color and translucency of conventional and low-shrinkage composites. *Journal of Biomedical Materials Research Part B: Applied Biomaterials,* 105**,** 7-13.

MINAGI, S., MIYAKE, Y., INAGAKI, K., TSURU, H. & SUGINAKA, H. 1985. Hydrophobic interaction in Candida albicans and Candida tropicalis adherence to various denture base resin materials. *Infection and Immunity,* 47**,** 11-14.

MOHAMMADI, Z., JAFARZADEH, H., SHALAVI, S. & PALAZZI, F. 2017. Recent Advances in Root Canal Disinfection: A Review. *Iranian Endodontic Journal,* 12**,** 402.

MOHMMED, S. A., VIANNA, M. E., HILTON, S. T., BONIFACE, D. R., NG, Y. L. & KNOWLES, J. C. 2017a. Investigation to test potential stereolithography materials for development of an in vitro root canal model. *Microscopy Research and Technique,* 80**,** 202-210.

MOHMMED, S. A., VIANNA, M. E., PENNY, M. R., HILTON, S. T. & KNOWLES, J. C. 2017b. The effect of sodium hypochlorite concentration and irrigation needle extension on biofilm removal from a simulated root canal model. *Australian Endodontic Journal*.

MOLANDER, A., LUNDQUIST, P., PAPAPANOU, P. N., DAHLÉN, G. & REIT, C. 2002. A protocol for polymerase chain reaction detection of Enterococcus faecalis and Enterococcus faecium from the root canal. *International Endodontic Journal,* 35**,** 1-6.

MOLVEN, O., OLSEN, I. & KEREKES, K. 1991. Scanning electron microscopy of bacteria in the apical part of root canals in permanent teeth with periapical lesions. *Dental Traumatology,* 7**,** 226-229.

MONSTEIN, H.-J., QUEDNAU, M., SAMUELSSON, A., AHRNÉ, S., ISAKSSON, B. & JONASSON, J. 1998. Division of the genus Enterococcus into species groups using PCR-based molecular typing methods. *Microbiology,* 144**,** 1171-1179.

MORIMOTO, T., YAMASAKI, M., NAKATA, K., TSUJI, M. & NAKAMURA, H. 2008. The expression of macrophage and neutrophil elastases in rat periradicular lesions. *Journal of Endodontics,* 34**,** 1072-1076.

MOTER, A. & GÖBEL, U. B. 2000a. Fluorescence in situ hybridization (FISH) for direct visualization of microorganisms. Elsevier.

MOTER, A. & GÖBEL, U. B. 2000b. Fluorescence in situ hybridization (FISH) for direct visualization of microorganisms. *Journal of Microbiological Methods,* 41**,** 85-112.

MULEME, M., STENOS, J., VINCENT, G., CAMPBELL, A., GRAVES, S., WARNER, S., DEVLIN, J. M., NGUYEN, C., STEVENSON, M. A. & WILKS, C. R. 2016. Bayesian validation of the indirect immunofluorescence assay and its superiority to the enzyme-linked immunosorbent assay and the complement fixation test for detecting antibodies against Coxiella burnetii in goat serum. *Clinical and Vaccine Immunology,* 23**,** 507-514.

NAIR, P. 1997. Apical periodontitis: a dynamic encounter between root canal infection and host response. *Periodontology 2000,* 13**,** 121-148.

NAIR, P., HENRY, S., CANO, V. & VERA, J. 2005a. Microbial status of apical root canal system of human mandibular first molars with primary apical periodontitis after “one-visit” endodontic treatment. *Oral Surgery, Oral Medicine, Oral Pathology, Oral Radiology, and Endodontology,* 99**,** 231-252.

NAIR, P. N. R., HENRY, S., CANO, V. & VERA, J. 2005b. Microbial status of apical root canal system of human mandibular first molars with primary apical periodontitis after “one-visit” endodontic treatment. *Oral Surgery, Oral Medicine, Oral Pathology, Oral Radiology, and Endodontology,* 99**,** 231-252.

NAIR, V., NAYAK, M., RAMYA, M., SIVADAS, G., GANESH, C., DEVI, S. & VEDAM, V. 2017. Detection of adherence of Enterococcus faecalis in infected dentin of extracted human teeth using confocal laser scanning microscope: An In vitro Study. *Journal of Pharmacy And Bioallied Sciences,* 9**,** 41-44.

NAKAMURA, V., PINHEIRO, E., PRADO, L., SILVEIRA, A., CARVALHO, A., MAYER, M. & GAVINI, G. 2017. Effect of ultrasonic activation on the reduction of bacteria and endotoxins in root canals: a randomized clinical trial. *International Endodontic Journal,* 51**,** e12-e22.

NAKAYAMA, N. & HAYASHI, T. 2007. Preparation and characterization of TiO2 and polymer nanocomposite films with high refractive index. *Journal of Applied Polymer Science,* 105**,** 3662-3672.

NALLAPAREDDY, S. R., QIN, X., WEINSTOCK, G. M., HÖÖK, M. & MURRAY, B. E. 2000. Enterococcus faecalis adhesin, ace, mediates attachment to extracellular matrix proteins collagen type IV and laminin as well as collagen type I. *Infection and Immunity,* 68**,** 5218-5224.

NALLAPAREDDY, S. R., SINGH, K. V., SILLANPÄÄ, J., GARSIN, D. A., HÖÖK, M., ERLANDSEN, S. L. & MURRAY, B. E. 2006. Endocarditis and biofilm-associated pili of Enterococcus faecalis. *Journal of Clinical Investigation,* 116**,** 2799-2807.

NAMEN, F. M., FERRANDINI, E. & GALAN JUNIOR, J. 2011. Surface energy and wettability of polymers light-cured by two different systems. *Journal of Applied Oral Science,* 19**,** 517-520.

NANCI, A. 2014. *Ten Cate's Oral Histology-Pageburst on VitalSource: Development, Structure, and Function*, Elsevier Health Sciences.

NEELAKANTAN, P., DEVARAJ, S. & JAGANNATHAN, N. 2016a. Histologic Assessment of Debridement of the Root Canal Isthmus of Mandibular Molars by Irrigant Activation Techniques Ex Vivo. *Journal of Endodontics,* 42**,** 1268-1272.

NEELAKANTAN, P., DEVARAJ, S. & JAGANNATHAN, N. 2016b. Histologic Assessment of Debridement of the Root Canal Isthmus of Mandibular Molars by Irrigant Activation Techniques Ex Vivo. *Journal of Endodontics,* 42**,** 1268-1272.

NETUSCHIL, L., AUSCHILL, T. M., SCULEAN, A. & ARWEILER, N. B. 2014. Confusion over live/dead stainings for the detection of vital microorganisms in oral biofilms-which stain is suitable? *BMC Oral Health,* 14**,** 2.

NEVES, M. A. S., PROVENZANO, J. C., RÔÇAS, I. N. & SIQUEIRA, J. F. 2016. Clinical Antibacterial Effectiveness of Root Canal Preparation with Reciprocating Single-instrument or Continuously Rotating Multi-instrument Systems. *Journal of Endodontics,* 42**,** 25-29.

NEWMAN, J. G., BRANTLEY, W. A. & GERSTEIN, H. 1983. A study of the cutting efficiency of seven brands of endodontic files in linear motion. *Journal of endodontics,* 9**,** 316-322.

NGUYEN, H. & VAI, M. 2010. Rapid prototyping technology. *Lincoln Laboratory Journal,* 18**,** 17-27.

NIELSEN, R. B., ALYASSIN, A. M., PETERS, D. D., CARNES, D. L. & LANCASTER, J. 1995. Microcomputed tomography: an advanced system for detailed endodontic research. *Journal of endodontics,* 21**,** 561-568.

NÓBREGA, L. M. M., MONTAGNER, F., RIBEIRO, A. C., MAYER, M. A. P. & GOMES, B. P. F. A. 2016. Molecular Identification of Cultivable Bacteria From Infected Root Canals Associated With Acute Apical Abscess. *Brazilian Dental Journal,* 27**,** 318-324.

NORMAN WELLER, R., NIEMCZYK, S. P. & KIM, S. 1995. Incidence and position of the canal isthmus. Part 1. Mesiobuccal root of the maxillary first molar. *Journal of Endodontics,* 21**,** 380-383.

NÚÑEZ-BELTRÁN, A., LÓPEZ-ROMERO, E. & CUÉLLAR-CRUZ, M. 2017. Identification of proteins involved in the adhesionof Candida species to different medical devices. *Microbial Pathogenesis,* 107**,** 293-303.

NYBERG, E. L., FARRIS, A. L., HUNG, B. P., DIAS, M., GARCIA, J. R., DORAFSHAR, A. H. & GRAYSON, W. L. 2017. 3D-Printing Technologies for Craniofacial Rehabilitation, Reconstruction, and Regeneration. *Annals of Biomedical Engineering,* 45**,** 45-57.

OLIVEIRA, W. F., SILVA, P. M., SILVA, R. C., SILVA, G. M., MACHADO, G., COELHO, L. C. & CORREIA, M. T. 2017. Staphylococcus aureus and Staphylococcus epidermidis infections on implants. *Journal of Hospital Infection,* 98**,** 111-117.

ÖNÇAĞ, Ö., HOŞGÖR, M., HILMIOĞLU, S., ZEKIOĞLU, O., ERONAT, C. & BURHANOĞLU, D. 2003. Comparison of antibacterial and toxic effects of various root canal irrigants. *International Endodontic Journal,* 36**,** 423-432.

ORDINOLA-ZAPATA, R., BRAMANTE, C. M., DUARTE, M. A. H., CAVENAGO, B. C., JARAMILLO, D. & VERSIANI, M. A. 2014. Shaping ability of Reciproc and TF Adaptive systems in severely curved canals of rapid microCT-based prototyping molar replicas. *Journal of Applied Oral Science,* 22**,** 509-515.

ORSTAVIK, D. & PITT FORD, T. 1998. Essential endodontology. *Prevention and treatment of apical periodontitis. Oxford: Blackwell Science*.

OSTI, G., WOLF, F. & PHILIPPI, P. Year. Spreading of liquid drops on acrylic surfaces. *In:* Proceedings of the 20th International Congress of Mechanical Engineering, International Congress of Mechanical Engineering, Gramado, RS, Brazil, 2009.

OZBEK, S. M., OZBEK, A. & YAVUZ, M. S. 2013. Detection of human cytomegalovirus and Epstein-Barr Virus in symptomatic and asymptomatic apical periodontitis lesions by real-time PCR.

ÖZEL, T., HSU, T.-K. & ZEREN, E. 2005. Effects of cutting edge geometry, workpiece hardness, feed rate and cutting speed on surface roughness and forces in finish turning of hardened AISI H13 steel. *The International Journal of Advanced Manufacturing Technology,* 25**,** 262-269.

OZSU, D., KARATAS, E., ARSLAN, H. & TOPCU, M. C. 2014. Quantitative evaluation of apically extruded debris during root canal instrumentation with ProTaper Universal, ProTaper Next, WaveOne, and self-adjusting file systems. *European Journal of Dentistry,* 8**,** 504-508.

PAIVA, S. S. M., SIQUEIRA, J. F., RÔÇAS, I. N., CARMO, F. L., FERREIRA, D. C., CURVELO, J. A. R., SOARES, R. M. A. & ROSADO, A. S. 2012. Supplementing the Antimicrobial Effects of Chemomechanical Debridement with Either Passive Ultrasonic Irrigation or a Final Rinse with Chlorhexidine: A Clinical Study. *Journal of Endodontics,* 38**,** 1202-1206.

PALMER JR, R. J., GORDON, S. M., CISAR, J. O. & KOLENBRANDER, P. E. 2003. Coaggregation-mediated interactions of streptococci and actinomyces detected in initial human dental plaque. *Journal of Bacteriology,* 185**,** 3400-3409.

PAPPEN, F. G., QIAN, W., ALEKSEJŪNIENĖ, J., DE TOLEDO LEONARDO, R., LEONARDO, M. R. & HAAPASALO, M. 2010. Inhibition of sodium hypochlorite antimicrobial activity in the presence of bovine serum albumin. *Journal of Endodontics,* 36**,** 268-271.

PAQUÉ, F., AL-JADAA, A. & KFIR, A. 2012. Hard-tissue debris accumulation created by conventional rotary versus self-adjusting file instrumentation in mesial root canal systems of mandibular molars. *International Endodontic Journal,* 45**,** 413-418.

PAQUÉ, F., BARBAKOW, F. & PETERS, O. 2005. Root canal preparation with Endo-Eze AET: changes in root canal shape assessed by micro-computed tomography. *International endodontic journal,* 38**,** 456-464.

PAQUÉ, F., LAIB, A., GAUTSCHI, H. & ZEHNDER, M. 2009. Hard-tissue debris accumulation analysis by high-resolution computed tomography scans. *Journal of Endodontics,* 35**,** 1044-1047.

PAQUÉ, F., RECHENBERG, D.-K. & ZEHNDER, M. 2012a. Reduction of hard-tissue debris accumulation during rotary root canal instrumentation by etidronic acid in a sodium hypochlorite irrigant. *Journal of Endodontics,* 38**,** 692-695.

PARHI, P., GOLAS, A. & VOGLER, E. A. 2010. Role of Proteins and Water in the Initial Attachment of Mammalian Cells to Biomedical Surfaces: A Review. *Journal of Adhesion Science and Technology,* 24**,** 853-888.

PARKER, J. M., MOL, A., RIVERA, E. M. & TAWIL, P. Z. 2017. Cone-beam Computed Tomography Uses in Clinical Endodontics: Observer Variability in Detecting Periapical Lesions. *Journal of Endodontics,* 43**,** 184-187.

PASSOS, V. F., MELO, M. A., VASCONCELLOS, A. A., RODRIGUES, L. K. & SANTIAGO, S. L. 2013. Comparison of methods for quantifying dental wear caused by erosion and abrasion. *Microscopy Research and Technique,* 76**,** 178-183.

PATEL, B., PRATTEN, J., MORDAN, N. & GULABIVALA, K. 2007. Development of an ex vivo model for the study of microbial infection in human teeth. *International Endodontic Journal,* 40**,** 405-405.

PATEL, S. & DUNCAN, H. F. 2011. *Pitt Ford's Problem-Based Learning in Endodontology*, John Wiley & Sons.

PECIULIENE, V., BALCIUNIENE, I., ERIKSEN, H. M. & HAAPASALO, M. 2000. Isolation of Enterococcus faecalis in Previously Root-Filled Canals in a Lithuanian Population. *Journal of Endodontics,* 26**,** 593-595.

PECIULIENE, V., MANELIENE, R., BALCIKONYTE, E., DRUKTEINIS, S. & RUTKUNAS, V. 2008. Microorganisms in root canal infections: a review. *Stomatologija,* 10**,** 4-9.

PEDULLÀ, E., GENOVESI, F., RAPISARDA, S., LA ROSA, G. R., GRANDE, N. M., PLOTINO, G. & ADORNO, C. G. 2017. Effects of 6 single-file systems on dentinal crack formation. *Journal of Endodontics,* 43**,** 456-461.

PERMAR, D. & MELFI, R. C. 1994. *Permar's oral embryology and microscopic anatomy: a textbook for students in dental hygiene*, Lea & Febiger.

PETERS, A. C. 1988. *A constant depth laboratov modelflm fermenter.* PhD thesis, University College Cardiff, Cardiff, UK.

PETERS, O., PETERS, C., SCHONENBERGER, K. & BARBAKOW, F. 2003a. ProTaper rotary root canal preparation: effects of canal anatomy on final shape analysed by micro CT. *International endodontic journal,* 36.

PETERS, O. A. & PAQUE, F. 2010. Current developments in rotary root canal instrument technology and clinical use: a review. *Quintessence international (Berlin, Germany: 1985),* 41**,** 479-488.

PETERS, O. A. & PAQUÉ, F. 2014. Shaping the Root Canal System to Promote Effective Disinfection. *Disinfection of Root Canal Systems: The Treatment of Apical Periodontitis***,** 91.

PETERS, O. A., PETERS, C. I., SCHONENBERGER, K. & BARBAKOW, F. 2003b. ProTaper rotary root canal preparation: effects of canal anatomy on final shape analysed by micro CT.

PETERS, O. A., SCHÖNENBERGER, K. & LAIB, A. 2001. Effects of four Ni–Ti preparation techniques on root canal geometry assessed by micro computed tomography. *International Endodontic Journal,* 34**,** 221-230.

PETZOLD, R., ZEILHOFER, H. F. & KALENDER, W. A. 1999. Rapid prototyping technology in medicine—basics and applications. *Computerized Medical Imaging and Graphics,* 23**,** 277-284.

PIRUSKA, A., NIKCEVIC, I., LEE, S. H., AHN, C., HEINEMAN, W. R., LIMBACH, P. A. & SELISKAR, C. J. 2005. The autofluorescence of plastic materials and chips measured under laser irradiation. *Lab on a Chip,* 5**,** 1348-1354.

PLOTINO, G., TESTARELLI, L., AL-SUDANI, D., PONGIONE, G., GRANDE, N. M. & GAMBARINI, G. 2014b. Fatigue resistance of rotary instruments manufactured using different nickel–titanium alloys: a comparative study. *Odontology,* 102**,** 31-35.

PODOLEANU, A. G. 2012. Optical coherence tomography. *Journal of Microscopy,* 247**,** 209-219.

PORTENIER, I., HAAPASALO, H., ØRSTAVIK, D., YAMAUCHI, M. & HAAPASALO, M. 2002. Inactivation of the Antibacterial Activity of Iodine Potassium Iodide and Chlorhexidine Digluconate Against Enterococcus faecalis by Dentin, Dentin Matrix, Type-I Collagen, and Heat-Killed Microbial Whole Cells. *Journal of Endodontics,* 28**,** 634-637.

PRADO, M. D., ROIZENBLIT, R. N., PACHECO, L. V., BARBOSA, C. A. D. M., LIMA, C. O. D. & SIMÃO, R. A. 2016. Effect of argon plasma on root dentin after use of 6% NaOCl. *Brazilian dental journal,* 27**,** 41-45.

PRATTEN, J., WIECEK, J., MORDAN, N., LOMAX, A., PATEL, N., SPRATT, D. & MIDDLETON, A. 2016. Physical disruption of oral biofilms by sodium bicarbonate: an in vitro study. *International Journal of Dental Hygiene,* 14**,** 209-214.

QING, Y., AKITA, Y., KAWANO, S., KAWAZU, S., YOSHIDA, T. & SEKINE, I. 2006. Cleaning Efficacy and Dentin Micro-Hardness After Root Canal Irrigation With a Strong Acid Electrolytic Water. *Journal of Endodontics,* 32**,** 1102-1106.

QUINTANA, R., JARDINE, A., MONTAGNER, F., FATTURI PAROLO, C., MORGENTAL, R., POLI KOPPER, P., #237 & CIA 2017. Effect of human, dentin, albumin and lipopolysaccharide on the antibacteerial activity of endodontic activity of endodontic irrigants. *Journal of Conservative Dentistry,* 20**,** 341-345.

RAZATOS, A., ONG, Y.-L., SHARMA, M. M. & GEORGIOU, G. 1998. Molecular determinants of bacterial adhesion monitored by atomic force microscopy. *Proceedings of the National Academy of Sciences,* 95**,** 11059-11064.

RENSLOW, R. S., MARSHALL, M. J., TUCKER, A. E., CHRISLER, W. B. & YU, X.-Y. 2017. In situ nuclear magnetic resonance microimaging of live biofilms in a microchannel. *Analyst,* 142**,** 2363-2371.

RHODES, J., FORD, T., LYNCH, J., LIEPINS, P. & CURTIS, R. 1999. Micro-computed tomography: a new tool for experimental endodontology. *International Endodontic Journal,* 32**,** 165-170.

RICUCCI, D. & SIQUEIRA, J. F. 2010. Biofilms and apical periodontitis: study of prevalence and association with clinical and histopathologic findings. *Journal of Endodontics,* 36**,** 1277-1288.

ROANE, J. B., SABALA, C. L. & DUNCANSON, M. G. 1985. The "balanced force" concept for instrumentation of curved canals. *Journal of Endodontics,* 11**,** 203-211.

ROBINSON, J. P., LUMLEY, P. J., CLARIDGE, E., COOPER, P. R., GROVER, L. M., WILLIAMS, R. L. & WALMSLEY, A. D. 2012. An analytical Micro CT methodology for quantifying inorganic dentine debris following internal tooth preparation. *Journal of dentistry,* 40**,** 999-1005.

ROBINSON, J. P., LUMLEY, P. J., COOPER, P. R., GROVER, L. M. & WALMSLEY, A. D. 2013. Reciprocating root canal technique induces greater debris accumulation than a continuous rotary technique as assessed by 3-dimensional micro–computed tomography. *Journal of endodontics,* 39**,** 1067-1070.

RÔÇAS, I. N., SIQUEIRA JR, J. F. & SANTOS, K. R. N. 2004. Association of Enterococcus faecalis With Different Forms of Periradicular Diseases. *Journal of Endodontics,* 30**,** 315-320.

RUDDLE, C. J., MACHTOU, P. & WEST, J. D. 2013. The Shaping Movement 5th Generation Technology. *Dentistry today*.

RUIZ-LINARES, M., AGUADO-PEREZ, B., BACA, P., ARIAS-MOLIZ, M. T. & FERRER-LUQUE, C. M. 2017. Efficacy of antimicrobial solutions against polymicrobial root canal biofilm. *International Endodontic Journal,* 50**,** 77-83.

RUIZ-LINARES, M., AGUADO-PÉREZ, B., BACA, P., ARIAS-MOLIZ, M. & FERRER-LUQUE, C. 2017. Efficacy of antimicrobial solutions against polymicrobial root canal biofilm. *International Endodontic Journal,* 50**,** 77-83.

SACHIDANANDHAM, R., YEW- HOONG GIN, K. & LAA POH, C. 2005. Monitoring of active but non-culturable bacterial cells by flow cytometry. *Biotechnology and Bioengineering,* 89**,** 24-31.

SAI SARASWATHI, V., KAMARUDHEEN, N., BHASKARARAO, K. V. & SANTHAKUMAR, K. 2017. Phytoremediation of dyes using Lagerstroemia speciosa mediated silver nanoparticles and its biofilm activity against clinical strains Pseudomonas aeruginosa. *Journal of Photochemistry and Photobiology B: Biology,* 168**,** 107-116.

SALEHRABI, R. & ROTSTEIN, I. 2004. Endodontic Treatment Outcomes in a Large Patient Population in the USA: An Epidemiological Study. *Journal of Endodontics,* 30**,** 846-850.

SALENTIJN, G. I., OOMEN, P. E., GRAJEWSKI, M. & VERPOORTE, E. 2017. Fused Deposition Modeling 3D Printing for (Bio) analytical Device Fabrication: Procedures, Materials, and Applications. *Analytical Chemistry,* 89**,** 7053-7061.

SAMARANAYAKE, L. P. 2006. *Essential microbiology for dentistry*, Elsevier Health Sciences.

SANGHVI, Z. & MISTRY, K. 2011. Design features of rotary instruments in endodontics. *The Journal of Ahmedabad Dental College and Hospital,* 2**,** 6-11.

SARGENT, R. G. 2013. Verification and validation of simulation models. *Journal of Simulation,* 7**,** 12-24.

SATHORN, C., PARASHOS, P. & MESSER, H. H. 2007. How useful is root canal culturing in predicting treatment outcome? *Journal of Endodontics,* 33**,** 220-225.

SAUER, K., CULLEN, M., RICKARD, A., ZEEF, L., DAVIES, D. & GILBERT, P. 2004. Characterization of nutrient-induced dispersion in Pseudomonas aeruginosa PAO1 biofilm. *Journal of bacteriology,* 186**,** 7312-7326.

SCARFE, W. C., FARMAN, A. G. & SUKOVIC, P. 2006. Clinical applications of cone-beam computed tomography in dental practice. *Journal-Canadian Dental Association,* 72**,** 75.

SCHACHERN, P. A., KWON, G., BRILES, D. E., FERRIERI, P., JUHN, S., CUREOGLU, S., PAPARELLA, M. M. & TSUPRUN, V. 2017. Neutrophil Extracellular Traps and Fibrin in Otitis Media: Analysis of Human and Chinchilla Temporal Bones. *JAMA Otolaryngology–Head & Neck Surgery,* 143**,** 990-995.

SCHÄFER, E. & FLOREK, H. 2003. Efficiency of rotary nickel–titanium K3 instruments compared with stainless steel hand K-Flexofile. Part 1. Shaping ability in simulated curved canals. *International Endodontic Journal,* 36**,** 199-207.

SCHNEIDER, S. W. 1971. A comparison of canal preparations in straight and curved root canals. *Oral Surgery, Oral Medicine, Oral Pathology,* 32**,** 271-275.

SCHNURR, P. J. & ALLEN, D. G. 2015. Factors affecting algae biofilm growth and lipid production: a review. *Renewable and Sustainable Energy Reviews,* 52**,** 418-429.

SCULLY, C., FLINT, S., PORTER, S. & MOOS, K. 2004. Oral and Maxillofacial Diseases: an illustrated guide to the diagnosis and management of diseases of the oral mucosa, gingiva, teeth, salivary glands, bones and joints. Taylor and Francis: Oxfordshire, UK.

SEDGLEY, C., NAGEL, A., DAHLÉN, G., REIT, C. & MOLANDER, A. 2006. Real-time quantitative polymerase chain reaction and culture analyses of Enterococcus faecalis in root canals. *Journal of Endodontics,* 32**,** 173-177.

SEDGLEY, C., NAGEL, A., HALL, D. & APPLEGATE, B. 2005. Influence of irrigant needle depth in removing bioluminescent bacteria inoculated into instrumented root canals using real-time imaging in vitro. *International Endodontic Journal,* 38**,** 97-104.

SÉNÉCHAL, A., CARRIGAN, S. D. & TABRIZIAN, M. 2004. Probing Surface Adhesion Forces of Enterococcus f aecalis to Medical-Grade Polymers Using Atomic Force Microscopy. *Langmuir,* 20**,** 4172-4177.

SHAH, N., MADHU, K., SREENIVASA MURTHY, B., HEMANTH, B., MATHEW, S. & NAGARAJ, S. 2016. Identification of presence of Candida albicans in primary root canal infections: An in vitro study. *Endodontology,* 28**,** 109-113.

SHANKAR, N., LOCKATELL, C. V., BAGHDAYAN, A. S., DRACHENBERG, C., GILMORE, M. S. & JOHNSON, D. E. 2001. Role of Enterococcus faecalissurface protein ESP in the pathogenesis of ascending urinary tract infection. *Infection and Immunity,* 69**,** 4366-4372.

SHEMESH, H., VAN SOEST, G., WU, M.-K., VAN DER SLUIS, L. W. M. & WESSELINK, P. R. 2007. The Ability of Optical Coherence Tomography to Characterize the Root Canal Walls. *Journal of Endodontics,* 33**,** 1369-1373.

SHEMESH, H., VAN SOEST, G., WU, M.-K. & WESSELINK, P. R. 2008. Diagnosis of vertical root fractures with optical coherence tomography. *Journal of endodontics,* 34**,** 739-742.

SHEN, Y., GAO, Y., QIAN, W., RUSE, N. D., ZHOU, X., WU, H. & HAAPASALO, M. 2010a. Three-dimensional Numeric Simulation of Root Canal Irrigant Flow with Different Irrigation Needles. *Journal of Endodontics,* 36**,** 884-889.

SHEN, Y., STOJICIC, S. & HAAPASALO, M. 2010b. Bacterial viability in starved and revitalized biofilms: comparison of viability staining and direct culture. *Journal of Endodontics,* 36**,** 1820-1823.

SHORT, F. L., MURDOCH, S. L. & RYAN, R. P. 2014. Polybacterial human disease: the ills of social networking. *Trends in Microbiology,* 22**,** 508-516.

SILVA, D. N., DE OLIVEIRA, M. G., MEURER, E., MEURER, M. I., DA SILVA, J. V. L. & SANTA-BÁRBARA, A. 2008. Dimensional error in selective laser sintering and 3D-printing of models for craniomaxillary anatomy reconstruction. *Journal of Cranio-Maxillofacial Surgery,* 36**,** 443-449.

SIMONSEN, G. S., SMÅBREKKE, L., MONNET, D. L., SØRENSEN, T. L., MØLLER, J. K., KRISTINSSON, K. G., LAGERQVIST-WIDH, A., TORELL, E., DIGRANES, A., HARTHUG, S. & SUNDSFJORD, A. 2003. Prevalence of resistance to ampicillin, gentamicin and vancomycin in Enterococcus faecalis and Enterococcus faecium isolates from clinical specimens and use of antimicrobials in five Nordic hospitals. *Journal of Antimicrobial Chemotherapy,* 51**,** 323-331.

SIMS, P., ALBRECHT, R., PAWLEY, J. B., CENTONZE, V., DEERINCK, T. & HARDIN, J. 2006. When Light Microscope Resolution Is Not Enough: Correlational Light Microscopy and Electron Microscopy. *Handbook of Biological Confocal Microscopy.* Springer.

SINGH, K. V., LA ROSA, S. L., SOMARAJAN, S. R., ROH, J. H. & MURRAY, B. E. 2015. The fibronectin-binding protein EfbA contributes to pathogenesis and protects against infective endocarditis caused by Enterococcus faecalis. *Infection and Immunity,* 83**,** 4487-4494.

SIQUEIRA, J. 2003. Microbial causes of endodontic flare-ups. *International Endodontic Journal,* 36**,** 453-463.

SIQUEIRA, J., MACHADO, A., SILVEIRA, R., LOPES, H. & UZEDA, M. D. 1997a. Evaluation of the effectiveness of sodium hypochlorite used with three irrigation methods in the elimination of Enterococcus faecalis from the root canal, in vitro. *International Endodontic Journal,* 30**,** 279-282.

SIQUEIRA, J., PEREZ, A., MARCELIANO-ALVES, M., PROVENZANO, J., SILVA, S., PIRES, F., VIEIRA, G., ROCAS, I. & ALVES, F. 2017. What happens to unprepared root canal walls: a correlative analysis using micro-computed tomography and histology/scanning electron microscopy. *International Endodontic Journal,* 51**,** 501-508.

SIQUEIRA, J. F. 2001. Aetiology of root canal treatment failure: why well-treated teeth can fail. *International Endodontic Journal,* 34**,** 1-10.

SIQUEIRA, J. F., ARAÚJO, M. C., GARCIA, P. F., FRAGA, R. C. & DANTAS, C. J. S. 1997b. Histological evaluation of the effectiveness of five instrumentation techniques for cleaning the apical third of root canals. *Journal of Endodontics,* 23**,** 499-502.

SIQUEIRA, J. F., LIMA, K. C., MAGALHÃES, F. A., LOPES, H. P. & DE UZEDA, M. 1999. Mechanical reduction of the bacterial population in the root canal by three instrumentation techniques. *Journal of Endodontics,* 25**,** 332-335.

SIQUEIRA, J. F., RÔÇAS, I. N., MORAES, S. R. & SANTOS, K. R. N. 2002a. Direct amplification of rRNA gene sequences for identification of selected oral pathogens in root canal infections. *International Endodontic Journal,* 35**,** 345-351.

SIQUEIRA, J. F., RÔÇAS, I. N., SOUTO, R., DE UZEDA, M. & COLOMBO, A. P. 2002b. Actinomyces species, streptococci, and Enterococcus faecalis in primary root canal infections. *Journal of Endodontics,* 28**,** 168-172.

SIQUEIRA JR, J., PEREZ, A., MARCELIANO-ALVES, M., PROVENZANO, J., SILVA, S., PIRES, F., VIEIRA, G., ROCAS, I. & ALVES, F. 2018. What happens to unprepared root canal walls: a correlative analysis using micro-computed tomography and histology/scanning electron microscopy. *International Endodontic Journal,* 51**,** 501-508.

SIQUEIRA JR, J. F. 2002. Endodontic infections: concepts, paradigms, and perspectives. *Oral Surgery, Oral Medicine, Oral Pathology, Oral Radiology, and Endodontology,* 94**,** 281-293.

SIQUEIRA JR, J. F., RÔÇAS, I. N. & LOPES, H. P. 2002a. Patterns of microbial colonization in primary root canal infections. *Oral Surgery, Oral Medicine, Oral Pathology, Oral Radiology, and Endodontology,* 93**,** 174-178.

SIQUEIRA JR, J. F., RÔÇAS, I. N., SOUTO, R., DE UZEDA, M. & COLOMBO, A. P. 2002b. Actinomyces Species, Streptococci, and Enterococcus faecalis in Primary Root Canal Infections. *Journal of Endodontics,* 28**,** 168-172.

SMALLWOOD, E., GHARBIA, S., WILLIAMS, J., GULABIVALA, K. & SHAH, H. Year. Isolation and direct nucleic acid detection of oral spirochaetes in root canal infections. *In:* International Endodontic Journal, 1998. 214-214.

SOAMES, J. V. & SOUTHAM, J. C. 2005. *Oral pathology*, Oxford University Press.

SOOD, S., MALHOTRA, M., DAS, B. & KAPIL, A. 2008. Enterococcal infections & antimicrobial resistance. *Indian Journal of Medical Research,* 128**,** 111.

SOUSA, B. C. D., GOMES, F. D. A., FERREIRA, C. M., ROCHA, M. M. D. N. P., BARROS, E. B. & ALBUQUERQUE, D. S. D. 2017. Persistent extra-radicular bacterial biofilm in endodontically treated human teeth: scanning electron microscopy analysis after apical surgery. *Microscopy Research and Technique,* 80**,** 662-667.

SPAIDE, R. F. & CURCIO, C. A. 2017. Evaluation of segmentation of the superficial and deep vascular layers of the retina by optical coherence tomography angiography instruments in normal eyes. *JAMA Ophthalmology,* 135**,** 259-262.

SPRATT, D., PRATTEN, J., WILSON, M. & GULABIVALA, K. 2001. An in vitro evaluation of the antimicrobial efficacy of irrigants on biofilms of root canal isolates. *International Endodontic Journal,* 34**,** 300-307.

STANLEY, H. R. 1989. Pulp capping: conserving the dental pulp—can it be done? Is it worth it? *Oral Surgery, Oral Medicine, Oral Pathology,* 68**,** 628-639.

STIFTER, D., BURGHOLZER, P., HÖGLINGER, O., GÖTZINGER, E. & HITZENBERGER, C. K. 2003. Polarisation-sensitive optical coherence tomography for material characterisation and strain-field mapping. *Applied Physics A: Materials Science & Processing,* 76**,** 947-951.

STOODLEY, P., SAUER, K., DAVIES, D. G. & COSTERTON, J. W. 2002. Biofilms as complex differentiated communities. *Annual Reviews in Microbiology,* 56**,** 187-209.

STOODLEY, P., WILSON, S., HALL-STOODLEY, L., BOYLE, J. D., LAPPIN-SCOTT, H. M. & COSTERTON, J. W. 2001. Growth and detachment of cell clusters from mature mixed-species biofilms. *Applied and Environmental Microbiology,* 67**,** 5608-5613.

STUART, C. H., SCHWARTZ, S. A., BEESON, T. J. & OWATZ, C. B. 2006. Enterococcus faecalis: Its Role in Root Canal Treatment Failure and Current Concepts in Retreatment. *Journal of Endodontics,* 32**,** 93-98.

SUMMITT, J. B. & DOS SANTOS, J. 2006. *Fundamentals of operative dentistry: a contemporary approach*, Quintessence Pub.

SUNDE, P. T., OLSEN, I., GÖBEL, U. B., THEEGARTEN, D., WINTER, S., DEBELIAN, G. J., TRONSTAD, L. & MOTER, A. 2003. Fluorescence in situ hybridization (FISH) for direct visualization of bacteria in periapical lesions of asymptomatic root-filled teeth. *Microbiology,* 149**,** 1095-1102.

SUNDQVIST, G. 1992. Associations between microbial species in dental root canal infections. *Oral microbiology and immunology,* 7**,** 257-262.

SUTHERLAND, I. W. 2001. The biofilm matrix–an immobilized but dynamic microbial environment. *Trends in microbiology,* 9**,** 222-227.

SVENSÄTER, G. & BERGENHOLTZ, G. 2004. Biofilms in endodontic infections. *Endodontic Topics,* 9**,** 27-36.

SWARTZ, D. B., SKIDMORE, A. E. & GRIFFIN, J. A. 1983. Twenty years of endodontic success and failure. *Journal of Endodontics,* 9**,** 198-202.

SYAKUR, A. & SUTANTO, H. Year. Determination of Hydrophobic Contact Angle of Epoxy Resin Compound Silicon Rubber and Silica. *In:* IOP Conference Series: Materials Science and Engineering, 2017. IOP Publishing, 012025.

TABASSUM, S. & KHAN, F. R. 2016. Failure of endodontic treatment: The usual suspects. *European Journal of Dentistry,* 10**,** 144-147.

TACHIBANA, H. & MATSUMOTO, K. 1990. Applicability of X-ray computerized tomography in endodontics. *Dental Traumatology,* 6**,** 16-20.

TAHMASBI, M., JALALI, P., NAIR, M. K., BARGHAN, S. & NAIR, U. P. 2017. Prevalence of Middle Mesial Canals and Isthmi in the Mesial Root of Mandibular Molars: An In Vivo Cone-beam Computed Tomographic Study. *Journal of Endodontics,* 43**,** 1080-1083.

TAO, P., LI, Y., SIEGEL, R. W. & SCHADLER, L. S. 2013. Transparent dispensible high-refractive index ZrO2/epoxy nanocomposites for LED encapsulation. *Journal of Applied Polymer Science,* 130**,** 3785-3793.

TCHORZ, J. P., BRANDL, M., GANTER, P. A., KARYGIANNI, L., POLYDOROU, O., VACH, K., HELLWIG, E. & ALTENBURGER, M. J. 2015. Pre-clinical endodontic training with artificial instead of extracted human teeth: does the type of exercise have an influence on clinical endodontic outcomes? *International Endodontic Journal,* 48**,** 888-893.

TEIXEIRA, F., SANO, C., GOMES, B., ZAIA, A., FERRAZ, C. & SOUZA-FILHO, F. 2003. A preliminary in vitro study of the incidence and position of the root canal isthmus in maxillary and mandibular first molars. *International Endodontic Journal,* 36**,** 276-280.

TEN CATE, A. 1998. Oral histology: Development, structure, and function, St. Louis, MO: Mosby-Year Book. Inc.

TERANAKA, A., TOMIYAMA, K., OHASHI, K., MIYAKE, K., SHIMIZU, T., HAMADA, N., MUKAI, Y., HIRAYAMA, S. & NIHEI, T. 2017. Relevance of surface characteristics in the adhesiveness of polymicrobial biofilms to crown restoration materials. *Journal of Oral Science***,** 16-0758.

THOMPSON, S. & DUMMER, P. 1997. Shaping ability of ProFile. 04 Taper Series 29 rotary nickel-titanium instruments in simulated root canals. Part 1. *International Endodontic Journal,* 30**,** 1-7.

TOLEDO-ARANA, A., VALLE, J., SOLANO, C., ARRIZUBIETA, M. A. J., CUCARELLA, C., LAMATA, M., AMORENA, B., LEIVA, J., PENADÉS, J. R. & LASA, I. 2001a. The enterococcal surface protein, Esp, is involved in Enterococcus faecalis biofilm formation. *Applied and environmental microbiology,* 67**,** 4538-4545.

TOLEDO-ARANA, A., VALLE, J., SOLANO, C., ARRIZUBIETA, M. J., CUCARELLA, C., LAMATA, M., AMORENA, B., LEIVA, J., PENADÉS, J. R. & LASA, I. 2001b. The Enterococcal Surface Protein, Esp, Is Involved in Enterococcus faecalis Biofilm Formation. *Applied and Environmental Microbiology,* 67**,** 4538-4545.

TOMÁS-CATALÁ, C. J., COLLADO-GONZÁLEZ, M., GARCÍA-BERNAL, D., OÑATE-SÁNCHEZ, R. E., FORNER, L., LLENA, C., LOZANO, A., MORALEDA, J. M. & RODRÍGUEZ-LOZANO, F. J. 2018. Biocompatibility of New Pulp-capping Materials NeoMTA Plus, MTA Repair HP, and Biodentine on Human Dental Pulp Stem Cells. *Journal of Endodontics,* 44**,** 126-132.

TORABINEJAD, M. & WALTON, R. E. 2002. *Principles and practice of endodontics*, Saunders Philadelphia.

TOWNSEND, C. & MAKI, J. 2009. An In Vitro Comparison of New Irrigation and Agitation Techniques to Ultrasonic Agitation in Removing Bacteria From a Simulated Root Canal. *Journal of Endodontics,* 35**,** 1040-1043.

VAN DER SLUIS, L., VERSLUIS, M., WU, M. & WESSELINK, P. 2007. Passive ultrasonic irrigation of the root canal: a review of the literature. *International Endodontic Journal,* 40**,** 415-426.

VAN VELTHOVEN, M. E., FABER, D. J., VERBRAAK, F. D., VAN LEEUWEN, T. G. & DE SMET, M. D. 2007. Recent developments in optical coherence tomography for imaging the retina. *Progress in Retinal and Eye Research,* 26**,** 57-77.

VENTOLA, C. L. 2014. Medical Applications for 3D Printing: Current and Projected Uses. *Pharmacy and Therapeutics,* 39**,** 704-711.

VERHAAGEN, B., BOUTSIOUKIS, C., HEIJNEN, G., VAN DER SLUIS, L. & VERSLUIS, M. 2012. Role of the confinement of a root canal on jet impingement during endodontic irrigation. *Experiments in Fluids,* 53**,** 1841-1853.

VERSIANI, M., ALVES, F., ANDRADE-JUNIOR, C., MARCELIANO-ALVES, M., PROVENZANO, J., RÔÇAS, I., SOUSA-NETO, M. & SIQUEIRA, J. 2016. Micro-CT evaluation of the efficacy of hard-tissue removal from the root canal and isthmus area by positive and negative pressure irrigation systems. *International Endodontic Journal,* 49**,** 1079-1087.

VERSIANI, M. A., PÉCORA, J. D. & DE SOUSA-NETO, M. D. 2011. Flat-oval root canal preparation with self-adjusting file instrument: a micro–computed tomography study. *Journal of Endodontics,* 37**,** 1002-1007.

VERSTRAETEN, J., JACQUET, W., DE MOOR, R. & MEIRE, M. 2017a. Hard tissue debris removal from the mesial root canal system of mandibular molars with ultrasonically and laser-activated irrigation: a micro-computed tomography study. *Lasers in Medical Science***,** 1-6.

VERSTRAETEN, J., JACQUET, W., DE MOOR, R. & MEIRE, M. 2017b. Hard tissue debris removal from the mesial root canal system of mandibular molars with ultrasonically and laser-activated irrigation: a micro-computed tomography study. *Lasers in medical science,* 32**,** 1965-1970.

VERTUCCI, F. J. 1984. Root canal anatomy of the human permanent teeth. *Oral Surgery, Oral Medicine, Oral Pathology,* 58**,** 589-599.

VILLEGAS, J. C., YOSHIOKA, T., KOBAYASHI, C. & SUDA, H. 2004. Frequency of transverse anastomoses with and without apical communication in Japanese population teeth. *Australian Endodontic Journal,* 30**,** 50-52.

VORUGANTI, K. 2008. Essential endodontology-prevention and treatment of apical periodontitis. *British Dental Journal,* 204**,** 536-536.

WAAR, K., VAN DER MEI, H. C., HARMSEN, H. J., DE VRIES, J., ATEMA-SMIT, J., DEGENER, J. E. & BUSSCHER, H. J. 2005. Atomic force microscopy study on specificity and non-specificity of interaction forces between Enterococcus faecalis cells with and without aggregation substance. *Microbiology,* 151**,** 2459-2464.

WAGNER, M. & HORN, H. 2017. Optical coherence tomography in biofilm research: A comprehensive review. *Biotechnology and Bioengineering,* 114**,** 1386-1402.

WAGNER, M., TAHERZADEH, D., HAISCH, C. & HORN, H. 2010. Investigation of the mesoscale structure and volumetric features of biofilms using optical coherence tomography. *Biotechnology and Bioengineering,* 107**,** 844-853.

WAKIMOTO, N., NISHI, J., SHEIKH, J., NATARO, J. P., SARANTUYA, J., IWASHITA, M., MANAGO, K., TOKUDA, K., YOSHINAGA, M. & KAWANO, Y. 2004. Quantitative biofilm assay using a microtiter plate to screen for enteroaggregative Escherichia coli. *The American Journal of Tropical Medicine and Hygiene,* 71**,** 687-690.

WALIA, H., BRANTLEY, W. A. & GERSTEIN, H. 1988. An initial investigation of the bending and torsional properties of Nitinol root canal files. *Journal of endodontics,* 14**,** 346-351.

WALLNER, G., AMANN, R. & BEISKER, W. 1993. Optimizing fluorescent in situ hybridization with rRNA-targeted oligonucleotide probes for flow cytometric identification of microorganisms. *Cytometry Part A,* 14**,** 136-143.

WALMSLEY, A., LUMLEY, P. & LAIRD, W. 1989. The oscillatory pattern of sonically powered endodontic files. *International Endodontic Journal,* 22**,** 125-132.

WALSCH, H. 2004. The hybrid concept of nickel–titanium rotary instrumentation. *Dental Clinics of North America,* 48**,** 183-202.

WALTERS, M. C., ROE, F., BUGNICOURT, A., FRANKLIN, M. J. & STEWART, P. S. 2003. Contributions of antibiotic penetration, oxygen limitation, and low metabolic activity to tolerance of Pseudomonas aeruginosa biofilms to ciprofloxacin and tobramycin. *Antimicrobial agents and chemotherapy,* 47**,** 317-323.

WALTON, R. E. 1976. Histologic evaluation of different methods of enlarging the pulp canal space. *Journal of Endodontics,* 2**,** 304-311.

WANG, L., ZHAO, Y., MEI, L., YU, H., MUHAMMAD, I., PAN, Y. & HUANG, S. 2017. Effect of application time of maleic acid on smear layer removal and mechanical properties of root canal dentin. *Acta Odontologica Scandinavica,* 75**,** 59-66.

WANG, R., SHEN, Y., MA, J., HUANG, D., ZHOU, X., GAO, Y. & HAAPASALO, M. 2015. Evaluation of the effect of needle position on irrigant flow in the C-shaped root canal using a computational fluid dynamics model. *Journal of Endodontics,* 41**,** 931-936.

WANG, Z., SHEN, Y. & HAAPASALO, M. 2012. Effectiveness of Endodontic Disinfecting Solutions against Young and Old Enterococcus faecalis Biofilms in Dentin Canals. *Journal of Endodontics,* 38**,** 1376-1379.

WANNER, O. & GUJER, W. 1986. A multispecies biofilm model. *Biotechnology and Bioengineering,* 28**,** 314-328.

WEBB, J. S., THOMPSON, L. S., JAMES, S., CHARLTON, T., TOLKER-NIELSEN, T., KOCH, B., GIVSKOV, M. & KJELLEBERG, S. 2003. Cell death in Pseudomonas aeruginosa biofilm development. *Journal of Bacteriology,* 185**,** 4585-4592.

WEBBER, J., MACHTOU, P., PERTOT, W., KUTTLER, S., RUDDLE, C. & WEST, J. 2011. The WaveOne single-file reciprocating system. *Roots,* 1**,** 28-33.

WEGE, H. A., AGUILAR, J. A., RODRÍGUEZ-VALVERDE, M. Á., TOLEDANO, M., OSORIO, R. & CABRERIZO-VÍLCHEZ, M. Á. 2003. Dynamic contact angle and spreading rate measurements for the characterization of the effect of dentin surface treatments. *Journal of Colloid and Interface Science,* 263**,** 162-169.

WEINE, F. S., KELLY, R. F. & LIO, P. J. 1975. The effect of preparation procedures on original canal shape and on apical foramen shape. *Journal of Endodontics,* 1**,** 255-262.

WELLER, R. N., BRADY, J. M. & BERNIER, W. E. 1980. Efficacy of ultrasonic cleaning. *Journal of Endodontics,* 6**,** 740-743.

WHITE, J. L. & SPRUIELL, J. E. 1981. Specification of biaxial orientation in amorphous and crystalline polymers. *Polymer Engineering & Science,* 21**,** 859-868.

WILSON, M. 1999. [21] Use of constant depth film fermentor in studies of biofilms of oral bacteria. *Methods in Enzymology,* 310**,** 264-279.

WOOD, N. K. & GOAZ, P. W. 1997. *Differential diagnosis of oral and maxillofacial lesions*, Mosby St. Louis.

WRIGHT, P. P. & WALSH, L. J. 2017. Optimizing Antimicrobial Agents in Endodontics. *Antibacterial Agents.* InTech.

WU, D., FAN, W., KISHEN, A., GUTMANN, J. L. & FAN, B. 2014. Evaluation of the antibacterial efficacy of silver nanoparticles against Enterococcus faecalis biofilm. *Journal of Endodontics,* 40**,** 285-290.

WU, M., CHEN, Q., HE, X., LI, P., FAN, W., YUAN, S. & PARK, H. 2018. Automatic Subretinal fluid segmentation of retinal SD-OCT images with neurosensory retinal detachment guided by enface fundus imaging. *IEEE Transactions on Biomedical Engineering,* 65**,** 87-95.

XI, C., MARKS, D., SCHLACHTER, S., LUO, W. & BOPPART, S. A. 2006a. High-resolution three-dimensional imaging of biofilm development using optical coherence tomography. *Journal of Biomedical Optics,* 11**,** 034001-034001-6.

XI, C., MARKS, D. L., SCHLACHTER, S., LUO, W. & BOPPART, S. A. 2006b. High-resolution three-dimensional imaging of biofilm development using optical coherence tomography. *Journal of Biomedical Optics,* 11**,** 034001.

XIA, T. & BAUMGARTNER, J. C. 2003. Occurrence of Actinomyces in infections of endodontic origin. *Journal of Endodontics,* 29**,** 549-552.

YADAV, H. K., YADAV, R. K., CHANDRA, A. & TIKKU, A. P. 2017. A Scanning Electron Microscopic Evaluation of the Effectiveness of Etidronic Acid, SmearClear and MTAD in Removing the Intracanal Smear Layer. *Journal of Dentistry,* 18**,** 118-126.

YAMADA, R. S., ARMAS, A., GOLDMAN, M. & LIN, P. S. 1983. A scanning electron microscopic comparison of a high volume final flush with several irrigating solutions: Part 3. *Journal of Endodontics,* 9**,** 137-142.

YOLDAS, O., YILMAZ, S., ATAKAN, G., KUDEN, C. & KASAN, Z. 2012. Dentinal microcrack formation during root canal preparations by different NiTi rotary instruments and the self-adjusting file. *Journal of Endodontics,* 38**,** 232-235.

YOON, H. Y. & LEE, S. Y. 2017. Establishing a laboratory model of dental unit waterlines bacterial biofilms using a CDC biofilm reactor. *Biofouling,* 33**,** 917-926.

YOU, S.-Y., BAE, K.-S., BAEK, S.-H., KUM, K.-Y., SHON, W.-J. & LEE, W. 2010. Lifespan of One Nickel-Titanium Rotary File with Reciprocating Motion in Curved Root Canals. *Journal of endodontics,* 36**,** 1991-1994.

YOUNES, J. A., LIEVENS, E., HUMMELEN, R., VAN DER WESTEN, R., REID, G. & PETROVA, M. I. 2017. Women and Their Microbes: The Unexpected Friendship. *Trends in Microbiology*.

YU, L. 2001. Amorphous pharmaceutical solids: preparation, characterization and stabilization. *Advanced Drug Delivery Reviews,* 48**,** 27-42.

YUSUF, H. 1982. The significance of the presence of foreign material periapically as a cause of failure of root treatment. *Oral Surgery, Oral Medicine, Oral Pathology,* 54**,** 566-574.

ZANESCO, C., SÓ, M. V. R., SCHMIDT, S., FONTANELLA, V. R. C., GRAZZIOTIN-SOARES, R. & BARLETTA, F. B. 2017. Apical Transportation, Centering Ratio, and Volume Increase after Manual, Rotary, and Reciprocating Instrumentation in Curved Root Canals: Analysis by Micro-computed Tomographic and Digital Subtraction Radiography. *Journal of Endodontics,* 43**,** 486-490.

ZEHNDER, M. 2006. Root Canal Irrigants. *Journal of Endodontics,* 32**,** 389-398.

ZHANG, K., CHENG, L., IMAZATO, S., ANTONUCCI, J. M., LIN, N. J., LIN-GIBSON, S., BAI, Y. & XU, H. H. 2013. Effects of dual antibacterial agents MDPB and nano-silver in primer on microcosm biofilm, cytotoxicity and dentine bond properties. *Journal of Dentistry,* 41**,** 464-474.

ZHENG, Y., HUANG, Y., LIAO, Q., ZHU, X., FU, Q. & XIA, A. 2016. Effects of wettability on the growth of Scenedesmus obliquus biofilm attached on glass surface coated with polytetrafluoroethylene emulsion. *International Journal of Hydrogen Energy,* 41**,** 21728-21735.

ZHU, J., YU, Z., BURKHARD, G. F., HSU, C.-M., CONNOR, S. T., XU, Y., WANG, Q., MCGEHEE, M., FAN, S. & CUI, Y. 2009. Optical Absorption Enhancement in Amorphous Silicon Nanowire and Nanocone Arrays. *Nano Letters,* 9**,** 279-282.

ZIMMER, M. 2014. *Introduction to fluorescent proteins*, CRC Press, Taylor & Francis Group: Boca Raton, FL, USA.